Universidad de Valladolid

Departamento de Bioquímica y Biología Molecular e Instituto de Biología y Genética Molecular (UVa-CSIC)

TESIS DOCTORAL:

Función de los canales de K^+ y Ca^{2+} en un modelo de hipertensión esencial

Presentada por Sendoa Tajada Esteban para optar al grado de doctor por la Universidad de Valladolid

Dirigida por el Dr. José Ramón López López y la Dra. Mª Teresa Pérez García

Abbreviations

5-HT	Serotonin
ABC	ATP-Binding Cassette
Ach	Acetylcholine
Ad	Adventitia
AID	Alpha Interaction Domain
ANP	Atrial Natriuretic Peptide
Ao	Aorta
AOTF	Accusto-Optic Tunable Filter
Ar	Artery
ATP	Adenosine triphosphate
BAPTA	1,2-bis(o-aminophenoxy)ethane-N,N,N',N'-tetraacetic acid
BID	Beta Interaction Domain
BK_{Ca}	Large conductance Ca^{2+}-dependent potassium channels
BP	Blood Pressure
BPH	Blood Pressure High
BPN	Blood Pressure Normal
BSA	Bovine Serum Albumin
cAMP	Cyclic Adenosine Monophosphate
CGRP	Calcitonin-Gene-Related-Peptide
CICR	Calcium-Induced Calcium Release
ClC	Chloride channel
CNN1	Calponin 1
CO	Cardiac Output
CS	Cardiovascular System
Ct	Threshold cycle
DAG	Diacylglycerol
DHP	Dihydropyridine
DHPs	Dihydropyridines
DMEM	Dulbecco's Modified Eagle's Medium
DP	Diastolic Pressure
DTE	1,4-Dithioerythritol
DTT	Dithiothreitol
EC_{50}	Half maximal effective concentration
EDHF	Endothelium-Derived Hyperpolarizing Factor
EGTA	Ethylene Glycol Tetraacetic Acid
E_K	Potassium equilibrium potential
EMCCD	Electron Multiplying Charge Coupled Device
eNOS	Endothelial Nitric Oxide Synthase
ER	Endoplasmic Reticulum
F	Fluorescence intensity of each pixel
F_o	Average resting fluorescence intensity
G/V	Conductance-Voltage relationship
GAPDH	Glyceraldehyde-3P-dehydrogenase
GBP	Gabapentin
GDP	Guanosine diphosphate
GFP	Green Fluorescent Protein
Glb	Glibenclamide
Gmax	Maximum conductance
GTP	Guanosine triphosphate
g_u	Unitary conductance

GUS	β-glucuronidase
HEKs	Human Embryonic Kidney 293 cells
HEPES	4-(2-hydroxyethyl)-1-piperazineethanesulfonic acid
HTN	Hypertension
HVA	High-Voltage Activated
I	Intima
I/V	Intensity-Voltage relationship
IK$_{Ca}$	Intermediate conductance Ca^{2+}-dependent potassium channels
IP$_3$	Inositol triphosphate
IP$_3$R	Inositol triphosphate recepptor
K$_{ATP}$	ATP-dependent potassium channels
K$_{Ca}$	Ca^{2+}-dependent potassium channels
K$_{IR}$	Inward rectifier potassium channels
Kv	Voltage-dependent potassium channels
L	Lumen
LA	Left atrium
LTCCs	L-type calcium channels
LV	Left ventricle
LVA	Low-Voltage-Activated
M	Media
MHC	Myosin Heavy Chain
MII	Myosin II-type
MLC	Myosin Light Chain
MLCK	Myosin Light Chain Kinase
MLCP	Myosin Light Chain Phosphatase
MP	Mean Pressure
MT	Myogenic Tone
NAd	Noradrenaline
NDPs	Nucleotide diphosphates
Nif	Nifedipine
NMDG	N-Methyl-D-Glucamine
NO	Nitric Oxide
NOS3	Nitric Oxide Synthase 3
nPs	Activity of Ca^{2+} sparklets
PA	Pulmonary Artery
PAF	Platelet Activating Factor
PGE	E type prostoglandins
PGF	F type prostoglandins
PGI$_2$	Prostacyclin
Phe	Phenylephrine
Pi	Phosphate group
PI3K	Phosphatidyl Inositol-3 Kinase
Pin	Pinacidil
PIP$_2$	Phosphatidylinositol 4,5-bisphosphate
PKA	Protein Kinase A
PKG	Protein Kinase G
PLC	Phospholipase C
PM	Plasmatic Membrane
PMCA	Plasma Membrane Ca^{2+}-ATPase pump
P$_o$	Open probability
PSS	Physiological Saline Solution
PVDF	Polyvinylidene difluoride membrane

qPCR	Quantitative real time Polymerase Chain Reaction
RA	Right Atrium
RAAS	Rennin-Angiotensin-Aldosterone System
ROCs	Receptor Operated Channels
RP18S	Ribosomal Protein 18S
RT	Room Temperature
RV	Right Ventricle
RyR	Ryanodine Receptor
SACS	Stretch-Activated Channels
SCG	Superior Cervical Ganglion
SDS-PAGE	Sodium Dodecyl Sulfate PolyAcrylamide Gel Electrophoresis
SEM	Standard Error of the Mean
SERCA	Sarcoplasmic Reticulum Ca^{2+}-ATPase pump
SHR	Spontaneously Hypertensive Rats
SK$_{Ca}$	Small conductance Ca^{2+}-dependent potassium channels
SMDS	Smooth Muscle Dissociation Solution
SOCs	Store Operated Channels
SP	Systolic Pressure
SR	Sarcoplasmic Reticulum
STOCs	Spontaneous Transient Outward Currents
SUR	Sulfonylurea Receptors
TBS	Tris Buffered Saline
TEA	Tetraethylammonium
TGM	Tris Glycine Methanol
TIRF	Total Internal Reflection Fluorescence
TLDA	TaqMan Low Density Array
TM	Transmembrane helices
TPR	Total Peripehrical Resistance
TRPs	Nonspecific cationic channels
V	Vein
VDCCs	Voltage-Dependent Calcium Channels
V$_M$	Membrane potential
VSM	Vascular Smooth Muscle
VSMCs	Vascular Smooth Muscle Cells
VWA	Von Willebrand factor type A

INDEX

1 INTRODUCTION

1.1 HYPERTENSION

Hypertension (**HTN**) or **arterial hypertension**, is defined as a chronic elevation of systolic blood pressure (BP) above 140 mmHg or diastolic BP over 90 mmHg or both in adults (Carretero & Oparil, 2000). Its high prevalence (close to 30% of adult population in developed countries (Chobanian *et al.*, 2003)), makes hypertension a relevant risk factor contributing to cardiovascular morbidity and mortality. HTN is associated with functional and structural cardiovascular pathologies such as ischemic heart disease, cerebrovascular disease, heart failure and renal failure, and is estimated to cause more than 7 million premature deaths per year worldwide.

About 95 per cent of all cases of hypertension are diagnosed as **essential hypertension** (or primary hypertension), in which it is not possible to identify a single, specific cause. The remaining cases are forms of hypertension secondary to other pathologies, such as renal artery stenosis, or pheochromocytoma. Essential hypertension tends to be familiar and is likely to be the consequence of a complex interaction between enviromental and genetic factors. More than 50 genes have been examined in association studies with hypertension, and the number is constantly growing. The genetic influence upon hypertension is not fully understood at the moment, although the majority of the studies support the concept that the inheritance is probably multifactorial. The prevalence of essential hypertension increases with age, and in these cases is also more likely to be multifactorial, involving mechanisms such as an increase in the stiffening of the arteries, a decrease in glomerular filtration rate or the developing of renal microvascular disease resulting in decreasing efficiency of sodium excretion. In addition to age, other factors contributing to the development of essential hypertension include obesity, renin elevation and metabolic syndrome or sodium rich diets. The complexity of this disease makes also difficult to create animal models of essential hypertension, and the best models to reproduce human hypertension are those strains obtained with a combination of genetic factors, by phenotypic selection.

Hypertension is a risk factor for all clinical manifestations of atherosclerosis. In addition, it is an independent predisposing factor for heart failure, coronary artery disease, stroke, renal disease and peripheral arterial disease. It is the most important risk factor for cardiovascular morbility and mortality in industrialized countries. Appropriate treatment, and even prevention, of hypertension depends upon better understanding of the underlying causes and mechanisms of the elevated BP.

1.2 OVERVIEW OF THE CARIOVASCULAR SYSTEM

The function of the cardiovascular system (CS) is to transport and distribute essential substances to the body tissues and to remove metabolic products. The circulatory system also maintains the homeostasis in all the tissue of the body for optimal survival and function of the cells. Also, the CS contributes to regulation of body temperature and pH, participates in humoral communication and defense against infections and allows the adjustments of O_2 and nutrients as a function of tissue needs. The heart and circulation in turn are controlled to provide the necessary cardiac output and arterial pressure to maintain the adequate tissue blood flow (Levy & Pappano, 2007).

The CS has two main components: the heart and blood vessels. The heart consists of two pumps in series: the right ventricle to propel blood through the lungs for exchange of O_2 and CO_2 (**The pulmonary circulation**) and the left ventricle to propel blood to all other tissues of the body (**The systemic circulation**) (Figure 1.1). The blood vessels consist of a series of distributing tubes, and an extensive system of thin vessels that permit rapid exchange between the tissues and the vascular channels.

CARDIOVASCULAR SYSTEM

PA

RA

RV

Pulmonar circulation

Ao

LA

LV

Systemic circulation
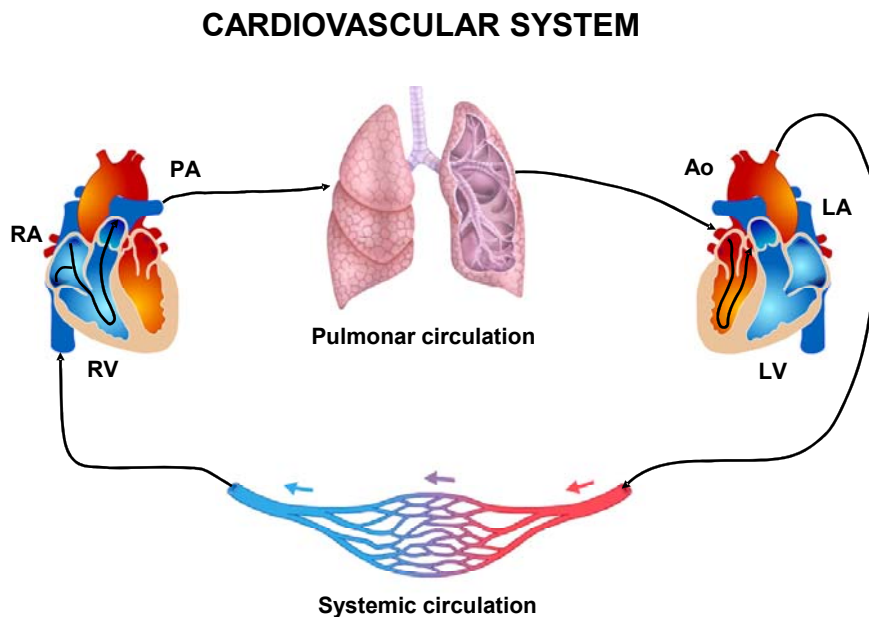
Figure 1.1. Overview of the cardiovascular system. The right side of the heart, pulmonary circulation, left side of the heart, and systemic circulation are arranged in series. RA, right atrium; RV, right ventricle; PA, pulmonary artery; Ao,aorta; LA, left atrium; LV, left ventricle (Klabunde, 2005).

The pulmonary circulation represents a "loop" through the lungs that is involved in the exchange of gases between the blood and alveoli. The systemic circulation is the circulation of the blood to all parts of the body except the lungs. The blood leaving the lungs enters the left atrium by way of the pulmonary veins. Blood then flows from the left atrium into the left

ventricle. The left ventricle ejects the blood into the aorta, which then distributes the blood to all the organs via the arterial system. The aorta gives raise to named conduit arteries. Theses branch repeatedly to form tiny arteries, which branch into even narrower vessels of high resistance, the arterioles. Arterioles branch into a vast number of fine, thin walled capillaries, which are the primary site of exchange. Blood flow from the capillaries enters venules, which form veins, returning blood flow to the right atrium via large systemic veins (Klabunde, 2005).

1.3 BLOOD VESSELS

Blood vessels of the cardiovascular system can be classified by size, function or cell composition.
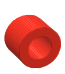
	Ascending aorta	Muscular artery	Arteriole	Capillary	Venule	Vein	Vena cava
Lumen Diameter	25mm	4mm	20 μm	5μm	20mm	5mm	30mm
Wall thickness	2mm	1mm	15μm	1μm	2μm	0.5mm	1.5mm

Figure 1.2. Cross sectional area of the different vascular bed (Aaronson & Ward, 2004).

Figure 1.2 represents different type of blood vessel, seen in cross section. Each blood vessel has different roles as detailed below:

a. **Arteries** (elastics and musculars): the function of the arteries is to transport blood under high pressure to the tissues. For this reason, the arteries have strong vascular walls, and the velocity of blood flow within them is elevated.

b. **Resistance vessels** (little arteries and arterioles): are the last small branches of the arterial system; they act as control conduits through which blood is released into the capillaries. The arteriole has a strong muscular wall that can induce large changes in the inner diameter of the vessel by contracting or relaxing, thus having the capability of vastly altering blood flow in each vascular bed in response to metabolic needs.

c. **Capillaries**: the function of the capillaries is to exchange fluid, nutrients, electrolytes, hormones, and other substances between the blood and the interstitial fluid. To serve this role, the capillary walls are very thin and have numerous minute capillary pores permeable to water and other small molecular substances.

    d. **Venules**: the venules collect blood from the capillaries, and they gradually coalesce into progressively larger veins.

    e. **Veins**: the veins function as conduits for transport of blood from the venules back to the heart; equally important, they serve as a major reservoir of extra blood. Because the pressure in the venous system is very low, the venous walls are thin. Even so, they are muscular enough to contract or expand and thereby act as a controllable reservoir for the extra blood, either a small or a large amount, depending on the needs of the circulation.

The main factor that drives blood along blood section is the pressure gradient (Figure 1.3). Ventricular ejection raises aortic pressure to ≈ 100 mm Hg. Also, because heart pumping is pulsatile, the arterial pressure alternates between a **systolic pressure** level of 120 mm Hg and a **diastolic pressure** level of 80 mm Hg. As the blood flows through the systemic circulation, its mean pressure falls progressively so that the pressure gradient dissipates completely at the entrance of the venae cavae into the right atrium of the heart (Levick J.R., 2003).
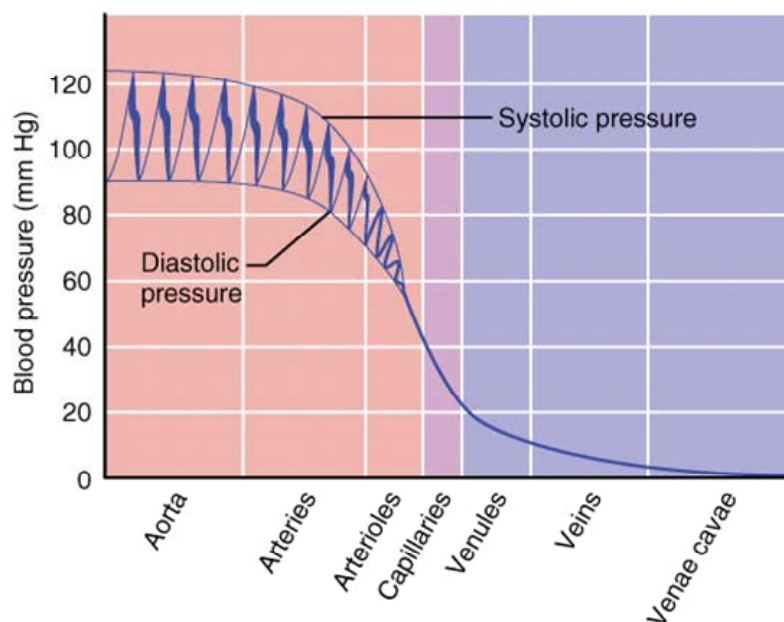
Figure 1.3. *Mean pressure in systemic curculation of human. The drop in mean pressure across the main arteries is only ≈ 2 mmHg. The large pressure drop across the terminal arteries and arterioles (diameter 20-400 µm) shows that they are the main resistance vessels. Adapeted from (Levick J.R., 2003)*

Changes in the diameter of blood vessels regulate arterial blood pressure, alter blood flow within organs, regulate capillary blood pressure, and distribute blood volume within the body. Changes in vascular diameters are brought about by activation of vascular smooth muscle cells (VSMCs) within the vascular wall by autonomic nerves, metabolic and biochemical signals from

outside of the blood vessel, vasoactive substances released by cells that line the blood vessels and intrinsic stretch-activated responses (Klabunde, 2005).

1.4 THE VASCULAR WALL

The wall of all blood vessels, both arteries and veins, consists of three layers: the tunica intima (innermost coat), tunica media (middle coat) and tunica adventitia (outer coat) (Figure 1.4).
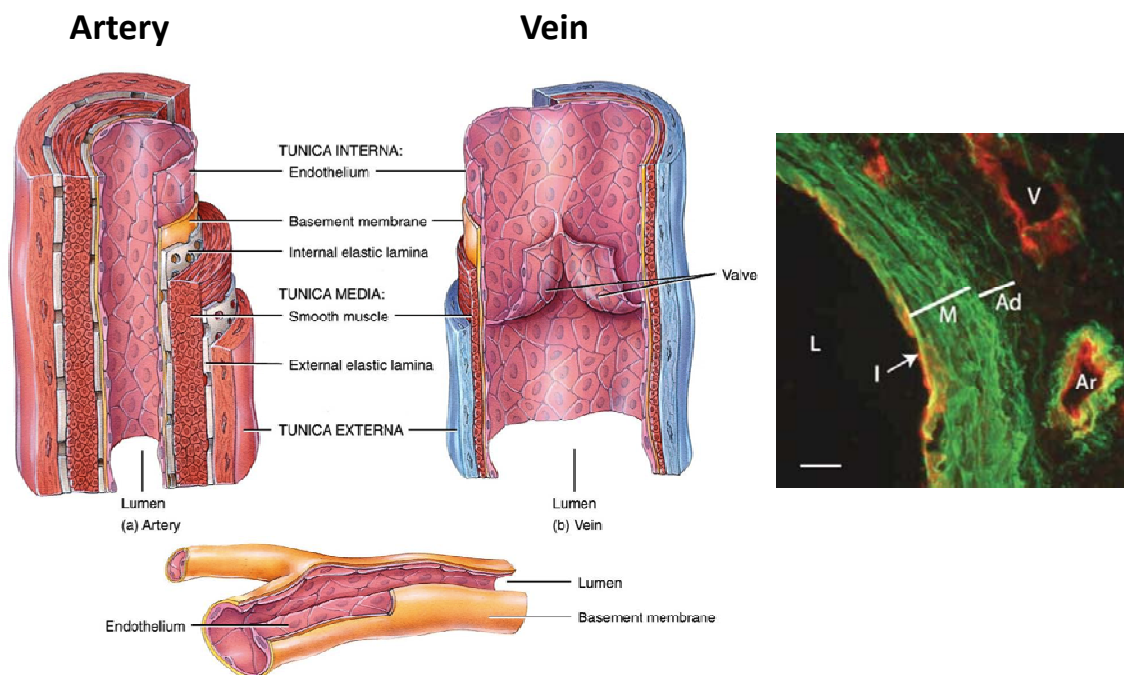
Figure 1.4. A. Structure of the wall of a small artery, vein and capilar. B. mmunofluorescence micrograph of mouse aorta. On the left is the lumen (L) of the artery. The intima (I) is evident as a single layer of red-staining endothelial cells. The media (M) contains dense layers of elastin, whereas the elastin in the adventitia (Ad) consists of fine fibers. The vein (V) on the top right shows the presence of endothelial cells but no elastin, whereas the small artery (Ar) directly below shows both. Scale bar = 100 µm (Wagenseil & Mecham, 2009).

1.4.2 The Tunica Intima

The **intima** is a sheet of flattened endothelial cells resting on a thin layer of connective tissue. Endothelial cells lining the vascular lumen of the vessel are sealed to each other by "tight junctions", restricting the diffusion of large molecules across the endothelium. The endothelial cells play a crucial role in controlling vascular permeability, vasoconstriction, angiogenesis (growth of new blood vessels) and hemostatic balance (Aird, 2007).

1.4.2 The Tunica Media

The **media** is separated from the intima by a fenestrated (perforated) sheath, the internal elastic lamina, mostly composed of elastin. The media contains smooth muscle cells (VSMCs) embedded in an extracellular matrix composed mainly of collagen, elastin and proteoglycans. This layer consists of spindle-shaped, smooth muscle cells, arranged helically, so that the vascular lumen narrows when they contract. Individual cells are long enough to wrap around small arterioles several times (McGrath *et al.*, 2005).

Adjacent VSMCs form gap junction. These are areas of close cellular contact in which arrays of large channels called connexons span both cell membranes, allowing ions to flow from one cell to another. The VSMCs therefore form a syncytium, in which depolarization spreads from each cell to its neighbors.

1.4.3 Tunica Adventitia

The **adventitia** is a connective tissue sheath with no distinct outer border. Its role is to tether the vessel loosely to the surrounding tissue. An external elastic lamina separates the tunica media from the adventitia. The adventitia of most vessels contains sympathetic nerve endings. Each terminal has numerous bead-like swellings ('varicosities') that release a vasoconstrictor agent, noradrenaline, which regulates local resistance and blood flow (Levick J.R., 2003). In large arteries and veins the adventitia also contains small blood vessels, called **vasa vasorum** (literally 'vessels of vessels'), which nourish the thick media (Aaronson & Ward, 2004).

1.5 VASCULAR SMOOTH MUSCLE

Vascular smooth muscle (VSM) is composed of cells (fibers) that are smaller than skeletal muscle fibers. VSM muscle can generally be divided into two major types, **multi-unit smooth muscle** and **unitary** (or single-unit) **smooth muscle** (Figure 1.5).

Multi-Unit Smooth Muscle. This type of smooth muscle is composed of discrete, separate smooth muscle fibers. Each fiber operates independently of the others and often is innervated by a single nerve ending, (as for skeletal muscle fibers). Some examples of multi-unit smooth muscle are the ciliary muscle of the eye, the iris muscle of the eye, and the piloerector muscles that cause erection of the hairs when stimulated by the sympathetic nervous system.

Unitary Smooth Muscle is a mass of hundreds to thousands of smooth muscle fibers that contract together as a single unit. The fibers usually are arranged in sheets or bundles, and their cell membranes are adherent to one another at multiple points so that force generated in

one muscle fiber can be transmitted to the next. In addition, the cell membranes are joined by many gap junctions through which ions can flow freely from one muscle cell to the next so that action potentials or ion fluxes without action potentials can travel from one fiber to the next and cause the muscle fibers to contract together. This type of smooth muscle is also known as **syncytial smooth muscle** because of its interconnections among fibers. It is also called **visceral smooth muscle** because it is found in the walls of most viscera of the body, including the gut, bile ducts, ureters, uterus, and many blood vessels.
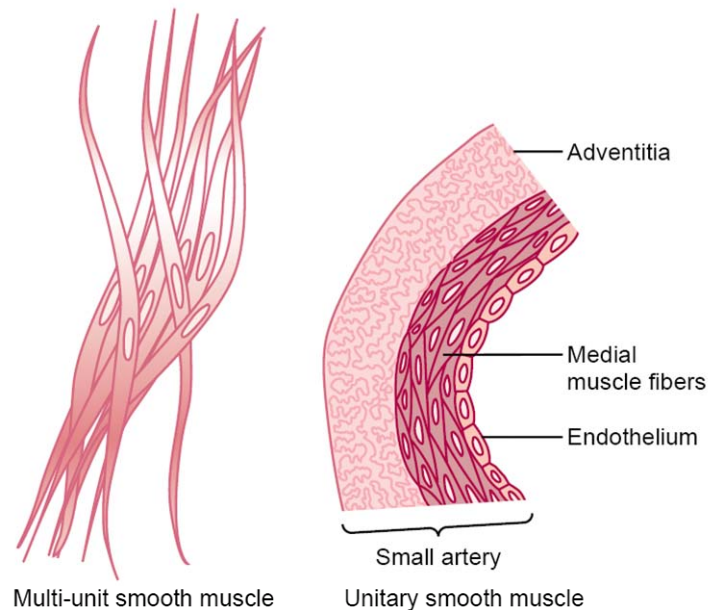
Figure 1 5. Multi-unit (A) and unitary (B) smooth muscle (Guyton, 2005).

1.6 VASCULAR SMOOTH MUSCLE CELLS STRUCTURE

Vascular smooth muscle cells (VSMCs), are located in the tunica media of arteries, arterioles, venules and veins, embedded in a matrix of collagen, elastin and various glycoproteins. The VSMCs are mononucleated and typically have a spindle or irregular elongate cylinder and its diameter decreases gradually in the end. These cells have a diameter between 5-10 µm and a length ranging between 50 and 200 µm (Figure 1.6)
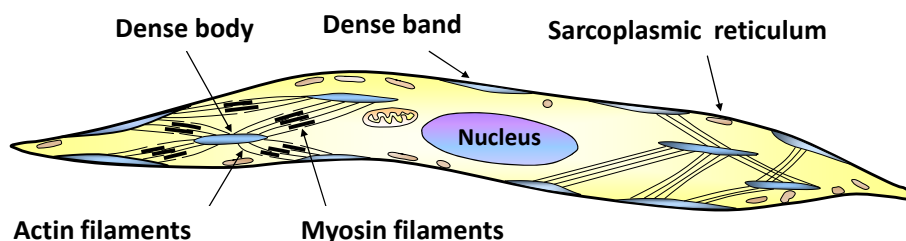
Figure 1.6. Smooth muscle cell ultrastructure. Modified from (Aaronson & Ward, 2004)

There are substantial differences in the way contraction is regulated in different blood vessels. At the level of the arteriole, where the media consists of a single layer of cells, smooth muscle cell organization is relatively simple. The small diameter of the arteriole and the length of a smooth muscle cell (≈100 μm) enable the cell to completely wrap the lumen. However, to ensure that the cell tips do not overlap, they are oriented slightly tilted with respect to the main axes of the vessel, therefore creating a partial helix. The next cell completes the helix and so on, giving a general helical or spiral appearance to the organization (McGrath *et al.*, 2005).

In resistance arteries, where there are multiple cell layers and a wider lumen, individual smooth muscle cells are set close to perpendicular (±10 deg) with the axis of flow. However, the smooth muscle cells are positioned in a diagonal offset pattern which creates the helical arrangement using groups of cells (Arribas *et al.*, 2007) (Figure 1.7).
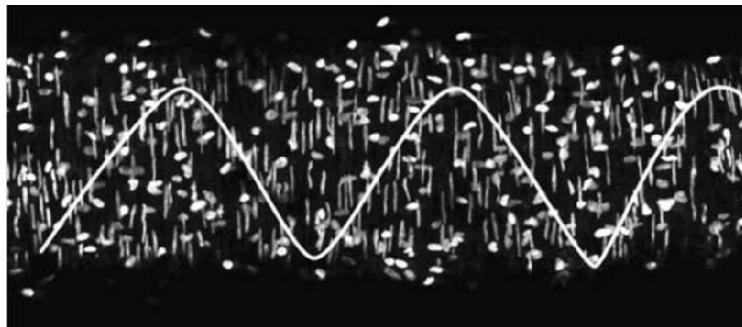
Figure 1.7. Nuclear stained mouse mesenteric artery. A live segment of artery was mounted on a perfusion myograph and maintained at 70 mmHg. All three cell types (nuclei) are visible. Smooth muscle cell nuclei run vertically. Adventitial nuclei are bright and roughly circular. Endothelial cell nuclei are fainter and are mostly associated with the position of the smooth muscle cells. White line represents a 'possible' path describing the helical nature of the cellular arrangement (McGrath et al., 2005).

In both cases the elongated shape of the VSMCs allows them to wrap helically around the vessel, so that changes in their contractility (tone) contract or dilate the vessel. This contraction is possible by a series of intracellular structures described below.

1.6.1 Caveolae

In the VSMCs membrane surface there are numerous small invaginations, called **caveolae,** which significantly increase the surface area of the cell by up to 75%. The cytoplasmic surface of each caveola has a striated coat of protein, caveolin-1, and the caveolar membrane is enriched in cholesterol and sphingomyelin. Caveolae are often in close proximity to the sarcoplasmic reticulum. There is evidence that caveolae are involved in the calcium transport and protein trafficking between the inner membrane and the cell surface (Levick J.R., 2003). Recent studies have suggested that caveolae play an important role in the smooth muscle

basic functions: contraction (Drab *et al.*, 2001), proliferation (Schwencke *et al.*, 2005) and celular metabolism (Raikar *et al.*, 2006). The exact function of caveolae is controversial, and more roles are continuously suggested. As several membrane proteins and signaling molecules (such as β-adrenergic receptors, G proteins, L-type Ca^{2+} channels (LTCCs), ATP-dependent potassium channels (K_{ATP} channels), adenyl cyclase and protein kinase C) have been found to locate preferentially in caveolae, it has been suggested that they could represent "signalosomes" where biochemical pathways are integrated. A recent study revealed that caveolae-associated LTCCs contribute to pro-hypertrophic signaling in cardiomyocytes (Makarewich *et al.*, 2012).

1.6.2 Sarcoplasmic reticulum

The smooth endoplasmic reticulum of VSM, or sarcoplasmic reticulum (SR), is the main releasable store of Ca^{2+} ions of the cell and can accumulate Ca^{2+} concentrations in the range of 10-100 μM (Gorlach *et al.*, 2006). Since the SR is relatively poorly developed, only 4% of the cell volume, the Ca^{2+} store is not very big, especially in small resistance vessels. Indeed, tonic vasoconstriction in resistance vessels requires not only store release but also extracellular Ca^{2+} influx.

The proximity between caveolae and SR suggest a rudimentary analog of the transverse tubule system of skeletal muscle. Therefore it has been proposed that membrane depolarization is transmitted into the caveolae and it can induce calcium release from the abutting sarcoplasmic tubules in the same way that action potentials in skeletal muscle transverse tubules cause release of calcium ions from the skeletal muscle longitudinal sarcoplasmic tubules.

Sarcoplasmic reticulum
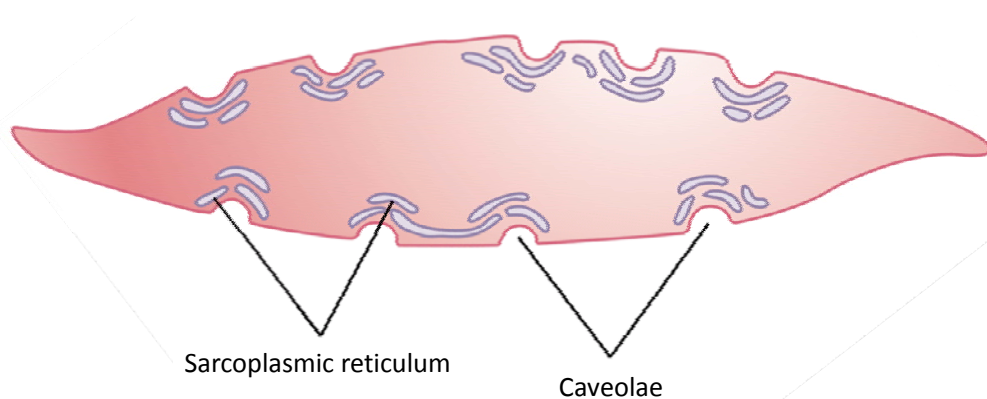
Caveolae

Figure 1.8. Sarcoplasmic tubules in a large smooth muscle fiber showing their relation to invaginations in the cell membrane called caveolae Guyton (2005).

Calcium can be released from the internal stores through two different pathways that have a different contribution to the physiological function of the VSMCs:

a. IP$_3$ Receptor

At some places within the cell, the cell membrane is in close proximity (around 15 nm) to the SR, which facilitates release of calcium from store by agonists, such as noradrenaline. The activation of the sarcolemmal agonist receptor triggers the formation of soluble factor, inositol triphosphate (IP$_3$), which quickly diffuses to the nearby SR, where IP$_3$ receptors are linked to Ca^{2+} release channels (IP$_3$-Ca^{2+} release channels). IP$_3$ thus releases the SR Ca^{2+} store. The subsequent global increase of cytosolic Ca^{2+} leads to increased vascular tone.

b. Ryanodine Receptor

The SR membrane also has a second type of Ca^{2+} release channel, the ryanodine receptor (RyR). At rest, ryanodine receptors spontaneously release brief bursts of Ca^{2+}, the so called Ca^{2+} sparks. These Ca^{2+} sparks will only raise the Ca^{2+} concentrations locally, in the subsarcolemmal region. This local signal activates nearby sarcolemmal Ca^{2+}-dependent K$^+$ channels (BKs), leading to hyperpolarization; so the RyR Ca^{2+} spark does not cause a direct contraction (Nelson *et al.*, 1995).
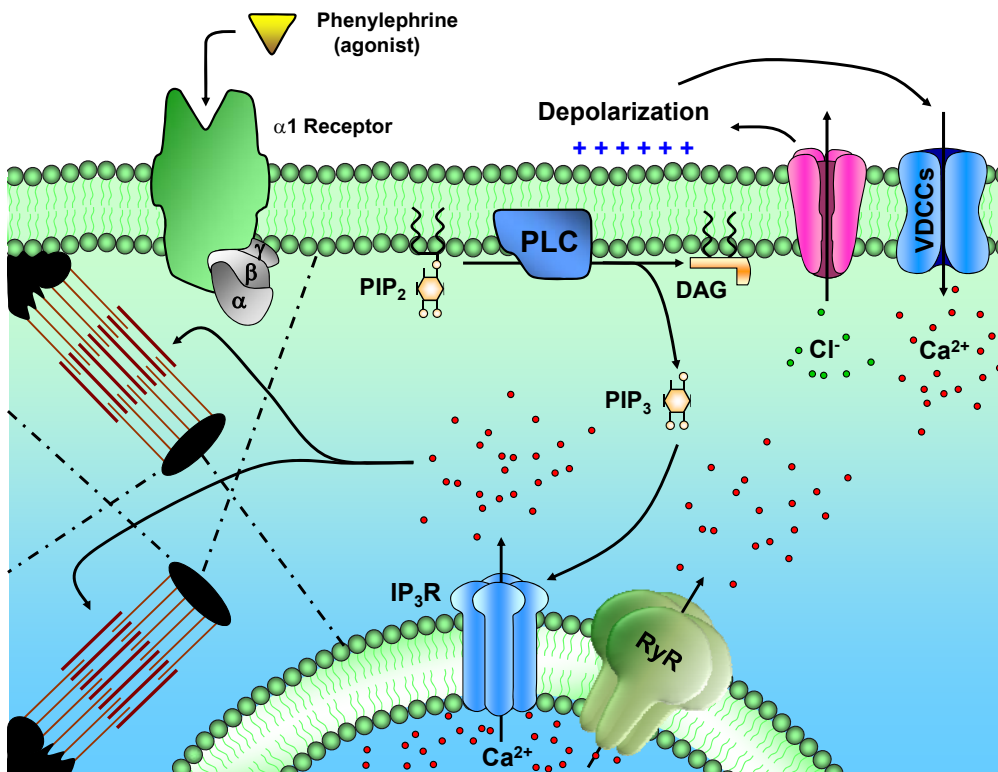
Figure 1.9. Phenylephrine binding to α_1 receptor activatin the G-protein G$_q$ and phospholipase C (PLC) to cleave phosphatidylinositol 4,5-bisphosphate (PIP$_2$) into inositol triphosphate (IP$_3$) and diacylglycerol (DAG). IP$_3$ causes intracellular Ca^{2+} release from the endoplasmic reticulum.

1.6.3 Contractile machinery

Contractile machinery of VSMCs is formed by two contractile proteins: actin and myosin. Monomers of these proteins polymerize into thin (actin) and thick filaments (myosin).

a. Actin thin filaments

The thin filaments that form part of the contractile machinery are predominantly composed of α- and γ-actin (Draeger *et al.*, 1990). In contrast, β-actin constitutes an important structural protein of the cytoskeleton just below the plasma membrane, playing an integral role in development of the mechanical tension generated during contracion (Gunst & Zhang, 2008). The actin filaments contain tropomyosin but lack of the Ca^{2+} sensitivity regulation protein, troponin, which is present in skeletal and striated muscle. Instead of troponin, smooth muscle cells have large amounts of another regulatory protein called calmodulin.

The vascular myocyte can shorten by a half or more, whereas striated muscle fibres shorten by only about one-third. The enhanced shortening of VSMCs is due to differences in the length of actin filaments and in the structure of myosin filaments. The ratio between myosin and actin filaments (number of filaments counted on transverse sections) in the smooth muscle is 10:1 (Gabella, 1984), and also differs with the skeletal muscle where the ratio is 2:1.

b. Myosin filaments

The myosin filaments bind to actin and possess ATPase enzyme activity. These filaments are mainly formed by myosin II-type (MII) (Eddinger & Meer, 2007). MII is a hexamer molecule composed of two heavy chains (MHC) and two pairs of myosin light chains (MLC). The MII hexamer consists of three differentiated regions. The **tail domain** is made up of the C-terminal ends of the MHCs, which are intertwined in an α-helical rod and form the major constituents of the thick myosin filaments. The **head domain** is composed of the globular N-terminal end of the MHCs that protrudes laterally from the filament. The head constitutes the "motor domain" that contains the actin-binding region as well as the ATP hydrolysis site that provides the energy required for force production. The intermediate **neck domain** is the region creating the angle between the head and tail. This hinge-like lever arm is the site of non-covalent binding of the MLCs—one from each pair binds to each MHC. The head and neck domains, along with the MLCs, that lean outward from the thick filaments are called cross-bridges to reflect their function as the parts of the myosin macromolecule that interact with the actin filaments during contractile activity. Myosin head organization in these filaments also differs with the skeletal muscle, because most of the myosin filaments have what are called "sidepolar" cross-

bridges arranged so that the bridges on one side hinge in one direction and those on the other side hinge in the opposite direction. This allows the myosin to pull an actin filament in one direction on one side while simultaneously pulling another actin filament in the opposite direction on the other side. This organization allows smooth muscle cells a better efficiency in the contraction (Craig & Woodhead, 2006).

c. Intermediate filaments

The VSM possesses other filaments that are not directly involved in the contraction, intermediate filaments. These filaments are composed of a large number of cytoskeletal proteins, although desmin and vimentin are the predominant constituents (Tang, 2008). Intermediate filaments form the structural network of the cytoskeleton and are largely responsible for the shape and spatio-temporal organization within the cell. Although there is no much information about the function of these filaments, they are believed to play important roles in signal transduction, contractile activity and other important processes (Taggart & Morgan, 2007;Tang, 2008).

d. Filaments organization

Smooth muscle does not have the same striated arrangement of actin and myosin filaments as is found in cardiac or skeletal muscle. The filaments are arranged in a more disorganized structure, but remaining a myosin filament surrounded by several actin filaments. The actin filaments are rooted in **dense bands** on the inner cell membrane and **dense bodies** in the cytoplasm, which function like Z-lines in cardiac myocytes. These structures are composed of α-actinin, the same protein as Z lines. The dense bodies are not aligned across the cell, but act to bridge thin filaments together along the contractile plane of the cell. Dense bodies serve as anchors from which the thin filaments can exert force to bring the polar cell membranes towards each other resulting in cell shortening. Interestingly, dense bodies also are associated with β-actin, which is the type found in the cytoskeleton, suggesting that dense bodies may integrate the functions of the contractile machinery and the cytoskeleton during contraction (Aguilar & Mitchell, 2010). In comparison, dense bands are associated with the plasmatic membrane (PM) and they are composed of a large number of proteins including α-actinin, vinculin and cytoskeletal actin. The actin filaments of the contractile machinery become tethered to the cytoskeleton by virtue of these dense bands, which thus play an important role in transmitting the forces from the contractile units toward the PM.

The structure of an individual contractile unit within a smooth muscle cell is composed of ≈10 actin filaments radiating from two dense bodies, the ends of these filaments overlap a myosin filament located midway between the dense bodies. This contractile unit is similar to the contractile unit of skeletal muscle.
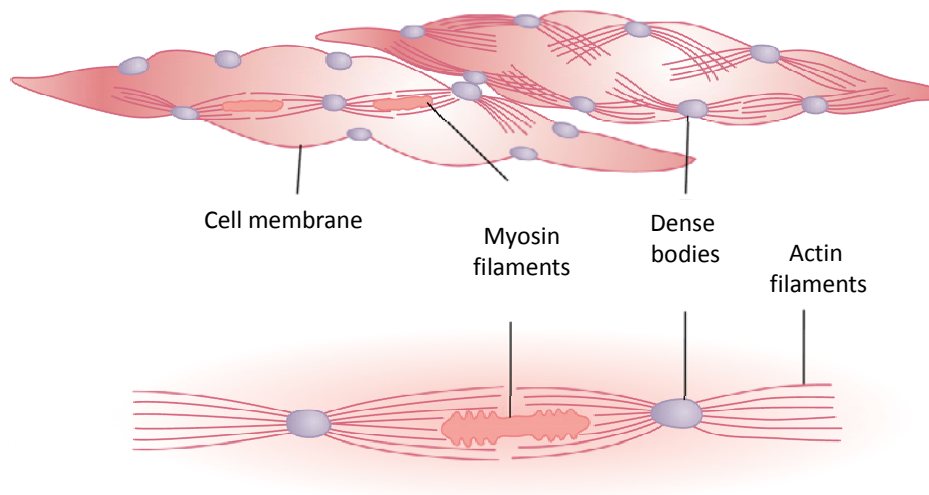
Figure 1.10. Physical structure of smooth muscle. The upper left-hand fiber shows actin filaments radiating from dense bodies. The lower lefthand fiber and the right-hand diagram demonstrate the relation of myosin filaments to actin filaments(Guyton 2005).

1.6.4 Gap-junctions

Similar to cardiac myocytes, vascular smooth muscle cells are electrically connected by gap junctions, also called nexus. The gap junctions is composed of six connexin molecules forming a hemi-tube (connexon), and the hemi-tubes of adjacent cells join end-to-end, connecting the cytoplasm of the two cells. These low-resistance intercellular connections allow propagating responses along the length of the blood vessels, however the spread is decremental and extends only about 3 mm along the vessel longitudinally (Christ *et al.*, 1996). That is why an electrical depolarization and contraction of a local site on an arteriole can result in depolarization at a distant site along the same vessel, indicating cell-to-cell propagation of the depolarizing currents (Christ *et al.*, 1996;Levick J.R., 2003).

The innermost myocytes of the tunica media also form gap junctions with the endothelial cells. Although its role has been a source of great controversy in the literature, these heterocellular or myoendothelial gap junctions transmit hyperpolarizing signals from the lining endothelium to the vascular myocytes (de Wit *et al.*, 2008)

1.7 VASCULAR SMOOTH MUSCLE FUNCTION AND REGULATION

1.7.1 Crossbridge cycle

VSMCs contraction depends on **crossbridge** formation between thick myosin filaments and thin actin filaments. This process promotes sliding of the actin filaments along the myosin filaments, shortening the cell and causing muscle contraction.
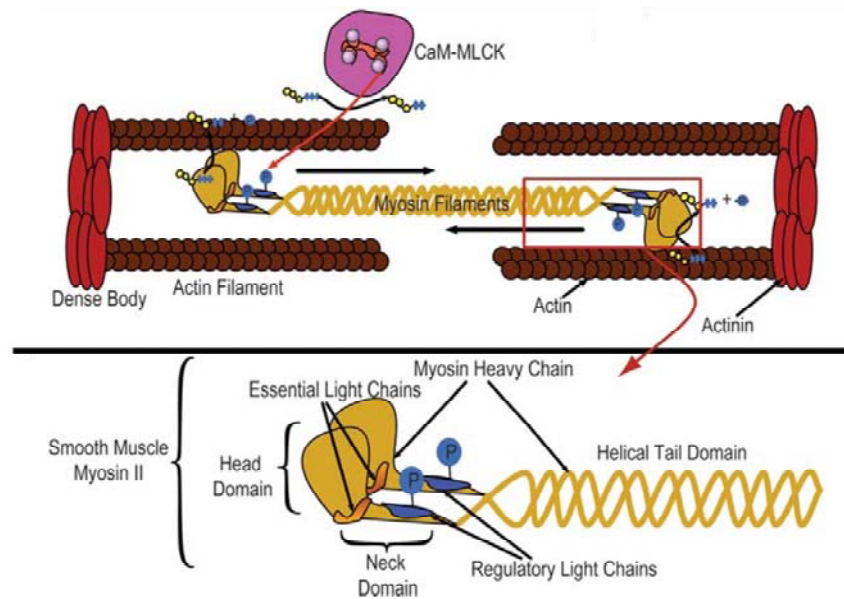
Figure 1.11. *The contractile elements are composed of myosin thick filaments and actin thin filaments anchored to dense bodies. The movement of thin filaments caused by phosphorylation of myosin light chains and subsequent ATP hydrolysis by the myosin II ATPase decreases the distance between anchor points. Myosin II is a hexamer composed of two heavy chains, two essential light chains and two regulatory light chains. Phosphorylation of the two regulatory light chains causes formation of a cross bridge between actin and myosin filaments and also creates a change in the angle of the neck region of myosin II, which causes motion of the actin thin filaments resulting in shortening of the cell (Aguilar & Mitchell, 2010).*

Vascular contraction depends primarily on global cytosolic Ca^{2+} ion concentration, which triggers myosin filaments activation. An increase in free intracellular calcium can result from either increased entry of calcium into the cell through L-type calcium channels (LTCCs) or release of calcium from internal stores (e.g., sarcoplasmic reticulum). The rise in cytosolic Ca^{2+} concentration causes the formation of the Ca^{2+}-calmodulin complex. Calmodulin is a cytoplasmic protein related to troponin C, that binds 4 Ca^{2+} ions (Johnson *et al.*, 1996). Ca^{2+}-calmodulin complex activates the enzyme myosin light chain kinase (MLCK). The light chain is a component of the myosin head involved in crossbridge formation with actin, and vascular myosin. When MLCK is activated, an immediate and marked increase in phosphorylation in the light chain is produced. This results in crosbridges formation and activation of the contractile

machinery (Somlyo & Somlyo, 2003). MLCK transfers a phosphate group from ATP to the myosin light chain, enabling the myosin head to form a crossbridge with actin, then the myosin head rotates to generate tension, as in striated muscle (Onishi *et al.*, 1983;Craig *et al.*, 1983)

Vascular relaxation occurs through myosin light chain phosphatase (MLCP), which turns off the myosin motor. When cytosolic Ca^{2+} concentration falls, MLCK activity declines. Meanwhile the MLCP increases its activity, removing the phosphate group of myosin light chain. This detaches preexisting crossbridges, and as new ones cannot form, the myocyte relaxes, leading to vasodilatation (Hartshorne *et al.*, 2004). Thus, the degree of contraction of smooth muscle degree is regulated by the balance between MLCK and MLCP.
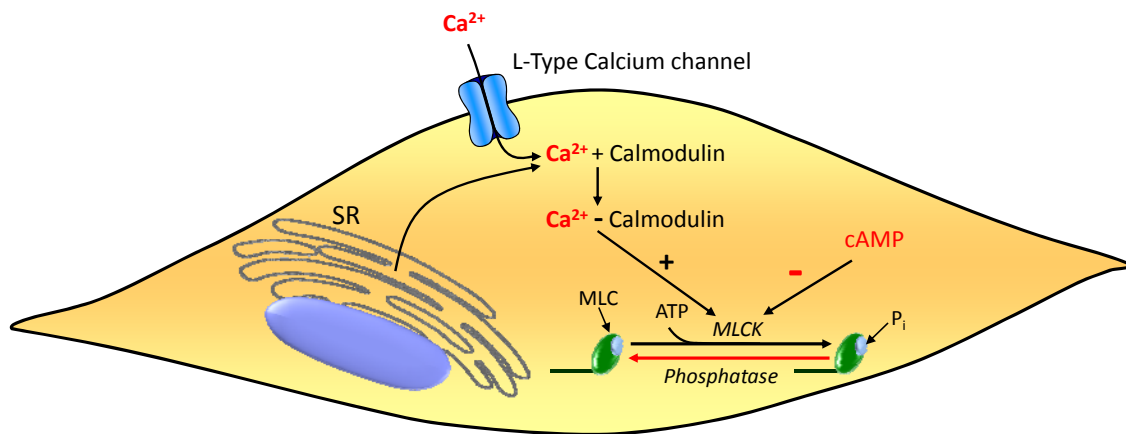
Figure 1.12. Regulation of vascular smooth muscle contraction by myosin light chain kinase (MLCK). Increased intracellular calcium, by either increased entry into the cell (through L-type Ca^{2+} channels) or release from the sarcoplasmic reticulum (SR), forms a complex with calmodulin, activating MLCK, which phosphorylates myosin light chains (MLC), causing contraction. Cyclic adenosine monophosphate (cAMP) inhibits MLCK, thereby causing relaxation. ATP, adenosine triphosphate; Pi, phosphate group(Klabunde, 2005).

One important characteristic of smooth muscle is that muscle tension can be maintained for a long period with little energy consumption by regulating the cross-bridge cycle velocity. This regulation is determined by the balance between myosin phosphorylation and dephosphorylation, which relies on Ca^{2+}-dependent activation process. Furthermore, the cross-bridge cycle in the VSM maintains contraction for longer periods of time than skeletal muscle, because the fraction of time that the cross-bridges remain attached to the actin filaments (the so called **latch-state**) is longer in smooth muscle. In this way, VSMC sustains the tension with a low ATP consumption rate. In adittion, there are Ca^{2+}-independent mechanisms that can modify contractile machinery-Ca^{2+} sensitivity by modulating the activity of the MLCP (Martinez-Lemus *et al.*, 2009;Murphy & Rembold, 2005).

1.7.2 Intracellular calcium homeostasis

The degree of contraction of VSMCs, that determines arterial tone, is tightly controlled by the concentration of free cytosolic calcium. In the VSM $[Ca^{2+}]_i$ is typically in the range 100-350 nM (Gorlach *et al.*, 2006) and these basal levels are mainly determined by 3 mechanism:

1. **Extracelular Ca^{2+} entry**. Extracellular Ca^{2+} enters the myocyte through Ca^{2+}-conducting channels in the sarcolema. These channels can be classified in two different groups:

    i. **Voltage-dependent calcium channels (VDCCs)** such as L- and T-type calcium channels (Nelson *et al.*, 1990;Sonkusare *et al.*, 2006b).

    ii. **Voltage independent calcium channels**. These latter include (1) receptor operated channels (ROCs), (2) capacitative or store-operated channels (SOCs) and (3) mechanosensitive or stretch-activated channels (SACs).

    Voltage-dependent Ca^{2+} channels (VDCCs) have a low but finite open-state probability under basal conditions, allowing a small extracellular Ca^{2+} influx. This design allows a tightly regulation of Ca^{2+} influx and therefore an excellent control of vascular basal tone, and blood pressure (Sonkusare *et al.*, 2006b). **Receptor operated channels (ROCs)** are regulated by agonist-receptor interaction independently of a previous change in membrane potential and in most cases, there is a transduction protein that mediates between receptor activation and channel opening (Bolton, 1979;Zhou *et al.*, 2006). **Store-operated channels (SOCs)** are activated by the emptying of intracellular Ca^{2+} stores (primarily the endoplasmic reticulum). Ca^{2+} store depletion activates Ca^{2+} entry from the extracellular space through plasma membrane channels to refill the store, as in a capacitor (Putney, Jr., 1986;Parekh & Penner, 1997;Sanders, 2001). Finally, **stretch-activated channels** are activated when tension or stretch is generated in the SMC plasma-membrane (Guharay & Sachs, 1984;Park *et al.*, 2003).

2. **Stored Ca^{2+} release**. Calcium is released from the sarcoplasmic reticulum (SR) through the IP3-dependent Ca^{2+} release channels, when the myocyte is stimulated by agonist such as noradrenaline (Berridge, 2008). Noradrenaline and adrenaline (via α_1-adrenoceptors), angiotensin II (via AT_1 receptors), endothelin-I (via ET_A receptors), and acetylcholine (via M_3 receptors) activate phospholipase C through the G_q-protein, causing the formation of soluble factor, inositol trisphosphate (IP_3) from PIP_2. IP_3 then quickly diffuses to the nearby SR, where IP_3 receptors are linked to Ca^{2+} release channels (IP_3-Ca^{2+} release channels). IP_3 thus directly stimulates the SR to release the Ca^{2+} store. The Ca^{2+} released often spreads into the cell as a Ca^{2+} wave. At the same

time, the SOCs are activated, increasing extracellular calcium influx (the capacitative calcium entry (Putney, Jr., 1986;Berridge, 1995)).
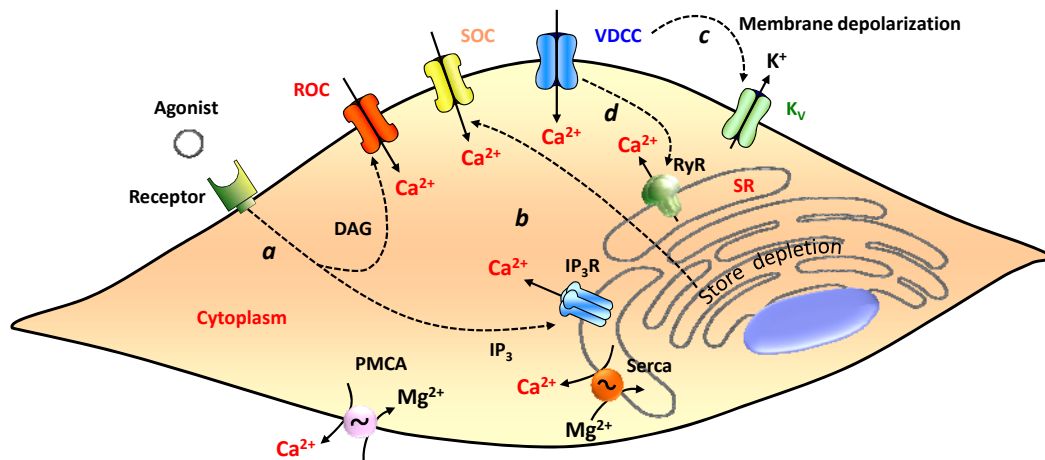
Figure 1.13*. Proposed mechanisms involved in the regulation of Ca^{2+} homeostasis in VSMC. a: DAG activates ROC-mediated Ca^{2+} influx and IP_3 activates IP_3R-mediated Ca^{2+} release. b: Depletion of Ca^{2+} from the SR activates SOC-mediated Ca^{2+} influx. c: Membrane depolarization leads to VDCC-mediated Ca^{2+} influx. d: A high level of local $[Ca^{2+}]_i$ is capable of triggering RyR-mediated Ca^{2+} release, a positive feedback mechanism known as Ca^{2+}- induced Ca^{2+} release (CICR). The low $[Ca^{2+}]_i$ under resting conditions is achieved and maintained mainly by active Ca^{2+} sequestration into the SR by the Ca^{2+}-ATPase (SERCA) and Ca^{2+} extrusion by the Ca^{2+}-ATPase in the plasma membrane (Landsberg & Yuan, 2004).*

3. **Ca^{2+}-ATPase pumps**. Cytoplasmic Ca^{2+} concentrations are tightly regulated by pumps (such as the sarcoplasmic–endoplasmic reticulum Ca^{2+} ATPase (SERCA) and plasma membrane Ca_{2+} ATPase (PMCA)) (Milner *et al.*, 1992). SR uptake from de cytoplasm by SERCA is called Ca^{2+} sequestration and the extracellular transfer by the PMCA is called Ca^{2+} expulsion. Na^+-Ca^{2+} exchanger also contributes to Ca^{2+} expulsion, although in VSMCs Ca^{2+}-ATPases predominate. At rest, there is a small but continuous influx of calcium through both VDCCs (because of their low open probability at resting membrane potential) and nonspecific cationic channels (TRPs), so that sarcolemmal Ca^{2+} pumps have to expel Ca^{2+} continuously, otherwise Ca^{2+} would accumulate in the cell.

1.7.3 Excitation contraction coupling in vascular smooth muscle

Vascular smooth muscle contraction can be initiated by electrical, chemical and mechanical stimuli (Davis & Hill, 1999). The processes involved in this contraction are called electromechanical coupling, pharmacomechanical coupling and mechanical coupling respectively.

a. Electromechanical coupling

Smooth muscle membrane potential (V_M) regulates muscle contractility by modulating Ca^{2+} influx through VDCCs. At rest, VSMCs potential is around -40 to -60 mV (Nelson & Quayle, 1995). In this range, calcium channels open probability increases exponentially, so that within a narrow range of membrane potential, influx of calcium through L-type calcium channels changes dramatically. VSMC depolarization increases the opening VDCCs leading to contraction, while hyperpolarization has the opposite effect.

The V_M is the net result of the activity of a number of active and passive ion transport mechanisms in the cell membrane. Among them, several types of potassium channels such as calcium-dependent potassium channels (BK_{Ca}), voltage-dependent potassium channels (Kv), inward rectifier potassium channels (K_{IR}), ATP-dependent potassium channels (K_{ATP}) and some ion-pumps (Na^+-K^+ ATPase) have been shown to modify membrane potential in VSMCs (see below).
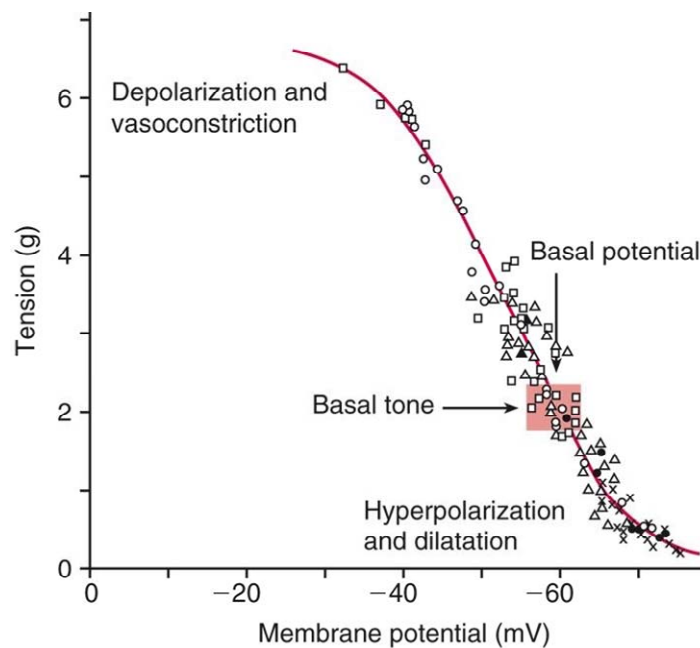
Figure 1.14. *Dependence of contractile tone on membrane potential in isolated artery. Membrane potential was altered by estracellular H^+ ($\triangle$), extracellular K^+ ($\square$), extracellular Ca^{2+} (●), noradrenaline (○) and oxigen tension (×). The highlighted box indicates membrane potential and tone in the "resting" basal state. (Siegel et al., 1991).*

b. Pharmacomechanical coupling

Binding of different agonist (circulating hormones, neurotransmitters, metabolites…) to its specific receptors on the cell membrane initiates a cascade of biochemical events leading to contraction or relaxation. The pathway from agonist to cellular response involves G protein-

coupled receptor activation and subsequent second messenger generation. Second messenger systems playing a major role in the contractile function of VSMCs are the **phosphatidylinositide** (described in section 1.7.2 part 2) and the **cAMP** pathways (Brown *et al.*, 1989). The latter involves adrenaline-dependent vasodilatation in those tissues where β_2-adreceptors are strongly expressed. The β_2-adrenoceptors is coupled to G protein, which activates membrane-bound adenylyl cyclase. The activation of adenylyl cyclase catalyzes the conversion of ATP into cyclic adenosine monophosphate (cAMP). cAMP activates the phosphorylating enzyme protein kinase A (PKA). PKA induces vascular relaxation by multiple actions: (1) phosphorylation of phospholamban, (2) phosphorylation of K_{IR}, K_{ATP} and K_{Ca} channels, which increases their open state probability or (3) inhibition of MLCK.
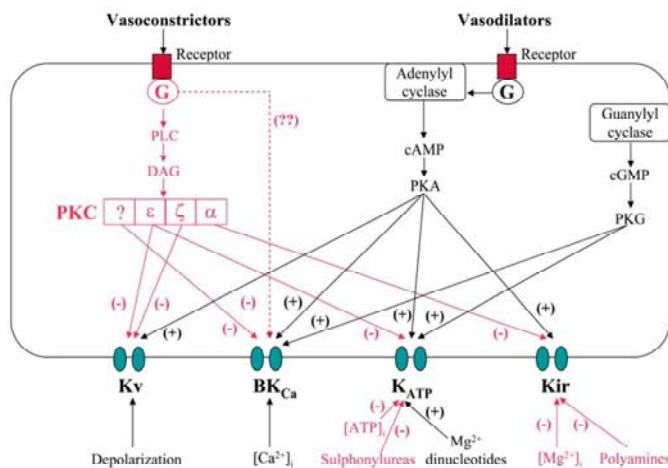
Figure 1.15. Pharmacomechanical coupling. Phosphatidylinositede and cAMP-PKA pathways modulating potassium channels and hence vascular response ina vascular smooth muscle cell. PLC, phospholipase C; DAG, diacylglycerol; PKC, protein kinase C; PKA, protein kinase A; PKG, protein kinase G(Ko et al., 2008).

c. Mechanichal coupling

A physical distortion of the cell or the cell membrane can activate second messenger systems and ion channels. Some TRP channels have been suggested to be activated by the tension of the vessel wall (Sharif-Naeini *et al.*, 2008), contributing to the contractile response of the vessel to stretch, the myogenic response.

1.8 VASCULAR TONE

The contractile activity of VSMCs in the walls of small arteries and arterioles is the major determinant of total peripherical resistance (TPR) in the vascular circulation. Vascular tone regulates the caliber of the vessel, and hence blood flow. According to Poiseuille's law (see Appendix 8.1) resistance is directly proportional to fluid viscosity η and tube lengh L and is

inversely proportional to tube radius raised to the fourth power, r⁴. Thus, small changes in the diameter of the vessels will lead to dramatic changes in resistance.

Blood vessels are normally in a state of partial contraction called **basal tone,** from which they can constrict further or dilate depending on the tissue demand for blood (Nelson & Quayle, 1995).
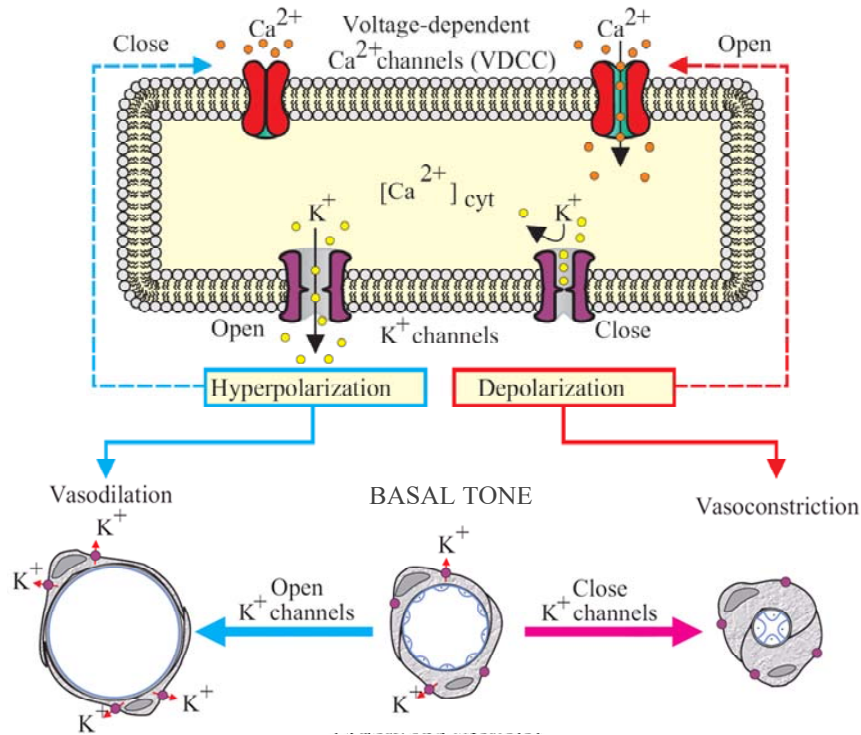
Figure 1.16. *Membrane potential and vascular tone. Inhibition of K⁺ channels causes membrane depolarization and leads to artery contraction. Modified from Jackson (Jackson, 2000).*

The average intracellular Ca^{2+} concentration in VSMCs in the wall of those vessels under basal tone is around 100-300 nM, several orders of magnitude lower than the extracellular fluid. Membrane potential, through activation of VDCCs, is a primary determinant of cytoplasmic Ca^{2+} and vascular tone (Knot & Nelson, 1998). Vascular tone plays an important role in the regulation of blood pressure and the distribution of blood flow between and within the tissues and organs of the body. Regulation of the contractile activity of vascular smooth muscle cells in the systemic circulation is dependent on a complex interplay of vasodilator and vasoconstrictor stimuli from circulating hormones, neurotransmitters, endothelium-derived factors, and blood pressure (Jackson, 2000). All of these signals are integrated by vascular muscle cells to determine the activity of the contractile apparatus of the muscle cells and hence the diameter and hydraulic resistance of a blood vessel.

1.8.1 Regulation of vascular tone

The processes that regulate vascular tone fall into two classes: intrinsic and extrinsic. Intrinsic regulation is regulation by factor located entirely within an organ or tissue. Extrinsic regulation is regulation by factors from outside the organ. Vascular regulation involves a hierarchy of control process, each of which can override and modify the lower one.
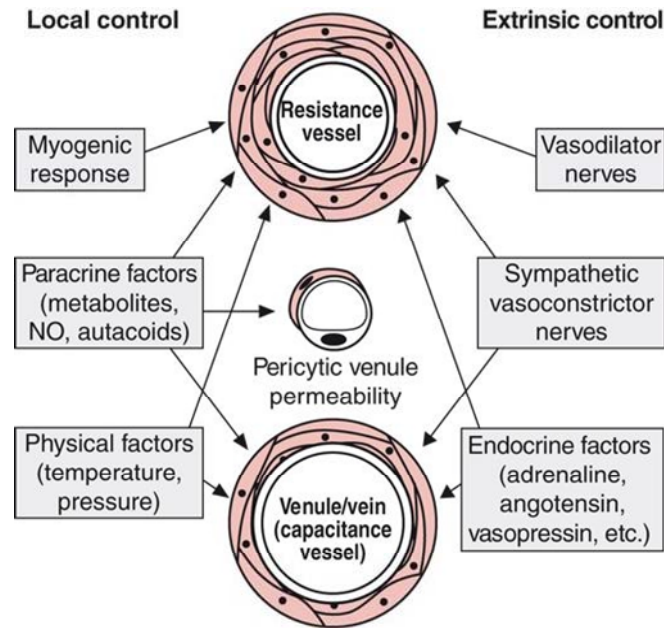
Figure 1.17. *Overview of vascular control. Vascular tone is determined by many different competing vasoconstrictor and vasodilator influences acting on the blood vessel. These influences can be separated into extrinsic factors that originate from outside of the organ or tissue in which the blood vessel is located, and intrinsic factors that originate from the vessel itself or the surrounding tissue (Levick J.R., 2003).*

a. Intrinsic mechanism

i The myogenic response

Myogenic response is a fundamental process for the development of resting vascular tone, converting mechanical force into an adaptive electrical and chemical biological response. The myogenic response was first described by Sir William Bayliss in 1906. When blood pressure is raised acutely in an artery or arteriole, the pressure at first distends the vessel. Within seconds, however, most systemic arterioles and arteries react and undergo a well-sustained contraction. This vital pressure-sensitive mechanism, called the **myogenic tone** (MT) or myogenic response, allows a constant blood flow despite changes in arterial pressure (Davis & Hill, 1999). Conversely, a fall in pressure triggers a fall in vascular tone and vasodilation. This pressure-dependent myogenic response is inherent to vascular smooth muscle and

independent of the endothelium or the nervous system. The myogenic response is important because a significant portion of the arterial tone is caused by transmural pressure and because it stabilizes tissue blood flow and capillary filtration pressure if arterial pressure changes (autoregulation).
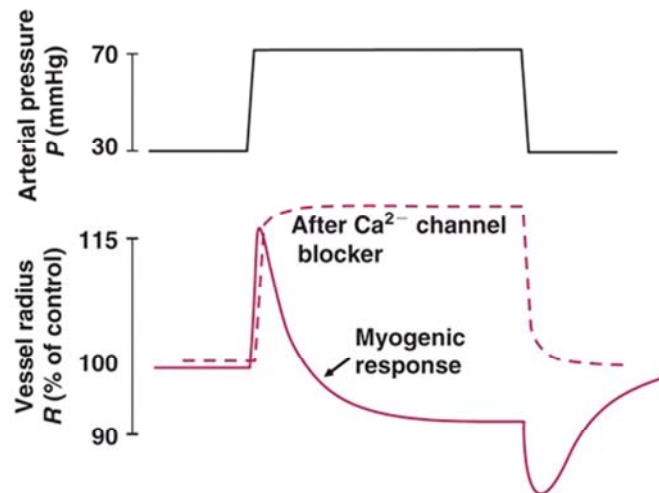
Figure 1.18*. Change in diameter of isolated cerebral artery upon raising luminal pressure P. Initial passive stretch is followed by active contraction-the bayliss myogenic response. This is abolished by L-type channel blockers (Levick J.R., 2003).*

The initial myogenic response is mediated by depolarization and Ca^{2+} concentration. When an arterial myocyte is stretched, it depolarizes to around -40mV. This activates L-type Ca^{2+} channels, leading to a rise in cytosolic free $[Ca^{2+}]$ and contraction. The depolarization is attributed to stretch-activated channels, namely TRP cation channels, volume-regulated chloride channels and ENaC-like channels (epithlelial Na^+ channels) because the myogenic response is impaired by these channels specific blockers.

The local (myocyte and endothelial) factors that maintain tonic arterial constriction, or 'tone', can be studied in isolated, cannulated small arteries. These arteries develop spontaneous MT when the lumen is pressurized. Indeed, the level of tone in isolated arteries is often comparable to that observed in the same vessels in vivo (Hill *et al.*, 2001), and may even be used to predict BP changes.

ii Endothelial secretions

Endothelium produces vasoconstrictor endothelin and the vasodilators nitric oxide (NO), endothelium-derived hyperpolarizing factor (EDHF) and prostacyclin (PGI_2). These are paracrine agents, acting locally on neighboring myocytes.

Nitric oxide (NO) is a freely diffusible gas with vasodilator properties. NO is generated from L-arginine by endothelial nitric oxide synthase (eNOS). eNOS activity is stimulated tonically by the shear stress exerted by flowing blood, and can be enhanced by agonist such as acetylcholine and inflammatory mediators.
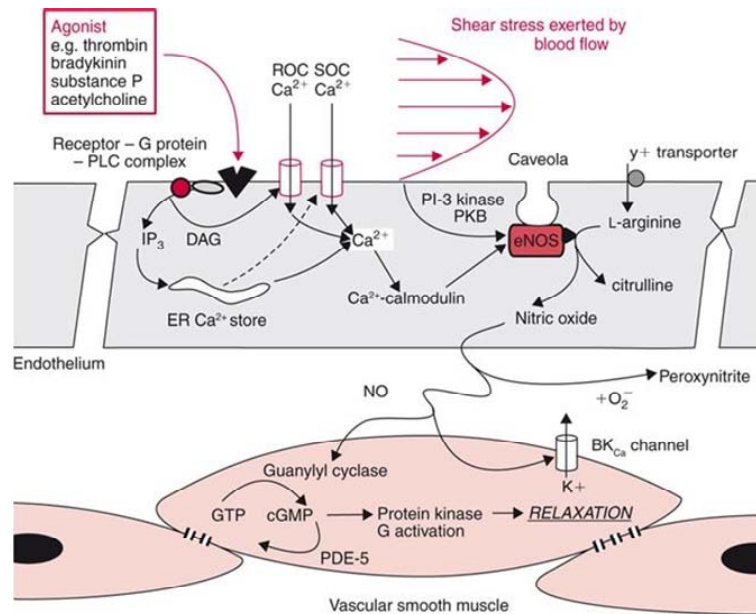
Figure 1.19. Regulation of NO production and its effect on neigbouring VSMC. eNOS endothelial nitric oxide synthase; ER endoplasmic reticulum; PDE-5 phosphodiesterase 5; PI3 kinase, phosphatidyl inositol-3 kinase (Levick J.R., 2003).

NO casuses vasodilation by two mechanisms: (1) NO diffuses rapidly into neighboring VSMCs, where it binds to the enzyme guanylyl cyclase. The activated guanylyl cyclase catalyzes the production of cyclic guanosine monophosphate (cGMP). The cGMP activates kinases such as protein kinase G (PKG) that promote vascular relaxation. (2) High concentrations of NO directly activate BK_{Ca} channels in the VSMCs membrane. This hyperpolarizes the smooth muscle, leading to vascular relaxation.

iii Metabolic vasoactive factors

The metabolic vasodilators act on the resistance vessels within the active tissue. Among the factors that increase in active tissues, and have a vasodilating effect, during metabolic hyperemia are: K^+ ions, H^+ ions (acidosis), hypoxia, adenosine, ATP, phosphate ions, hyperosmolarity and hydrogen peroxide.

iv Autacoids

Autoacoids are paracrine, vasoactive agents, which can be vasoconstrictor, such as serotonin (5-HT), E type prostoglandins (PGE), thromboxane, leukotrienes and platelet activiating factor (PAF) or vasodilators such as bradykinin and F type prostoglandins (PGF). Histamine is another autoacoid that can produce both effects depending on the type receptor present on the vessel on which it is released. Histamine H_1 receptors are coupled to Gq-PLC pathway, leading to vasoconstriction, however H_2 receptors are coupled to Gs-adenylyl cyclase-cAMP pathway, producing the relaxation of the vessel.

b. Extrinsic mechanism

i Vasomotor nerves

Sympathetic vasoconstrictor nerves constitute a fundamental system to control the total peripheral resistance and blood pressure. Most small arteries and resistance arteries are richly innervated, whereas arterioles are poorly innervated, being controlled chiefly by intrinsic mechanism. The terminal axon varicosities contain numerous dense-cored vesicles filled with noradrenaline. The released noradrenaline bind to the α-adrenorecptors on the vascular myocyte membrane, leading to vascular contraction.

Sympathetic vasoconstrictor fibres are tonically active contributing substantially to resting vascular tone, so a fall sympathetic vasomotor activity causes vasodilatation (Mohrman DE &
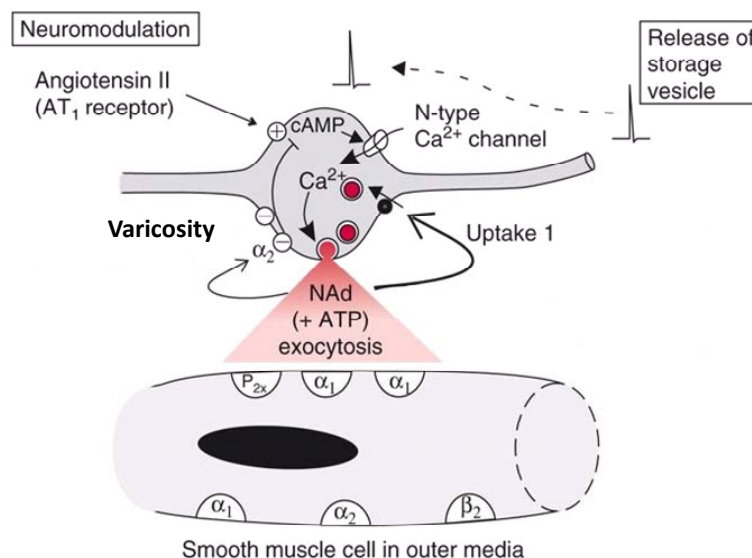
Figure 1.20. *Sympathetic neuromuscular transmission. Noradrenaline (NAd) binds to post-juntional α₁-receptors leading to vasocontriction. Pre-juntional α₂-receptors inhibir cAMP production to attenuate Ca²⁺ channel opening and vesicle release (Levick J.R., 2003).*

Heller LJ, 2003). On the other hand, parasympathetic terminals release the classic neurotransmitter acetylcholine, which elicits vasodilatation.

ii Vasoactive hormones

The main cardiovascular hormones that control VSMCs activity are: catecholamines (adrenaline and noradrenaline), angiotensin, vasopressin and atrial natriuretic peptide.

Adrenaline and noradrenaline can produce arterial and venus constriction in tissues with a predominace of vascular α-adrenoreceptors, such as skin and intestines or vasodilation in myocardium, skeletal muscle and liver due to their abundance of β_2-adrenoceptors. The β_2-adrenoceptors are coupled to the vasodilator G_s-adenylyl cyclise-cAMP pathway.

Angiotensin II is a vascocontrictor peptide whose productions increase through the renin-angiotensin-aldosterone system (RAAS), when blood pressure falls. Angiotensin II stimulates aldosterone secretion; and it causes vasoconstriction both directly and by enhancing sympathetic activity.

Vasopressin or antidiuretic hormone is a vasoconstrictor synthesized in the magnocelular neurons of the hypothalamus.

Atrial natriuretic peptide (ANP) is potent vasodilator secreted by the atria in response to distention.

1.9 VSMCs ION CHANNELS AND VASCULAR TONE

As seen above, regulation of the contractile state of VSMCs in the systemic circulation depends on multiple vasoactive stimuli including hormones, endothelial secretions, neurotransmitters, and blood pressure. All of these signals are integrated by VSMCs within the vessel wall to determine the degree of contraction and hence the diameter and hydraulic resistance of a blood vessel. Ion channels play a central role in this process. Briefly, when a potassium channel opens in the VSMC membrane, K^+ efflux increases, causing membrane potential (V_M) hyperpolarization, closure of VDCCs decreased Ca^{2+} entry, and vasodilatation. Conversely, closure of a K^+ channel causes V_M depolarization, opening of VDCCs, increased cytosolic Ca^{2+} concentration, and vasoconstriction (Sobey, 2001).

Therefore, contraction in the vascular smooth muscle is closely coupled to membrane potential with depolarization augmenting it and hyperpolarization inhibiting it (Haeusler, 1983a). Consequently, factors that modulate V_M have a direct effect on contraction and

vascular resistance (Nelson *et al.*, 1990). It should be noted that contractile function can also be modified by factors that have a direct effect at the contractile protein level, including the regulation of Ca^{2+} sensitivity of the contractile apparatus (Horowitz *et al.*, 1996). Membrane potential in most tonic smooth muscles including vascular is generally thought to be a K^+ and Cl^- channel equilibrium potential, with Ca^{2+} and nonselective cation channels possibly contributing to the total potential (Nelson et al., 1990). Because the VSMC plasma membrane has high input impedance and the resting membrane potential is close to the activation threshold for K^+ channels, it appears that K^+ channels play a major role in determining V_M. Consequently, K^+ channel activity is an important determinant of vascular tone and blood vessel diameter. At least four different types of K^+ channels have been identified in arterial SMCs. These include the inward rectifier (K_{IR}), voltage-dependent (K_V), ATP-dependent (K_{ATP}) and Ca^{2+}-dependent K^+ (BK_{Ca}) channels (Nelson & Quayle, 1995).

In addition VSMCs also express 2 types of voltage-dependent Ca^{2+} channels (Nelson *et al.*, 1990), 2 types of Cl^- channels (Large & Wang, 1996), store-operated Ca^{2+} channels (Gibson *et al.*, 1998) and stretch-activated cation channels (Davis *et al.*, 1992) in their plasma membranes, all of which may be involved in the regulation of vascular tone.

Expression of these channels varies among vessels and tissues, and consequently VSM shows very diverse electrical behaviour. The expression of the four types of K^+ channels has been reported to vary among vascular beds as well as with vessel size (Michelakis *et al.*, 1997). However, K_V and high-conductance Ca^{2+} gated K^+ (BK_{Ca}) channels are present in virtually all vascular myocytes and have been shown to strongly influence contractile responses (Nelson & Quayle, 1995).
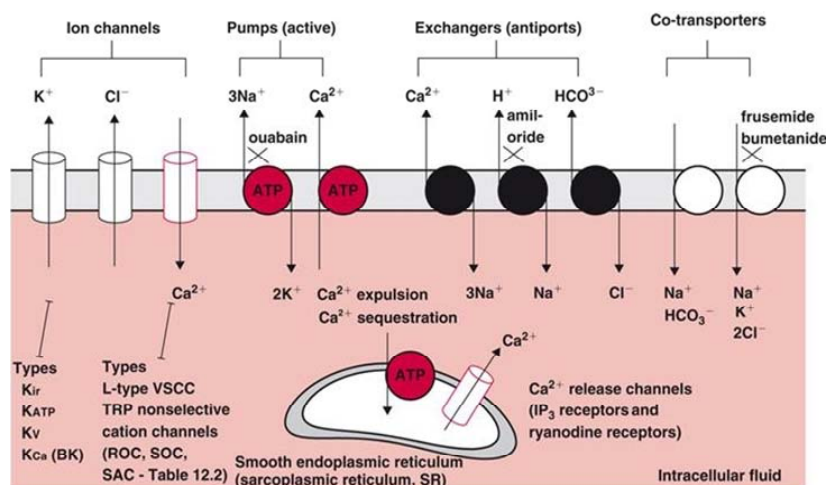
Figure 1.21. Ion channels, pumps, exchangers and co-trasnporters in sarcolema of VSMCs (Levick J.R., 2003).

1.9.1 Potassium channels

VSMCs have a higher intracellular K^+ concentration, generated by the sarcolemal Na^+-K^+ pump. A fraction of the sarcolemal K^+ channels is open at any moment, transmiting a small outward current of K^+ ions down the electrochemical gradient. K^+ channel status (open/closed) is important because it determines the negative membrane potential.

a. Inward-rectifier potassium channels

Inward-rectifier potassium channels (K_{IR}) are composed of two transmembrane helices (TM1 and TM2) and a short loop between them (referred to as the P-loop). This canonical architecture referred to as 2TM/P is essentially a universal feature of K^+ channels. P-loop region serves as the "ion-selectivity filter" (Hibino *et al.*, 2010) that shares with other K^+-selective ion channels. K_{IR} channel structures lack the S4 voltage sensor region that is conserved in voltage-gated Na^+, Ca^{2+}, and K^+ channels. As a result, K_{IR} channels are insensitive to membrane voltage and would be active at all V_M. Their defining characteristic, inward rectification, turns out not to be an intrinsic function of the channel protein but a result of the block of outward K^+ flux by intracellular substances such as Mg^{2+} and polyamines. These substances block the channel pore when V_M is more depolarized than potassium equilibrium
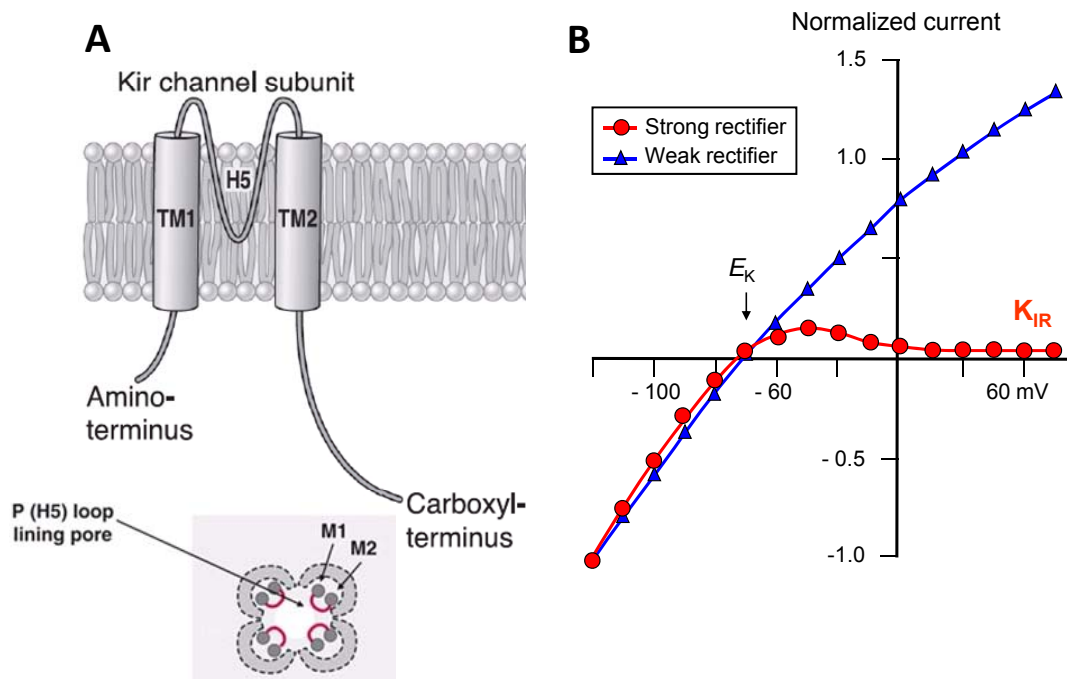
Figure 1.22. *A: Primary structure of the K_{IR} channel subunit. Each K_{IR} subunit contains two transmembrane (TM1 and TM2) regions, a pore-forming (H5) loop, and cytosolic NH_2 and COOH termini. Top view of tetrameric complex of a K_{IR} channel (bottom panel). B: Current–voltage curves of a strong and a weak inward rectifier (Hibino et al., 2010;Bichet et al., 2003).*

potential (E_K). The primary structure of two transmembrane strands is insufficient to form a complete ion channel, and functional K_{IR} channels are made up of four such subunits in a tetrameric complex (Yang *et al.*, 1995) (Figure 1.22A).

To date, 15 K_{IR} subunit genes have been identified (Kir1.x to Kir7.x) and classified into four functional groups: (1) classical K_{IR} channels (Kir2.x), (2) G protein-gated K_{IR} channels (Kir3.x), (3) ATP-sensitive K^+ channels (Kir6.x), and (4) K^+-transport channels (Kir1.x, Kir4.x, Kir5.x, and Kir7.x).

These ion channels pass inward K^+ current much more readily than outward current with physiological ion gradients and also show a parallel rightward shift in the potential at which rectification appears (activation potential) (Jackson, 2000). However, not all types of K_{IR} channels show the same degree of inward rectification. There are "strong" (Kir2.x and Kir3.x), "intermediate" (Kir4.x), and "weak" (Kir1.1 and Kir6.x) rectifiers (Hibino *et al.*, 2010) (Figure 1.22B). The channel serves as a sensor of external K^+ concentration, being the only K^+ channel whose open probability is increased by a rise in extracellular [K^+], in the range 5-15 nM (Knot *et al.*, 1996). The increased K^+ conductance shifts the membrane potential toward E_K, causing hyperpolarization and hence vasodilation. K_{IR} channels provide part of outward current for basal membrane potential. These channels are important in the vessels of tissues with high activity such as: exercising muscle, myocardium and brain, where increased metabolic activity raised the local intersticial [K^+]. The resulting vascular hyperpolarization and vasodilatation helps raise blood flow, to match demand (Nelson & Quayle, 1995). By contrast, a very high, non-physiological extracellular [K^+] will depolarized the myocyte, because it abolishes the K^+ gradient responsible for the membrane potential. The depolarization actives Ca^{2+} channels, leading to contraction.

Blockers most commonly used for K_{IR} channels are Ba^{2+} and Cs^+ (Ko *et al.*, 2008). Externally applied these cations suppress K_{IR} currents in a voltage-dependent manner. Ba^{2+} at micromolar concentrations is relatively specific to K_{IR} channels (Quayle *et al.*, 1993).

b. ATP-dependent potassium channels

The ATP-dependent K^+ channel (K_{ATP}) are functional hetero-octomers composed of four K_{IR} channel subunits (Kir 6.1 or Kir 6.2) forming the ion channel pore and four auxiliary proteins: the sulfonylurea receptors (SURx), that confers sensitivity to ATP (Hibino *et al.*, 2010) (Figure 1.23). SUR subunits are four ATP-binding cassette (ABC) family proteins containing 17 transmembrane regions grouped into 3 transmembrane domains (TM0-2) (Standen & Quayle,

1998;Teramoto, 2006). Each SUR unit has two nucleotide-binding domains between TM1 and TM2 and in the COOH terminus.

SUR1, SUR2A, and SUR2B represent pancreatic, cardiac, and vascular smooth muscle types of SUR, respectively, and different combinations of Kir6.1 and Kir6.2 and the SURx determine the properties of each native channel (Brayden, 2002). K_{ATP} channels in vascular smooth muscle most likely contain Kir6.X/SUR2B, as co-expression of SUR2B with Kir6.1 or Kir6.2 has been shown to produce channels with the properties of native K_{ATP} channels in smooth muscle (Standen & Quayle, 1998;Cui *et al.*, 2002).
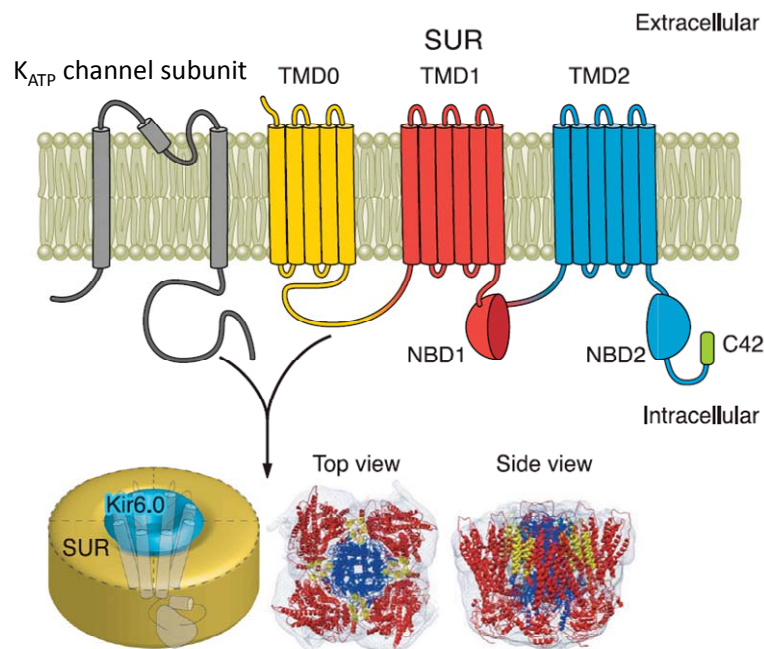
Figure 1.23*. Molecular constituents of K_{ATP} channels. K_{ATP} channels are composed of pore-forming Kir6.x subunits and SUR subunits. SUR subunits contain 17 transmembrane regions grouped into 3 transmembrane domains TMD0, -1, and -2 (top panel). Each SUR unit has two nucleotide-binding domains (NBD, depicted as hemispheres) between TMD1 and TMD2 (NBD1) and in the COOH terminus.A functional K_{ATP} channel is a heterooctamer made up of four Kir6.x subunits and four SUR subunits (bottom left). Bottom right images show top and side views of the entire K_{ATP} channel complex. Blue represents Kir6.x. Yellow represents TMD0 of SUR. Red represents the rest of SUR (Hibino et al., 2010).*

The K_{IR} subunits are responsible for ATP inhibition and the SUR proteins for nucleotide diphosphates (NDPs) activation. Thus, the channel open probability is increased by a fall in intracelular ATP (ischaemia) and by a rise in ADP, GDP, adenosine and [H^+] (hypoxia). Therefore, the K_{ATP} channel help links cellular metabolism with vascular tone through its effects on membrane potential (Standen & Quayle, 1998). In VSM a decrease in metabolic activity open K_{ATP} channels leading membrane hyperpolarization, decreased intracellular calcium concentration, vasorelaxation and increase O_2 delivery. In addition to metabolic sensitivity, the channels are opened under normal conditions, due to phosphorylation by

background levels of active PKA. Functional work has shown that K_{ATP} channels in arterial smooth muscle cells provide a background potassium conductance important in the regulation of membrane potential and so arterial tone and blood flow in a number of vascular beds.

A variety of pharmacological agents can either stimulate or inhibit K_{ATP} channels by binding to SUR. The inhibitory agents include sulfonylureas, such as chlorpropamide, tolbutamide, and glibenclamide (Wickenden, 2002). The stimulatory agents are known as K^+ channel openers and they include pinacidil, nicorandil, and diazoxide (Terzic *et al.*, 1995).

c. Voltage-dependent potassium channels

Voltage-dependent potassium channels (K_V) are heteromultimeric complexes being composed of membrane-integrated tetramer of $K_V\alpha$ subunits that form the ion conductive pore of the channels along with accessory $K_V\beta$ subunits (Pongs & Schwarz, 2010). To date, more than 30 genes encoding several subfamilies of K_V α-subunits are currently recognized (Ko *et al.*, 2008). Structurally, α-subunits contain six transmembrane domains (S1–S6) with an S4 voltage-sensing transmembrane domain (Korovkina & England, 2002), this structure is called 6TM/P. Each α-subunit can associated with ancillary β-subunits, which influences the characteristics of the channel (Bahring *et al.*, 2001).
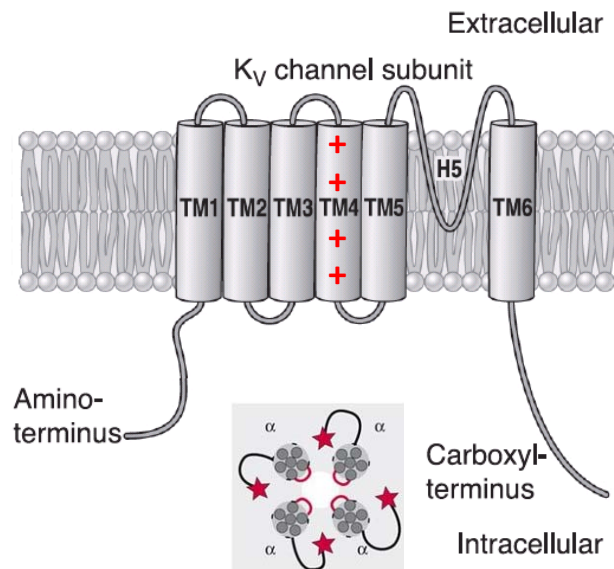
Figure 1.24. *Structure of voltage-gated K^+ (Kv) channel subuit, which possesses six transmembrane (TM1-TM6) regions. The positively charged, arginine-rich S4 loop is the voltage sensor. Bird's eve view of heterotetrameric Kv channel (bottom panel) (Hibino et al., 2010).*

K_V channels open to allow an efflux of K^+ in response to depolarization of the membrane potential, resulting in repolarization and a return to the resting membrane potential. In vitro studies have demonstrated that the activity of K_V channels contributes to resting membrane

potential and smooth muscle tone (Cheong *et al.*, 2001). These channels can be activated by the cAMP-protein kinase A signaling pathway (Aiello *et al.*, 1998) such that they may be involved in the mechanism of action of vasodilators such as adenosine, PGI2 and calcitonin-gene-related-peptide (CGRP). Decreased intracellular pH activates K_V channels in coronary myocytes (Berger *et al.*, 1998). As with K_{ATP} channels, vasoconstrictors tend to close K_V channels through signaling pathways involving protein kinase C (Aiello *et al.*, 1996) and Ca^{2+} (Cox & Petrou, 1999).

d. Calcium-dependent potassium channels

Based on their biophysical properties, calcium-dependent potassium channels K_{Ca} have been classified into three subtypes: one, exhibiting large unitary conductance and gated by the cooperative action of membrane depolarization and $[Ca^{2+}]_i$, is termed BK_{Ca}, a second one displaying small conductance and gated solely by $[Ca^{2+}]_i$, is referred to as SK_{Ca} and a third one showing intermediate conductance, called IK_{Ca} (Sah, 1996).

BK_{Ca} channels are comprised of a pore-forming α-subunit and a regulatory β-subunit (Tanaka *et al.*, 2004) α-Subunits contain six transmembrane spanning domains (S1–S6), including a voltage sensor (S4), which form the pore (Nelson & Quayle, 1995). However, the α-subunits contain an additional seventh transmembrane region (S0) at exoplasmic NH_2 terminus (Tanaka *et al.*, 2004). The large intracellular COOH terminus domain contains a binding site(s) for Ca^{2+}, whose occupancy provides one source of energy for channel opening (Schreiber & Salkoff,
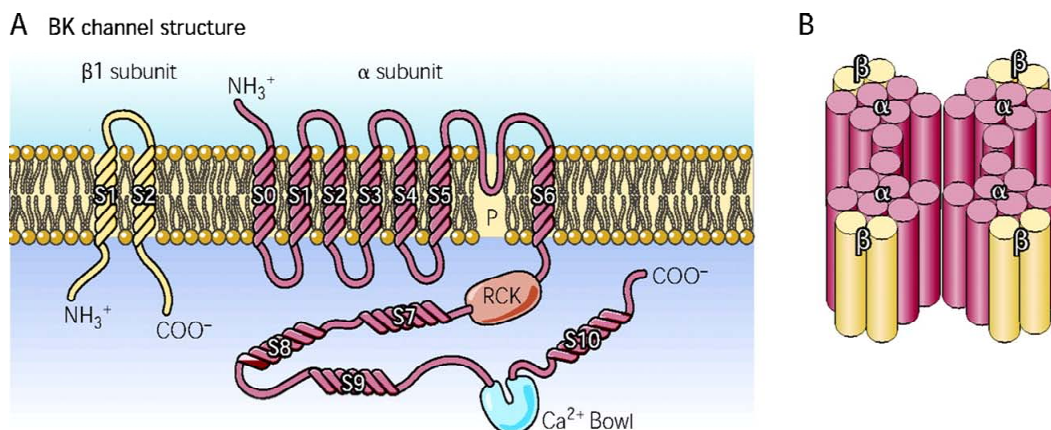
Figure 1.25*. Schematic diagrams of the BK and the SK channels. A: structure of the α and β₁-subunits of the BK channel. The β₁-subunit consists of 2 transmembrane domains and the α-subunit of 11 (S0–S10) hydrophobic domains, with S0–S6 located in the cytoplasmic membrane and the pore region (P) between S5 and S6. B:association of four α and four β₁-subunits forms the native BK channel (Ledoux et al., 2006).*

1997). In addition, there are four β-subunit isoforms (β1-4), each with two transmembrane domains. Of the four isoforms, β1 subunit is the predominant isoform in vascular smooth muscle (Ko *et al.*, 2008).

Large-conductance BK_{Ca} channels are found in most cells. In VSMCs BK_{Ca} channels have been implicated in the regulation of vascular tone (Meredith *et al.*, 2004). Under basal conditions the BK_{Ca} channels are activated intermittently by the spontaneous SR Ca^{2+} sparks (Ca^{2+} released from intracellular stores by RyR receptors), generating "spontaneous transient outward currents" (STOCs), that contribute to membrane potential. BK_{Ca} channels activation oppose vascular contraction, because, as Ca^{2+} enters the myocyte, BK activation makes the membrane potential more negative, which reduces the voltage-sensitive Ca^{2+} channel open probability.

BK_{Ca} channel may be blocked by external TEA, iberiotoxin, paxiline and charybdotoxin (Ko *et al.*, 2008).

1.9.2 Calcium channels

a. Voltage-dependent calcium channels

Voltage-dependent Ca^{2+} channels (VDCCs) play a central role in the regulation of vascular tone by membrane potential: hyperpolarization closes these channels and leads to vasodilatation, whereas depolarization opens them, which results in vasoconstriction (Nelson *et al.*, 1990).

VDCCs can be divided into two subgroups based on their activation threshold, low-voltage-activated (LVA) and high-voltage activated (HVA). LVA calcium channels activate at a membrane voltage positive to −70 mV. Because of the small amplitude of single channel conductance and its fast decay, these channels were also called **T-type calcium channels** (T for tiny and transient). HVA channels have an activation threshold at membrane voltages positive to −20 mV. Because of its large-single channel conductance amplitude and slow kinetics of current decay, it was named **L-type calcium channel** (LTCCs; L for large and long-lasting). A pharmacological hallmark of all L-type channels is their sensitivity to 1,4-dihydropyridines (DHPs)– a wide class of drugs with either inhibitory (nifedipine, nisoldipine, isradipine) or activatory (Bay K 8644) action on the channel. In addition, there are calcium channels, insensitive to DHPs and with single-channel conductances between those of T-type and L-type channels. These channels were named N-type calcium channels (N for neuronal and blocked by ω-conotoxin), P/Q-type calcium channel (P for Purkinje cells and blocked by agatoxin) and R-type calcium channel (R for resistant to both toxins) (Lacinova, 2005).

VDCCs are highly selective for divalent cations (Ca^{2+} and Ba^{2+}), and its open probability is increased by depolarization. Depolarization leads to a conformational change within the α_1 subunit that gates the channel and activates the Ca^{2+} current. As a result, vascular tension is graded function of membrane depolarization in many vessels. In VSM the predominant VDCCs are the L-type Ca^{2+} channels (LTCCs), specifically a splice variant of the $Ca_V1.2$ (Jackson, 2000) and are particularly important because influx of extracellular Ca^{2+} is essential for muscle contraction and generation of vascular tone. LTCCs are expressed more abundantly in arterioles and terminal arteries than in large arteries, so their contribution to myogenic reactivity and vasomotion increase in small resistence arteries (Davis & Hill, 1999).

i LTCCs structure

LTCCs are multi-subunit complexes, composed of a central pore-forming α_1 subunit and additional β, $\alpha_2\delta$ and γ subunits arranged in 1:1:1:1 stoichometry (Catterall & Curtis, 1987).

1. α_1 subunit

Structure: α_1 subunits are large proteins with molecular weight between 212 and 273 kDa. The structure of the α_1 subunit includes four repeat domains (I, II, III, IV) each composed of 6 transmembrane segments and a pore region between segments S5 a S6 (Catterall, 2000a).
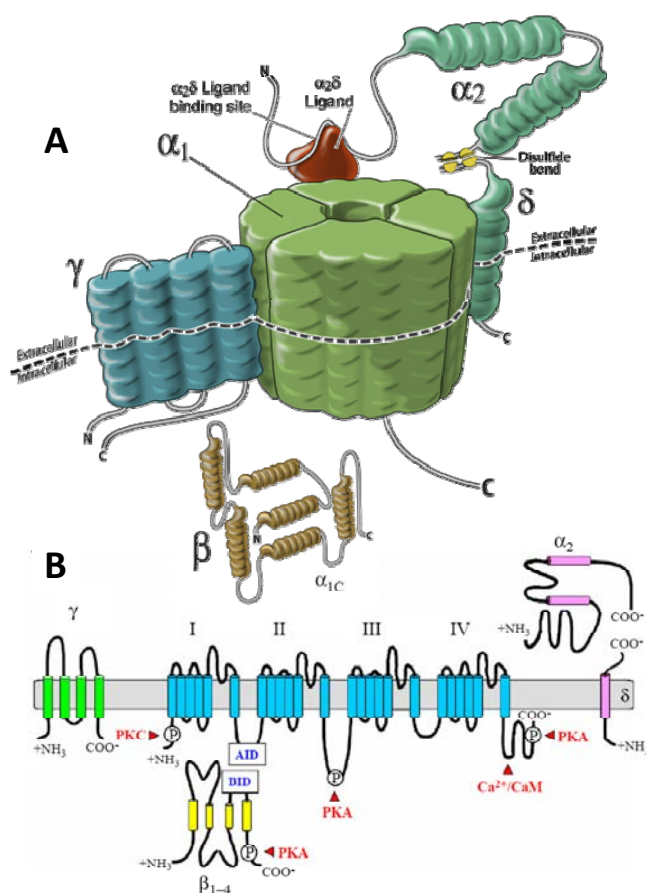
Figure 1.26. *A: Proposed schematic structure of VDCC. The principal α_1 subunit is a transmembrane protein containing a conducting pore, through which calcium ions can pass upon opening. α_1 subunit is further regulated by auxiliary subunits: intracellular β subunit, transmembrane γ subunit and a complex of extracellular α_2 subunit and transmembrane δ subunit, connected by a disulphide bridge. B: Proposed membrane topology of the LTCCs. The central α_1 subunit is a single large polypeptide of 4 repeat domains (I–IV). The intracellular linkers and N- and C-termini of the α_1 subunit interact with β subunits and intracellular signaling molecules. Abbreviations: AID, alpha interactive domain; BID, beta interactive domain; CaM, calmodulin; PKA, protein kinase A; PKC, protein kinase C (Doan, 2010).*

The length of α_1 subunit ranges approximately between 1870 and 2420 amino acids. S4 segments contain five to six positively charged arginins and lysines, so that these segments bear a net positive charge and can act as voltage sensors controlling VDCC gating. The pore region contains a putative selectivity filter, which ensures high selectivity of the channel pore for calcium ions. Furthermore, the α_1 subunit sequence contains sites of interaction with auxiliary subunits, binding sites for various activators and blockers, including G-proteins, as well as several putative phosphorylation sites. Some of these interaction sites are common, e.g., the site of the interaction with β subunit, while others are channel type specific, e.g., the binding sites for specific channel ligands (Lacinova, 2005). Modulation of channel behaviour by phosphorylation is enabled by intracellular binding domains for signalling molecules including protein kinase A (PKA) and protein kinase C (PKC).

Expression: Out of the ten α_1-subunits identified to date, $Ca_v1.2$ is the predominant isoform expressed in VSMCs. In addition, $Ca_v1.2$ is expressed in many tissues including heart, brain, lung, uterus, the gastrointestinal system, and vascular system (Koch *et al.*, 1990). Several alternatively spliced isoforms have been identified. One of these splices results in two different N termini of $Ca_v1.2$ (isoforms A and B). Isoform A (cardiac form) is specifically expressed in the heart, whereas isoform B (noncardiac form) is ubiquitously expressed in many cell types, including VSMCs (Pang *et al.*, 2003).

Function: the α_1 subunit confers most functional properties to the L-type Ca^{2+} channel, including voltage sensing, Ca^{2+} permeability, Ca^{2+}-dependent inactivation, and inhibition by Ca^{2+} channel blockers.

2. β subunit

Structure: the β subunit is the only entirely cytoplasmic Ca^{2+} channel subunit (Obermair *et al.*, 2008). Some forms, however, including β_{1b} and rat β_{2a} isoforms, can associate with the plasma membrane independent of the α_1 subunit (Arikkath & Campbell, 2003). β subunits are smaller proteins than α_1 with molecular weight between 57 and 69 kDa. β subunits have a general structure comprised at least four domains in the protein, namely a PDZ-like domain (PSD-95/disc large/zona occludens, this domain helps anchor transmembrane proteins to the cytoskeleton and hold together signaling complexes), an SH3 domain, a guanylate kinase-like domain and beta Interaction domain (BID). β subunits associate with the α_1 subunit through a highly conserved high affinity interaction that is mediated by the alpha interaction domain (AID) in the α_1 subunit and the BID in the β subunit (Arikkath & Campbell, 2003).

Expression: there are four known isoforms of the β subunits. The β_1 subunit is expressed in skeletal muscles. The β_2 gene is expressed abundantly in the heart and, to a lower degree, in aorta, trachea, lungs and brain, whereas the β_3 specific mRNA is detectable in the brain and a variety of smooth muscle tissues (Hullin *et al.*, 1992;Lacinova, 2005). However, the β_3 subunit is the main subtype in VSMCs (Murakami *et al.*, 2003b).

Function: The intracellular β subunits modulate the biophysical and physiological properties of the channel. The β subunits are believed to play a key role in trafficking of α subunits to the plasma membrane (Dolphin, 2009). Recent studies have proposed β subunits as an important target for modulation, both via PKA, PI3K/Akt pathway and CaMKII (Catalucci *et al.*, 2009).

3. $\alpha_2\delta$ subunit

Structure: The $\alpha_2\delta$ subunit ($\approx$ 120 kDa) is a heavily glycosylated protein that is post-translationally cleaved intro α_2 and δ peptides, which remain associated via disulfide bonds.

The δ part anchors the α_2 protein to membrane via a single transmembrane segment (Lacinova, 2005). Extracellular α_2 domain provides the structural elements required for channel stimulation (Gurnett *et al.*, 1996). The extracellular sequence of all $\alpha_2\delta$ subunits presents the von Willebrand factor type A (VWA) domain, which mediates binding to collagen and factor VIII, among other proteins. Recently, another domain called Cache has been identified in $\alpha_2\delta$ subunits, which contains methyl-sensing receptors. These domains might be relevant to the ability of the $\alpha_2\delta_{1-2}$ subunits to bind to gabapentinoid drugs (Davies *et al.*, 2007).

Expression: there are four $\alpha_2\delta$ subunits widely distributed in excitable tissues. The $\alpha_2\delta_1$ subunit is predominantly expressed in skeletal muscles, heart, brain (Lacinova, 2005) and vascular smooth muscle (Sonkusare *et al.*, 2006a;Bannister *et al.*, 2012). $\alpha_2\delta_2$ is importantly expressed in the heart, skeletal muscles, lungs, pancreas, testes, brain and smooth muscle (Hobom *et al.*, 2000;Sonkusare *et al.*, 2006a). The $\alpha2\delta_3$ subunit is mostly expressed in the brain (Klugbauer *et al.*, 1999). The $\alpha_2\delta_4$ gene has been detected in the heart and skeletal muscles and the protein has been noticed in the pituitary gland, adrenal gland, small intestines and foetal liver tissue (Qin *et al.*, 2002).

Function: The $\alpha_2\delta$ subunits both enhance calcium channel expression and also influence the properties of the channels, increasing channel gating and producing a hyperpolarizing shift in voltage activation (Klugbauer *et al.*, 2003;Davies *et al.*, 2007). Although the δ subunit is the portion of the protein that is anchored in the membrane, the extracellular α_2 subunit also interacts with the α_1 subunit (Sonkusare *et al.*, 2006b). The accessory subunit $\alpha_2\delta$ includes the

binding site for gabapentinoids such as gabapentin and pregabalin, two anti-epiletic-drugs that have lately also been used in the theraphy of neurophatic pain. The effect of gabapentin (GBP) on physiological activity of calcium channels is not clearly understood. GBP was found to bind specifically to $\alpha_2\delta_1$ and $\alpha_2\delta_2$ of VDCCs (Marais *et al.*, 2001c;Dolphin, 2009). The effects of gabapentin on native Ca^{2+} currents are controversial: some but not all authors report a small inhibition of Ca^{2+} currents, in different cell types, with a relatively slow onset of several minutes (Sutton *et al.*, 2002). In addition, because VDCCs are involved in the control of electrical excitability of neurons, it has been postulated that this drug reduces calcium current by modulating α_1 subunit of HVA channel indirectly through its association with $\alpha_2\delta_1$ (Gee *et al.*, 1996a).

4. γ subunit

Structure: The γ subunit is a highly glycosylated integral membrane protein, consisting of 222 amino acids with a predicted molecular mass of 25.1 kDa. The γ structure includes four putative transmembrane helices with intracellularly located N- and C-termini.

Expression: there are 8 genes for gamma subunits γ_{1-8}. The γ_1 subunit is typically expressed in skeletal muscles. The γ_2 subunit was identified in brain is expressed mostly in the cerebellum, olfactory bulb, cerebral cortex, thalamus, CA3, and dentate gyrus of the hippocampus (Letts *et al.*, 1998).

Function: γ has been associated with the skeletal muscle and neural voltage-gated channel complex. However the exact role of this protein γ_1 still remains unclear, and the function of the more recently cloned homologs, γ_{2-8}, specifically as calcium channel subunits now seems unlikely. Indeed, γ_{2-8} have been identified to have a major role in AMPA glutamate receptor trafficking (Dolphin, 2009).

1.9.3 Other channels

a. Transient receptor potential channels (TRPs)

The transient receptor potential (TRP) family of ion channels is a large family of cation selective ion channels, which are expressed and functional in a variety of tissues.

37
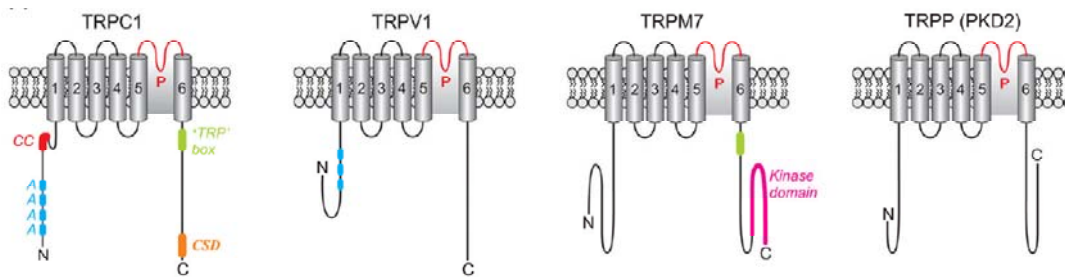
Figure 1.27. *Structure of TRP Channels. Representative topological structure of TRPC1, TRPV1, TRPM7, and TRPP (PKD2). Six transmembrane domains (TM1–TM6), ankyrin repeats or ankyrin-like domains (A), pore region (P), TRP box, caveolin-scaffolding (CSD) and coiled-coil (CC) domains are shown(Firth et al., 2007).*

The mammalian TRP channel comprises a ring of four TRP proteins, each with six transmembrane helices, similar to K_V. TRP subunits do not possess a voltage sensing moiety, making their activity insensitive to changes in membrane potential. TRP channels therefore function as voltage-independent, non-selective cation channels which are permeable to Na^+, K^+, Cs^+, Li^+, Ca^{2+}, and Mg^{2+} (Owsianik *et al.*, 2006) (Figure 1.27). TRP subunits are split into several subfamilies according to their activation stimuli and the presence of regulatory domains on the cytosolic N- and C-termini. **Canonical** TRP (TRPC) is activated by G protein-coupled receptors and receptor tyrosine kinases linked to phosphoinositide hydrolysis via phospholipase C (PLC) activation. A variety of chemical and physical stimuli including capsaicin, lipids, acid, heat, shear stress, and hypoosmolarity can activate **vanilloid** receptor related TRP (TRPV). **Melastatin** related TRP (TRPM) are either constitutively active or activated in response to increased $[Ca^{2+}]_i$, oxidative stress, or exposure to the cold (Pedersen *et al.*, 2005).

TRP channels in vascular smooth cells have been implicated in Ca^{2+} induced smooth muscle cell proliferation and migration, contraction, hypoxia sensing by pulmonary smooth muscle and stretch or mechanical sensing by vascular smooth muscle cells (Vennekens, 2011). Several TRPs have been implicated already in blood pressure regulation, but direct evidence for regulation of basal blood pressure by TRP channels is only available for three examples, TRPM4, TRPC1 and TRPC6 (Dietrich *et al.*, 2005;Mathar *et al.*, 2010).

b. Chloride channels

In mammals, the chloride channel family (ClC) consists of nine known members (Jentsch, 1996). The ClCs are α-helical membrane proteins, predicted to traverse the membrane 10-12 times. Both the N- and C-termini domains in mammalian are cytoplasmic and the C- terminal transmembrane helices are important for the function of the molecule (Mindell, 2008).

ClC display a variety of important physiological and cellular roles that include regulation of pH, volume homeostasis, organic solute transport, cell migration, cell proliferation and differentiation. In the VSMCs membrane chloride-conducting channels activated by cytosolic Ca^{2+} (Cl_{Ca}) are abundantly distributed and present a higher conductance than the corresponding conductances in skeletal and cardiac muscle cells. ClC in vascular cells contributes to (1) membrane depolarization, with the subsequent contraction being due to Ca^{2+} release from the intracellular store sites, and (2) Cl^- movements through the membrane of the Ca^{2+} store sites also regulate Ca^{2+} release and Ca^{2+} uptake from/into the store sites.

1.10   ION CHANNELS AND HYPERTENSION

Hypertension or high blood pressure is a multi-factorial disease, which arises because of complex interactions of various genes with the environment. Using Darcy´s Law (see appendix 2), blood pressure is determined by two important physical parameters, cardiac output (CO) and total peripheral resistance (TPR). Multiple pathways including the autonomic nervous system, renin–angiotensin system, aldosterone and other vasoactive substances affect CO and TPR to tightly regulate blood pressure and thus ensure appropriate flow of blood to various organs in the body (Blaustein, 1996). In most clinical cases, CO is normal whereas TPR is elevated due to an abnormal constriction of the small arteries and arterioles. The diameter of small arteries and arterioles is maintained mainly by the dynamic interplay of Ca^{2+} and K^+ channels expressed on the plasma membrane of VSMCs.

The elevated vascular tone observed in human hypertension and in several experimental models of hypertension thus points to abnormalities in the expression and function of Ca^{2+} and/or K^+ channels in VSMCs (Cox & Rusch, 2002). Indeed, the VSMCs are more depolarized as a consequence of the "ion channel remodelling" that occurs during chronic hypertension (Harder *et al.*, 1983).

1.10.1 Vascular ion channels remodelling during hypertension

Small arteries and arterioles undergo biological and structural adaptation in response to elevated intraluminal pressure that occurs during chronic hypertension. The underlying pathophysiological processes appear to be complex, and likely involve vascular remodeling, endothelial dysfunction, smooth muscle cell hypertrophy, and changes in extracellular matrix composition and function (Mehta & Griendling, 2007). The net effect of these adaptive changes is augmented vasoconstrictor responses and attenuated vasodilator responses to

various physiological stimuli, resulting in elevated vascular tone in the arteries and arterioles that are exposed to persistent high blood pressure (Heistad *et al.*, 1990).

The elevated vascular tone observed in the small arteries of cerebral, coronary and renal circulations during hypertension is thought to buffer the transmission of the high systemic pressure to the fragile capillaries of the brain, heart and kidneys (autoregulation), respectively, to prevent pressure-induced damages (Hayashi *et al.*, 1996). However, in the case of small arteries and arterioles of the mesenteric and skeletal muscle beds that contribute substantially to total peripheral resistance, elevated vascular tone during hypertension would further accentuate the increase in systemic blood pressure.

Similar to other components of the vasculature, during persistent high blood pressure, ion channels in the plasma membrane of VSMCs also undergo "electrical remodelling" such that the arteries maintain a heightened vascular tone. In this electrical remodelling, VSMC membranes exposed to high blood pressure exhibited increased transmembrane Ca^{2+} and K^{+} flux in arteries from different experimental models of hypertension. Actually, changes contributing to sustain the higher levels of Ca^{2+} influx required for persistent arterial contraction coexist with adaptive responses aimed to compensate for the pro-hypertensive changes. To date, two fundamental events have been implicated in this process: VSMC membrane depolarization increasing the open probability of VDCCs (Harder et al. 1985; Cox & Rusch, 2002), and up regulation of the expression of the principal subunit (α_{1C} subunit) of VDCCs, determining the increase in the number of functional VDCCs in VSMCs (Pesic et al. 2004).

1.10.2 Effect of hypertension on V_M

The final common pathway for the control of vascular reactivity, and ultimately peripheral vascular resistance, is located at the level of membrane and intracellular processes of the vascular smooth muscle cell (Pinterova *et al.*, 2011). Since changes of few millivolts in membrane potential cause significant changes in blood vessel diameter (Nelson & Quayle, 1995), knowledge of the membrane processes responsible for vascular smooth muscle cell activation seems to be crucial for understanding of the complete scope of blood pressure regulation. Indeed, the relevance of the VSMC membrane potential in hypertension was indicated by the proportionality between the magnitude of membrane potential and vascular smooth muscle contractile force (Harder *et al.*, 1985).

The resting V_M of VSMCs is reported to be more depolarized in arteries from hypertensive versus normotensive animals (Cheung, 1984;Harder *et al.*, 1983). Increased vascular depolarization is associated with enhanced myogenic tone in arteries from hypertensive animals (Harder *et al.*, 1985). The effect of hypertension on V_M may be more profound in smaller resistance vessels, especially in vascular beds that play a significant role in the regulation of peripheral resistance (Martens & Gelband, 1996).

1.10.3 Effect of hypertension on potassium channels

Since the pioneering studies reporting an abnormally low permeability of the plasma membrane to K^+ ions in VSMCs from hypertensive animals (Harder *et al.*, 1983), a loss of resting K^+ efflux resulting in membrane depolarization is a common finding in VSMCs from many vascular beds under high blood pressure (Sonkusare *et al.*, 2006b). Molecular biology studies reveal a large diversity of K^+ channel subtypes expressed in normal conditions in VSMCs, but there is little information available at the molecular level regarding regulation of the expression and function of K^+ channels in essential hypertension. Moreover, the available data regarding the functional contribution of these channels to the hypertensive phenotype show clear discrepancies. Different changes in the functional expression of both BK_{Ca} and several Kv channels have been described in hypertensive models. In fact, there are contradictory reports even in the direction of the changes. In the case of BK_{Ca} channels, larger currents with increased Ca^{2+} sensitivity have been found in arteries from hypertensive rats (reviewed by (Cox & Rusch, 2002;Sobey, 2001), while decreased currents with lower Ca^{2+} sensitivity have been reported in other studies (Amberg *et al.*, 2003;Moreno-Dominguez *et al.*, 2009). Regarding Kv channels, changes in the expression of Kv1.x channels (up and down regulations, (Cox & Rusch, 2002), decreased functional expression of Kv2 channels (Moreno-Dominguez *et al.*, 2009) and downregulation of Kv7.4 channels (Jepps *et al.*, 2011) are among the changes associated with essential hypertension. In addition to species differences, vascular-bed-specific differences and/or differences in the experimental models, several explanations can account for these discrepancies. First, our knowledge of the signalling pathways that regulate K^+ channel expression and function in VSMCs is incomplete. Second, altered vascular K^+ channel function during hypertension could be either a cause related to the pathogenesis of the disease or a compensatory mechanism directed to limit the progression of the disease.

Using hypertensive and normotensive mice strains (BPH and BPN mice, for blood pressure high and normal, respectively) obtained by phenotypic selection after crossbreeding of eight

different strains (Schlager & Sides, 1997) we have previously determined the functional expression of Kv channels and their contribution to VSMC excitability. Our results showed that in VSMCs from mesenteric arteries of BPH mice there is a remodelling of Kv2 currents leading to a decreased Kv current amplitude that contributes to the hypertensive phenotype in resistance arteries (Moreno-Dominguez *et al.*, 2009). However, while VSMCs from BPH mice were significantly more depolarized than BPN VSMCs, we found no clear differences in the contribution of Kv channels (or BK_{Ca} channels) to setting resting V_M between BPN and BPH cells. This observation implies that in addition to the decrease in both BK_{Ca} and Kv currents (Moreno-Dominguez *et al.*, 2009), there must be changes in other non-Kv conductances in the BPH mesenteric VSMCs responsible for the more depolarized resting V_M. Inward rectifier K^+ channels (K_{IR} and K_{ATP} channels) are more active at negative membrane potentials and therefore represent good candidates for regulating the VSMC membrane potential in arteries in the absence of extrinsic depolarizing influences such as pressure or vasoconstrictors. The expression and the functional role of K_{IR} and K_{ATP} channels in VSMCs have been extensively characterized in many VSMC preparations (reviewed by (Quayle *et al.*, 1997;Sobey, 2001;Ko *et al.*, 2008;Hibino *et al.*, 2010)).

a. K_{IR} channels in hypertension

K_{IR} channels have been identified in small, resistance arteries (Smith *et al.*, 2008), and their activity is a function of both membrane potential and extracellular K^+ concentration (Nelson & Quayle, 1995). Kir2.1 gene expression in VSMCs is required for K_{IR} currents and K^+-induced dilations in cerebral arteries (Zaritsky *et al.*, 2000). However, neither the changes in the expression nor their contribution to pathologies such as systemic hypertension has been explored. Although there is indirect evidence suggesting that this function of K_{IR} channels is impaired in cerebral arteries of hypertensive animals (McCarron & Halpern, 1990) there are contradictory reports (reviewed by (Sobey, 2001)).

b. K_{ATP} channels in hypertension

K_{ATP} channels are expressed in VSMCs from both small and large vessels, and their activity has been proposed to represent the functional link between cellular metabolism and membrane excitability. In addition, the channels are opened by vasodilators and closed by many vasoconstrictors, a modulation that is relevant for their physiological role. K_{ATP} provides a background K^+ conductance important for the regulation of V_M, and hence arterial tone and blood flow (Quayle *et al.*, 1997;Hibino *et al.*, 2010). However, K_{ATP} channel contribution to

resting tone varies among vascular beds. In some cases (e.g. coronary, mesenteric and renal arteries), there is strong support for the channel contribution to the regulation of the V_M of VSMCs, even in normoxia and in the absence of vasodilators. In contrast, K_{ATP} channel blockers such as glibenclamide generally do not affect vascular resistance, tone or membrane potential in cerebral arteries, although K_{ATP} channels are functional in these vessels (Quayle *et al.*, 1997;Sobey, 2001). If K_{ATP} channels are inactive at basal conditions, increased vascular tone during chronic hypertension is unlikely to be related to impaired channel function (Kitazono *et al.*, 1993). However, other studies suggest that K_{ATP} channels in hypertensive arteries are dysfunctional but can recover upon long-term treatment of high blood pressure (Ohya *et al.*, 1996). Characterization of vascular function in transgenic mice with selective knockout of the two molecular constituents of K_{ATP} channels in VSMCs, namely SUR2B and Kir6.1, did not provide consistent results. Both transgenic models displayed sudden death from coronary artery vasospasm, highlighting the importance of K_{ATP} channels in the tonic regulation of vasomotion in coronary arteries, but while SUR2$^{-/-}$ animals were hypertensive (Chutkow *et al.*, 2002), Kir6.1$^{-/-}$ mice had normal blood pressure (Miki *et al.*, 2002).

c. BK$_{Ca}$ channels in hypertension

There is strong evidence that the functional role of BK$_{Ca}$ channels is altered in vascular muscle during chronic hypertension, however, the direction of these changes is not so obvious. Some authors propose that the BK$_{Ca}$ channels are increased during the hypertension, because increases in both Ca^{2+} influx and BK$_{Ca}$ channel activity can be detected even in prehypertensive spontaneously hypertensive rats (SHRs) (Asano *et al.*, 1995). Electrophysiological measurements obtained under voltage-clamp conditions in arterial myocytes isolated from hypertensive animals have confirmed that the whole-cell K^+ current through BK$_{Ca}$ channels is enhanced in comparison with currents recorded from normotensive myocytes (Rusch *et al.*, 1992). This fact may be due to several reasons: (1) a higher density of BK$_{Ca}$ channel current in SHRs and a greater expression of the BK$_{Ca}$ channel α-subunit (Liu *et al.*, 1998) or (2) a increased BK$_{Ca}$ channel open probability in the renal vasculature owing to higher intracellular Ca^{2+} levels during hypertension (Martens & Gelband, 1996). However, increased BK$_{Ca}$ channel function may also be a consequence of elevated blood pressure, as it can be induced over several weeks by surgical or pharmacological interventions that cause hypertension (Rusch *et al.*, 1992) and it can be reversed by antihypertensive therapy (Rusch & Runnells, 1994). Therefore, BK$_{Ca}$ channel function may be increased in arterial smooth muscle cells as a protective mechanism against progressive increases in blood pressure and may provide a negative-feedback mechanism that helps to restrict the increased pressure and vascular tone. Such a

mechanism would therefore act to limit pressure-induced vasoconstriction and to preserve local blood flow.

In contrast, other authors proposed that the increased prevalence of hypertension with age is correlated with a reduction of BK_{Ca} channel expression (Ledoux *et al.*, 2006). A number of recent findings support the importance of the smooth muscle BK_{Ca} channel in the regulation of vascular tone and blood pressure. Ablation of the gene for the smooth muscle specific β_1-subunit of the BK_{Ca} channel leads to an increase in vascular tone and hypertension (Plüger *et al.*, 2000). In adittion, a reported a mutation of the human β_1 gene leading to a gain of function of the BK_{Ca} channel associated with a low incidence of human diastolic hypertension (Fernandez-Fernandez *et al.*, 2004). Moreover, β_1 relative to the α-subunit expression is downregulated in chronically hypertensive rats (Amberg & Santana, 2003). Consistent with the effects of the β_1 subunit knockout, ablation of the BK gene leads to an increase in vascular tone and hypertension (Sausbier *et al.*, 2005).

1.10.4 Effect of hypertension on calcium channels

a. Ca^{2+} channels in hypertension

As mentioned above, under dynamic conditions, arterial tone of VSMCs within the vessel wall is regulated by multiple vasoactive stimuli controlling myofilament Ca^{2+} sensitivity (Somlyo & Somlyo, 2003), and/or intracellular $[Ca^{2+}]$. Cytosolic $[Ca^{2+}]$ is tightly coupled to Ca^{2+} influx through VDCCs, especially L-type Ca^{2+} channels (LTCCs). Therefore, the myogenic response relies on the opening of LTCCs in the VSMCs for contraction (Nelson *et al.*, 1990). In fact, the requisite role of LTCCs in mediating pressure-induced contraction is evident by the absence of myogenic tone in the arteries of mice in which the LTCCs ($Ca_V1.2$) gene is inactivated (Moosmang *et al.*, 2003).

Several studies have conclusively demonstrated that an upregulation of LTCCs ($Ca_V1.2$) channel function in VSMCs is a hallmark feature of hypertension. A strong positive correlation exists between blood pressure and the number of functional $Ca_V1.2$ channels in the VSMCs in vivo. For example, systolic blood pressure was found to be linearly correlated to membrane densities of $Ca_V1.2$ channel currents in VSMCs from small mesenteric arteries of SHR and WKY rats (Lozinskaya & Cox, 1997). Other studies have also shown that the profound increase in $Ca_V1.2$ channel function observed during hypertension is an abnormality shared among VSMCs of several vascular beds (Sonkusare *et al.*, 2006b;Lozinskaya & Cox, 1997). Electrophysiological studies have demonstrated elevated Ca^{2+} currents in freshly isolated VSMCs of cerebral,

mesenteric, renal, skeletal and pulmonary arteries from various hypertensive animal models (Sonkusare *et al.*, 2006b;Lozinskaya & Cox, 1997;Simard *et al.*, 1998;Pesic *et al.*, 2004;Hirenallur-S DK *et al.*, 2008).

Single channel experiments and other studies have further shown that the elevated Ca^{2+} currents observed in VSMCs during hypertension are not the result of altered single channel conductance, open-time distribution or voltage sensitivity, but rather due to an increased number of $Ca_V1.2$ channel openings (Ohya *et al.*, 1993). Complementing the electrophysiological studies, contractile studies in isolated arteries further proved that compared to normotensive animals, arteries from hypertensive animals develop more Ca^{2+}-dependent spontaneous tone that was sensitive to $Ca_V1.2$ channel blockers (Pesic *et al.*, 2004). For example, renal arteries from SHRs, a genetic model of hypertension, and aortic-banded rats, that develop hypertension due to elevated angiotensin II levels, develop more Ca^{2+}-dependent spontaneous tone that was reversed by nifedipine (1 µmol/L), a $Ca_V1.2$ channel specific blockers, compared to their normotensive counterparts (Sonkusare *et al.*, 2006b). This authors propose that, if blood pressure is not restored to normal levels by compensatory neural and renal mechanisms, the VSMCs of the arterial circulation appear to ''electrically remodel'' as an adaptive response to sustain the higher levels of voltage-gated Ca^{2+} influx required for persistent arterial contraction. This adaptation is postulated to rely, at least in part, on the development of a ''disease-specific'' profile of vascular ion channels that promotes arterial contraction and Ca^{2+} influx.

The profound upregulation in vascular $Ca_V1.2$ channel function observed in hypertensive animals is largely attributed to increased expression of the channel. Immunoblot analyses show that the expression of the pore-forming α_1 subunit of the $Ca_V1.2$ channel is elevated in arteries of hypertensive animals compared to age-matched normotensive animals (Hirenallur-S DK *et al.*, 2008;Pratt *et al.*, 2002). For example, the protein expression of α was higher in mesenteric, renal and skeletal muscle arteries of SHR compared to age-matched WKY rats (Sonkusare *et al.*, 2006b). Other evidences suggest that depolarization per se promotes α_1 subunit expression in the VSMCs of small arteries, suggesting that this ''myogenic stimulus'' may both activate existing LTCCs and increase the number of Ca^{2+} channels in VSMCs during the evolution of hypertension (Pesic *et al.*, 2004).

In other study, increased expression of α_1 protein was observed in aorta and mesenteric arteries of SHR compared to WKY rats (Wang *et al.*, 2006). Further, the increase in α1 protein was specific to vasculature, and was not observed in brain or visceral smooth muscles. Increased expression of pore-forming α_1 subunit was also seen in renal arteries of aortic-

banded rats compared to Sham rats, suggesting that the increased expression of vascular $Ca_V1.2$ channel is an anomaly shared between hypertensive animal models with different etiologies (Pesic *et al.*, 2004). In the same study, the authors found that renal arteries that were exposed to high blood pressure for as little as 2 days exhibited increased expression of α_1 subunit, implying that the abnormal increase in vascular $Ca_V1.2$ channels may be an early event occurring during the development of hypertension.

However, is not now well established the mechanisms that lead to increased protein expression of the pore-forming α_1 subunit. Data available so far points to the involvement of multiple cellular mechanisms in the upregulated protein expression of vascular $Ca_V1.2$ channels during hypertension. In addition to transcriptional activity (Hirenallur-S DK *et al.*, 2008), post-transcriptional mechanisms (Kharade *et al.*, 2013) such as increased translation efficiency, increased trafficking of channel proteins to plasma membrane and increased stability of channel protein complex may also contribute to the upregulation of α_1 protein during hypertension.

In a recent study, through the use of β_3 knockout ($\beta3^{-/-}$) mice, authors. demonstrated that in mesenteric arteries from angiotension II-induced hypertensive mice, the β_3 subunit is required for the upregulation of $Ca_V1.2$ channels, increased calcium-dependent tone, and the development of high blood pressure (Kharade *et al.*, 2013). In heterologous expression systems, the β_3 subunit has been shown to promote plasma membrane expression of $Ca_V1.2$ channels by binding to the pore-forming α_{1c} subunit and potentially masking an ER retention signal. Contrary, other authors propose that a hypertension-associated increase in $\alpha_2\delta_1$ elevates $Ca_V1.2\alpha_1$ surface expression in arterial myocytes leading to pressure- and depolarization-induced vasoconstriction (Bannister *et al.*, 2012).

To date, no studies have investigated pathological or disease-associated molecular changes in LTCCs auxiliary subunits, in VSMCs of resistance-sized arteries. In addition, it is unclear whether the subunit composition of arterial myocyte surface LTCCs is altered in disease. Alternative splicing of mRNA encoding LTCC subunits confer tissue-selective channels with distinct pharmacological and electrophysiological profiles (Keef *et al.*, 2001;Bannister *et al.*, 2011). Channel function is further influenced by interaction with a variety of regulatory and structural proteins, and is subject to modification by several ubiquitous kinases and phosphatases, which serve to finely tune channel function to cellular demand (Catterall, 2000b;Keef *et al.*, 2001). Importantly, alteration of LTCC expression or function has been linked to multiple human pathological conditions including cardiac arrhythmia, hypertension,

immune deficiency and autism(Liao & Soong, 2010). Further studies will be required to determine the subunit composition of LTCCs and investigated the involvement of accessory subunits in this pathological alteration.

Evidence from a recent study also points to clustering and coordinated gating of Ca$_V$1.2 channels in the plasma membrane of VSMCs during hypertension (Navedo *et al.*, 2010). The authors in this study observed a higher frequency of coupled Ca$_V$1.2 channel gating events, measured as persistent Ca^{2+} sparklets, in VSMCs of angiotensin II-induced hypertensive animals, and raised the possibility of transient interaction of 2–6 adjacent Ca$_V$1.2 channels via their C-terminus during hypertension. Such a transient interaction of adjacent Ca$_V$1.2 channels and their simultaneous activation would result in enhanced Ca^{+2}influx per gating event and elevated myogenic tone during hypertension. Interestingly, persistent Ca^{2+} sparklet activity by Ca$_V$1.2 channels in VSMCs requires recruitment of PKCα by AKAP150 to the plasma membrane, suggesting that scaffolding proteins that 'organize' signaling molecules and ion channels may be important in mediating the vascular ion channel phenotype observed during hypertension (Navedo *et al.*, 2008). Consistent with this hypothesis, AKAP150 knockout mice showed a lack of persistent Ca^{2+} sparklets, decreased myogenic tone, and did not develop angiotensin II-induced hypertension. Although more mechanistic studies are needed in the future, information available thus far suggests the involvement of multiple regulatory pathways in the enhanced expression of vascular Ca$_V$1.2 channels during hypertension.

To summarize, the diameters of small arteries and arterioles are tightly regulated by the dynamic interaction between Ca^{2+} and K$^+$ channels in the vascular smooth muscle cells. Calcium influx through LTCCs induces vasoconstriction, whereas the opening of K$^+$ channels mediates hyperpolarization, inactivation of voltage-gated Ca^{2+} channels, and vasodilation. Here we explore the expression levels and function of four types of ion channels, that have been implicated in the regulation of resting vascular tone. These include the classical inward rectifiers (K$_{IR}$), ATP sensitive K$^+$ channels (K$_{ATP}$), large conductance Ca^{2+}-dependent K$^+$ channels (BK$_{Ca}$) and the L-type calcium channels (LTCCs). We use a mice model of essential hypertension obtained by phenotypic selection, the normotensive (BPN) and hypertensive (BPH) mice. This model shares many features common to human hypertension and thus allows a pathophysiological analysis of the factors responsible for the development and maintenance of the disease. Using resistance mesenteric arteries, we also characterize the functional contribution of these channels to control VSMC excitability and vessel tone, measured in intact arteries with pressure myography.

2 OBJECTIVES

Our goal in this thesis is the characterization of the changes in the functional expression of VSMCs ion channels in a mouse model of essential hypertension. This specific goal includes:

1. The study of the remodelling of inwardly rectifier K^+ channels in VSMCs from hypertensive animals, relevant as they are key determinants of resting V_M and hence vascular tone. To achieve that objective we explored:

    a. The expression and the functional electrophysiological properties of classical inward rectifiers (K_{IR} channels) and ATP-sensitive K^+ channels (K_{ATP} channels) in mesenteric VSMCs from BPN and BPH mice.

    b. The contribution of these channels to set the resting membrane potential in isolated VSMCs and to determine vascular tone in isolated mesenteric arteries of BPN and BPH mice.

2. The characterization of the differences between BPN and BPH mice in the functional expression of L-type calcium channels (LTCCs), as key elements regulating intracellular calcium levels and vascular reactivity. To achieve this objective we explored:

    a. The changes in local and global calcium influx through LTCCs in BPN and BPH VSMCs, studying both microscopic currents ("sparklets") and macroscopic whole-cell currents. We study the effect of these changes in the excitation-contraction coupling in VSMCs by characterizing calcium release from intracellular stores (calcium "sparks") and calcium-induced K^+ efflux ("STOCs") in both preparations

    b. The changes in LTCCs chanelosome in BPN and BPH VSMCs, to determine whether the functional differences observed can be atributted to changes in the molecular composition of the LTCCs in the plasma membrane.

3 MATERIALS & METHODS

3.1 APPARATUS

3.1.1 Electrophysiology set-up

The electrophysiology set-ups dedicated to measure electrical activity of the cells have several basic elements.

a. **Perfusion chamber for recording**

The perfusion chamber consists of two parts: a polycarbonate chamber (RC-24E, Warner Instruments, Hamden, CT, USA), and an aluminium platform (P1, Warner Instruments). The chamber is attached by screws to the platform allowing perfect sealing with the coverslip that forms the bottom part. In addition, the chamber has a perfusion inlet and aspiration outlet to place the associated perfusion lines. The chamber is designed to allow a laminar flow and rapid exchange of the solution. The small bath volumes are especially useful when using drugs in small quantities. Cells are placed at the bottom of the chamber either directly or previously attached to glass coverslips.

b. **Inverted microscope**

IX70 (Olympus, Tokyo, Japan) and Eclipse TE300 (Nikon, Tokyo, Japan) inverted microscopes were used in the electrophysiological experiments. Both were adapted with a support for the micropipette, the "electrode holder" (2.0mm 64-840 QSW, Warner Instruments), a perfusion chamber and a macro and micromanipulation system. The "holder" is attached to the micromanipulator through the amplifier headstage (AU CV201, Axon Instruments). The "holder" provides support to the pipette and transmits the electrical signal to the amplifier through a silver wire.

c. **Macro and micromanipulators**

The macro and micromanipulator (PSC-5000 Series, Burleigh, Newton, NJ, USA) and (423 Series, Newport, Irvine, CA, USA) are used for positioning the micropipette tip onto the cell membrane in a controlled manner. First, the recording pipette is positioned in the vicinity of the cell by the macromanipulador. Next, the piezoelectric micromanipulator is employed to establish contact between the pipette tip and the cell, performing fine adjustment movements in the three spatial axes. Finally, a slight negative pressure is applied through a syringe connected to the "holder" with a silicone tube to achieve a high resistance seal.

d. Amplifiers

The Axopatch-200 and the Multiclamp 700A (Axon Instruments, Inc., Foster City, CA, USA) amplify the signal current, that flows between the recording electrode and the ground. In addition, patch clamp amplifiers process the experimental commands, such as holding potential and voltage steps. Signal conditioning, which includes filtering, further amplification and data reduction, can be performed by the amplifier, in addition to basic control commands such as current/voltage clamp selection, offset control, capacitance and series resistance compensation, holding potential setting and gain.

e. Digitizers

Digidata 1322A and 1440A (Axon Instruments) are data acquisition systems for electrophysiological recordings of low noise and high resolution. Digitizers enable communication between the computer and the amplifier, and other peripheral devices (perfusion system controler, temperature, stimulators, etc.) by AxoScope software. Currents generated by the cells are digitized with the analog-digital converter by digitizers. Similarly, the voltage pulse protocols generated on the computer are converted to analog with digital-analog converter of the Digidata.

f. Anti-vibration table

The table (63-544 microg, TMC, Peabody, MA, USA) provides an excellent work surface free of vibrations. Vibration isolation properties work on the principle of air cushions in the table legs that support a heavy table top. The table top is kept afloat by a gas-source from nitrogen tank. Inverted microscope is placed on the table top, isolating it from vibrations of the surrounding area. This is essential for stable recording, as it prevents vibrations of the pipette that could detach the cell from the pipette or crush it against the bottom.

Perfusion system and microscope are placed inside a Faraday cage, isolating our sample of external electric fields

g. Perfusion system

Cultured or dissociated cells are placed on the recording chamber and perfused by gravity at a rate of 1-2 ml/min from a stand with six reservoirs. Reservoirs containing solutions communicate with the recording chamber via flexible silicone tubes, which converge into one very close to the recording chamber, allowing quick solution changes with low residual volume. Reservoirs function as Mariotte´s bottles, maintaining a constant infusion rate

independent of the volume of solution in the reservoir. Solution changes are controlled by an electrovalves system. The level of the chamber is maintained constant by a suction system that uses a vacuum pump.

h. PC-Computer

Computer is a necessary tool to communicate with analogical-digital/digital-analogical interface for most patch-clamp applications and to perform data analysis. pClamp 10.2® (Axon Instruments) software was installed in the computer. This software comprises Clampex® application to edit stimulation protocols and Clampfit® application to analyze the obtained data. Furthermore, Clampex® allows us to edit stimulation protocols, sample at different frequencies, filter data, subtracting "leak" current and store records from the cells.

3.1.2 Equipment for manufacturing micropippetes

a. Glass

Borosilicate glass capillaries with an outer diameter of 2 mm, an inner diameter of 1.12 mm and provided with an inner filament (12B, World Precision Instruments, Inc., Sarasota, FL, USA) are used for making micropipettes. These thick-walled capillaries minimize electrical noise, while the filament within the rod lumen greatly aids filling of microelectrode by increasing capillary action, avoiding bubbles on the pipette tip.

b. Pipette pullers

PP-83 vertical puller (Narishige, Tokyo, Japan) and a P-97 automatic puller (Sutter Instruments, Novato, CA, USA) were used to stretch the capillaries. The vertical puller heats the capillary in two successive stretching steps. A glass rod is mounted in two clamps, of which one can move by means of a carriage. The two rod clamps are located on either side of a heated coil. For extra regulation, the current flowing through the resistance at both stretching is controlled independently by two potentiometers.

Ciclo Press = 600	Heat	Pull	Velocity	Time
1	600	-	21	150
2	600	-	21	150
3	550	-	21	150
4	550	-	21	150

Table3.1 Puller P97 protocol for micropippetes stretch.

The automatic puller has a larger number of parameters that can be set for each pulling cycle, providing better control and hence greater reproducibility.

For pipettes with a tip of 3-4 mm and resistances of 2-3 MΩ, we have used a 4 stages program (Table 3.1)

c. Microforge

Micropipette tips are sharp and can have jagged edges, which could easily destroy the cell. The problem is solved by fire polishing of the tip in a microforge, (MF-830 Narishige, Tokio, Japan). The pipette tip is melted using a platinum/iridium incandescent filament to make the edge rounded and smooth. This step facilitates the seal between the glass and the cell plasma membrane. Once polished, micropipettes and filled with internal solution, exhibit resistance between 6-10 MΩ for VSMCs and 2-4 MΩ for HEK cells.

3.1.3 Myography set-up

The Pressure myograph system (111P, DMT Aarhus, Denmark) was used to measure the physiological function and properties of small arteries, veins and other vessels.
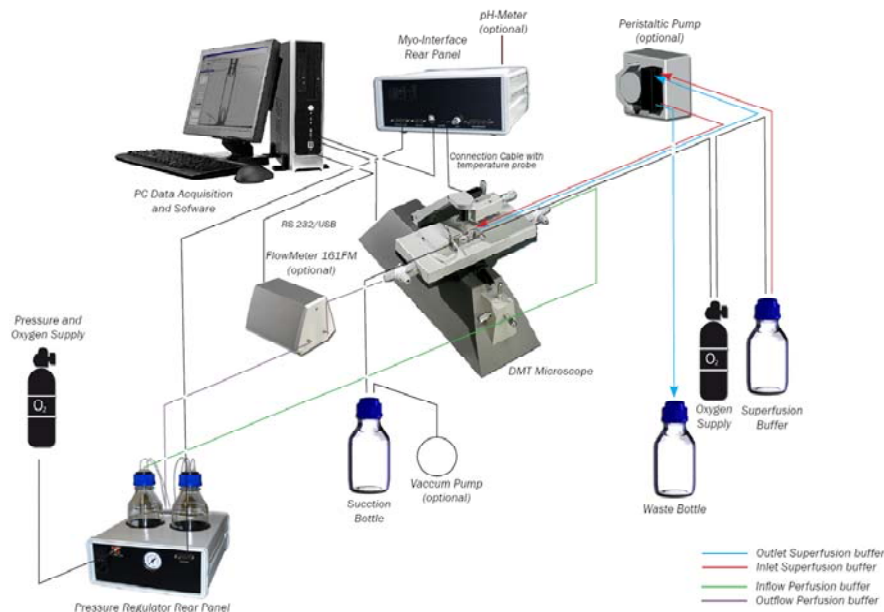
Figure 3.1 *Example of the Complete Pressure Myograph.*

a. Pressure myograph unit

In pressure myography unit, an intact small segment of an artery is mounted onto two small glass cannulae and pressurized to a suitable transmural pressure under near-physiological conditions. A built-in heating system maintains the chamber temperature, eliminating the need for continuous and often costly superfusion. The chamber cover includes ports for superfusion, for rapid draining and filling, for cumulative addition of drugs and for oxygenation.

The pressure myograph unit contains two pressure transducers based on Wheatstone bridge circuit. The pressure sensors measures liquid pressure inside the pipette, generating a electrical signal as a function of the pressure imposed. In addition, the myography unit is equipped with a force transducer to keep the vessel stretched after application of drugs or pressure stimuli.
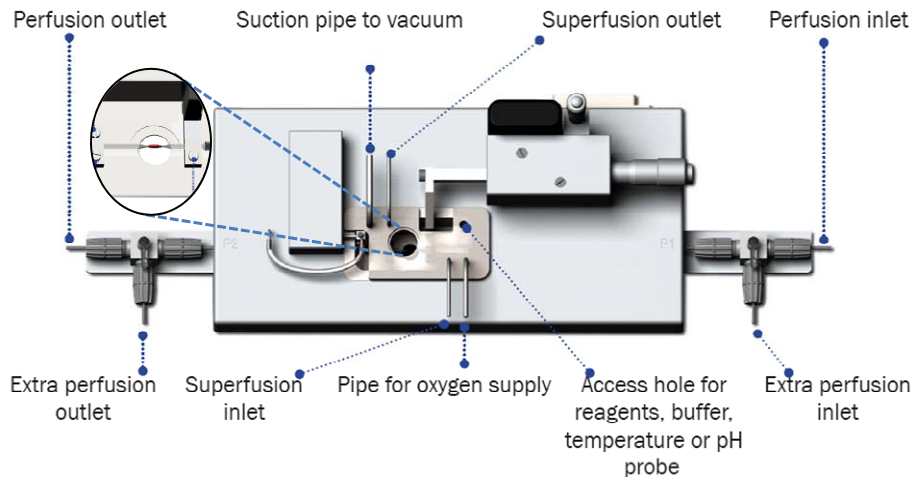
Figure 3.2 *Pressure myograph unit.*

b. Inverted microscope

The DMT Microscope is an inverted microscope equipped with a Zeiss Achromat 10X / 0.25 objective and build-in CCD camera. The objective is adjustable in all X Y Z directions using the three micropositioners on the front. DMT Microscope has a build-in infrared light source to avoid the surroundings light from having influence on the data acquisition and analysis.

c. The pressure regulator

The Pressure Regulator controls the flow and pressure applied to the vessel mounted in the pressure myograph chamber via settings in the Myo-Interface and the MyoView™ software. The Pressure Regulator consists of two individual circuits, an air circuit and a buffer circuit. The Pressure Regulator transfers the pressure and flow settings from the Myo-Interface by individual control of the air pressure in the two buffer bottles.

3.1.4 TIRF imaging-set-up

TIRF (total internal reflection fluorescence) microscopy is a technique with a very high z resolution (< 200 nm) ideally suited for the study of membrane associated processes.

a. Laser Line Combiner

The Laser Line Combiner (TILL Photonics, Gräfelfing, Germany) is a modular system combining two different laser lines (488nm and 561nm) by feed them into a single fiber. An accusto-optic tunable filter (AOTF) allows controlling gating and attenuating of every single laser via software. Fast switching of laser wavelength and intensity using the AOTF ensures minimal exposure of cells to the laser light, reducing phototoxicity and photobleaching. After passing the AOTF the light from the lasers is coupled into a monomode fiber. This fiber accommodates in wavelengths from 400 to 650 nm and maintains the laser's original polarization.

b. Polytrope

The Polytrope Imaging-Mode Switch (TILL Photonics, Gräfelfing, Germany) is a fast beam switching device, which allows changing between widefield fluorescence illumination and laser illumination in milliseconds increasing time resolution with reduced bleaching and phototoxicity. This is achieved by turning a galvanometric mirror in the center of the Polytrope. This galvo mirror allows changing the beam path of the laser coming from a light source from epifluorescence illumination to laser illumination.

In TIRF experiments where the light passes four highly reflective mirrors and a lens, causing the tube lense inside the microscopy to focus the laser light onto the back focal plane of the objective lens. The position in the back focal plane can be changed by the angle of the galvo mirror. In combination with an PlanApo TIRF objective with a NA >1.49 this enables changing the TIRF angle and consequently changing the penetration depth of the evanescent field in the specimen.

c. Camera

Andor iXON 597 EMCCD (Electron Multiplying Charge Coupled Device) uses a quantitative digital camera technology that is capable of detecting single photon events whilst maintaining high quantum efficiency, achievable by way of a unique electron multiplying structure built into the sensor. This camera has very fine nanosecond resolution for the 512x512 back-illuminated sensor. Also, due to our faster vertical speeds it could acquire images at 100 Hz.

d. Software

Live Acquisition software is the application that allows recording of multi-position, multi-dimensional, multi-channel series in real-time and at highest speed with more than 300 fps. In addition, it controls all the hardware for TIRF experiments.
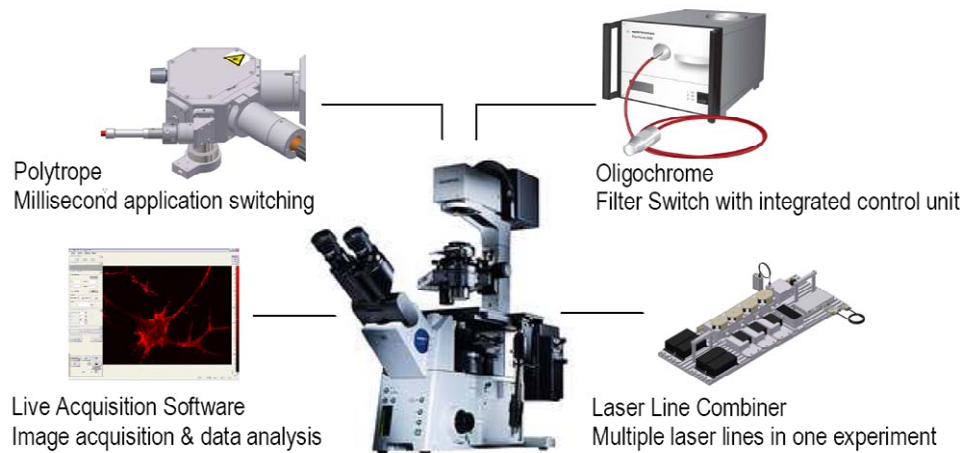
Figure 3.3 *TIRF set-up squeme.*

3.2 SOLUTIONS

3.2.1 Electrophysiological solutions

To record and isolate different-ionic currents it is necessary to control the concentration of the major permeable ions on both sides of the membrane. The solution that perfuses the recording chamber is called external solution, and the solution inside the micropipette is called internal solution. The external solution has an ionic composition similar to the extracellular medium, while the internal solution tries to reproduce intracellular ionic composition and some intracellular mediators in some cases.

a.   Solutions for K_{IR} and K_{ATP} currents recording

Internal solution: The internal solutions were designed according to Table 2. GDP, GTP and ATP are added to ice-cold solutions to prevent degradation, and after that pH was adjusted to 7.2. Finally, 1 ml aliquots were prepared and stored frozen at -80 ° C. The internal solution was filtered before filling the pipettes and always kept on ice.

The K_{ATP} internal solution was designed to amplify the magnitude of K_{ATP} currents in VSMCs, as previously described (Beech & Bolton, 1989).

Resting membrane potential measurements were performed using the perforated-patch solution, and a different intracellular solution was used in these experiments (Table 3.2).

| Composition | K_{IR} Currents | | K_{ATP} Currents | | Int. Solution |
	Int. Solution (mM)	Ext. Solution ↑K^+ (mM)	Int. Solution (mM)	Ext. Solution (mM)	Perf-patch (mM)
NaCl		85.7		141	
K-Glutamate			100		95
KCl	125	60	25	4.7	40
$MgCl_2 \cdot 6H_2O$	4	1.2	2	1.2	
$CaCl_2$		1.8		1.8	8
Hepes	10	10	10	10	10
EGTA	10		10		
Glucose		10		10	
Amphotericin B					300µg/ml
Na_2-GTP			0.1		
Mg-ATP	5		0.1		
Na_2-GDP			1		
pH	7.2 (KOH)	7.4 (NaOH)	7.2 (KOH)	7.4 (NaOH)	7.2 (KOH)

Table3.2 Solutions for K_{IR} and K_{ATP} currents recordings

External Solutions: External solutions were designed according to Table 3.2. An external solution with high K^+ has been used to increase the amplitude of the currents.

b. Solutions for Ca^{2+} currents recording

Internal solution: In the internal solution (table 3.3) KCl has been substituted by caesium chloride to block potassium currents.

| Composition | Cav Currents | | Int. Solution |
	Int. Solution (mM)	Ext. Solution (mM)	Perf-patch (mM)
NaCl		140	
KCl		2.7	
CsCl	130		40
$MgCl_2 \cdot 6H_2O$	2		
$CaCl_2$			8
$BaCl_2$		10	
Hepes	10	10	10
EGTA	10		
Glucose		10	
Cs Aspartate			95
Amphotericin B			300µg/ml
Na_2-GTP	2		
Mg-ATP	2		
pH	7.2 (CsOH)	7.4 (NaOH)	7.2 (CsOH)

Table 3.3 Solutions for Ca^{2+} currents recording

External solution: external solution was designed according to table 3.3. This solution contains barium as a charge carrier, which increases the amplitude of the currents through calcium

channels due to its increased permeability and the reduction of the calcium-induced inactivation (Lee & Tsien, 1984).

c. Solutions for STOCs recording

Composition	Ext. Solution BK (mM)	Int. Solution BK (mM)
NaCl	130	10
L-aspartic acid		110
KCl	5	30
$MgCl_2 \cdot 6H_2O$	1	1
$CaCl_2$	2	
Hepes	10	10
Glucose	10	
EGTA		0.5
pH	7.4 (NaOH)	7.3 (KOH)

Table 3.4 *Solutions for BK_{Ca} currents recording*

d. Solutions for single channel recording of BK channels

Composition (nM)	0 Ca^{2+}	1 mM Ca^{2+}	5.5 mM Ca^{2+}	10 mM Ca^{2+}	100 mM Ca^{2+}
KCl	125	125	125	125	125
EGTA	5	5	5	5	-
HEDTA	-	-	-	-	5
HEPES	10	10	10	10	10
$CaCl_2$	-	3.86	4.73	4.86	4.84
pH	7.3 (KOH)				

Table 3.5 *Solutions for single channel recordings of BK_{Ca} channels*

3.2.2 VSMCs isolation solutions

Composition	SMDS (mM)	SMDS 10µM Ca^{2+} (mM)
NaCl	145	145
KCl	4.2	4.2
$MgCl_2 \cdot 6H_2O$	1.2	1.2
$CaCl_2$		0.01
Hepes	10	10
Glucose	11	11
pH	7.4 (NaOH)	

Table 3.6 *Solutions for VSMCs isolation*

a. SMDS

The smooth muscle dissociation solution (SMDS) is used for surgery and dissection of the arteries (Table 3.6). The SMDS is also used as basis for preparing the enzymatic solution used for the isolation of the vascular smooth muscle cells.

b. Enzymatic solution

The solutions to dissociate the mesenteric arteries VSMCs are prepared immediately prior to dissociation and kept at 4 ° C until used. Dissociation of VSMCs (described in Section 3.5.3) is performed in two stages, using sequentially solutions A and B (Table 3.7).

Composition	A solution (mg/ml SMDS)	B Solution (mg/ml SMDS 10µM Ca^{2+})
DTE (1,4-Dithioerythritol, Sigma)	1	
BSA (Bovine serum albumin, Sigma)	1	1
Papain (3119, Worthington)	0.4-0.6	
Collagenase F (7926, Sigma)		0.4-0.8
Time (min.)	9-15	12-16

Table3.7 *A and B solutions to VSMCs isolation*

3.2.3 HEKs culture media

Transfected HEK cells were maintained using standard Dulbecco's Modified Eagle's Medium, (DMEM, Gibco) supplemented with the antibiotic mixture: penicillin 100 U / ml, streptomycin 100 U / ml, Fungizone 0.25 µg / ml (Lonza), and fetal bovine serum at 5% (FBS, Lonza). In some experiments, we used stably transfected clones with the calcium channel α1c subunit, and in these cases the medium contains the antibiotic G418 at a final concentration of 50mg/ml, as the stable clones also express the antibiotic resistance gene.

	HEKs MEDIUM in DMEM	CLONES MEDIUM in DMEM
Fetal bovine serum (Lonza)	5%	5%
Penicillin (Lonza)	100U/ml	100U/ml
Streptomycin (Lonza)	100U/ml	100U/ml
Fungizone (Lonza)	0.25µg/ml	0.25µg/ml
G418 (345812, Calbiochem)		8µl/ml

Table 3.8 *Trasnfected HEKs culture mediums*

3.2.4 Western-blot solutions

a. K_{IR} and K_{ATP} channels

Proteins were precipitated by Trizol ® and dissolved in 0.1% SDS.

Loading mix: 10-20μg of proteins, 1x XT Reducing agent and 1x XT sample buffer (Bio-Rad, Laboratories, Hercules, CA, USA).

Running buffer: running buffer depends on the type of gels.

- Criterion Precast Gel 10% Bis-Tris: MOPS (Bio-Rad).

- Criterion TGX 4-15%: Tris/Gly/0.1% SDS (Bio-Rad). 25 mM Trizma base pH 8.3, 192 mM glycine, 0.1% SDS. In some experiments.

Transfer buffer (TGM): 25 mM Trizma base pH 8.3, 192 mM glycine, 20% methanol.

TBS: 10 mM Trizma base pH 7.5, 150 mM NaCl.

TTBS: 1x TBS with 0.1% Tween 20 .

Blocking Buffer: we used two different blocking solutions:

For Kir 6.1 and β-actin: 5% skim milk in TTBS.

For Kir 2.1, Kir 4.1 and SUR2: 0.5% Tropix® I-Block^{TM} (Applied Biosystems).

Antibodies: see table 3.14.

b. L-type calcium channels

Freezing solutions:

Solution 1: 10% TCA, 10 mM DTT in acetone.

Solution 2: 10 mM DTT in acetone.

Sample buffer: 60mM Tris HCl (pH 6.8), 10% glycerol, 2% SDS, 0.01% bromophenol blue.

Homogenization solution: 1x sample buffer and 100mM DTT.

Electrophoresis gels: Criterion TGX 4-15%.

Running buffer: /Tris/Gly/0.1% SDS (Bio-Rad).

Transfer buffer (TGM): 25 mM Trizma base pH 8.3, 192 mM glycine, 20% methanol.

Blocking Buffer: 5% skim milk in TTBS.

Antibodies: see table 3.14.

3.2.5 Myography solutions

A physiological saline solution (PSS) was used in the myography experiments. The composition of this solution is shown in table 3.9.

Composition	PSS (mM)	PSS-ØCa^{2+} Nifedipine (mM)	PSS-ØCa^{2+} EGTA (mM)
NaCl	120	120	120
KCl	5	5	5
CaCl$_2$	2.5		
NaHCO$_3$	25	25	25
NaH$_2$PO$_4$	1.18	1.18	1.18
MgSO$_4$	1.17	1.17	1.17
Glucose	10	10	10
Nifedipine		0.01	
EGTA			3
pH	7.4 (NaOH)	7.3 (NaOH)	7.4

Table 3.9 *PSS composition.*

3.2.6 Calcium imaging solutions

Composition	Ca^{2+} sol. for TIRF (mM)	20mM Ca^{2+} sol. for TIRF (mM)	Int. Solution for TIRF (mM)
NMDG	140	113	
Cs-Aspartate			87
CsCl	5	5	20
MgCl$_2$	1	1	1
CaCl$_2$	2	20	
Glucose	10	10	
HEPES	10	10	10
BAPTA			10
Fluo-5F (Invitrogen)			250µM
Mg-ATP			5
pH	7.4(NaOH)	7.4(NaOH)	7.2(CsOH)

Table 3.10 *Sparklets registration solutions.*

a. **"Sparklets" recording solutions (TIRF)**

A 2 mM Ca^{2+} solution was used to make the seal and then was switch to a 20 mM Ca^{2+} solution to record sparklets.

b. **"Sparks" recording solutions**

Dissociation of the cells was performed as described in material and methods section 3.5.8. After dissociation, the cells were washed and let rest in the dissociation solution SMC for 30

minutes. Before Ca^{2+} imaging experiments, Fluo-4AM was added to an aliquot of cells at a final concentration between 3-5 µM.

Composition	SMC Solution (mM)	Ext. Sol. for Sparks (mM)
NaCl	125	130
KCl	5.4	5
$MgCl_2 \cdot 6H_2O$		1
$NaHCO_3$	15.4	
Na_2HPO_4	0.33	
KH_2PO_4	0.34	
$CaCl_2$		2
Glucose	10	10
Sucrose	3	
HEPES	11	10
Fluo-4AM (Invitrogen)	3-5µM	
pH	7.4 (NaOH)	7.4 (NaOH)

Table 3.11 *Sparks registration solutions.*

3.3 PLASMIDS

Dr. D. A. Castellano provided us the plasmids containing the complete rabbit coding sequences of Cav1.2, $\alpha_2\delta$ and β_2 (CACNA1C, CACNA2D1 and CACNAB2) cloned into their respectively expression vectors as follows: Cav1.2 into pCARDi (Mikami *et al.*, 1989), $\alpha_2\delta$ into pk CRα2 (Zong *et al.*, 1994) and β_2 into pSG5 (Castellano *et al.*, 1993).

These plasmids were co-expressed with GFP to determine the efficiency of transfection and to identify the transfected cells. The expression vector that has been used for GFP was the gWIZ-GFP, commercially available from Gene Therapy Systems Inc. This vector contains a modified and much brighter than the original GFP (Cheng *et al.*, 1996).

3.4 DRUGS

Phenylephrine (Phe) (phenylephrine hydrochloride, P6126, Sigma-Aldrich) is a selective α-adrenergic receptors agonist.

Acetylcholine (Ach) (acetylcholine chloride, A6625, Sigma Aldrich) neurotransmitter used to activate the endothelial nitric oxide synthase pathway.

Nifedipine (Nif) (481981, Calbiochem) dihydropyridine L-type Ca^{2+} channel blocker. It is used to determine the maximum diameter on a relaxed artery.

Bay K-8644 (BayK) (Methyl 2,6-dimethyl 5-nitro 4-[2-(trifluoromethyl) phenyl] 1,4-dihydropyridine 3-carboxylate, B-350, Alomone) is an opener of all LTCCs.

Glibenclamide (Glb) (G0639, Sigma-Aldrich) sulfonylurea ATP-sensitive potassium channel blocker.

Pinacidil (Pin) (Pinacidil monohydrate, P154, Sigma-Aldrich) cyanoguanidine ATP-sensitive potassium channel activator.

Gabapentin (GBP) (G154, Sigma-Aldrich): amino butyric acid analogue (GABA). Described as an antagonist of calcium currents because of its union with the L-type calcium channels $\alpha_2\delta$ subunit.

3.5 METHODS

3.5.1 Hypertension mouse model

Samples were obtained from hypertensive mice strain, BPH (Blood Pressure High) and the corresponding control strain, BPN (Blood Pressure Normal), from Jackson Laboratories (The Jackson Laboratories, Bar Harbor, ME, USA). We use only male adults (aged between 3-12 months). BPN and BPH mice were maintained by inbreeding crossing in the animal facility of the School of Medicine of Valladolid under temperature-controlled conditions (21°C) and with free access to water and food.

These mice were obtained by phenotypic selection of individuals that showed higher blood pressure after crossbreeding of eight different strains. This allowed the identification of hypertensive (BPH) and normotensive (BPN) lines sharing a comparable genetic background (Schlager & Sides, 1997;Schlager, 1981).

BPH mice show elevated systolic blood pressures (SP) at five weeks old. In addition, BPH mice strain shows lower levels of renin, aldosterone and angiotensin than BPN (Schlager & Sides, 1997;Schlager, 1981) and a reduced lifespan (Schlager, 1981)).

All animal protocols were approved by the Institutional Care and Use Committee of the University of Valladolid, and are in accordance with the European Community guiding principles regarding the care and use of animals.

3.5.2 Blood pressure measurements

Blood pressure measurements were made in BPN and BPH mice to confirm that the two strains really exhibit consistent and significant differences in blood pressure values.

Blood pressure was measured in awake mice with a tail cuff pressure meter (LSI Letica Scientific Instruments, Barcelona, Spain). This system consists of a cuff that occludes the blood flow in the mouse tail and a transducer, which monitored systolic (SP) and diastolic (DP) pressure and calculated mean arterial pressure (MP) according to the following equation:

$$MP = DP - \frac{SP - DP}{3}$$

The mice were placed in a thermostated cage and heated for 20-30 minutes at 37 ° C before each measurement. Repeated measurements were carried out in each animal in different sessions over several days to reduce stress and to obtain reliable values. Heart rate was monitored by the pulse transducer to ensure that the animal was in resting conditions (heart rate <600 beats / min).

SP values were (mean ± SEM) 134.9 ± 1.5 mmHg in BPN versus 155.8 ± 3.5 mmHg in BPH and DP values were 90.7±2.8 mmHg in BPN versus 109.0±3.6 mmHg in BPH. MP values averaged 105.0 ± 2.1 mmHg in BPN and 124.9 ± 3.7 mmHg in BPH (P <0.001 in all cases, n =15 animals in each group).

3.5.3 VSMCs isolation

a. Surgery

BPN and BPH mice aged between 3-12 months and weighing between 22-33 g were anesthetized using isoflurane (5% O_2 2.5l min^{-1}) and sacrificed by cervical dislocation. VSMCs from mesenteric arteries were obtained as previously described (Moreno-Dominguez *et al.*, 2009). Briefly, mice were placed in supine position and a laparotomy was carry out to get access into the abdominal cavity, after incision the small intestine was excised and placed on a Sylgard®-coated plate filled with ice cold 10µM Ca^{2+} SMDS (Table 3.6).

Subsequently, 2nd and 3rd order mesenteric arteries were located under a dissecting microscope and cleaned of fat and surrounding connective tissue. After the cleaning, we proceed in different ways depending on the use of the arteries: (1) the arteries were either frozen at −80◦C to further extract RNA and proteins (in both cases the endothelial layer of the artery was removed), (2) subjected to an enzymatic digestion to get fresh dispersed VSMCs or (3) used to carry out myography experiments.

b. Enzymatic digestion

The mesenteric arteries were cut into small pieces and subjected to two consecutive processes of enzymatic digestion to obtain acute isolated VSMCs. In a first step, the arteries are added to a 37 °C preheated vial for 15' with SMDS Ø Ca^{2+} (Table 3.7: Solution A), containing 0.4-0.6 mg/ml papain, 1 mg/ml BSA and 1mg/ml 1,4-dithioeritritol (DTE). After 9-15' at 37 °C, a second incubation was carried out in a 37 °C preheated vial with 10µM SMDS Ca^{+2} (Table 3.7: Solution B) containing 0.4-0.8mg/ml collagenase F and 1mg/ml BSA solution. The arteries were transferred to this second vial and incubated at 37 °C in the bath for 12-16'. After three washings in SMDS containing 10µM Ca^{2+}, single cells were obtained by gentle trituration with a wide-bore glass pipette of different diameter tips. Cells are stored at 4 °C and used within the same day for the electrophysiological records. The ionic composition of SMDS and 10µM SMDS Ca^{+2} was described in table 3.6.

3.5.4 RNA isolation and real-time PCR

The mRNA expression levels of different potassium channel genes were studied by RT-real time PCR. This study was carried out in VSMCs from five different vascular beds from BPN and BPH mice.

Gen name	Acronyms	Applied Biosystems identification number
KCNJ1	Kir1.1	Mm00444727_s1
KCNJ2	Kir2.1	Mm00434616_m1
KCNJ12	Kir2.2	Mm01237201_m1
KCNJ3	Kir3.1	Mm00434618_m1
KCNJ6	Kir3.2	Mm00440070_m1
KCNJ9	Kir3.3	Mm00434622_m1
KCNJ10	Kir4.1	Mm00445028_m1
KCNJ8	Kir6.1	Mm00434620_m1
KCNJ11	Kir6.2	Mm00440050_s1
ABCC9	Sur2	Mm00441638_m1*
CNN1 (Calponin 1, smooth muscle)	CNN1	Mm00487032_m1
NOS3 (Nitric oxide synthase 3, endothelial)	NOS3	Mm00435204_m1
GAPDH (Glyceraldehyde-3P-dehydrogenase)	Gadph	**
GUS (β-glucuronidase)	Gus	**

Table 3.12 *Genes whose expression was studied using Taqman probes, with the acronyms used in this work and the reference probe from Applied Biosystems. * The SUR2 probe recognizes both SUR2A and SUR2B isoform. ** Probes designed in our laboratory.*

a. RNA samples homogenization and isolation

Total RNA from arteries was isolated with a MELT Total RNA Isolation System Kit (Ambion, Life Technologies Corporation) following the manufacturer's instructions. Five or six mesenteric arteries (second and third order), the femoral and renal arteries and the thoracic aorta of five mice, and the basilar artery from 40–50 mice were employed for each assay.

For adequate enzymatic disruption, arteries were cut in fragments less than 3 mm in length, added to "MELT digestion master mix" and shaked for 10 min, until the samples become fully homogenized. Next, samples were transferred to the "Binding Beads master mix" containing magnetic small balls with chaotropic salts (the binding beads) that bind to nucleic acids.
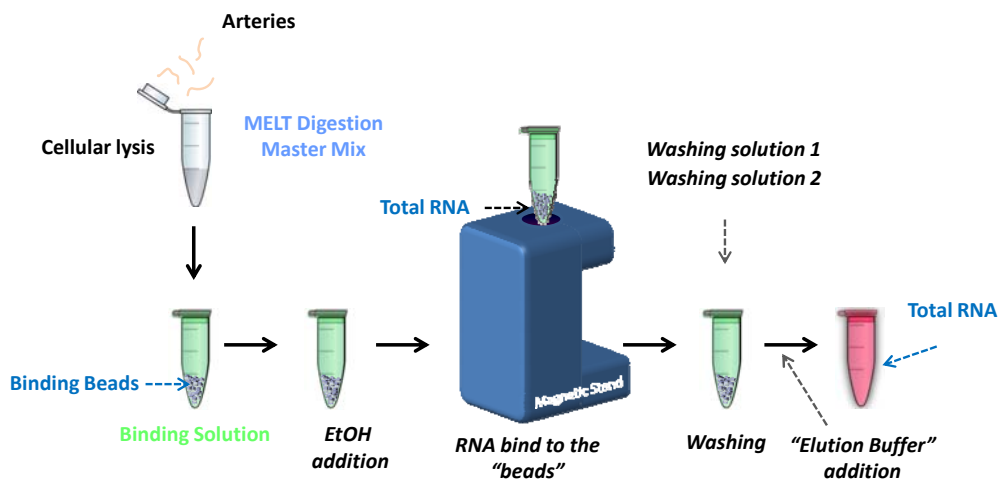

Figure 3.4 Total RNA samples extraction process, using the commercial extraction kit MELT Total RNA Isolation System Kit (Ambion, Life Technologies Corporation). EtOH: 70 % ethanol.

After two hours incubation, the reaction tube was transferred to a magnetic stand, allowing the Binding Beads to be captured for 1–3 min at room temperature. After three washings in "washing solution 1 and 2", purified RNA was transferred into the elution buffer and stored at -80°C or used within the same day to check RNA purity and integrity.

b. RNA quantification and treatment with DNAse

RNA yield varies greatly depending on many factors such as type of tissue, sample handling during dissection, storage, and extraction method. Once RNA was purified, quantification and verification of their quality was performed by two methods: optical density measurements at 260 and 280nm in the spectrophotometer (NanoDrop ND-1000, Thermo Scientific) and electrophoresis on agarose gels.

RNA concentration can be calculate by Lambert-Beer's Law (see appendix 8.2), because the absorbance measured in the NanoDrop is directly proportional to the concentration of RNA.

c. Synthesis of complementary DNA

In this stage, cDNA (RT+) is synthesized by reverse transcription from RNA samples with the reverse transcriptase enzyme MuLvRT. This enzyme uses a single-stranded RNA as a template in the presence of a primer to synthesize a complementary cDNA strand.
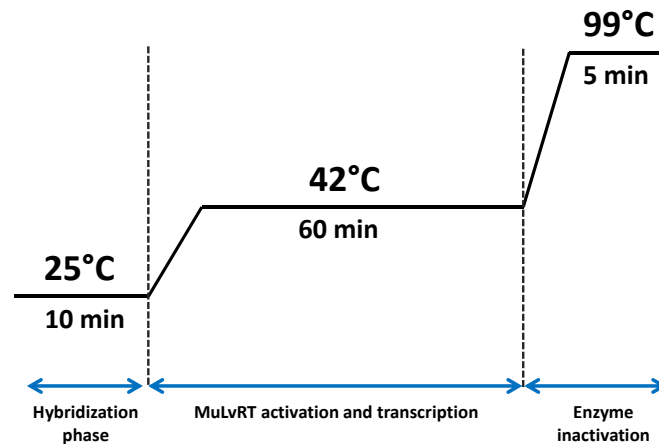

Figure 3.5 *cDNA synthesis protocol using the MuLvRT (Applied Biosystems). 25°C for 10 min to mRNA hybridize with the enzyme, 42°C for 60 min to the enzyme activation and amplify the cDNA and 99°C for 5 min to inactivate the enzyme and denature the mRNA-cDNA complex.*

After DNAse I treatment, 500–750 ng of RNA was reverse transcribed with MuLvRT (2.5 u μl^{-1}) in the presence of 1 u μl^{-1} of RNAse inhibitor, 2.5 µM random hexamers, 1× PCR buffer, 5mM $MgCl_2$ and 4mM mixed dNTPs. All reagents were from Applied Biosystems. The mixture was subjected to the following temperature cycle: 10 min at 25°C, 60 min at 42°C, and finally 5min at 99°C to get cDNA (RT^+). The amplified cDNA was immediately stored at -20°C.

From the same samples, 200–350 ng of total RNA was used as genomic control in reverse transcriptase reaction in the absence of MuLv and RNase inhibitor using the same temperature protocol. This sample was designated as RT^-.

d. Relative amplification and quantification by real time PCR

Gene expression was detected using TaqMan assay (Applied Biosystems, Live Technologies) which is based on a 5' nuclease fluorogenic reaction. Taqman assays consit of a pair of primers and a probe that binds to a target sequence which is located between the primers, allowing amplification of our gene of interest and avoiding the nonspecific amplifications.

TaqMan probes consist of a fluorophore covalently attached to the 5' end and a quencher at the 3' end. The quencher molecule accepts the energy emitted by the fluorophore which is dissipated as heat or fluorescence, when the fluorophore is close to the quencher.

Thus, when the DNA polymerase starts the amplification process, the 5'>3' exonuclease activity of the Taq DNA polymerase cleaves the fluorophore from the probe. This fluorescence can be measured and the level is directly proportional to the amount of target DNA accumulated during the PCR reaction.
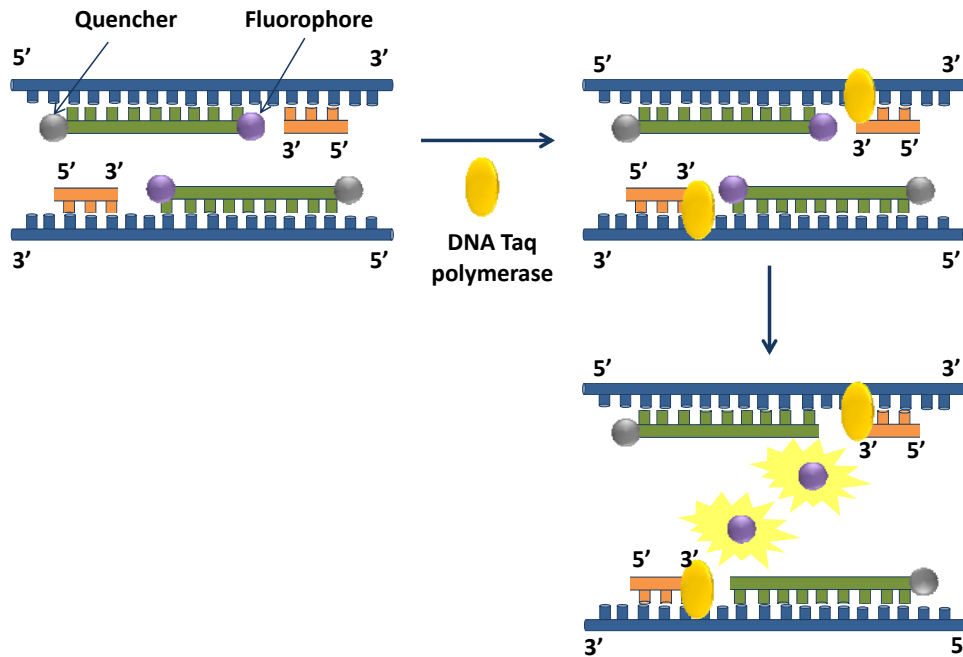
Figure 3.6 *TaqMan probes action mechanism.*

A small fraction of these cDNAs were used for real-time amplifications of selected control genes (Gapdh and Gus) in a Rotor-Gene RG3000 (Corbett Life Science, Qiagen) thermocycler to check the quality and integrity of the samples. Primer sets and TaqMan probes for these genes were designed in the laboratory:

mGADPG	Primer 5'-3'	5'-TGTGTCCGTCGTGGATCTG-3'
	Primer 3'-5'	5'- GATGCCTGCTTCACCACCTT-3
	Taqman probe	5'-FAM-TGGAGAAACCTGCCAAGTATGATGACATCA-BHQ2-3
mGus	Primer 5'-3'	5'-CAATGGTACCGGCAGCC-3'
	Primer 3'-5'	5'-AAGCTAGAAGGGACAGGCATGT-3'
	Taqman probe	5'-FAM-TACGGGAGTCGGGCCCAGTCTTG-BHQ2-3

Amplifications were performed in a final volume of 20 µl, using 10 µl of Absolute QPCR mix (ABgene, Thermo Fisher Scientific Inc), 1 µl of each primer, 1µl of the probe and 1 µl of cDNA. Cycling conditions were 15 min at 95° C, 40 cycles of 95° C for 15 s and 60 °C for 1min. These amplifications were used to compare the different samples, and also to check the efficiency of the DNase treatment by comparing expression levels of these genes between RT$^+$ and RT$^-$ samples.
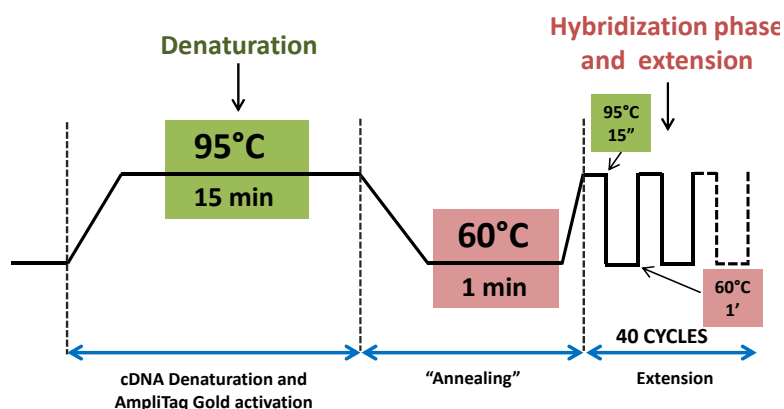
Figure 3.7 *Amplification protocol.*

Real-time PCR was carried out with TaqMan Low Density Arrays (TLDA, Applied Biosystems, Life Technologies Corporation). TLDA arrays allow the analysis of multiple genes using real-time qPCR. The selected genes were the potassium channels (Kir1, Kir2, and Kir6 Kir4) and the accessory subunit SUR2. It has also included an endogenous control gene (18S rRNA), a smooth muscle marker (calponin) and an endothelial cells marker (eNOS). A complete list of the genes studied is provided in (Table 3.13).

Figure 3.8 *Amplification protocol for TDLA cards.*

TLDA were processed at the Genomic Service of the Centro Nacional de Investigaciones Científicas (CNIC Madrid, Spain), with an ABI Prism 7900HT Sequence detection system (Applied Biosystems) using SDS 2.1. software from Applied Biosystems.

Analysis of the PCR reaction results requires the setting of a detection threshold Ct (cycle treshold) within the exponential phase of all amplification curves. Ct is defined as the number of cycles required to produc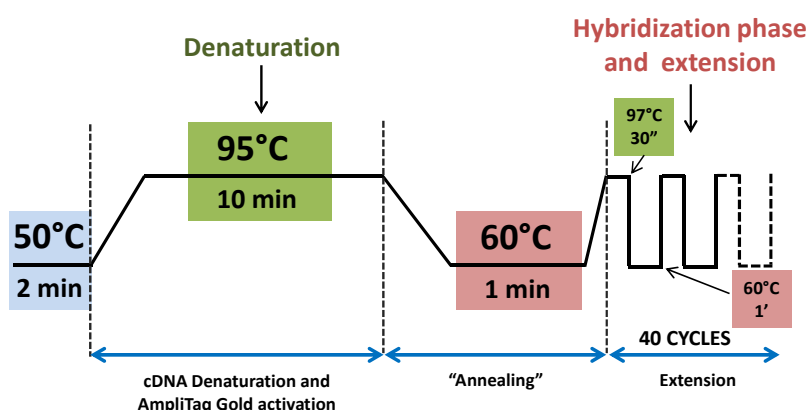e a significantly fluorescence increases compared with the baseline signal, and it is inversely proportional to the initial amount of cDNA molecules.

e. Quality control of qPCR

In order to extract meaningful conclusions for the qPCR data, we ensure that the conditions of our PCR reaction are optimized so that the efficiency of the reactions is close to 1 (when efficiency is defined as percentage from 0 to 1) meaning that the amount of template doubles in each cycle. Efficiency of the qPCR for the analysis of the housekeeping gene expression (Gapdh and Gus) was calculated by examining the correlation between Ct number and different concentration of some control tissues using cDNA serial dilutions, and was always close to 1.

All the expression assays used with the Taqman low density arrays were inventoried and validated by the manufacturer, so that under their specified conditions for the amplification, the efficiencies of all the genes studied are also 1 and differ among them in less than 10%, so that the ΔΔCt method could be applied (Livak & Schmittgen, 2001).

f. Statistical analysis

Data were analyzed using the relative quantification comparative (ΔΔCt) method (Livak & Schmittgen, 2001). This method is based on comparison of the threshold cycle of different genes, which are normalized by the internal control rRNA 18S or Gapdh genes. Where ΔCt was calculated from:

$$\Delta C_t = C_{t,Channel} - C_{t,18s}$$

The expression level of the same gene under different conditions was compare using the relative quantification method ΔΔCt, which is calculated from:

$$\Delta \Delta C_t = \Delta C_{t,sample} - \Delta C_{t,calibrator}$$

The fold increase of one normalized gen to another is expressed as $2^{-\Delta\Delta Ct}$. Thus, differences between hypertensive and normotensive VSMCs within the different vascular beds were calculated from this equation, where:

$$\Delta\Delta C_t = \Delta C_{t,BPH} - \Delta C_{t,BPN}$$

For comparisons, $\Delta Ct_{(BPN)}$ was designated as the calibrator, and the data in BPH samples are presented as the fold change in gene expression. In order to do statistical comparisons, ΔCt values obtained in each sample ($Ct_{,Channel} - Ct_{,18S}$), were subtracted from the mean ΔCt of the calibrator to provide the S.E.M. Each data point was obtained from duplicate determinations from at least three different assays. In the cases in which expression of a gene was not detected in one of the conditions, a Ct value of 40 was assigned in order to do the comparisons. When changes are represented as log $2^{(-\Delta\Delta Ct)}$, a higher expression in BPH mice has a positive value, whilst a lower expression is negative, and absolute values of 0.3, 0.7 and 1 represent 2-, 5- and 10-fold changes respectively.

The statistical analysis was performed with two different housekeeping genes, RP18s and Gapdh to choose the most adequate. Ribosomal protein 18s has the advantages of being an ubiquitous and relatively stable gen that is included in the Taqman low density arrays so that is also an internal control of the reaction. However, its expression levels are high and therefore it could be less sensitive to variations in the expression range of the genes of interest. On the contrary, Gapdh, whose expression levels are closer to the levels of the genes under study, serves as external control as its expression is determined from the same samples in an independent reaction. The data obtained with the two sets of ΔCt values showed no important discrepancies, as illustrated in the table 3.13 (see below), so we used RP18s as the housekeeping gene for representing the data.

	ENDOGENOUS CONTROL		SAPHYRO-WILKS TEST		STUDENT T TEST			MANN-WHITNEY-WILCOXON	
	BPN	BPH	BPN	BPH	t	p	Confidence interval	W	p
	Ct (mean±SD)	Ct (mean±SD)	p	p					
Rp18S	11.72±0.62	11.31±0.60	0.083	0.190	1.48671	0.15707	(-0.216,1.03)	31	0.166
Gapdh	19.78±0.87	19.73±0.86	0.437	0.139	0.04626	0.96361	(-0.8,0.836)	50	0.969

Table 3.13 *Statistical analysis of the Ct values obtained for the two housekeeping genes*

Statistical analysis was performed with the STATGRAPHICS Centurion XVI software (StatPoint Technologies Inc.) using different test for comparison between BPN and BPH samples.

For each set of data, we evaluated first if the data distribution could be adjusted to a normal distribution by using the Saphyro-Wilks test, where p values > 0.05 indicate a normal distribution (null hypothesis). As this was the case for all data set in our study, we applied a student t-test for independent samples to determine if we have statistically significant differences when comparing the means of the two groups (BPN and BPH).

In addition, we also use the Mann-Whitney-Wilcoxon test, a non-parametric test, that represents a more robust statistical analysis as it compares the median of the two groups to decide whether two populations are equal or not without assuming them to follow the normal distribution.

Although several statistical approaches can be taken to analyze real time data, including multiple regression models, a recent study comparing several statistical methods indicates that more simplified alternatives such as t-test and Wilcoxon two group tests can be used with no differences in the final outcome (Yuan *et al.*, 2006).

Using these tools, we evaluated first the distribution and the possible existence of differences in the expression levels of the two housekeeping genes, RP18s and Gapdh. As shown in Table 3.13, when comparing the data set obtained in BPN and BPH samples, they both show a normal distribution with no statistical differences.

3.5.5 Western blot

a. K$_{IR}$ channels protein isolation

For total protein isolation, were used 20–25 mesenteric arteries obtained from six animals. The arteries were placed in a tube with TRIzol® Reagent (Invitrogen, Life Technologies Corporation). TRIzol® is a chemical reagent for the isolation of high-quality total RNA or the simultaneous isolation of RNA, DNA, and protein from a variety of biological samples.

Later, samples were lysed and homogenized in a Precellys 24 homogenizator (Bertin Technologies, Montigny-le-Bretonneux, France) using ceramic beads (CK14) following the manufacturer's instructions.

After homogenizing the sample with TRIzol® Reagent, chloroform is added and the homogenate is allowed to separate into a clear upper aqueous layer (containing RNA), an interphase, and a red lower organic layer (containing the DNA and proteins). RNA is precipitated from the aqueous layer with isopropanol. Isolated RNA can be used in RT-PCR within the same day or stored in 75% ethanol at least 1 year at -20°C.

b. Calcium channels protein isolation

For calcium channels protein isolation, aproximatelly 50 arteries from 4 animals were used. Arteries were flash-frozen in an ice-cold mixture of 10% trichloroacetic acid (TCA) and 10 mM dithiothreitol (DTT) in acetone. Arteries were washed in ice-cold acetone containing 10 mM DTT and lyophilized overnight. Prior to protein extraction, the lyophilled vessels were weighted in an ultra precision scale to normalize the western load.

For protein extraction, ≈ 1000 μl of sample buffer (3.2.4.b section) was added to 20-25 pooled messenteric vessels per experimental group. Samples were heated at 95 °C for 10 min and rotated end-over-end overnight at 4 °C prior to electrophoresis. Multiple freeze/thaw cycles were avoided to limit protein degradation

c. Western Blot

Protein samples were dissolved in 1% SDS. Samples of 10–20 μg were incubated with XT Reducing Agent and XT Sample Buffer (Bio-Rad Laboratories, Hercules, CA, USA) for 5min at 95∘C.

Proteins were separated by SDS-PAGE (Criterion Precast Gel 10% Bis-Tris for Kir2.1, Kir4.1 and Kir6.1 or Criterion TGX 4–15% for SUR2 detection, Bio-Rad) and transferred onto polyvinylidene difluoride membrane (PVDF). Membranes were blocked in either 5% non-fat dry milk (Kir6.1 and β-actin) or 0.5% Tropix® I-Block^{TM} (Applied Biosystems, Kir2.1, Kir4.1 and SUR2) in TTBS (Tris-buffered saline with 0.1% Tween 20) for 1 h. Membranes were then incubated with the primary antibodies in blocking solution for 1 h under spinning. Antibodies used were:

Antibodies Name	Dilution	Company and Ref.
Mm monoconal anti-β-actin	1:1000	Abcam, 8226
Rb polyclonal anti-Kir2.1	1:333	Alomone Labs, APC-026
Rb polyclonal anti-Kir4.1	1:400	Alomone Labs, APC-035
Rb polyclonal anti-Kir6.1	1:1000	Alomone Labs, APC-105
Rb polyclonal anti-SUR2	1:250	Santa Cruz Biotechnology, sc-25684 *
Mm monoclonal anti-Cav1.2	1:1000	Neuromab, 75-053
Mm monoclonal anti-β$_2$	1:200	Santa Cruz Biotechnology, sc-81990
Mm monoclonal anti-α$_2$δ	1:500	Santa Cruz Biotechnology, sc-271697

*Table 3.14. Antibodies used to study protein expression with the dilution at which have been used and the commercial reference. * The SUR2 antibody reacts both the isoform SUR2A as SUR2B.*

After three washings in TTBS, membranes were next incubated with horseradish peroxidase-conjugated anti-rabbit IgG (Santa Cruz Biotechnology, Santa Cruz, CA, USA) or anti-mouse IgG (Bio-Rad Laboratories) at a final concentration 1:10,000 for 1 h under spinning at RT. Protein signals were detected in the VersaDoc 4000 Image System (Bio-Rad) with SuperSignal West Femto Maximum Sensitivity Substrate (Thermo Scientific, Rockford, IL, USA). Quantification was carried out with the densitometric analysis of the bands for each antibody and normalized to their corresponding β-actin signals, using the Quantity One software (Bio-Rad).

Calcium channels subunits proteins were separated by SDS-PAGE and transferred onto nitrocellulose membranes (Trans-Blot®, Bio-Rad Laboratories, Hercules, CA, USA). After blockade of the membranes with 5% non-fat dry milk in TTBS (TBS with 0.1% Tween 20), membranes were incubated with either mouse monoclonal antibodies anti-Cav1.2 (75-053, Neuromab), anti-$\alpha_2\delta$ (SC-271697, Santa Cruz) and anti-β_2 (SC81890, Santa Cruz) in blocking solution for 1 h. Membranes were next incubated with horseradish peroxidase-conjugated goat anti-mouse IgG (K-4065, Dako Diagnósticos, Barcelona, Spain), at a final concentration of 1:10000 for 1 h. Protein signals were detected in the VersaDocTM 4000 Image System (Bio-Rad) with SuperSignal R® West Femto Maximum Sensitivity Substrate.

3.5.6 Electrophysiological methods

a. Experimental procedure

Electrodes. In patch clamping usually only two **electrodes** are used: the pipette electrode and the bath electrode. It is important that both electrodes are identical in type of material and have small redox potentials, such as silver chloride. Silver chloride electrodes consist of silver wire or pellets that have been "chlorided", forming AgCl layer on the outside. The layer will wear of, particularly from the pipette electrode where repeated pipette changes will scrape away the silver chloride, increasing the offset, so it chloriding silver wire to form AgCl electrodes must be routinely performed.

Superfusion system. It consists of a set of reservoirs connected to the bath inlet by several tubes. Reservoirs and tubes must be free of dirt and salts, therefore before the experiments 8% acetic solution followed by distilled water is perfused through them. After filling the reservoirs with final solutions, the system must be drain to avoid bubbles reaching the recording chamber. In addition is important to check that the chamber is clean and without leaks. In case the coverslip is damaged or dirty, it must be replaced and sealed to the base of the chamber with silicone grease (RS Components, Corby, UK).

Micropipettes. They are filled with the corresponding internal solution with an insulin syringe, whose end has been previously heat-stretched to obtain a very thin duct. The internal solution is previously filtered through PVDF filters Ø 0.22 mm pore (Millex®, Millipore Corp., Bedford, MA, USA) to remove any particles that may block the tip of the micropipette. In addition, after filling micropipettes with internal solution, is important remove air bubbles into the micropipette to improve electrical contact between electrode and solution. Micropipettes are made as indicated in 3.1.2 section.

Cells. The coverslips with the attached cells were placed at the bottom of the recording chamber and perfused by gravity with the bath solution, while freshly isolated **VSMCs** were placed directly on the recording chamber and left to settle for a 15 minutes before starting superfusion with the external solution.

b. Seal and Whole-cell

Before starting the experiment, the micropipette must be firmly attached to the electrode holder (Holder, Axon Instruments) and there must be contact between internal solution and microelectrode.

The Clampex "seal test" software applied a small block pulse (-10 mV) through the micropipette, these pulses are displayed as a negative deflection current line on the computer screen. The seal test calculates the micropipette tip resistance automatically and continuously by Ohm's law:

$$V = I \cdot R$$

Where V is voltage in (V), I is current in (A) and R is the resistance in (Ω).

Thus, the resistance can be calculated easily by dividing the test pulse amplitude by the current response amplitude. When the pipette is outside the bathing solution, no current will flow because the resistance in the circuit is infinite.

When the pipette is lowered into the bathing solution using the macromanipulator, the current changes to a large square response from which pipette resistance can be calculated. Once the target cell is chosen, the pipette tip is positioned near the cell using the fine micromanipulator. The final approach is monitored simultaneously on the microscope and on the oscillating seal test. Cell contact is indicated by an increased resistance caused by occlusion of the pipette by the cell. The next step is to apply negative pressure into the pipette, which should drop the test pulse response considerably to form a high resistance seal (more than 1GΩ "Gigaseal").
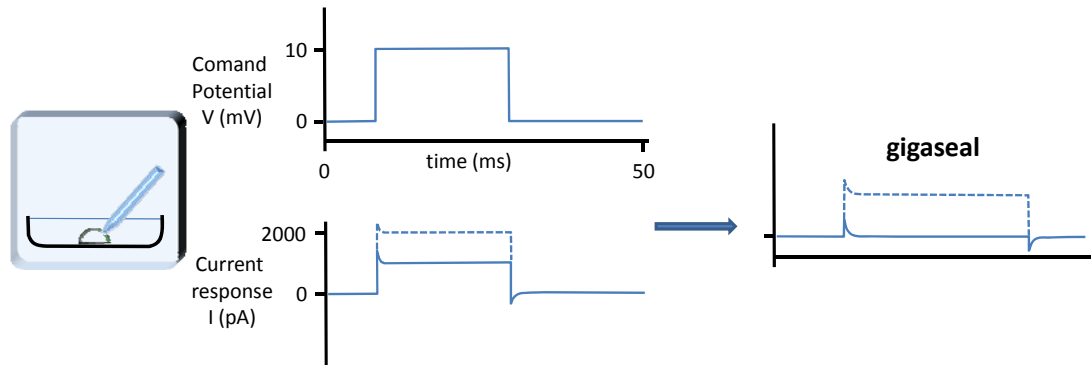
Figure 3.9*. Current response to a square pulse with the patch pipette touching the cell. The response drops in amplitude, indicating incresed resistance and finaly a gigaseal formation (Molleman, 2003).*

At this point we are in the cell-attached configuration. After gigaseal formation, it is helpful to switch the pipette potential to a value near the membrane potential (-80mV). This will make the patch more stable and to prevent a sudden depolarization when the whole-cell is achieved. The whole-cell is obtained from the cell-attach configuration when the membrane patch isolated inside the pipette tip is broken by application of additional suction pressure thought the pipette tube. The pipette solution is then in direct contact with the cytoplasm, establishing electrical contact between the cytoplasm and the electrode placed inside the pipette.

A successful breakthrough is indicated by the observation of capacitative transient. The transient is formed by the cell capacitance (R_m) in series with the pipette ($R_{pipette}$) plus the access resistance (R_{access}). R_m is the largest resistor, so this configuration allows study the sum of currents through all channels of the cell, also called macro-currents. Before starting the whole-cell experiments, membrane capacitance and series resistances must be correctly compensate. Good quality recording can be defined with the following criteria: a seal resistance > 1GΩ, the resistance series lower than 20MΩ and both must be stable.

c. Perforated-patch

The perforated-patch configuration was used to study membrane potential and several K^+ and Ca^{2+} currents. This configuration allows a good electrical access and preservation of the intracellular milieu. The pipette tip is dipped briefly into the perforated patch solution (Table 3.2 and 3.3) and is filled with the same solution containing amphotericin B (300µg/ml). Amphotericin B is an antifungal that creates holes in the membrane patch, permeable to monovalent ions but no large molecules, most critically second messenger molecules.

Gigaseal formation is performed as usual, a good electrical access to the cell cytoplasm was assessed by monitoring the current response to a test pulse. The capacitative transients

indicating electrical access to the cell cytoplasm can be observed slowly increasing over time, with decreasing access resistance as indicated by a progressively faster capacitative transient. At this point, the amplifier can be switched to current-clamp mode to record membrane potential. The high Ca^{2+} content of the pipette solution ensures the correct performance of the perforate-patch technique, as accidental rupture of the patch (changing to whole-cell configuration) leads to a sudden Ca^{2+} load and cell death.
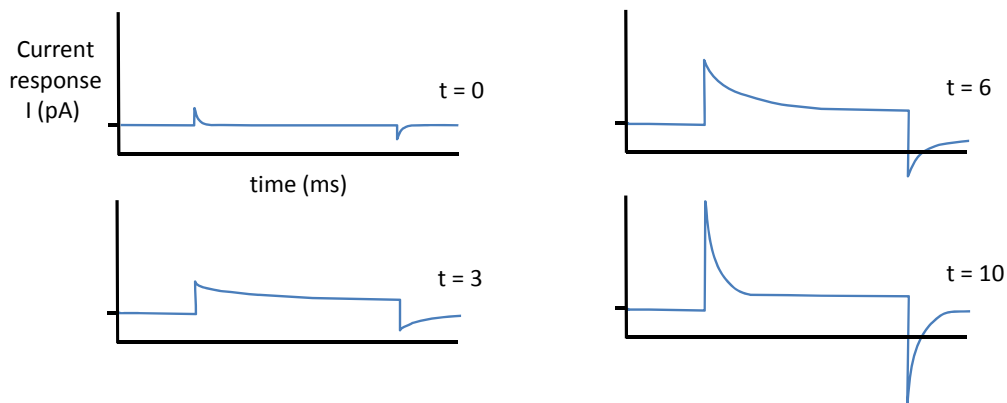

Figure 3.10*. Establishment of perforated patch configuration. The gigaseal is formed at t=0 min. The patch initially appears to become leaky and then the capacitative transients develops (Molleman, 2003).*

d. Data acquisition and analysis

Electrophysiological data acquisition and part of the analyses were performed with the Clampfit subroutine of the pCLAMP software (Axon Instruments) and with Origin 7.5 software (OriginLab Corp., Northampton, MA, USA). Electrical stimulation protocols were designed and controlled with the Clampex 2.10 subrutine included in the same software. The graphical representation of the data and part of the analysis was performed with the ORIGIN 7.5 (OriginLab Corp., Northampton, MA, USA). Pooled data are expressed as means ± standard error of the mean (S.E.M.). Statistical comparisons between groups of data were carried out with Student's two-tailed t test for paired or unpaired data, and values of $P<0.05$ were considered statistically different.

e. Protocols for ion channels recording

i K_{IR} and K_{ATP} currents

Ionic K_{IR} and K_{ATP} currents were recorded at room temperature (RT, 20–25∘C) using the whole cell or the perforated patch configurations of the patch-clamp technique.

Current–voltage relationships were obtained from a holding potential of −80 mV in 2 s ramps from −150 to +30 mV (Figure 3.11). The perforated-patch technique was used to explore the currents elicited by the same voltage ramps without manipulation of the intracellular medium.
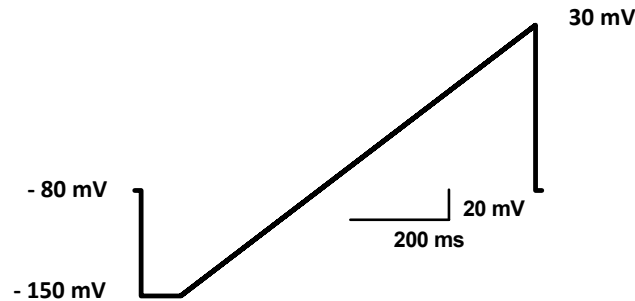

Figure 3.11. *Ramp protocol used for K_{IR} and K_{ATP} currents.*

ii Calcium currents

Whole cell calcium currents were recorded at RT in isolated myocytes using the whole cell patch clamp configuration. Inward Ba^{2+} currents were evoked by stepwise depolarizing pulses in 10 mV intervals between -70 mV and +70 mV from a holding potential of -80 mV (Figure 3.12A). The perforated-patch technique was used to explore the calcium currents without intracellular medium manipulation.
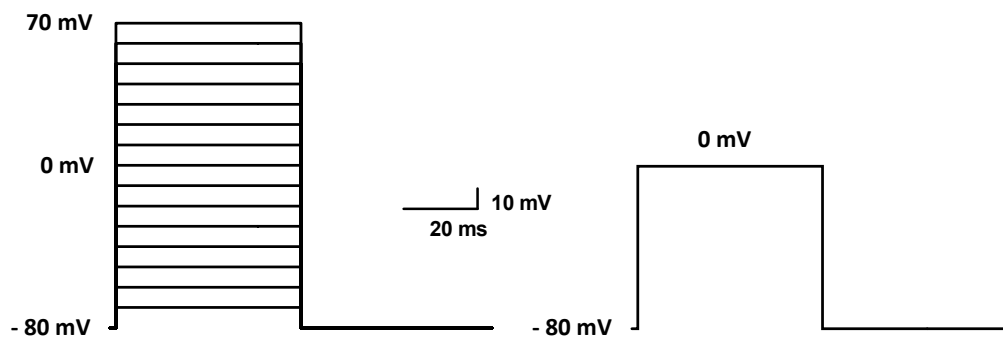
Figure 3.12. *Calcium channels protocols. A: Stepwise depolarizing pulses in 10 mV intervals between -70 mV and +70 mV from a holding potential of -80 mV. B: depolarizin pulse at 0 mV for time curse records.*

Time course of the calcium peak current amplitude was studied using a 50 ms depolarizing pulse from a holding potential of −80 mV to a test potential of 0 mV (Figure 3.12B).

iii Voltage membrane measurements

V_M measurements were performed at room temperature using the perforated-patch technique and recordings were obtained with an Axopatch 700A patch-clamp amplifier. We used amphotericin B (300 µg/mL) and a gap-free acquisition mode.

iv STOCs currents

Spontaneous BK currents were measured using the whole-cell patch clamp technique in the amphotericin B (300 µg/mL) perforated patch configuration with the gap-free acquisition mode at -40mV. Cells were continuously superfused with BK external solution (Table 3.4). We analyzed BK currents with an amplitude ≥ 6 pA, which based on the unitary current of BK channels at –40 mV (≈ 2pA) (Nelson *et al.*, 1995), requires the simultaneous opening of at least three BK channels.

v Single channel currents

BK single channel currents were recorded from inside-out patches under symmetrical (140 mM) K^+ conditions. Smooth muscle cells were bathed in solutions in which different $CaCl_2$ concentrations were added to obtain titrated concentrations of free Ca^{2+}, determined using Maxchelator software; (Chris Patton, Stanford University) (Table 3.5). Pipettes were filled with the same 140 mM K^+ solution without Ca^{2+}-supplementation. The number of BK channels per patch was estimated while patches were held at 100 mV in the presence of 100 µM Ca^{2+}, which maximizes the open probability (P_o) of these channels. Records were obtained in gap-free mode at different holding potentials as indicated.

3.5.7 Myography methods

a. Myography fundaments

The pressure myograph technique allows the characteriztation of a large variety of physiological functions and properties of vessels. The system also allows the study of pharmacological effects of drugs and other vasoactive compounds on small isolated vessels under near physiological conditions. In these preparations, vessels retain many of their in vivo characteristics.

In pressure myography, an intact small segment of healthy artery is mounted onto two small glass cannulae and pressurized to a suitable transmural pressure. This near physiological condition permits the investigation of intrinsic mechanism such as (myogenic) responses, endothelial secretions, vasoactive metabolites and autacoids, which can be extrapolated to the in vivo behaviour of the entire vascular bed. Various pharmacological agents can then be studied by adding these to the superfusate or luminal solution. Both constriction and dilation can be readily measured as changes in diameter of the preparation via digital video edge-

detection. Since intrinsic myogenic constriction is present, the role and function of the endothelium for this phenomenon can be studied.

b. Arteries dissection

A common finding in miography studies is that responsive and stable preparations are associated with the development of spontaneous tone in nearly all arterial vessels. Consequently, the tone is easily compromised by excessive levels of anesthesia, extensive surgical manipulation, or trauma (Davis & Hill, 1999). For this reason, a similar procedure as described in section 3.5.3 must be followed for dissection of the arteries, but in the case of the myograph experiments certain precautions must be keep in mind.

Once the animal is euthanized in accordance to section 3.5.3, a midline laparotomy is performed to expose the mesenteric bed. From this point, around 10cm of intestine together with its feeding vasculature, including part of the superior mesenteric artery are removed with scissors. The excised intestine section is placed in a Petri dish (about 9cm in diameter) coated with a thick layer of Sylgard at the bottom to hold the fixing pins. Immediately the Petri dish is filled with cold PSS well aerated carbogen. The dissection is performed without further oxygenation of the PSS. The proximal end of the intestine section is pinned down on the left-hand side of the Petri dish without stretching the vessels. The remaining of the intestine section is pinned down in an anti-clockwise direction. In this configuration the feeding vasculature is placed on the upper side and the veins are located usually bellow. Afterwards, the vessel segment to be cleaned is localized under a dissecting microscope. In this case vessel segments from the second or third branch from the superior mesenteric artery (unpressurized approximate external diameter 150-200µm) were selected. The vessel segment of interest is dissected using high quality forceps and dissection scissors. The mesenteric membrane is cut through along both sides of the vessel, about 1-2mm from the vessel. To avoid accidentally cutting the artery it is recommended to always cut along the length of the vessels and never perpendicular to them. The adipose tissue around the vessels was dissected away to distinguish between the artery and vein. The artery can easily be identified by the following characteristics:

1. The branch points of arteries are V-shaped whereas those of veins are more U-shaped.

2. The arterial wall contains a thick layer of smooth muscle cells compared to the vein wall, which only contains a single or a few layers of smooth muscle cells. The histological difference is clearly visible in the stereomicroscope.

3. When the differentiation is difficult and the vein and artery still contain some blood, a last test can be done, moving the blood forward by very gently squeezing the vessels with a forceps. In the artery the blood will run back quickly whereas in the vein the blood will run back very slowly if it even does so. It is important to perform this on vessels other than those will be used as this procedure damages the vessels.
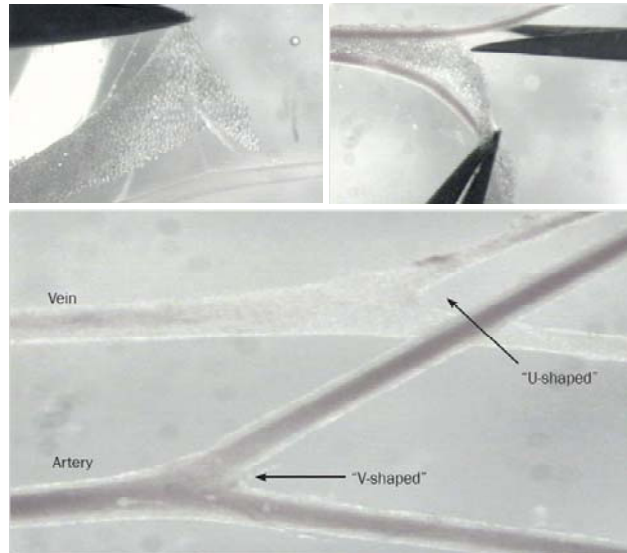

Figure 3.13. *Cleaning the artery by removing any remaining adipose or connective tissue (upper panels). Distinguishing between artery and vein(bottom panels)(DMT's user manual).*

After this, the vein is dissected away using scissors to cut the adipose and connective tissue between the artery and vein. One method is to cut the vein in one position and afterwards gently to pull the vein away from the artery. In this way a fine membrane of connective tissue becomes visible between the adipose tissue and the artery. Carefully the fine membrane is cut to remove the vein and adipose tissue while avoiding any direct contact between the scissor and artery.

Once the artery is isolated is cleaned by removing any remaining adipose or connective tissue. The adipose or connective tissue is gently pulled away to make the connective tissue membrane become visible. Finally, the artery section to be investigated is removed cutting the distal and the proximal end, while ensuring that the vessel segment has the correct length.

c.   Mounting protocol for arteries

First of all, the Pressure Myograph Chamber (DMT, Aarthus, Denmark) is filled with cold PSS (Table 3.9) aerated with 5% CO_2-95% air. After drain the ways and micropipettes through the both valves (P1 and P2) using a vacuum system, the isolated vessel segment is transferred to the Pressure Myograph Chamber. The end of the vessel is carefully cannulated on the right

side glass cannula connected to P1 and the vessel is gently secured with two fine nylon sutures (DMT, Aarthus, Denmark). After a gently flush of the lumen of the mounted vessel with PSS to remove any blood or debris, the other end of the vessel is carefully cannulate with two fine nylon sutures.

The pressure myograph unit is placed on an inverted microspcope with a built-in infrared light source and CCD camera, which measures the differences in light intensity passing through the walls of the mounted vessel segment. Thus, it is possible to continuously measure the diameter of the arteries using Myoview software (DMT, Aarhus, Denmark). Arteries were superfused with physiological saline solution (PSS) at 37∘C equilibrated with 5% CO_2–95% air. The chamber cover is placed over the pressure myograph chamber connecting the temperature sensor, the CO_2 supply (to prevent calcium carbonate precipitation) and the drain system (to remove the excess of PSS).

The endothelium was removed, prior to pressurization of the artery, by passing air bubbles through the lumen for a few seconds. Viability of mesenteric arteries was evaluated by their ability to constrict in response to 0.5–1 µM phenylephrine, and the endothelium denudation was confirmed by the absence of dilation in response to 10 µM acetylcholine.

After draining pressure regulator ways with PSS at 37 °C equilibrated with 5% CO_2–95% air, these are connected to myograph unit valves (P1 and P2). First, a slightly flow is maintained along the vessel around 20 minutes, establishing a pressure difference between the inlet and outlet of the vessel. The mounted vessel is gradually pressurised from 10 to 70 mm Hg over a period of about 30 minutes, increasing the pressure in 10mmHg steps every 5 minutes to reach 70mmHg. After this gradual pressurization, the mounted vessel is allowed to equilibrate at an intraluminal pressure of 70mm Hg in a "No-flow" state for about one hour before starting the experiment. During this period, around 30–50% of the mounted arteries developed significant myogenic tone.

d. Myography protocols

Different experiments were performed using the MyoViewTM software, where the inlet as the outlet pressure, temperature and the duration of each parameter can be controlled. When a dilatory response was tested, initial constriction was potentiated by adding 0.5-1 µM phenylephrine to facilitate analysis of the response. All chemical agents were added to the superfusate. At the end of each experiment, vessels were superfused either with a solution

containing 10 μM nifedipine or with a 3 mM EGTA, Ca^{2+}-free PSS solution to determine maximal vessel diameter upon relaxation.

For characterization of the myogenic response, pressure–diameter curves elicited by pressure steps from 20 to 140 mmHg were obtained in control conditions (active tone) and in the presence of 10 μM nifedipine (passive tone), and myogenic tone was defined as the difference between the two curves. The myogenic tone was defined in correspondence with the following equation:

$$Myogenic\ Tone\ (\%) = \frac{D_{nif} - D_{control}}{D_{nif}} \cdot 100$$

For study of the contribution of K_{IR} and K_{ATP} channels to vessel excitability, we determined the changes in diameter elicited by selective blockers and/or openers of the channels at least at two different pressure values. Data analysis was performed with Origin 7.5 software.

3.5.8 Calcium imaging methods

a. TIRF technique

Total internal reflection fluorescence (TIRF) microscopy is a high signal-to-noise ratio technique that can be used to obtain a very thin optical section specimen whilst background noise (Axelrod, 2001).

TIRF utilises the evanescent field created when a beam of light strikes an interface between two media with different refractive indices, such as glass (n=1.51) and watter (n=1.33). When a beam of light hits an interface between the medium in which it is travelling an a medium of lower refractive index, part of the beam is refracted and part is reflected. The relative proportions of refracted and reflected light depend on the angle that the beam strikes the interface (termed the angle of incidence). As the angle of incidence increase, the amount of light reflected also increases. Once the angle of incidence exceeds a known as the critical angle all light is reflected. This is known as total internal reflection.

Equation for calculate the critical angle:

$$\theta_c = sen^{-1} \frac{n_2}{n_1}$$

where, θ_c= critical angle, n_1= refractive index of first medium (glass) and n_2= refractive index of second medium (water).

When light is totally internally reflected, some of the incident energy generates a very thin electromagnetic field that penetrates into a second medium (Figure 3.14). The intensity of this

field decreases exponentially as it moves away from the interface and, as such, is called the evanescent vawe.

The evanescent wave retains the frequency of the incident light and is capable of exciting fluorophores within approximately 100nm of the coverslip, it gives a very thin optical section that eliminates background fluorescence.

b.   Through-the lens technique

In the through-the-lens technique, the angle of illumination is varied by positioning the light beam off-axis at the back focal plane of the objective. The further off-axis the beam is positioned, the higher the angle of the incident beam and, therefore, the thinner the optical section.
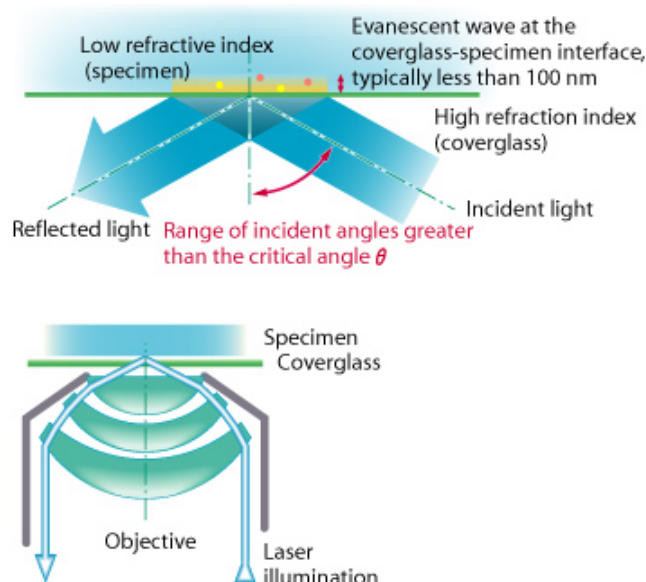

Figure 3.14. Creation of evanescent wave at the coverglass-specimen interface (upper panel) and through-the-lens laser TIRF.

c.   "Sparklets" records

Ca^{2+} sparklet images were acquired using a through-the-lens TIRF microscope built around an inverted Olympus IX-71 microscope equipped with an Olympus PlanApo TIRF (60X, NA = 1.49) oil immersion lens and an Andor iXON 597 EMCCD camera. Images were acquired at 100 Hz using TILL Image software. To monitor $[Ca^{2+}]_i$, cells were loaded with the calcium indicators fluo-5F (Invitrogen). Excitation of fluo-5F was achieved with 488 nm solid state argon laser. Excitation and emission light was separated with the appropriate set of filters. Ca^{2+} sparklets were recorded in cells exposed to 1 μmol/L thapsigargin to eliminate Ca^{2+} release from intracellular stores.

Background-subtracted fluorescence signals were converted to concentration units using the "F_{max}" equation (Maravall *et al.*, 2000):

$$[Ca^{2+}] = K_d \cdot \frac{F/F_{max} - 1/R_f}{1 - F/F_{max}}$$

Where:

F is fluorescence. Fmax is the fluorescence intensity of fluo-5F in the presence of a saturating free Ca^{2+} concentration. K_d is the dissociation constant of the fluorescence indicator used (fluo-5F = 1280 nmol/L) R_f (fluo-5F = 280) is this indicator's F_{max}/F_{min}. F_{min} is the fluorescence intensity of fluo-5F in a solution where the Ca^{2+} concentration is 0. K_d and R_f values for Fluo-5F was determined in vitro using standard methods (Woodruff *et al.*, 2002). F_{max} was determined at the end of experiments by exposing cells to a solution to which the Ca^{2+} ionophore ionomycin (10 μM) and 20 mM external Ca^{2+} had been added.

Ca^{2+} sparklets were detected and defined for analysis using an automated algorithm written in IDL language. Ca^{2+} sparklets had an amplitude equal to or larger than the mean basal $[Ca^{2+}]_i$ plus 2.5 times its standard deviation. For a $[Ca^{2+}]_i$ elevation to be considered a sparklet, a grid of 3 X 3 contiguous pixels had a $[Ca^{2+}]_i$ value at or above the amplitude threshold. These detection criteria for Ca^{2+} sparklets are similar to those used by other investigators (Cheng *et al.*, 1999;Demuro & Parker, 2004).

Analogous to single-channel data analysis, the activity of Ca^{2+} sparklets is determined by calculating the "nPs" of each sparklet site, where n is the number of quantal levels and Ps is the probability that a quantal Ca^{2+} sparklet event is active. To do this, we used the single channel analysis module of pCLAMP 10.2. First, $[Ca^{2+}]_i$ from previously identified sparklet sites were imported into this program, defining a baseline. To estimate nPs, Ca^{2+} sparklet events were detected using pCLAMP's "threshold detection analysis" using no duration constraints and a unitary Ca^{2+} elevation of 38 nM as a starting point for event detection (note that the amplitude of the unitary event was not fixed). Each one of the events detected with this analysis were then cross-referenced with the original image stack to verify that they met the amplitude and spatial criteria described above. Only Ca^{2+} influx events that met the spatial and amplitude criteria were used to estimate nPs for each experimental condition.

As previously reported (Navedo *et al.*, 2005), Ca^{2+} sparklet activity was bimodal in arterial myocytes, with sites of low activity and sites of high activity. Based on this behavior, Ca^{2+} sparklets were grouped into two categories: low (*nPs* between 0 and 0.2), and high (*nPs* higher than 0.2).

Amplitude histograms were constructed using the amplitudes of the detected Ca^{2+} sparklet events. By simultaneously recording single Ca^{2+} channel currents and Ca^{2+} sparklets in arterial myocytes, it has been reported that at -70 mV and with 20 mM external Ca^{2+} a single Ca^{2+} channel current of ≈0.5 pA produced a Ca^{2+} sparklet of ≈37 nM (Navedo *et al.*, 2005). As shown in figure 4.37, histograms from all $[Ca^{2+}]_i$ records obtained from arterial myocytes had multiple, clearly separated peaks and could be fit with the following multi Gaussian function.

$$N = \sum_{j=1}^{n} a_j \cdot \exp\left[-\frac{([Ca^{2+}]_i - jq)^2}{2jb}\right]$$

Where a and b are constants, $[Ca^{2+}]_i$ and q are intracellular Ca^{2+} and the quantal unit of Ca^{2+} influx, respectively. The term "quantal" is defined as the minimum amount of Ca^{2+} influx through LTCCs. Using this analysis, a q value of 37 nM was obtained in the histogram, a value that is similar to that obtained in previous stidies (Navedo *et al.*, 2005). This analysis provides further support to the hypothesis that Ca^{2+} sparklets are quantal in nature and that the size of Ca^{2+} sparklet depends on the number of quanta activated.

d. "Sparks" records

Imaging of Ca^{2+} sparks was performed on cells loaded with the fluorescent Ca^{2+} indicator fluo-4-AM (F14201, Invitrogen). VSMCs were loaded with 3 µM fluo 4-AM for 15 minutes at RT in the perfusion chamber. Fluorescence was recorded using a livescan swept field confocal system (Nikon) coupled to a Nikon TE300 inverted microscope equipped with a Nikon 60x water immersion lens (numerical aperture N.A=1.4) (Nikon Inc., Melville, New York, USA). Ca^{2+} sparks were imaged using the line-scan mode of the confocal microscope. Images were analyzed using custom software written in IDL language (Research Systems Inc, Boulder, Colorado, USA). Ca^{2+} sparks were identified using a computer algorithm similar to the one used in sparklets records. Images were normalized by dividing the fluorescence intensity of each pixel (F) by the average resting fluorescence intensity (F_0) of a confocal image to generate an F/F_0 image.

3.5.9 Maintenance and transfection of cultured HEK cells

HEK293 cells were maintained in Dulbecoo's modified Eagle's medium (DMEM) supplemented with 10% fetal bovine serum (Gibco), 100 U ml^{-1} penicillin, 100 g ml^{-1} streptomycin and 2 mM L-glutamine. Cells were grown as a monolayer to confluences up to 80% in 35 mm Petri dish prior to transfection. Transient transfections were performed using Lipofectamine 2000 (Invitrogen) according to manufacturer instructions, with 1 µg of plasmid DNA encoding Cav1.2

alone or in combination with 2 μg of plasmid DNA encoding $\alpha_2\delta$ and β_2 subunits (molar ratio Cav$_{1.2}$: $\alpha_2\delta$: β_2; 1 : 2 :2). In all cases, 0.2 μg of plasmid DNA encoding the green fluorescent protein (GFP) was included to permit transfection efficiency estimates (20–60%) and to identify cells for voltage-clamp analysis. The plasmids pCARDI-Cav$_{1.2}$ (Mikami *et al.*, 1989), pKCR-$\alpha_2\delta$ (Zong *et al.*, 1994) and pS13-β_2 were provided by Dr A. Castellano (Instituto de Biomedicina de Sevilla (IBIS), Universidad de Sevilla, Spain).

After transfection, cells were tripsinized and plated on glass coverslip for electrophysiological experiments.

4 RESULTS

Essential hypertension is a multifactorial disorder and one of the main risk factors responsible for renal and cardiovascular diseases. Essential HTN involves a sustained increase in total peripheral resistance (TPR), which is dynamically regulated by the vasoconstriction/dilation state of VSMCs within small "resistance" arteries wall, the so called vascular tone. Contraction of VSMCs is ultimately dependent on an increase of intracellular calcium concentration ($[Ca^{2+}]_i$). The major pathways for this increase are the influx through voltage-dependent Ca^{2+} channels (VDCC) and non-selective cation channels at the plasma membrane or release from intracellular stores through the internal store release channels. There is a well-established correlation between vascular tone and resting membrane potential (V_M) of VSMCs (Nelson & Quayle, 1995). Global $[Ca^{2+}]_i$ is mainly regulated by the open probability of VDCC, which is finely controlled by the membrane potential (V_M). Thus, there is a close coupling between V_M, Ca^{2+} influx, $[Ca^{2+}]_i$ and force maintenance in VSMC, implying that factors that modulate V_M have a direct effect on contraction and vascular resistance. As a major regulator of V_M, the K^+ channels are important determinant of vascular tone and blood vessel diameter (Dick & Tune, 2010).

4.1 ESSENTIAL HYPERTENSION MOUSE MODEL

The role of VSMCs potassium channels (in particular K_{IR}, K_{ATP} and BK_{Ca}) and L-type calcium channels (LTCCs) in the genesis and mainteninance of hypertension was studied in this work using a mouse model of essential hypertension.
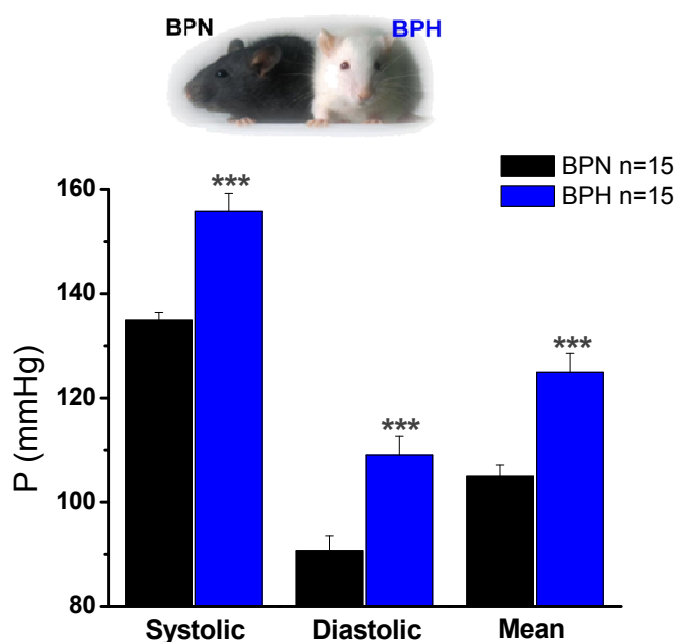

Figure 4.1 Systolic, diastolic and mean arterial blood pressures are more elevated in hypertensive BPH than normotensive BPN mice. Bar graphs showing different pressures were obtained from BPN (n=15) and BPH (n=15) mice by tail cuf. *** indicates P<0.001 when compared BPH and BPN mice.

This model consists in hypertensive (BPH) and normotensive (BPN) mice strains obtained by phenotypic selection. These lines share a comparable genetic background as they were obtained by crossbreeding of eight different mice strains (Schlager & Sides, 1997).

BPH and BPN diastolic, systolic, and mean arterial blood pressures were measured by tail-cuff sphygmomanometer in conscious mice. At 12 weeks of age, diastolic, systolic, and mean arterial pressures were ≈ 20 mm Hg higher in BPHs than BPN mice. (Figure 4.1).

4.1.1 Characterization of VSMC excitability in BPN and BPH mesenteric arteries

Essential hypertension is associated with physiological and morphological changes in blood vessels including phenotypic changes in vascular smooth muscle cells, hypertrophy, as well as arterial hyperreactivity (Anwar *et al.*, 2012).

Pressure-induced changes in vessel diameter in both BPH and BPN mesenteric arteries were explored with a pressure myograph as depicted in Figure 4.2.
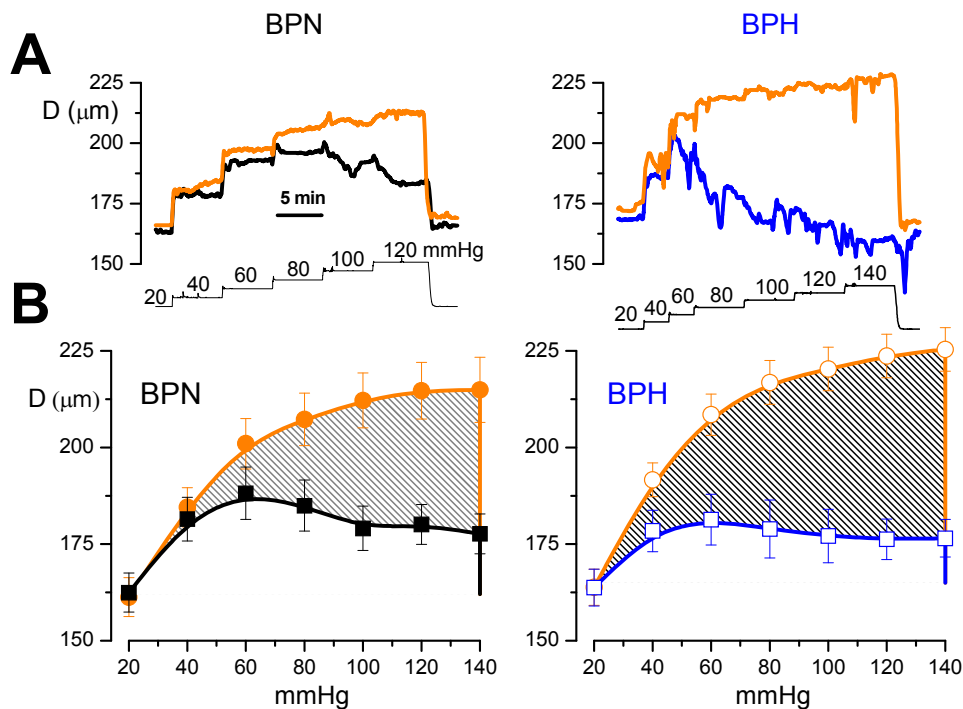
Figure 4.2 A: Pressure–diameter curves obtained from mesenteric BPN and BPH arteries mounted on a pressure myograph, and subjected to step pressure changes (in mmHg) with the protocol shown in the insets. For each artery, pressure protocol was applied in control conditions (active diameter, Dcontrol, squares) and in the presence of nifedipine (passive diameter, Dnif, circles). B: The average diameters obtained at the different pressures studied from m11 arteries in each group are shown in the lower panels. The shaded areas represent the difference between passive and active diameter, i.e. the myogenic tone

In each preparation, the pressure–diameter relationship was determined under control conditions (active diameter curves) and in the presence of 10 µM nifedipine (passive diameter curves). The difference between passive and active diameter at each pressure (Figure 4.2B, shaded areas) is a measure of the myogenic tone. Myogenic tone was significantly larger at all pressures in BPH mesenteric arteries, suggesting an increased vascular reactivity in the hypertensive animals (Figure 4.3).
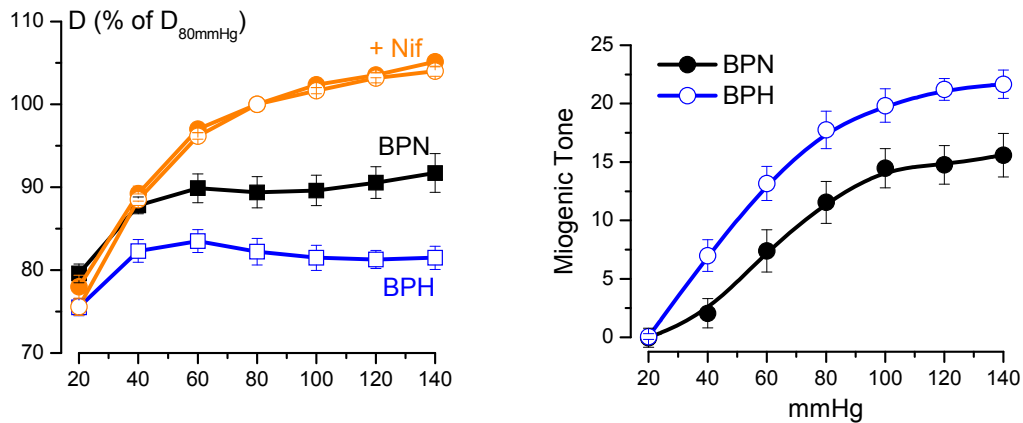

Figure 4.3 The left panel shows passive diameter (nifedipine, circles) and active diameter (squares) after normalizing each artery to the passive diameter obtained at 80 mmHg. The average myogenic tone obtained from BPN and BPH arteries and measured as 100 × (Dnif – Dcontrol)/Dnif is represented in the right panel. n = 11 and 12 for the BPN and BPH groups, respectively.

Since vascular tone is very dependent of V_M, we have measured resting V_M in freshly dissociated VSMCs under the current-clamp (I=0) perforated patch configuration (Figure 4.4). We found a clear difference between BPH and BPN cells. Resting V_M was approximately -35.2 ± 1.3 mV in VSMCs from BPH, significantly more depolarized than resting V_M in VSMCs from BPN (-45.8 ± 1.7 mV). These results are in agreement with previous data obtained in our laboratory (Moreno-Dominguez *et al.*, 2009).
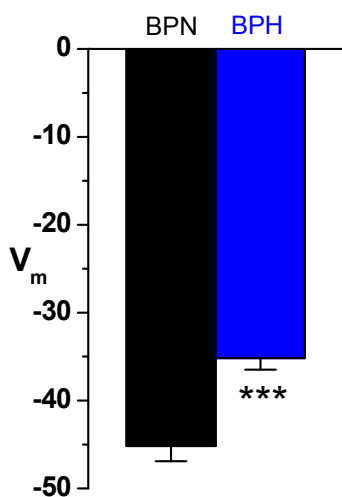

Figure 4.4 Resting V_M was obtained with direct measurements from current-clamp experiments. Data are from 37 BPN and 34 BPH cells

In order to determine the ionic currents underlying the differences in resting V_M between BPN and BPH cells, we characterized the total ionic currents in both cases under voltage clamp with the perforated patch configuration of the patch-clamp technique. Currents elicited with voltage ramps between -150 mV and +30 mV, in the presence of Standard$_e$ bath solution, showed clear differences between BPN and BPH VSMCs (Figure 4.5).
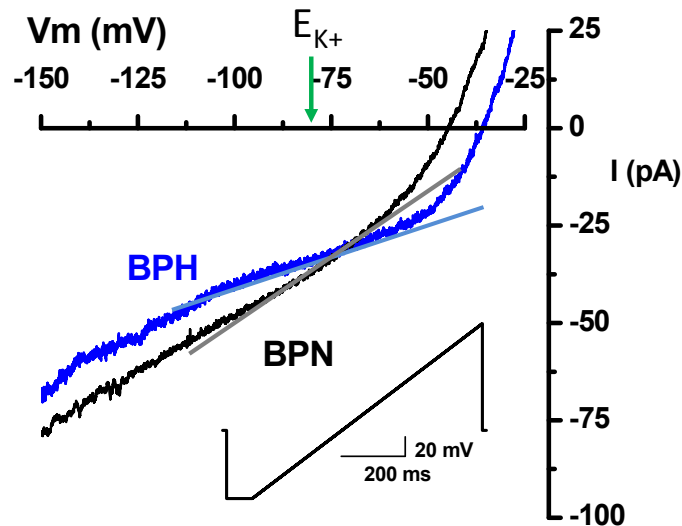

Figure 4.5 *Currents obtained in depolarizing ramps from −150 to +30 mV (ramp protocol show in the inset graph) in acutely dissociated VSMCs from BPN and BPH mesenteric arteries. Currents were recorded with the perforated patch configuration of the patch-clamp technique while cells were bathed in standard saline solution. Each trace is the average current from 9–11 cells. E_{K+} -80 mV in our experimental conditions where the slope conductances were caclculated.*

Currents depicted in Figure 4.5 are average traces obtained in BPN (n=9) and BPH (n=11) cells. A simple inspection of the data reveals that BPH cells (as compared to BPN) show:

- A decrease of the current elicited at hyperpolarizing potentials.

- A decrease in the slope conductance of the current voltage relationship at potentials around -80 mV (the estimated E_K).

- A more depolarized resting V_M (membrane potential at I = 0).

- An increase in the slope conductance at the values around V_M.

The slope conductance at certain voltage is the gradient of the tangent to the curve at that voltage, indicating how the membrane changes with voltage from one conductive steady state to another. On the other hand, the chord conductance at certain voltage can be simply defined as the ratio between the current and the voltage measured at that potential (Thompson, 1986).
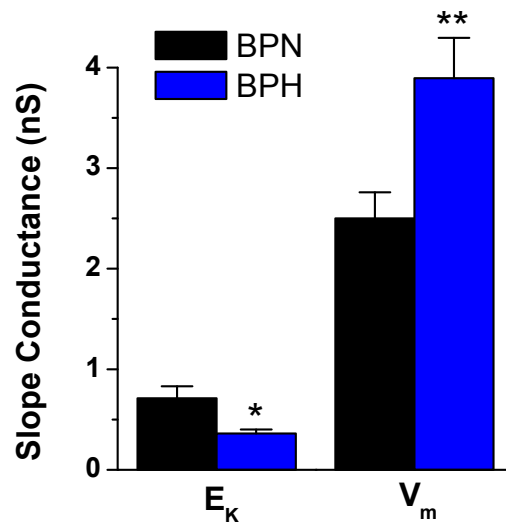
Figure 4.6 *Slope conductance was calculated from the linear fit of the current traces obtained from each individual cell around (±5 mV) E_K (–80 mV in our experimental conditions) and V_M (V at I = 0). Each bar shows the mean ± SEM of 13–16 determinations in each group. $*P < 0.05$, $**P < 0.01$, $***P < 0.001$, Student's t test for unpaired data.*

The averages of the slope conductances measured in each cell both at membrane resting potential and at E_K, are shown in Figure 4.6. Differences were statistically significant both at E_K and at V_M. However, while the slope conductance at E_K is significantly reduced, the changes in the chord conductance at E_K are not statistically different between BPN and BPH cells (0.54±0.046 nS in BPN vs. 0.60±0.08 nS in BPH, p=0.09), indicating that ionic currents mediated by other ions than K^+ are very similar in BPN and BPH VSMCs. These data suggest that the more depolarized V_M observed in VSMCs from BPH mice could be explained by a decrease in K^+ conductance. Furthermore, it seems reasonable to assume that changes in other conductances have only a minimal contribution to the more depolarized V_M observed in BPH VSMCs.

Therefore, we hypothesized that a K^+ conductance relevant at resting V_M is decreased in BPH VSMCs. Since we have already excluded Kv conductances as possible candidates to explain differences in V_M between BPH and BPN cells (Moreno-Dominguez *et al.*, 2009), we decided to explore the role of other K^+ channels such as the fammilly of inward-rectifier channels, K_{IR} and K_{ATP}.

4.2 CHARACTERIZATION OF INWARD-RECTIFIER CHANNELS IN VSMCs FROM BPN AND BPH MICE

4.2.1 mRNA expression profile of inward-rectifier channel subunits

In order to study the contribution of inward rectifiers to modulate V_M in BPN and BPH VSMCs, we decided to start by characterizing the expression profile of the channel subunits encoding inward-rectifier K^+ channels in mesenteric VSMCs as well as in several other vascular beds from BPN and BPH mice. The genes explored included members of K_{IR} subfamilies (Kir1-6) as well as the SUR2 subunit. A total of 10 channel genes were studied, together with control genes such as calponin as a control for VSMC, endothelial nitric oxide synthase (eNOS) as a control for endothelial cell contamination and ribosomal protein 18S (RP18S) as endogenous control for the qPCR. The preparations studied included VSMCs from aorta, femoral, renal, mesenteric and cerebral arteries of BPN and BPH animals, and two non-vascular preparations, cardiac muscle cells from the left ventricle and nervous tissue from the prefrontal cortex. In all cases, we explored both the relative abundance of the channel genes expressed in the normotensive preparations and the changes observed in the BPH animals. These data are summarized in figures 4.7-4.10.
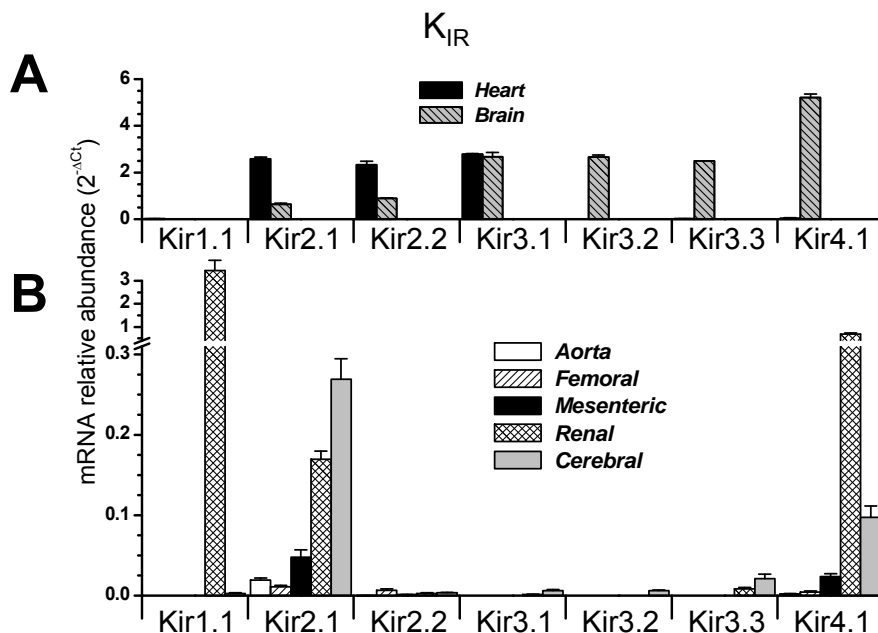
Figure 4.7 *Expression levels of K_{IR} channel genes explored were determined in two control tissues (heart and brain, A panel)) and five vascular beds (aorta, femoral, mesenteric, renal and cerebral, B panel). Expression levels are normalized with respect to RP18S. Relative abundance was expressed as 2−ΔCt, where ΔCt = Ct$_{channel}$−Ct$_{18S}$.*

Figures 4.7 and 4.8 show the relative abundance of all the genes studied in both control tissues (heart and brain) and vascular tissues (aorta, femoral, mesenteric, renal and cerebral), and

figure 4.9 and 4.10 depict their changes upon hypertension only in VSMCs, as no changes in these genes were detected when comparing heart and brain preparations from BPN and BPH mice (data not shown). The expression level of K_{IR} channels (Figure 4.7) and K_{ATP} (Figure 4.8) are represented in different plots due to the higher expression of K_{ATP} channels (note the different scales).

We found that Kir2.1 and Kir4.1 are expressed in all vascular beds studied, being more abundant in mesenteric, renal and cerebral vessels (Figure 4.7B). Kir1.1 is also especially abundant in renal arteries whilst Kir2.2 and Kir3.x are minimally represented. As previously described, K_{IR} channel genes are abundantly expressed in brain (all but Kir1.1) and in cardiac tissue (Kir2.x and Kir3.1) (Figure 4.7A). Regarding K_{ATP} channel genes, we detected high levels of mRNA expression for Kir6.1 channel and SUR2 receptor, the main constituents of the vascular K_{ATP} channels (Seino & Miki, 2004) in all vessels studied. The more abundant expression of Kir6.2 mRNA in cardiac and neural tissues is also consistent with previous reports (Figure 4.8).
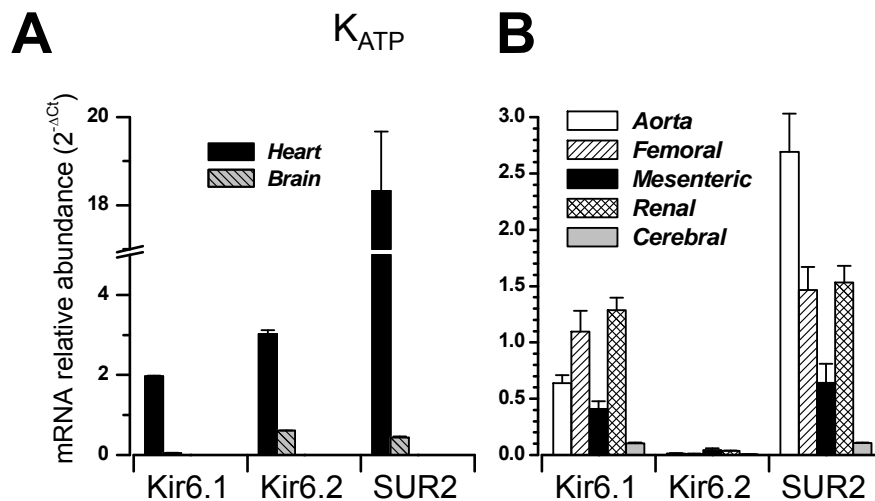
Figure 4.8 *Expression levels of K_{ATP} channel genes in control tissues (A) and in vascular tissues (B).*

Expression changes in BPH are depicted in figure 4.9 and 4.10. In these plots, positive values represent increased levels of expression compared to BPN whilst negative values represent decreased expression (see methods). The most relevant changes were the lower expression of Kir2.1, Kir4.1 (Figure 4.9) and SUR2 (Figure 4.10) in BPH mesenteric arteries, as well as the general decrease in the expression of Kir6.1 in all BPH vascular beds tested (Figure 4.10). Other significant changes were the evident increase of Kir1.1 in renal arteries and Kir3.2 (Figure 4.9) and SUR2 (Figure 4.10) in cerebral arteries. Other changes, although statistically significant, may be considered less relevant if we take into account the low levels of expression.

Altogether, these data show that the hypertensive phenotype associates with a decrease in the expression pattern of the mRNA encoding the most abundant vascular K_{IR} channels (Kir2.1, Kir4.1 and Kir6.1 and SUR2 channels). Of note, all changes are found in the mesenteric bed, pointing to these arteries as a good model to study their functional impact.
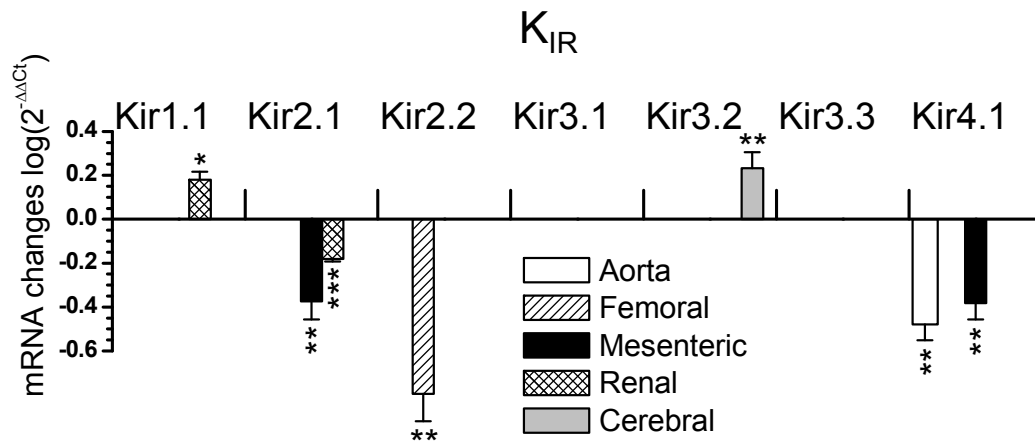
Figure 4.9 *Changes in K_{IR} channel expression in BPH arteries (using BPN expression levels as calibrator) in all the vascular beds explored. The changes were calculated as 2−ΔΔCt, where ΔΔCt = ΔCt$_{(BPH)}$ − ΔCt$_{(BPN)}$. Data are represented on log scale, so the absence of changes will give values close to 0, negative values mean decreased expression and positive values increased expression. Statistical analysis in this plot was by Student's t test for two independent samples (ΔCt$_{(BPH)}$ and ΔCt$_{(BPN)}$) obtained with RP18S as endogenous control. For the shake of clarity, only statistically significant changes are plotted. Each bar shows the mean of 6–12 determinations obtained in 3–6 duplicate assays. ∗P < 0.05, ∗∗P < 0.01, ∗∗∗P < 0.001.*

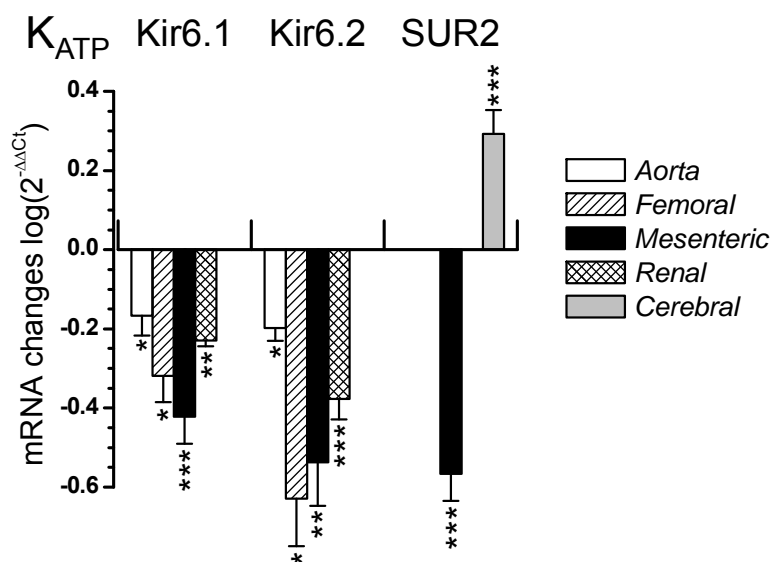**Figure 4.10** *Changes in K_{ATP} channel mRNA expression levels in BPH vs BPN arteries in all the vascular beds explored.*

4.2.2 Expression of K$_{IR}$ and K$_{ATP}$ channels-encoding proteins in BPN and BPH VSMCs

Next we determined whether the mRNA changes correlate with protein expression levels of VSMCs extracts obtained from BPN and BPH mesenteric arteries. Figures 4.11 and 4.12 show representative immunoblots for Kir2.1, Kir4.1, Kir6.1 and SUR2 proteins with their quantification from 3-5 different experiments (bar plots). In agreement with the mRNA expression levels, we found a decreased expression of all the proteins in BPH VSMCs, although this decrease was not statistically significant for Kir2.1 protein. Changes in expression were particularly large in the case of Kir6.1 channels (Figure 4.12), in which protein levels were hard to detect in BPH samples.
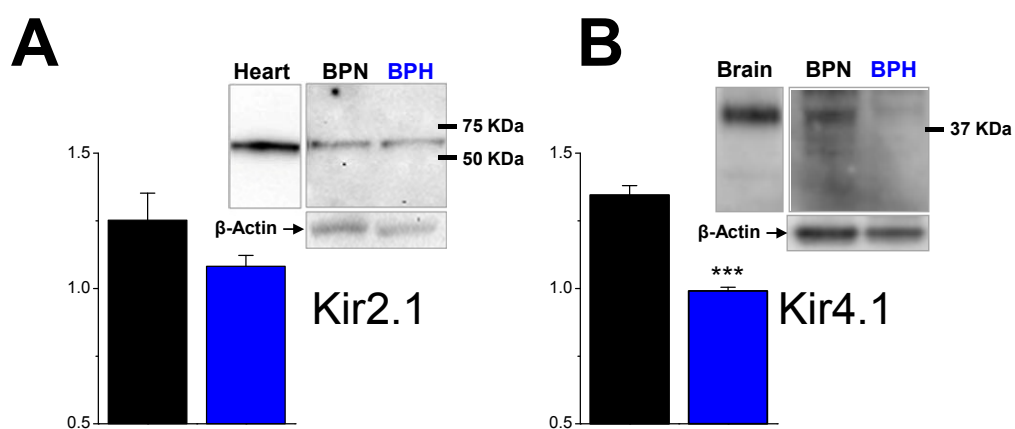
Figure 4.11 *Expression of Kir2.1 and Kir4.1 proteins in BPN and BPH mesenteric VSMCs. Representative immunoblots of mesenteric VSMC lysates from BPN and BPH arteries showing a band of the expected size for Kir2.1 and Kir4.1 as indicated. Loading control (β-actin) of the same membranes is also shown, as well as positive controls for the antibodies (heart homogenates for Kir2.1 and brain lysates for Kir4.1). Quantification of these data (bars plots) was obtained via densitometric analysis of 3–5 immunoblots for each antibody, normalized to their corresponding β-actin signals. ∗∗P < 0.01, ∗∗∗P < 0.001.*
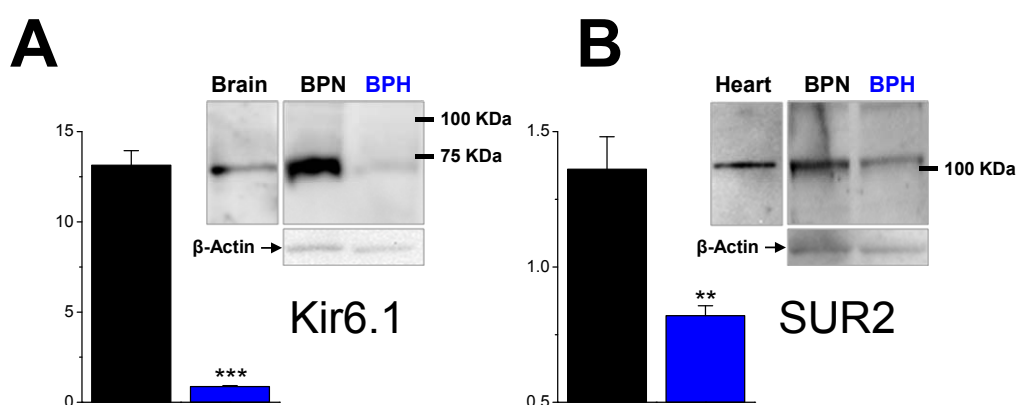
Figure 4.12 *Expression of Kir6.1 and SUR2 proteins in BPN and BPH mesenteric VSMCs. Here also shown positive controls for the antibodies (brain lysates for Kir6.1 and heart homogenates for SUR2).*

4.2.3 Functional characterization of K_{IR} and K_{ATP} channels in isolated VSMCs

The functional expression of inward rectifying K^+ channels was evaluated with electrophysiological studies in freshly dispersed mesenteric VSMCs from BPN and BPH mice. Membrane currents were studied using a ramp-pulse protocol as the one shown in figure 4.5 Total current density at -150 mV was significantly larger in BPN cells than in BPH (-9.6 ± 1.6 pA/pF versus -6.4 ± 0.69 pA/pF, p<0.05, n=20 cells in each group). This decrease in current density is due to a small decrease in the total current amplitude in BPH cells (see averaged data in figure 4.5) and to an increase in the cell size of the VSMCs from BPH mesenteric arteries, as previously reported (Moreno-Dominguez *et al.*, 2009).
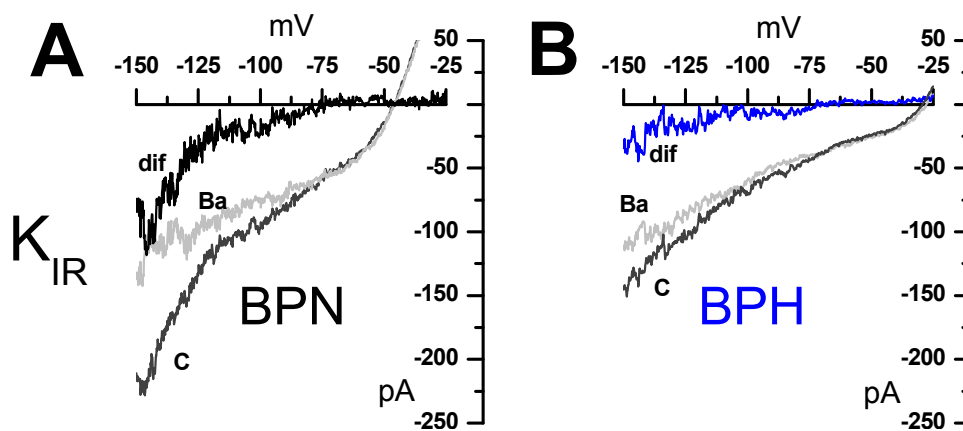
Figure 4.13 *Pharmacological dissection of K_{IR} in BPN (A) and in BPH (B) mesenteric VSMCs. K_{IR} currents were defined as the fraction of current sensitive to 100 µM BaCl$_2$ (dif, black and blue for BPN and BPH respectively), and were obtained by subtracting current traces elicited by voltage ramps in the presence of BaCl$_2$ (Ba, light gray) from traces in control conditions (C, gray). Sample traces were obtained using the perforated patch configuration.*
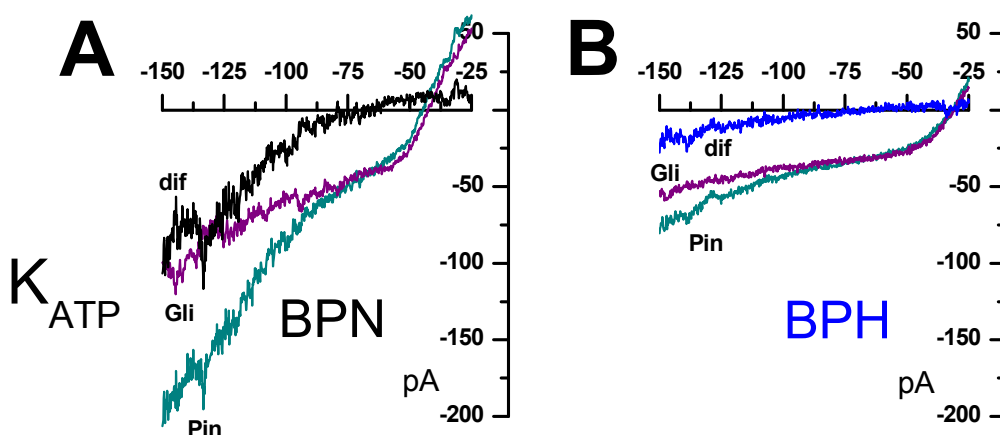
Figure 4.14 *Pharmacological dissection of K_{ATP} in BPN (A) and in BPH (B) mesenteric VSMCs. K_{ATP} currents were defined as the difference (dif, black and blue for BPN and BPH respectively) between currents recorded in the presence of 100 µM pinacidil (Pin, cyan) and currents recorded in the presence of 20 µM glibenclamide (Gli, purple). Current–voltage plots show representative traces obtained with the perforated patch configuration.*

A pharmacological approach was used to dissect the contribution of both K_{IR} and K_{ATP} channels to the total current. K_{IR} currents (Figure 4.13) were defined as the 100 µM $BaCl_2$-sensitive fraction of the current, whereas K_{ATP} currents (Figure 4.14) were estimated as the difference between the current in the presence of 100 µM pinacidil and the current in the presence of 20 µM glibenclamide.

Figure 4.13 and 4.14 show representative examples of the effect of these drugs on the currents recorded from BPN and BPH cells in perforated-patch experiments, and the estimated K_{IR} and K_{ATP} currents. In both cases, the small size of the currents and the inward rectification preclude a reliable estimation of the reversal potential of the subtracted currents, although in all cases it approximated the estimatedvalue for E_K.

The average density at -150 mV of the 100 µM $BaCl_2$-sensitive component of the current (the K_{IR} current) both with perforated-patch and with whole-cell experiments is represented in figure 4.15A. In the same way figure 4.15B shows the average K_{ATP} current density at -150 mV. A comparison of the bar plots of these two figures (figure 4.15A and B) shows that K_{ATP} currents in BPN cells represented a larger fraction of the total outward current than K_{IR} currents (values in perforated patch were -4.28 ± 0.77 pA/pF and -2.11 ± 0.32 pA/pF respectively). Also, when comparing with BPH cells, the decrease in the fraction of the current due to K_{ATP} channels was larger than the decrease of K_{IR} currents. Again, in perforated patch and at -150 mV, K_{ATP} current density in BPH cells represented a 36% of the current in BPN cells, while K_{IR} current density was reduced to a 50% of the BPN current.
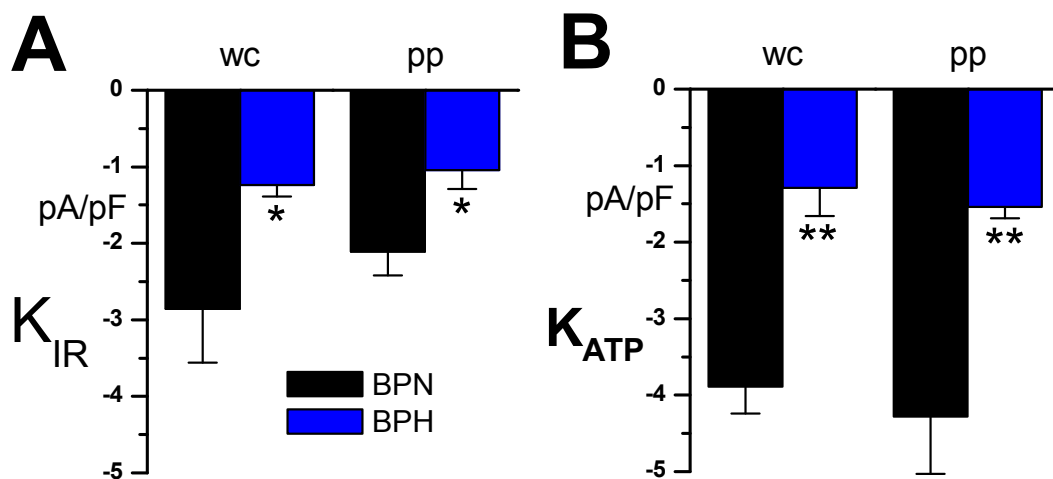

Figure 4.15 *A: K_{IR} average current densities obtained at −150 mV, both with the perforated patch (pp) or the whole-cell configuration (wc) of the patch clamp technique, are depicted in the bar plot. B: bar graphs depict the K_{ATP} average current densities obtained at −150 mV. Each bar, in both A and B, is the mean ± SEM of 7–10 cells. ∗P < 0.05, ∗∗P < 0.01.*

Results

To complete the electrophysiological characterization, we explored K_{IR} and K_{ATP} contribution to mesenteric VSMCs excitability by analyzing the changes in resting V_M observed upon application of selective channel blockers and openers (Figure 4.16 and 4.17). Figure 4.16A illustrates the effect of $BaCl_2$ at two concentrations that are below the reported K_d of K_{ATP} channels for $BaCl_2$ (Ko *et al.*, 2008) and may be considered selective for K_{IR} (30 and 100µM). The depolarizing response to $BaCl_2$ was decreased to 45-60% of that observed in BPN cells (Figure 4.16B).
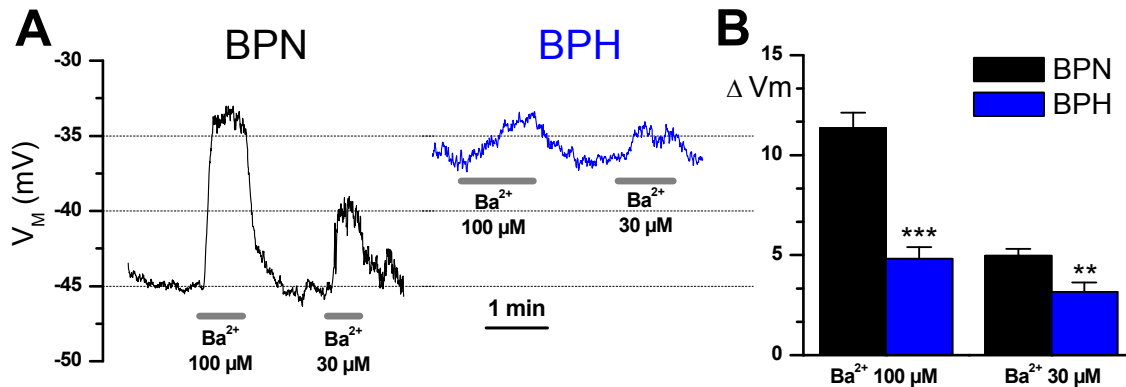
Figure 4.16 *Contribution of K_{IR} channels to resting V_M in BPN and BPH mesenteric VSMCs. A: Current clamp records illustrating the effects of two different $BaCl_2$ concentrations (30 and 100 µM) in representative BPN and BPH cells. B: Bar graphs showing the average data of the barium effects between BPN and BPH cells.*

Figure 4.17A depicts two representative examples of the effects of pinacidil (100µM) and glibenclamide (20µM) in a BPN and a BPH cells. The differences in the response of BPN and BPH cells were very evident in these representative traces and in the averaged data (Figure 17B).

When comparing with the data from figure 4.16B for the effects of the K_{IR} channels blocker, it is clear that the changes in the response to K_{ATP} channel modulators in BPH cells were more prominent (Figure 4.17B). Glibenclamide-induced depolarization was reduced to 33% of that seen in BPN cells, while the hyperpolarizing response to pinacidil was absent in 7 out of 22 cells, and represented on average 17% of the amplitude of the response in BPN cells. If we assume that pinacidil and glibenclamide open and close respectively all available channels, we can estimate the percentage of K_{ATP} channels open at rest as shown in Figure 4.17C. Whilst there are around 50% of K_{ATP} channels open at rest in BPN cells, this percentage increases to almost 70% in BPH cells.
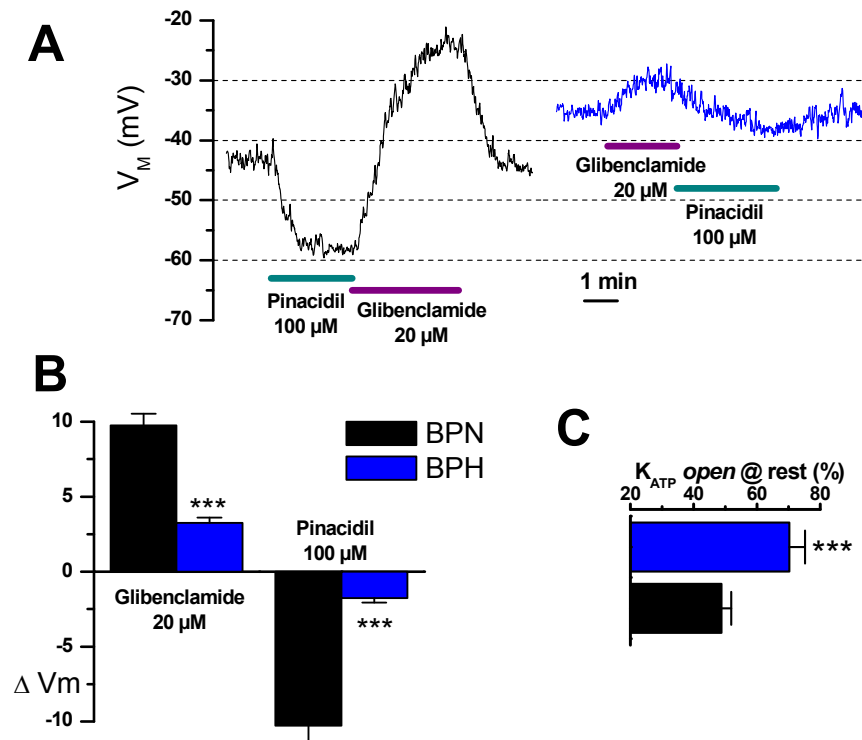
Figure 4.17 *Contribution of K_{ATP} channels to resting V_M in BPN and BPH mesenteric VSMCs. A: The upper graph shows a record illustrating the effects of 100 µM pinacidil and 20 µM glibenclamide in BPN and BPH cells. B: Both resting V_M and the amplitude of the drug-induced changes are clearly different between BPN and BPH cells. These differences were consistent and significant, as shown in the summary data on the bar graphs. n = 9–18 cells in each group, Student's unpaired t test. C: Horizontal bar plot shows the fraction of K_{ATP} channels that are open at resting membrane potential, calculated as 100 × ΔV_M,glibenclamide/(ΔV_M,glibenclamide + ΔV_M,pinacidil). Each value is the mean ± SEM of 18 (BPN) and 16 (BPH) cells. ∗∗P < 0.01, ∗∗∗P < 0.001.*

4.2.4 Characterization of K_{IR} and K_{ATP} channel contribution to vascular tone in pressurized mesenteric arteries from BPN and BPH mice

The functional data obtained in isolated VSMCs showed a good correlation with the expression data for Kir2.1, Kir4.1 and Kir6.x channels, suggesting that the decreased expression of K_{IR} and K_{ATP} channels could be contributing to the hypertensive phenotype. To explore this hypothesis, we studied the effects of pharmacological modulation of these channels on the diameter of BPN and BPH mesenteric arteries pressurized in physiological conditions.

The contribution of K_{IR} channels to vascular tone was analyzed by the changes in diameter observed in response to increasing $BaCl_2$ concentrations (Figure 4.18A shows the effects of 3, 30 and 300 µM) at two different pressures, 40 and 100 mmHg. The concentration response curve for the vasoconstriction induced by $BaCl_2$ in BPN and BPH arteries is plotted in Figure 4.18B.
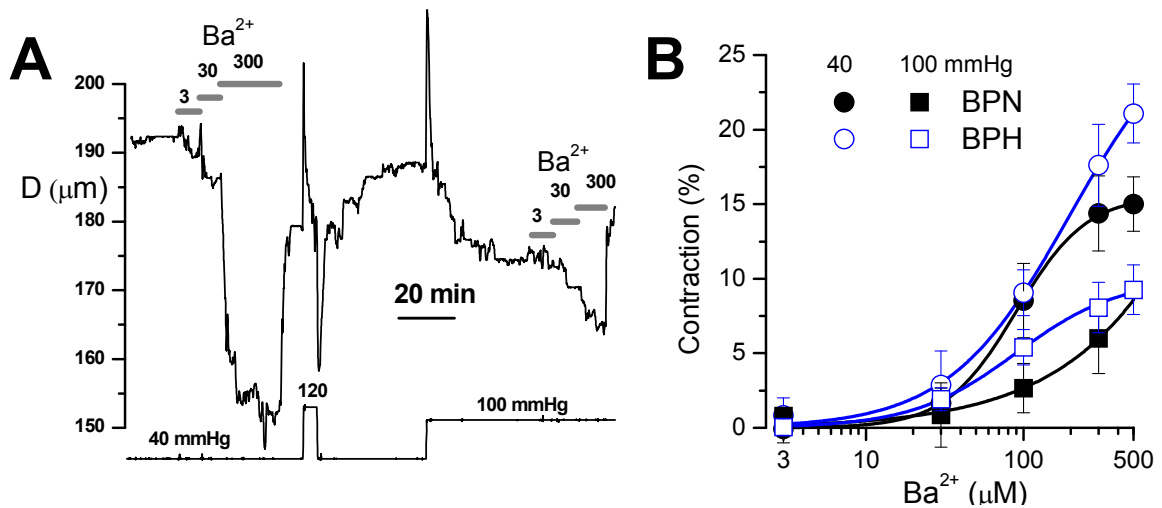
Figure 4.18 *Contribution of K_{IR} channels to vascular tone in mesenteric BPN and BPH arteries. A: time course of the changes in diameter in a BPN artery subjected to the pressure protocol shown at the bottom. At each pressure value, increasing concentrations of $BaCl_2$ were applied as indicated, to obtain a dose–response curve for the barium-induced contraction. Myogenic tone was clearly observed in this artery when pressure was raised from 40 to 120 or 100 mmHg. B, dose–response curves for barium are represented for the two experimental conditions (BPN, grey symbols; BPH, white symbols) and the two pressure values explored (40 mmHg, circles; 100 mmHg, squares). n = 7–8 arteries.*
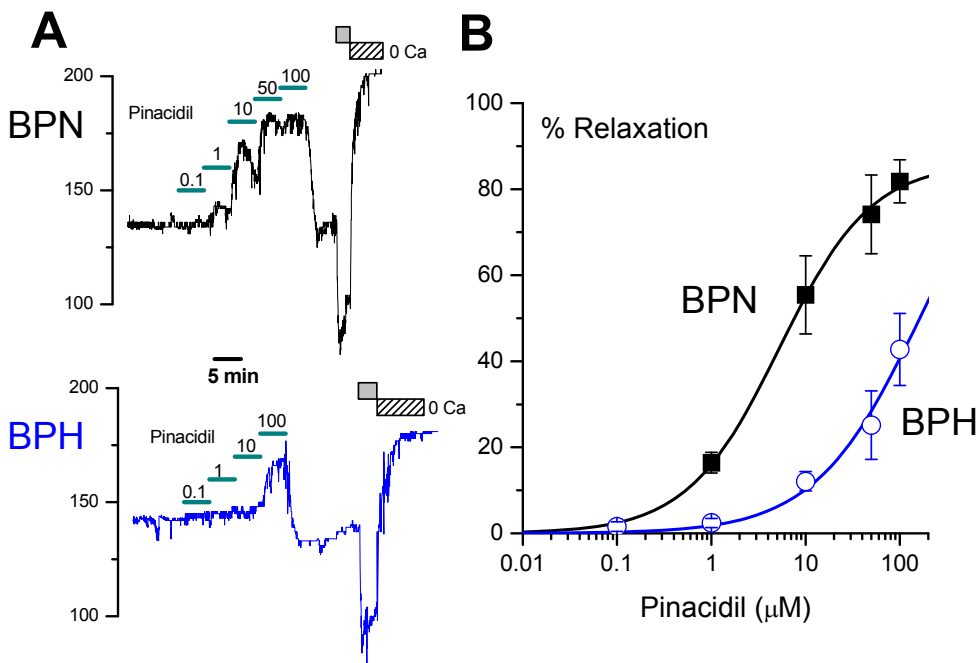
Figure 4.19 *Contribution of K_{ATP} channels to vascular tone in BPN and BPH arteries. A: dose–response effect of pinacidil on the changes in diameter obtained in representative BPN and BPH arteries. The minimal and maximal arterial diameters were determined by sequential application of 10 µM phenylephrine (grey box) and a Ca^{2+}-free solution (hatched box), respectively. B, summary of the effects of pinacidil at different concentrations in BPN (squares) and BPH (circles). Data are normalized to the maximal diameter values obtained in Ca^{2+}-free solution and are expressed as a percentage of relaxation.*

As expected from the well-established correlation between resting V_M of VSMCs and arterial tone (Nelson & Quayle, 1995;Smith *et al.*, 2008), $BaCl_2$ induced contraction was larger at lower vascular pressures. However, no significant differences were observed in the whole organ response between BPN and BPH arteries.

The contribution of K_{ATP} channels to vascular reactivity was explored by analyzing the vasodilation in response to increasing concentrations of pinacidil, ranging from 0.1 to 100 µM (Figure 4.19A). In these experiments, in order to facilitate the analysis of the vasodilatory effect, arteries were preconstricted with 0.5-1 µM phenylephrine and pressure was maintained all through the experiment at 70 mmHg. In this group of experiments the differences in the response of BPH and BPN arteries were evident, as illustrated in figure 4.19B. Both the EC_{50} for the pinacidil-induced relaxation and the maximal vasodilation observed were significantly reduced in BPH arteries, suggesting a decreased contribution of K_{ATP} channels to set the vascular tone in these arteries.

4.3 FUNCTIONAL AND MOLECULAR CHARACTERIZATION OF LTCCS IN VSMCs FROM BPN AND BPH MICE

As mentioned in the introduction, hypertension is associated with an elevation in arterial contractility that increases systemic blood pressure. LTCCs are the primary Ca^{2+} entry pathway in arterial myocytes and are essential for contractility regulation by a wide variety of stimuli, including intravascular pressure, membrane potential, and vasoconstrictors (Wamhoff *et al.*, 2006). To date many studies have shown that hypertension is associated with Ca^{2+} channels abnormalities, including changes in the expression, the trafficking and/or the modulation of LTCCs. LTCCs channels are heteromeric complexes composed of a pore-forming α_1 and auxiliary $\alpha_2\delta$, β and γ subunits. To date, it is unclear whether the subunit composition of arterial myocyte surface LTCCs channels is altered in hypertension, and if so, what can be the functional consequences of this molecular remodeling. For this reason, we investigated whether LTCCS from BPH mesenteric VSMCs exhibit changes in their functional properties as compared to BPN cells, whether these changes are due to disease-associated molecular changes in LTCCs and finally whether these changes could contribute to the altered vascular tone characteristic of hypertension in mesenteric arteries of BPH mice .

4.3.1 Functional characterization of LTCCs channels in isolated VSMCs

First, the functional expression of LTCCs was evaluated with electrophysiological studies in freshly dispersed mesenteric VSMCs from BPN and BPH mice. Membrane currents were studied using 10mM Ba^{2+} as a charge carrier, since LTCCs show a higher permeability to Ba^{2+} than Ca^{2+} (Lee & Tsien, 1984). Inward Ba^{2+} currents were evoked by stepwise depolarizing pulses in 10 mV intervals between -70 mV and +70 mV from a holding potential of -80 mV. Current records were obtained with the whole-cell configuration of the patch-clamp technique (Figure 4.20). BPH and BPN mesenteric VSMCs showed depolarization-activated, inward currents with a tail current on repolarization (Figure 4.20A). The comparison of the traces depicted in part A of the figure 4.20 in a single BPN and BPH cell show clearly that the amplitude of Ba^{2+} currents in BPH cells is significantly smaller than in BPN cells. These differences remain when we express the data as current density (Figure 4.20B).
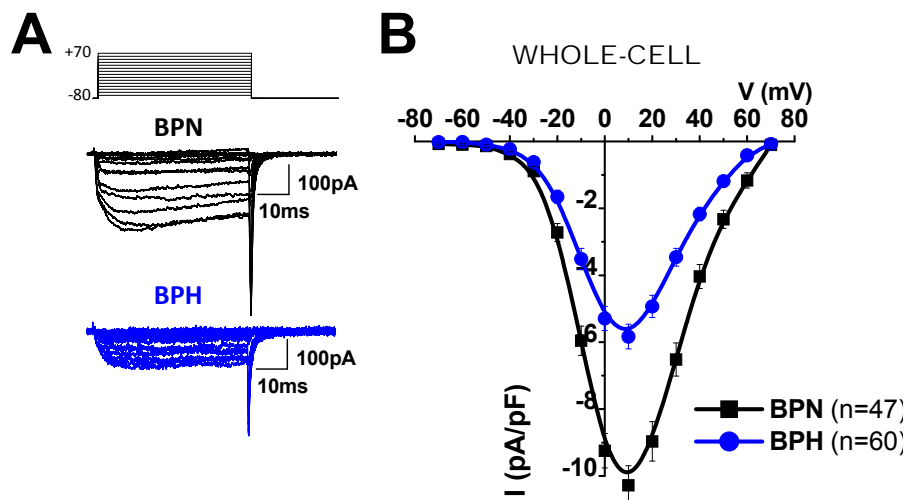
Figure 4.20 *A: Representative traces of VDCCs currents elicited by 10mV steps from -70 mV to +70 mV in mesenteric BPN and BPH VSMCs. Ca^{2+} currents were studied using 10mM Ba^{2+} as charge carrier (more permeable than Ca^{2+} to these channels) using whole cell configuration. B: Average of Ba^{2+} current-density versus voltage curves obtained in BPH (n=60) and BPN (n=47) VSMCs.*

The current density at +10 mV was significantly smaller in BPH cells than in BPN (-5.8 ± 0.4 pA/pF versus -10.2 ± 0.6 pA/pF, p<0.001, n=47 and 60 cells respectively in each group). The voltage-dependence, the time course and the kinetic properties of these currents are typical of the currents mediated by L-type Ca^{2+} channels in VSM cells (Fernandez-Tenorio *et al.*, 2010;Moosmang *et al.*, 2003;Franco-Obregon *et al.*, 1995).

The reduced Ba^{2+} current density observed in BPH VSMCs could be due to some intracellular mediator that could act as an inhibitor of LTCCs and could be differentially expressed in the hypertensive strain. To test this hypothesis, we compared channel activity recorded in

mesenteric VSMCs either under the conventional whole cell configuration with EGTA (10 mM) or under the perforated-patch configuration with amphotericin B (250μg/ml) included in the pipette. Under perforated patch clamp conditions, we found that in both BPN and BPH Ba^{2+} current densities were decreased (Figure 4.21). However, the differences in the current density when comparing BPH relative to BPN were still evident (≈ 49% , -2.5 ± 0.8 pA/pF versus -4.9 ± 0.5 pA/pF).
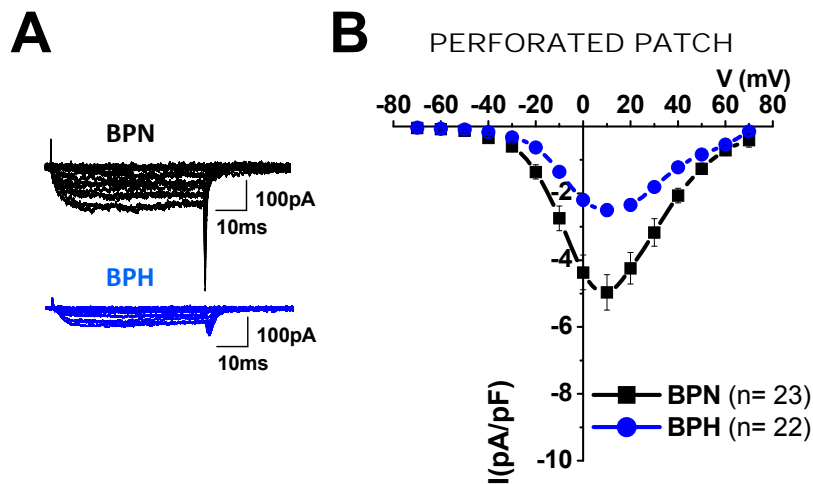
Figure 4.21 *A: Representative Ca^{2+} currents density recordings from BPN and BPH mice arterial smooth muscle cells in perforated-patch configuration. B: IV curves showed a decreased Ba^{2+} current density in BPH relative to BPN.*

The identification of the inward Ba^{2+} currents as mediated by L-type Ca^{2+} channels was accomplished following both kinetic and pharmacological criteria (Catterall *et al.*, 2005), and our results are summarized in figures 4.22, 4.23 and 4.24.

Ba^{2+} currents from both BPN and PBH VSMCs were almost completely blocked by application of a selective blocker of LTCCs such as nifedipine, a dihydropyridine (DHP) antagonist (Figure 4.22). Part A of the figure shows representative records at +10 mV from a BPN and a BPH cell before and during application 5μM nifedipine. Nifedipine reduced peak LTCCs current density in BPN cells to -2.6 ± 0.3 pA/pF and to -1.1 ± 0.1 pA/pF in BPH cells (Figure 4.22B). The effect, expressed as percentage of inhibition at +10 mV, was similar in both strains (Figure 4.22C). Of note, the kinetics and voltage-dependence of the remaining currents were not different from the control curve, before nifedipine application. We did not observe a leftward shift in the current/voltage curve in the presence of nifedipine. That shift would be expected if T-type calcium channels were present. Moreover, the best fit of deactivation curves was obtained with a single exponential (not shown), confirming that only L-type calcium channels were functional both in BPN and BPH VSMCs.
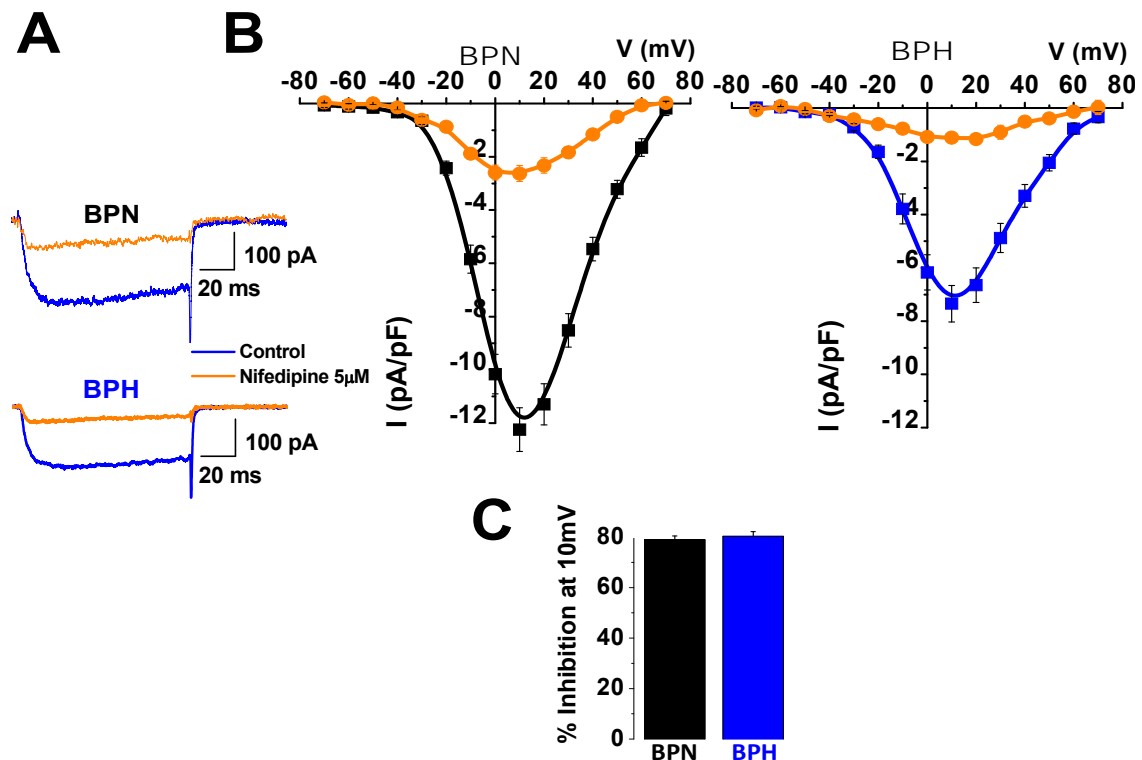
Figure 4.22 A: Representative calcium currents from BPN and BPH VSMCs redorded in control conditions and in the presence of 5µM nifedipine (a dihydropyridine, DHP). B: Mean current density-voltage relationship of BPN and BPH were almost completely blocked by 5µM nifedipine C: The proportion of nifedipine-sensitive current at +10 mV was similar in both strains.

In order to further characterize the electrophysiological and pharmacological properties of the LTCCs we used an agonist of L-type calcium channels, BayK 8644. This DHP increases Ca^{2+} influx through voltage-dependend calcium channels by lengthening the mean open times (Peterson & Catterall, 2006).

Application of 10 µM BayK 8644 led to a dramatic current increase in both experimental groups (Figure 4.23A). Current density at 0 mV increased from -9.24±0.5 pA/pF to -12.6±0.9 pA/pF in BPN and from -5.29±0.3 pA/pF to -10.3±1 pA/pF in BPH, n=33 and 32 cells respectively in each group. The effect of BayK was significantly larger in BPH cells (Figure 4.23B), and the differences in the I/V curves of BPN and BPH cells became smaller (compare with figure 4.20B).
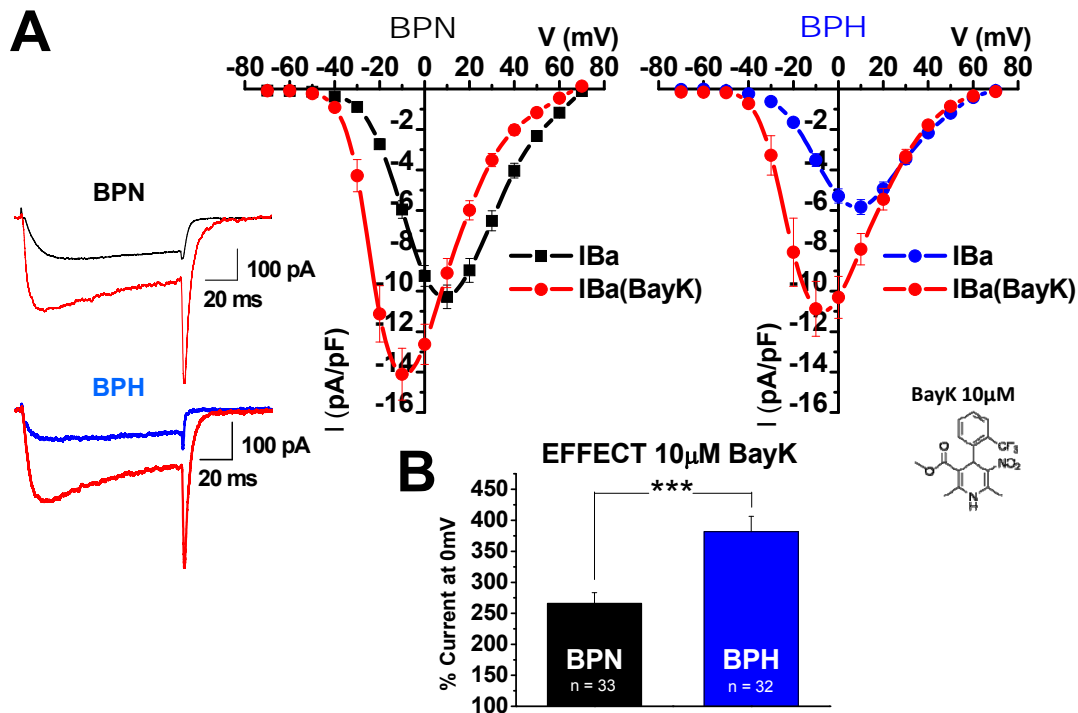
Figure 4.23 *A: Representative Ca^{2+} currents density recordings from BPN and BPH mice VSMCs in whole-cell configuration in control and in presence of the L-type Ca^{2+} channel agonist BayK 8644. Application of BayK led to a dramatic increase of the currents in both experimental groups. However, the potentiating effect of BayK was significantly larger in BPH cells, and the differences in the I/V curves of BPN and BPH cells tend to disappear (compare with figure 4.20B). B. The effect of BayK is represented as the percentage of increase of Ba^{2+} currents at 0mV. *** p<.001*

To compare the voltage-dependent activation of BPN and BPH LTCCs currents in control and in the presence of BayK, we analyzed tail currents to get an estimate of the conductance to voltage (G/V) relationship for each cell. Averaged data in each condition and the corresponding Bolzmann fits are depicted in Figure 4.24.

G/V curves show the same differences between BPN and BPH VSMCs than those observed in the I/V curves: BPN conductaces (data and fits in black) are significantly higher than BPH conductances (data and fits in blue), both in control conditions and in the presence of BayK (Figure 4.24A). Fits to a Boltzmann function were performed individually for each cell and the averaged fit parameters in each condition are depicted in parts B and C of figure 4.24.

Maximal conductances (G$_{max}$) were represented in figure 4.24B. Large and significant differences between BPN and BPH cells can be observed, both in control and in the presence of BayK. However, while in control conditions, BPN G$_{max}$ was 2.96 times higher than BPH (68.08±9.8 *vs.* 24.76±3.5 pS/pF), in the presence of BayK this difference decreased to 1.7 (199.17±26.6 *vs.* 115.71±18.7 pS/pF). These differences in the effect of BayK were analyzed

individually in each cells, and the average ratios between the G_{max} obtained with BayK and the G_{max} obtained in control in BPN and BPH cells are depicted in figure 4.24B (left).

The average voltage for half-maximum Ba^{2+} current activation ($V_{0.5}$) and the steepness (dx) of the Boltzman functions are shown in Figure 4.24C. These parameters were not significantly different between BPN and BPH cells, suggesting that in both cases L-type calcium channels are the only responsible for the inward currents.

Calcium current through LTCC channels can be described by the following equation,

$$I_{Ca} = n \cdot P_o \cdot g_u (V_M - E_{Ca})$$

where **n** is the number of channels in the membrane, **P_o** is the open probability, **g_u** is the unitary single channel conductance, **V_M** is the membrane potential and **E_{Ca}** is the reversal potential for calcium ions. Assuming that BayK effect on **P_o** is similar in BPN and BPH cells, and assuming that **g_u** are also similar, the only factor accounting for a different current is the number of channels (**n**). That is, BPH should have fewer LTCCs in the membrane. Otherwise, the different effect of BayK between both strains could reflect a different modulation of **P_o** by BayK or differences in **g_u** in LTCCs from BPH cells. These differences could be the result of
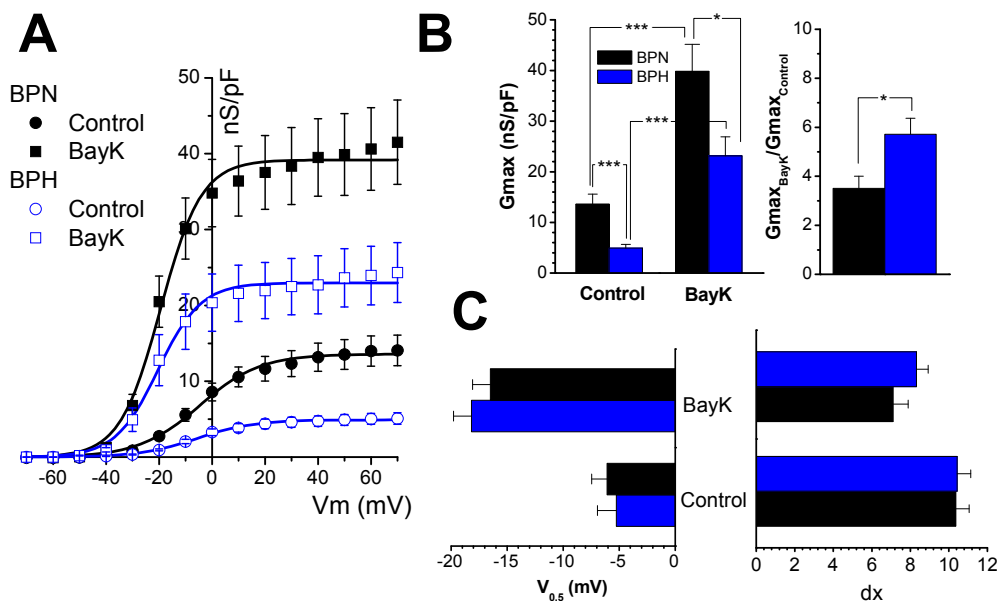
Figure 4.24 *A: Average conductance/voltage curves (G/V) obtained from BPN and BPH VSMCs in control and in presence of 10µM BayK, with the corresponding Boltzman fits. B: Average maximal conductances (G_{max}) obtained in BPN and BPH from the Boltzman fits to the individual cells in both conditions. In the right panel BayK G_{max} in each cells was normalized with respect to the control G_{max}. C: Average parameters for the Boltzman fit to the the individual cells from BPN and BPH in control and in the presence of BayK. $V_{0.5}$ is the voltage for half-maximum Ba^{2+} current activation, and dx is the steepness of the Boltzman relationship. Conductance (G) was calculated from the tail peak current amplitude as $G = I/(V_M - V_{rev})$, where V_{rev} is the assumed reversal potential, V_M is the membrane potential, and I is the tail peak current.*

differences in the composition of auxiliary subunits of the functional channel in BPH cells. So, we decided to explore this posibilty.

4.3.2 mRNA expression profile of LTCCs ancillary subunits

As a first step to determine the LTCCs subunit composition, we studied the expression pattern of the genes encoding pore forming α_1 and its accessory subunits ($\alpha_2\delta$, β and γ) in BPN and BPH mesenteric vessels. A total of 12 genes were studied together with several control genes such as calponin as a control of VSMCs, endothelial nitric oxide synthase (eNOS) as a control of endothelial cells and RP18S as endogenous control of the qPCR.

Figure 4.25A shows the relative abundance of the channel genes expressed in mesenteric arteries from normotensive animals (n=20). Expression levels of some accessory subunits, particularly $\alpha_2\delta_1$ and γ_6 genes are particularly abundant. No expression could be detected for $\alpha_2\delta$-4, γ-2, γ-3 and γ-5.
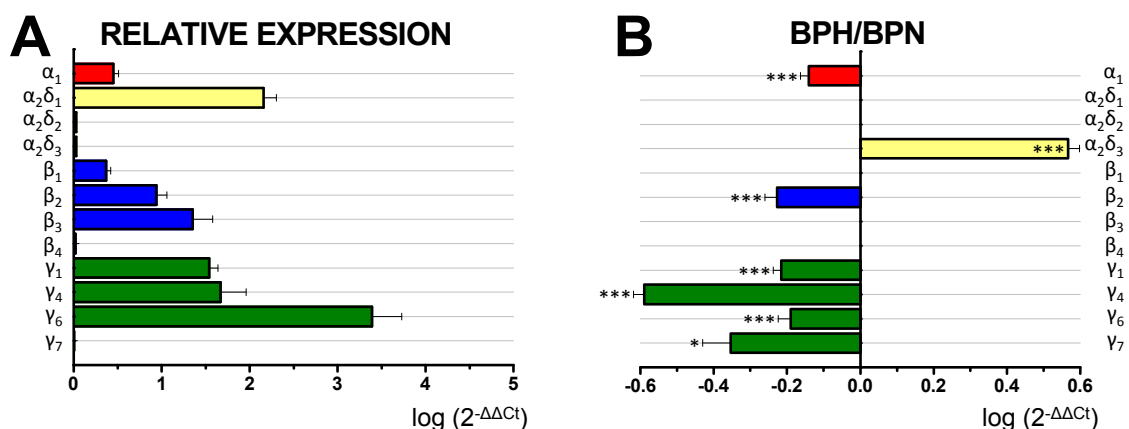
Figure 4.25 *A: Relative abundance of LTCCs principal subunit (α_1) and calcium channels accessory subunits in BPN mesenteric arteries. B: The mRNA expression levels differences in BPH arteries using BPN expression levels as calibrator. Changes in expression levels were calculated as $2^{-\Delta\Delta Ct}$, where $\Delta\Delta Ct = \Delta Ct_{(BPH)} - \Delta Ct_{(BPN)}$.*

Differences in expression in BPH VSMCs (Figure 4.25B) include a significant reduction in the mRNA expression levels of the pore forming α_1 subunit, which correlates with the decreased Ba^{2+} current density described above (see Figure 4.21). In addition, all the γ and the β_2 accessory subunits exhibited a decreased expression in BPH. In contrast, $\alpha_2\delta_3$ subunit showed an increased expression in BPH. Interestingly, changes in the expression of $\alpha_2\delta$ (Bannister *et al.*, 2012) and the β_3 (Kharade *et al.*, 2013) accessory subunits have been recently associated with hypertension.
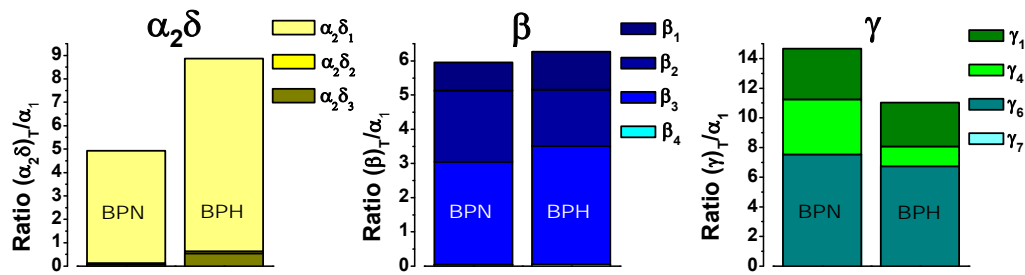
Figure 4.26 *The ratio of accessory subunit $\alpha_2\delta$, β and γ was normalized to Cav1.2 α_1. This ratio suggest an increased in $\alpha_2\delta$ and a decreased in γ in BPH VSMCs.*

Since LTCCs channelosome is composed of α_1, $\alpha_2\delta$, β and γ subunits with a stoichiometric ratio 1:1:1:1, we calculated the mRNA ratio of each different accessory subunit to the main subunit as a first approximation to get a tentative picture of the possible differences in the composition of the LTCC channelosome in BPN and BPH cells. The amount of mRNA for $\alpha_2\delta$, β and γ auxiliary subunits was pooled and normalized to that of α_1 in mesenteric arteries VSMCs for the BPN and BPH mice (Figure 4.26). This analysis disclosed a significant relative increase (1.8 fold) in the expression of the auxiliary subunits $\alpha_2\delta$ in BPH cells. On the other hand, there were no substantial changes in the proportion of β and we found a small decrease in the γ ratio in BPH relative to BPN. These differences in the mRNA levels of the different subunits between BPN and BPH were suggestive of a different composition of the functional calcium channels, and a possible way of explaining the functional differences described above. Obviously, this analysis has some important limitations, because mRNA levels do not necessarily reflects protein level, and because the relationship between the expression level of certain subunit and the functional properties of the currents do not need to be linear. Therefore, we decided to explore some additional electrophysiological properties that could correlate with the changes in the subunit composition of the channels.

4.3.3 Functional characterization of $\alpha_2\delta$ LTCCs accessory subunit in isolated VSMCs

To test whether the $\alpha_2\delta$ mRNA increase contributes to the different functional expression of LTCCs currents in VSMCs obtained from BPH mice, we used a pharmacological approach. Gabapentin (GBP), a drug originally developed as a GABA analogue and employed for the treatment of epilepsy (Field *et al.*, 2006;Tzellos *et al.*, 2008), was found to be an specific $\alpha_2\delta$ ligand (Gee *et al.*, 1996b;Taylor, 2009b). Therefore we used this drug to quantify the functional contribution of $\alpha_2\delta$ subunits to the inward Ba^{2+} currents in BPN and BPH cells. We tested GBP effect on membrane currents applying 50 ms depolarizing pulses from a holding potential of −80 mV to a test potential of 0 mV every 10 seconds. Figure 4.27 illustrates the time course of the peak current amplitude of LTCCs currents (at 0 mV) and the changes in this amplitude in response to acute application of GBP 100μM. GBP caused a little increase of the inward current in BPN cells (1.18 folds in the example shown in figure 4.27A). In contrast, GBP induced a large increment in BPH VSMCs (2.15 fold in the cell depicted in figure 4.27B).

4.3.4 Specific interaction of gabapentin with the $\alpha_2\delta$ accessory subunit of VSMCs LTCCs

The exact mechanism by which gabapentin exerts its actions at the molecular level remains unclear. However, gabapentin has been found to bind to two of the $\alpha_2\delta$ subunit subtypes, $\alpha_2\delta$-1 and $\alpha_2\delta$-2, but not to $\alpha_2\delta$-3 or $\alpha_2\delta$-4, which do not contain the extracellular epitope that is key to gabapentin binding (Brown *et al.*, 1998;Davies *et al.*, 2006;Davies *et al.*, 2007). To support the hypothesis that, also in our preparation, the effects of gabapentin on Ca^{2+} currents
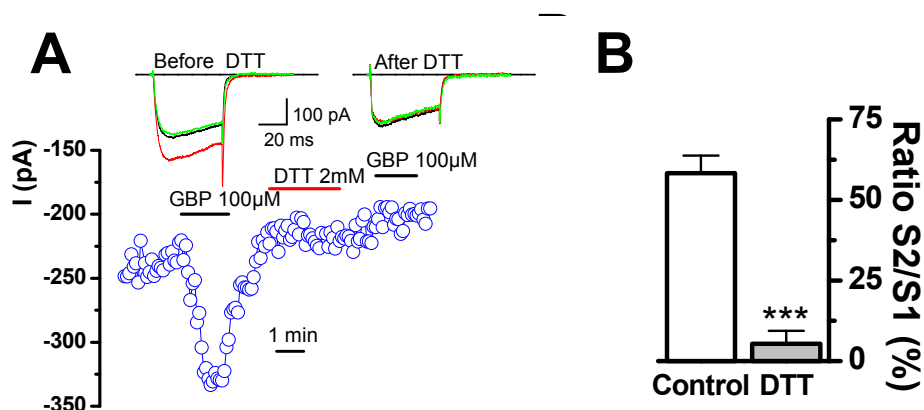
Figure 4.28 *A: Representative currents elicited by a depolarazing pulse at 0 mV before and after DTT aplication. Control conditions (black), activation by acute 100 μM GBP (red) and recovery (green). The effect of GBP is abolished after DTT 2 mM treatment, demonstrating the specific binding of GBP to $\alpha_2\delta$ subunit. B: The average effect of 100 μM GBP on the peak inward current at 0mV.*

are mediated by its binding to $\alpha_2\delta_x$ subunits, we explored the effects of gabapentin after treating cells with the reducing agent 1,4-dithiothreitol (DTT). DTT cleaves the $\alpha_2\delta$ subunit breaking the disulfide bridge that binds the α_2 and the δ subunits, eliminating the binding site of GBP (Marais *et al.*, 2001d). Figure 4.28A represents the time-course of Ba^{2+} current amplitudes recorded from a holding potential of -80 mV to a test potential of 0 mV in an isolated BPH VSMCs. Application of GBP 100 µM significantly increased the peak amplitude of Ca^{2+} currents to 146.3% of control. In contrast, after the reducing agent DTT (2 mM) was applied in the bath solution, the effect of a second application of GBP was abolished. Since the
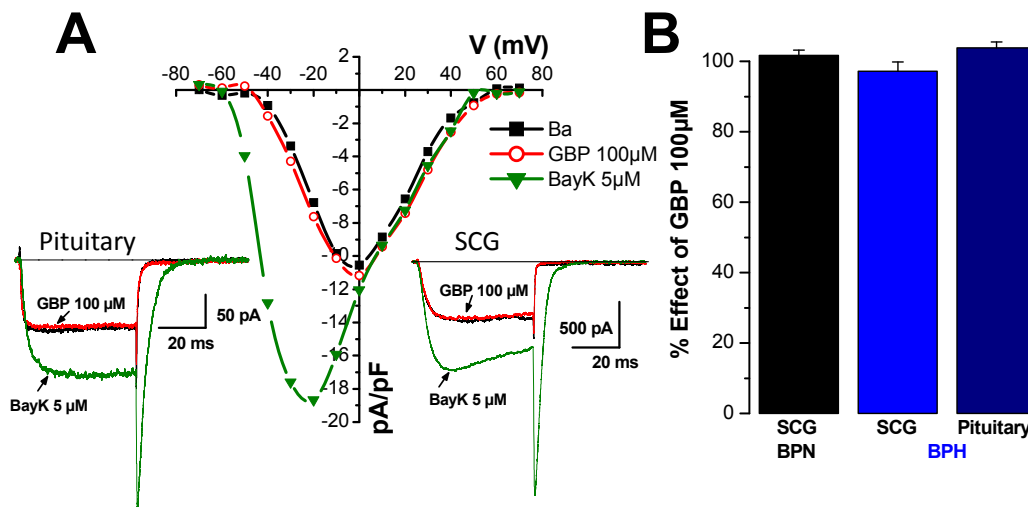
Figure 4.29 *A: Mean current density–voltage relationship of pituitary isolated cells from BPH mice under control conditions (black), in acute aplication of 100 µM GBP (red) and current increasing with 5 µM BayK (green). Representative currents elicited by a depolarazing pulse at 0 mV under each condition (inset). B: Average effect of GBP 100 µM at 0 mV in superior cervical ganglions isolated cells from BPN and BPH and in pituitary cells from BPH.*

effect of GBP tended to be smaller in the second application (see figure 4.27), we quantified the effect of DTT measuring the ratio between the second and first stimulus (S2/S1ratio) in several cells with and without DTT application between the two stimuli (Figure 4.28B). S2/S1 ratio was 58% when two sequential GBP applications were performed, and decreased to a 5% after treatment with 2 mM DTT. These results strongly suggest that the effect of GBP on calcium currents in our preparation required the presence of the $\alpha_2\delta$ accessory subunit.

There is no agreement in the literature about the effect of GBP on native Ca^{2+} currents. Some authors report a small acute inhibition of Ba^{2+} currents in different cell types (Sutton *et al.*, 2002) but other studies report a chronic inhibition of calcium channel trafficking (Hendrich *et al.*, 2008b). Our data add more elements to this controversy, as we found a clear and reproducible increase in the calcium currents in response to 100 µM GBP in BPH but not in

BPN VSMCs. Nevertheless, since individual $\alpha_2\delta$ subtype may associate (or form complexes) with different α_1 subunits, GBP could affect various types of Ca^{2+} channels depending on the tissue and/or cell studied. Therefore, we have explored if the effect of GBP was specific of VSMCs from mesenteric arteries by looking at the changes in Ba^{2+} currents in other tissues from BPN and BPH mice (Figure 4.29). Part A of figure 4.29 shows the Ba^{2+} current-density/voltage relationship obtained from isolated pituitary cells from BPH mice, in control conditions and after applying either 100 µM GBP or 5 µM BayK-8644. The inward Ba^{2+} current was significantly enhanced by BayK, since LTCCs are the main voltage-gated calcium channels described in this preparation (Cohen & McCarthy, 1987). However, GBP had no effect on these currents. We also explored the effect of 100 µM GBP in superior cervical ganglion (SCG) neurons, where calcium channels are mainly of the N-type (Mintz *et al.*, 1992), obtaining similar results (figure 4.29B). Representative current traces obtained in BPH SCG neurons and in BPH pituitary cells with depolarizing pulses from -80 mV to 0 mV in control conditions and after applying either 100 µM GBP or 5 µM BayK-8644 are also depicted in figure 4.29A.

4.3.5 Concentration response effects of GBP in native VSMCs and in LTCC HEK transfected cells

The different sensitivity of LTCCs to GBP in BPN and BPH VSMCs was further characterized measuring a concentration response curve for the drug effect at 0 mV. Results of this analysis are summarized in Figure 4.30A. GBP increased the total Ba^{2+} currents in a concentration-dependent manner in BPH VSMCs, with a maximal effect of 179.1 ±7.7 % and an apparent IC_{50} of 16 µM. The effect of GBP was dramatically different in BPN VSMCs, where the concentration response curve has a bell shape with a peak (177.04 ±14.9 % increase over control values) at a concentration of 10 µM GBP. A further increase of GBP concentrations (we explored the range from 20 µM to 1 mM) led to progressive smaller increases of the Ba^{2+} inward currents, that were not different from control at 1 mM GBP (105.4 ±4 % of control).

These results were completely unexpected and difficult to explain simply in terms of an amount of the proportion of channels with $\alpha_2\delta$ subunits in BPH cells. Therefore we hypothesized that changes in other auxiliary subunits could modulate GBP binding to the channels. Inspecting mRNA expression differences (Figure 4.25), a possible candidate was the β_2 subunit, whose mRNA levels decreased significantly in BPH cells. In order to test this possibility, we studied the effects of GBP in the currents obtained from different subunit combinations of LTCCs expressed in HEK293 cells.
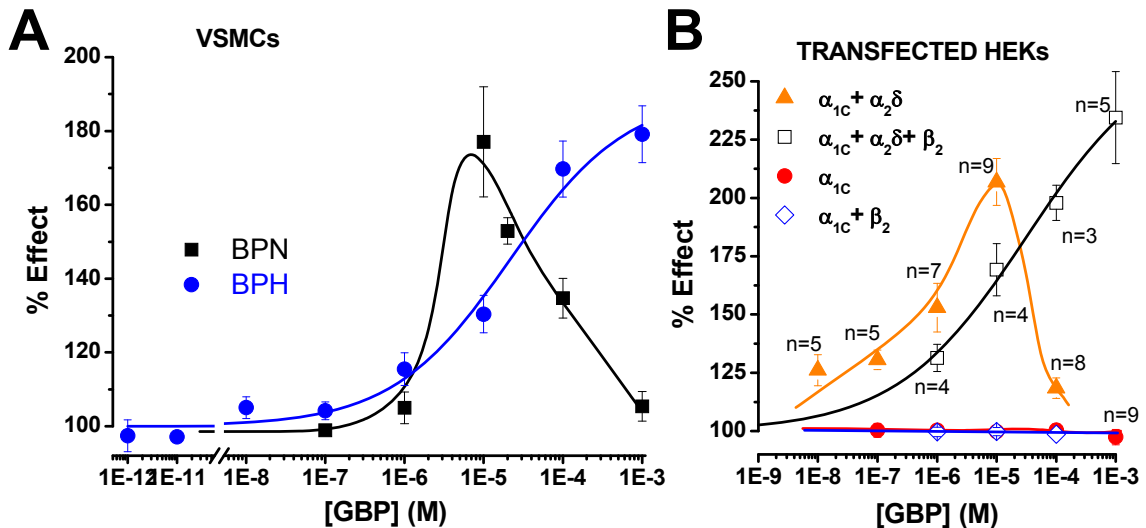
Figure 4.30 A: Dose-response relationship for GBP are represented for two experimental conditions BPN (squares) and BPH (circles) VSMCs. Data are expressed as a percentage of GBP effect. Average data were fitted by eye, obtaining an apparent EC_{50} of 16 µM in BPH cells and a maximal effect ~ 10 µM in BPN cells. B: Dose-response curves for different LTCCs subunits in a heterologous system pointing to similarities between $\alpha_{1C}+\alpha_2\delta+\beta_2$ transfected HEK and BPH and between $\alpha_{1C}+\alpha_2\delta$ and BPN.

For that purpose, α_1, $\alpha_2\delta$ and β_2 subunits were co-transfected in this heterologous system for electrophysiological characterization. Results are depicted in figure 4.30B. As expected, GBP required the presence of $\alpha_2\delta$ subunits to have an effect on Ba^{2+} currents. GBP-sensitive Ba^{2+} currents were completely absent in α_1 and $\alpha_1+\beta_2$ transfected cells (red circles and blue diamonds respectively), while clear responses could be observed in all combinations where $\alpha_2\delta$ subunits were present. When just α_1 and $\alpha_2\delta$ subunits were co-expressed (orange triangles) we obtained a bimodal response, with a maximal increase in the Ba^{2+} current at ~10 µM GBP (206.8 ±10.06 % of the control effect). Interestingly, when α_1 subunits were co-expressed with $\alpha_2\delta$ and β_2 subunits (open squares), the GBP dose-response relationship became sigmoidal, with an apparent IC_{50} ~1µM and a maximal effect of 234.4 ±19.75 %.

The simple inspection of figure 4.30 reveals a close resemblance between curves obtained in BPH cells and in HEK cells transfected with α_1 ,$\alpha_2\delta$ and β_2 subunits and between curves obtained in BPN cells and in HEK cells transfected with just α_1 and $\alpha_2\delta$ subunits. These results confirm that the presence of $\alpha_2\delta$ is required for GBP sensitivity, and strongly suggest that the differences in the response between BPN and BPH VSMCs could be due to a different proportion of β_2 subunits. However, while β_2 mRNA expression is reduced in BPH cells, the concentration-response curve obtained in those cells corresponds to the curve obtained with β_2 in HEK cells.
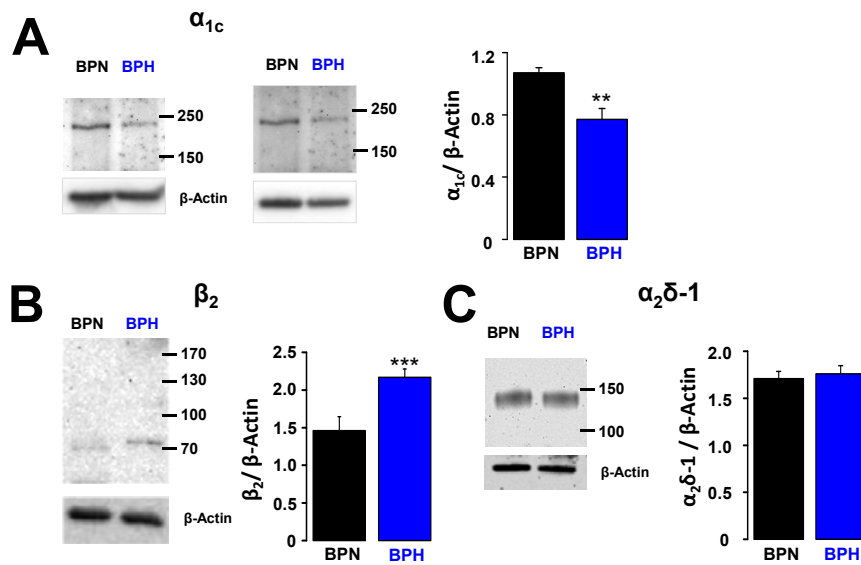
Figure 4.31 *A: Sample western blot ilustrating α_1 protein from BPN and BPH whole arterial lysates. Blot were cut at 50 KDa to allow pobing for acting. Right panel, mean data illustrating that α_1 protein is downregulated in hypertension. **P<0.01. B: Representative western western blot ilustrating that β_2 subunit is elevated in BPH arteries. To the right, average densitiometric values for β_2 subunit. ***P<0.001 C: Wester blot showing adjacent lines loaded with mesenteric artery protein lysate pooled from either 2 BPN or hypertensive mice and probed with anti-$\alpha_2\delta$. B-actin was a loading control.*

4.3.6 Expression of LTCCs proteins in BPN and BPH VSMCs

This discrepancy could be explained if β_2 mRNA expression does not correlate with protein levels. To test that possibility, we decided to perform western blot experiments in order to measure protein levels of α_1, $\alpha_2\delta$ and β_2 subunits in mesenteric arteries lysates from BPN and BPH mice. Results are shown in Figure 4.31. In agreement with mRNA levels, α_1 protein was downregulated 0.28 ± 0.07 fold in the BPH mice compared with BPN mice (Figure 4.31A). On the other hand, β_2 protein was upregulated in BPH mice, in clear disagreement with the mRNA expression levels. The immunodensity of the β_2 band was 1.54 ± 0.13 fold higher in mesenteric arteries lysate from BPH mice compared with BPN mice (Figure 4.31B). Interestingly, this result correlates well with the GBP effect found in the heterolgous system. Regarding $\alpha_2\delta$ subunit proteins, since $\alpha_2\delta$-1 is the main GBP binding subunit and is the more abundant $\alpha_2\delta$ subunit both in BPN and BPH cells, we investigated its possible upregulation in BPH mesenteric arteries. In agreement with mRNA expression levels, $\alpha_2\delta$-1 protein levels were similar in BPN (1.71 ± 0.07) and BPH (1.76 ± 0.08) mesenteric arteries (Figure 4.31C).

4.4 DIFFERENCES IN LTCC ACTIVITY MEASURED AT PHYSIOLOGICAL MEMBRANE POTENTIALS

The data presented so far strongly suggest the existence of differences between BPN and BPH LTCCs attributable to a different subunit composition that leads to changes in the electrophysiological and pharmacological properties of the currents. In order to explore the physiological relevance of these differences, we decided to explore whether LTCCs could have a different behavior at membrane potentials closer to the physiological membrane resting potential and with physiological $[Ca^{2+}]_e$, combining voltage–clamp electrophysiology with evanescent field total internal reflection fluorescence microscopy (TIRF). VSMCs were loaded with the ''fast'' Ca^{2+} indicator Fluo-5F (200 μM) and the ''slow'' Ca^{2+} buffer EGTA (10 mM). With this indicator-buffer combination, Ca^{2+} entering the cell through LTCCs binds to Fluo-5F,
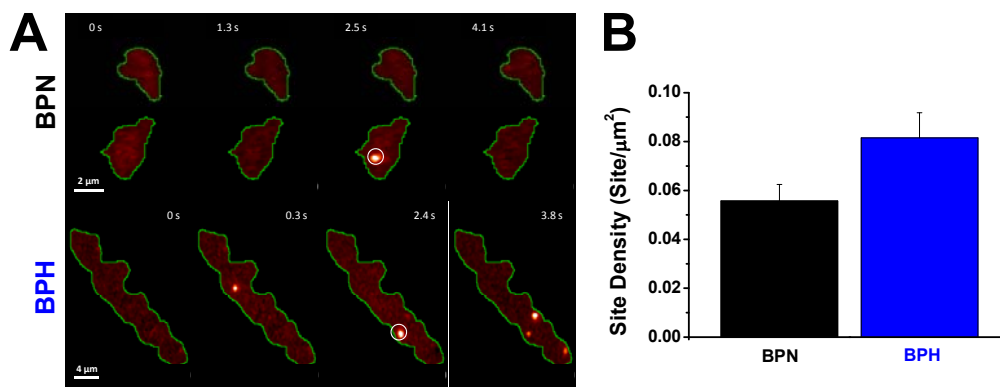
Figure 4.32 A: Image secuencies from BPN and BPH VSMCs loaded with Fluo-5F 200μM showing Ca^{2+} sparklets. B. Bar plot of the mean ± SEM of the Ca^{2+} sparklets site density. BPH showed 0.08 sites/μm² and BPN 0.055 sites/μm² but theses differences are not significative.

resulting in a fluorescence signal, called "Ca^{2+} sparklets" (Navedo *et al.*, 2005). VSMCs were patch-clamped in the whole-cell configuration and V_M was held at -70mV, slightly under the typical resting membrane potential to increase the driving force for Ca^{2+} entry and to maintain a low LTCCs open probability. Under these conditions we characterized the sparklet activity in BPN and BPH cells answering the following questions: 1) How many sparklets sites are per cell, 2) what is the opening frequency of these channels, 3) how long are the openings and, 4) how many channels assemble to form a site.

4.4.1 Ca^{2+} sparklet site density

Figure 4.32A shows a sequence of 4 images obtained from a BPN and a BPH VSMC showing one and four active Ca^{2+} sparklet sites respectively. On average, the number of Ca^{2+} sparklets
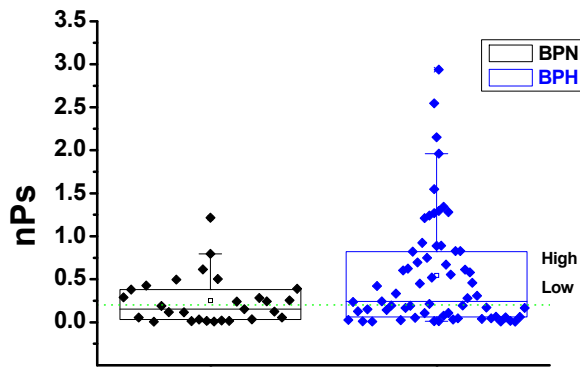
Figure 4.33 Summarized data of nP_s sites. The distribution of nP_s Ca^{2+} sparkleets sites were bimodal. Therefore, we grouped sparklets sites in low open probability (0< nP_s<0.2) and high open probability (nP_s>0.2).

sites per cell was higher in BPH (1.84 ± 0.16) than in BPN (1.43 ± 0.09) VSMCs. Since the number of sparklet sites depends on the total surface of the cell attached to the cover-slip, this data was normalized to VSMCs footprint area. Figure 4.32B shows the mean ± SE of the Ca^{2+} sparklet site density in both mice strains. In spite of the fact that BPH showed a higher sparklets site density (0.081 sites/μm^2) than BPN (0.055 sites/μm^2) these changes are not significantly different.

4.4.2 Ca^{2+} sparklet open probability

The opening of one or more LTCCs defines the activity of single sparklet site, thus we determined the activity of Ca^{2+} sparklets by calculating the **nPs** of each site, where **n** is the number of quantal levels of $[Ca^{2+}]_i$ increase, and **Ps** is the probability that a given Ca^{2+} sparklet site is active. The box plot showing the distribution of Ca^{2+} sparklet sites **nPs** is plotted in figure 4.33. Mean values of sparklet activity was 0.25±0.05 (*n* =28) in BPN cells and 0.54±0.08 (*n* = 64) in BPH cells. Differences were statistically different (p<0.05). A simple inspection of the sparklet activity distribution obtained in BPH cells reveals a bimodal distribution, with sparklets highly active and sparklets clearly less active. Following previous descriptions of this observation (Navedo *et al.*, 2005), we grouped Ca^{2+} sparklet sites into two categories: low Ca^{2+} sparklet **nPs** sites, that had a minimal level of activity (0 < nPs < 0.2), and high **nPs** sites (nPs > 0.2), with a nearly continuous Ca^{2+} influx that persisted for seconds.

Results of this analysis are depicted in figure 4.34. Part A of the figure represents examples of the time-course of $[Ca^{2+}]_i$ changes observed in Ca^{2+} sparklet sites working in low and high open probability mode from BPN and BPH cells. Figure 4.34B represents the mean±SE **nPs** of Ca^{2+} sparklet sites after they have been grouped into low and high open probability. As suspected, the differences observed between BPN and BPH are mainly due to the differences between high Ca^{2+} sparklet **nPs** sites, and open probability of BPH high activity sites (0.93 ± 0.11) were significantly higher than BPN sites (0.47 ± 0.076).
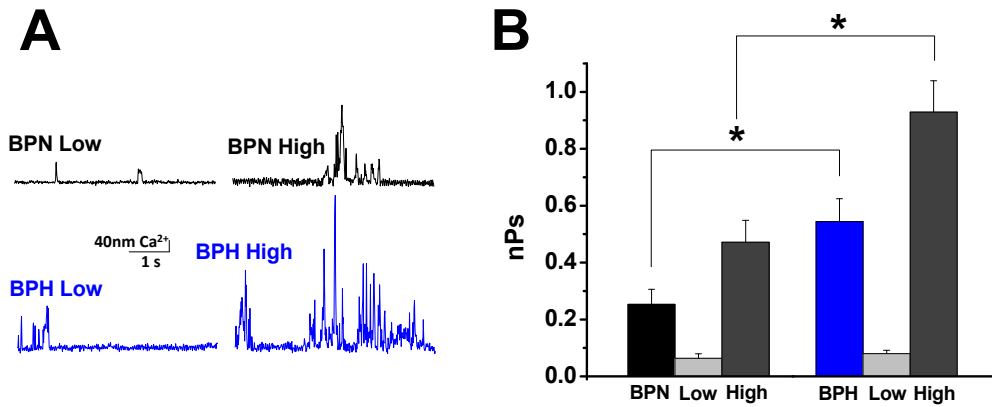
Figure 4.34 *A: Sample $[Ca^{2+}]_i$ traces of low and high nP_s sites. B: Summarized data of nP_s sites. The distribution of nP_s Ca^{2+} sparkleets sites were bimodal. Therefore, we grouped sparklets sites in lowopen probability (0< nP_s<0.2) and high open probability (nP_s>0.2).*

Taking together, these results demonstrate that although Ca^{2+} sparklet site density was similar between BPN and BPH cells, LTCCs open probability was higher in BPH sites.

4.4.3 Ca^{2+} sparklets dwell time

The analysis of LTCCs open dwell times provides relevant insights concerning ion channel function. Figure 4.35A displays representative sparklet site traces obtained from BPN and BPH
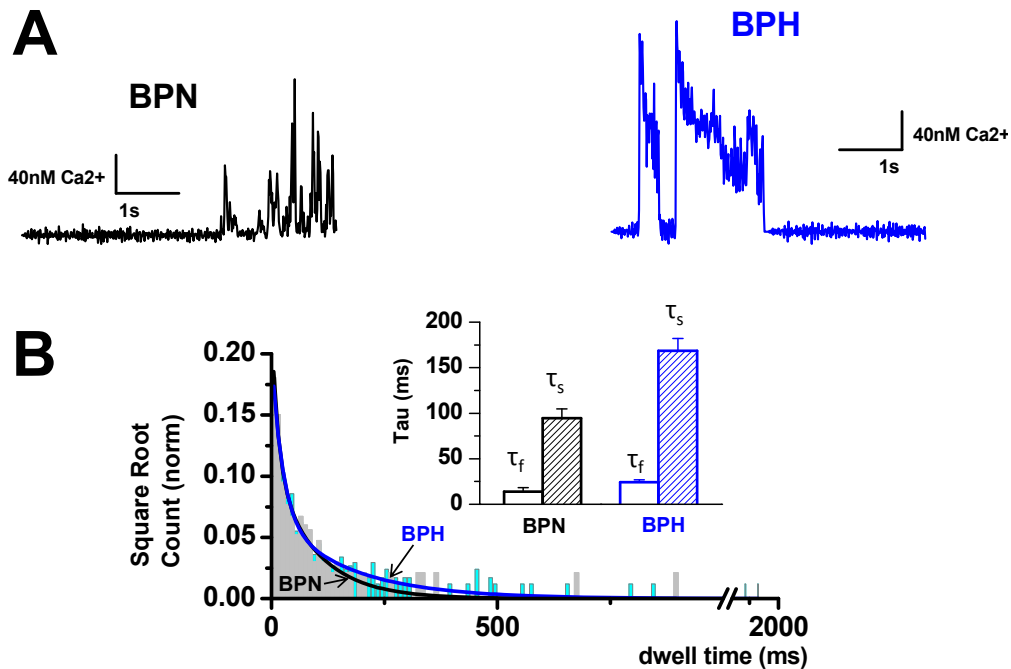
Figure 4.35 *A: Sample BPN and BPH sparklets site traces showing differences in the LTCCs mean open time. B: Super-imposed BPN and BPH dwell time amplitude histograms showing the LTCCs open time distribution in both strains. The inset shows the mean LTCCs open times (τ1 and τ2) obtained by fitting the histograms to the sum of two exponential functions.*

cells, in which clear differences in the LTCCs open times can be observed. It is important to point that in spite of this variable length of Ca^{2+} influx events, Ca^{2+} influx sites were stable, showing clear signs of activity for the duration of the experiments ($\approx$ 5–20 min). Total BPN and BPH time intervals for LTCCs opening were compiled into dwell time histograms for statistical analysis. Since dwell-time data were difficult to interpret because there were several widely quantitative components, we used Sigworth & Sine alternative presentation (Sigworth & Sine, 1987) and plotted data on a square root scale. Figure 4.35B shows superimposed the BPN and BPH dwell time histograms showing the open time distributions of LTTCs. Data were fitted to the sum of two exponentials, with the time constants depicted in the inset of figure. Both components are longer in BPH than in BPN (168.5±13.5 *vs.* 94.4±10.39 and 24.17±2.7 *vs.* 14±4.26 ms).

Therefore, LTCC open more frequently in the sparklet sites from BPH cells and when they are open, they remain open longer than in BPN sites.

4.4.4 Ca^{2+} sparklet amplitude distribution

Electrophysiological studies indicate that approximately 5000–10000 functional LTCCs channels ($\approx$ 5–15 channels/μm^2) are expressed in a typical vascular myocyte (Rubart *et al.*, 1996). LTCCs are broadly distributed throughout the sarcolemma of smooth muscle cells (Navedo *et al.*, 2006;Rubart *et al.*, 1996). However, the local spatial distribution of LTCCs into a Ca^{2+} sparklet sites in arterial myocytes varies between cells, since LTCCs may be found alone or grouped in clusters of several channels. Then, the amplitude of the change in $[Ca^{2+}]$ elicited by a sparklet site is function of the number of channels, the single current amplitude and their open probability.

Figure 4.36: Mean ± SEM of total BPN and BPH Ca^{2+} sparklets amplituds. P<0.001.

When the total amplitudes were measured (Figure 4.36) we found that average values were significantly higher in BPH (70.05 ± 1.25 nM) than in BPN (54.90 ± 2.22 nM). We have already seen that open probability of LTCC is larger in sparklets form BPH cells, and this fact could account for the observed higher amplitudes. Nevertheless, the number of channels and their single current amplitude could also be different in BPH sparklets. To test this possibility, we pooled all data obtained in different cells in order to construct and analyze the amplitude
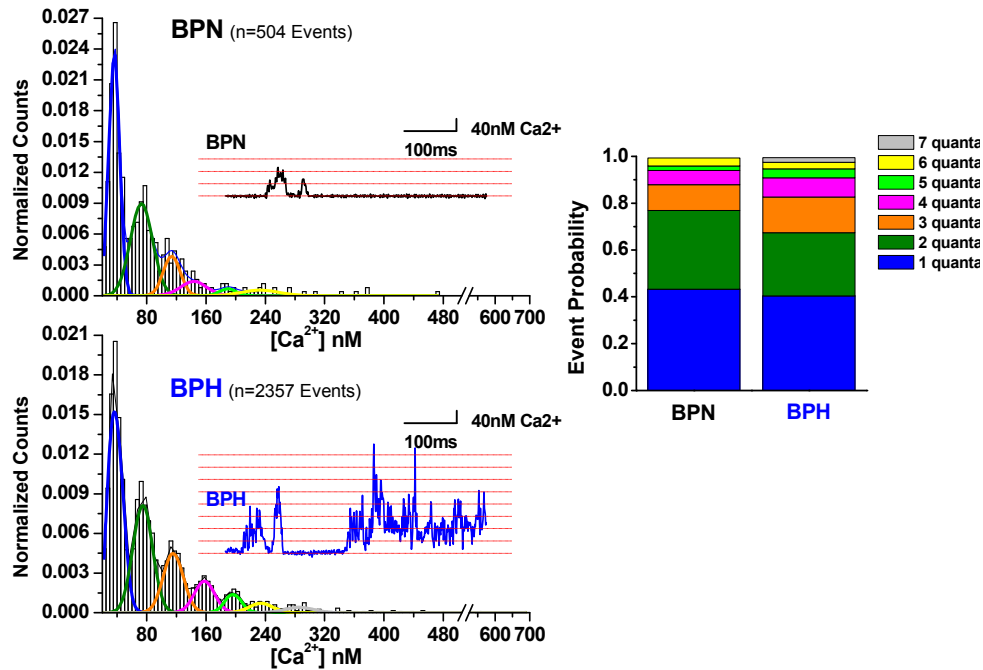
Figure 4.37 *Amplitude histogram of Ca^{2+} sparklets at 20 mM $[Ca^{2+}]_o$. Data were fitted with a multicomponent Gaussian function with a quantal unit elevation of 38 nM. The inner graphs show a representative traces of BPN and BPH sparklets amplituds. Dotted lines in the insets mark the quantal levels. Color bar plots in the right represent the different quanta of BPN and BPH LTCCs clusters.*

histograms of Ca^{2+} sparklets obtained with an extracellular concentration of 20mM$_i$ (Figure 4.37). Using an approach similar to the one implemented by del Castillo and Katz (DEL CASTILLO & Katz, 1954), we fitted our histograms with several Gaussian functions. This analysis revealed 5 clearly discrete peaks in BPN and 7 in BPH, corresponding to the number of LTCCs present in the corresponding sparklets. Both in BPN and in BPH cells, calcium influx through a single LTCC produced a Ca^{2+} elevation of 37.5 nM. This calcium increase is the so called "quantal unit". This value was identical in BPN and BPH cells, demonstrating that single channel current is the same in both preparations. Then, we can conclude that differences between LTCC currents in BPN and BPH cells are not due to differences in single channel conductance. The insets of Figure 4.37 show representative $[Ca^{2+}]_i$ records from BPN and BPH Ca^{2+} sparklets sites with two (BPN) and eight (BPH) quantal events. The right panel of figure 4.37 represents the probability of finding 1 to 7 calcium channels open in the same cluster of LTCCs. It can be seen that BPH VSMCs are more likely to present clusters with more channels than BPN VSMCs (32.08% vs 22.4% for n>4).

All together, these data suggest that Ca^{2+} sparklets are more active in BPH cells because 1) the number of channels larger, 2) their open probability is higher and 3) they remain open longer times.
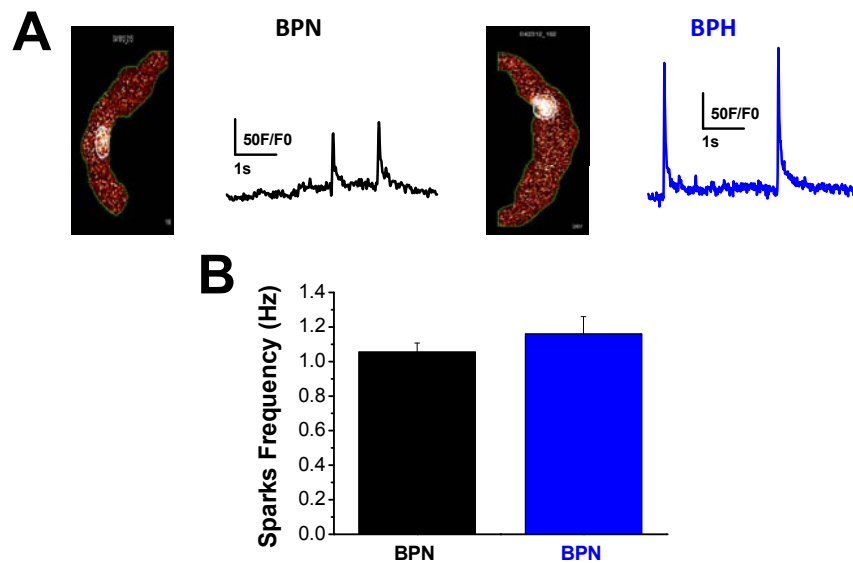
Figure 4.38 *A: Representative swept-field confocal images of Ca^{2+} sparks from BPN and BPH myocytes. The traces to the right show the time course of [Ca^{2+}]$_i$ in the regions of the images delimited by the white circle located in the middle of each image.B: Bar plots summarizing mean ± SEM Ca^{2+} spark frequencies. and amplitudes (right).P>0.05.*

4.5 FUNCTIONAL CHARACTERIZATION OF Ca^{2+} SPARKS AND BK$_{Ca}$ ACTIVITY IN BPN AND BPH CELLS

Ca^{2+} sparklets are local events that activate the ryanodine receptors (RyRs) present in the sarcoplasmic reticulum (SR) closely located beneath the plasma membrane. This mechanism of activation is known as Ca^{2+}-induced Ca^{2+} release (CICR). In vascular smooth muscle, these localized Ca^{2+} release events from SR through RyRs are called "Ca^{2+} sparks". These events activate the large-conductance, Ca^{2+}-sensitive, K$^+$ channels (BK$_{Ca}$) present in the nearby plasma membrane, producing Spontaneous Transient Outward Currents (STOCs) that tend to hyperpolarize the cells. This coupling between Ca^{2+} sparks and BK$_{Ca}$ channel activity operates as a negative feedback mechanism that opposes vasoconstriction. Therefore, a BPH myocyte showing LTCCs channels with an increased activity, longer mean open times and grouped in bigger clusters, should have a higher spark activity and a consequent increase in BK$_{Ca}$ activity. Since this chain of events would eventually lead to vasodilation, we could conclude that changes in BPH LTCC activity would be designed to compensate the hypertensive status in these animals. To test this hypothesis, we examined Ca^{2+} sparks and BK$_{Ca}$ current activity at rest in VSMCs from BPN and BPH mice.
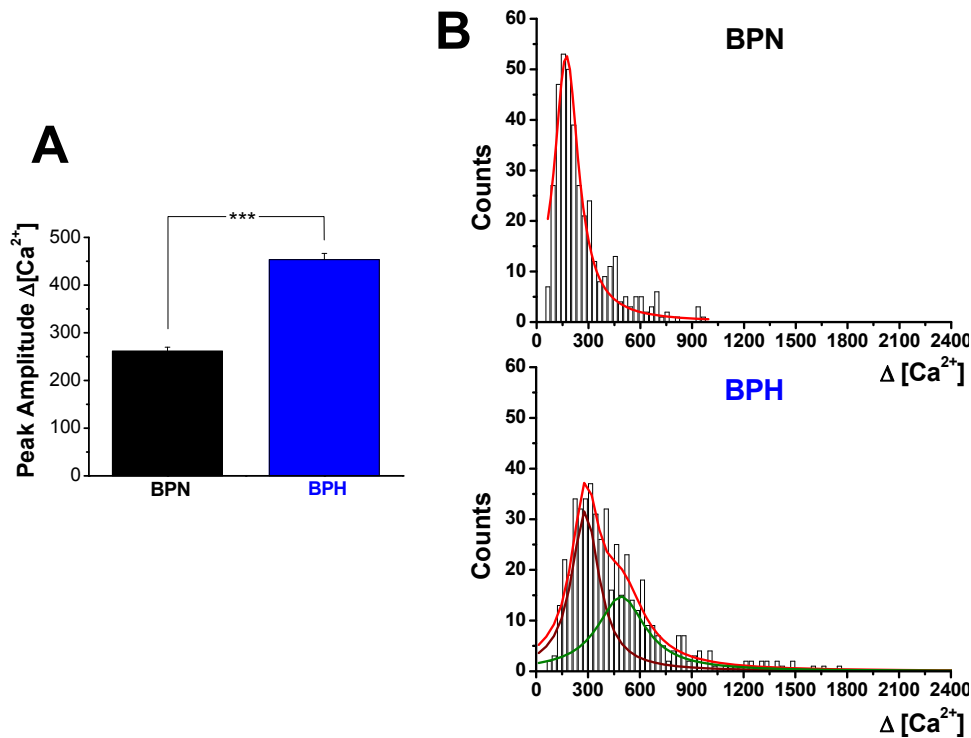
Figure 4.39 *A: Bar plots summarizing mean ± SEM Ca²⁺ spark amplitudes.***P<0.001. B: Distributions of Ca²⁺ sparks for Δ[Ca²⁺] in BPN (n= 25 cells, n= 389 sparks) and BPH (n= 27 cells, n= 493 sparks). Data were fitted with a one component Gaussian function in BPN and two components in BPH.*

4.5.1 Spark frequency and amplitude

We used swept-field confocal microscopy to detect Ca²⁺ sparks in BPN and BPH myocytes at rest. Figure 4.38A shows representative images of BPN and BPH arterial myocytes exhibiting Ca²⁺ sparks. The spatial widths of Ca²⁺ sparks show that Ca²⁺ diffusion from the center of Ca²⁺ sparks to periphery was asymmetric, indicating that the distribution of RyRs in a cluster of Ca²⁺ release channels is inhomogeneous in both BPN and BPH cells. Traces represent the F/Fo values recorded at the area where Ca²⁺ sparks were active (white circle). We found that Ca²⁺ spark frequency was very similar in BPN (1.05 ± 0.05 Hz, n=25) and BPH (1.16 ± 0.09 Hz, n=27) cells (Figure 4.38B). However, when we analyze the size of spontaneous Ca²⁺ sparks in BPN and BPH cells we found that the amplitude of Ca²⁺ sparks was about 73% higher in BPH than in BPN (Figure 4.39A). The amplitude of Ca²⁺ sparks was further analyzed by constructing the corresponding histograms for Δ[Ca²⁺] of sparks events in BPN and BPH (Figure 4.39B). The histograms were fitted either with one (BPN) or two (BPH) Gaussian functions. The peak value for Δ[Ca²⁺] in BPN was ≈ 171 nM, and the two Gaussians used to fit BPH data peak ≈ 268 nM and 493 nM. These data show that smooth muscle cells from hypertensive (BPH) animals exhibit larger Ca²⁺ sparks, as expected if we take into account the Ca²⁺ sparklet activity in these cells.
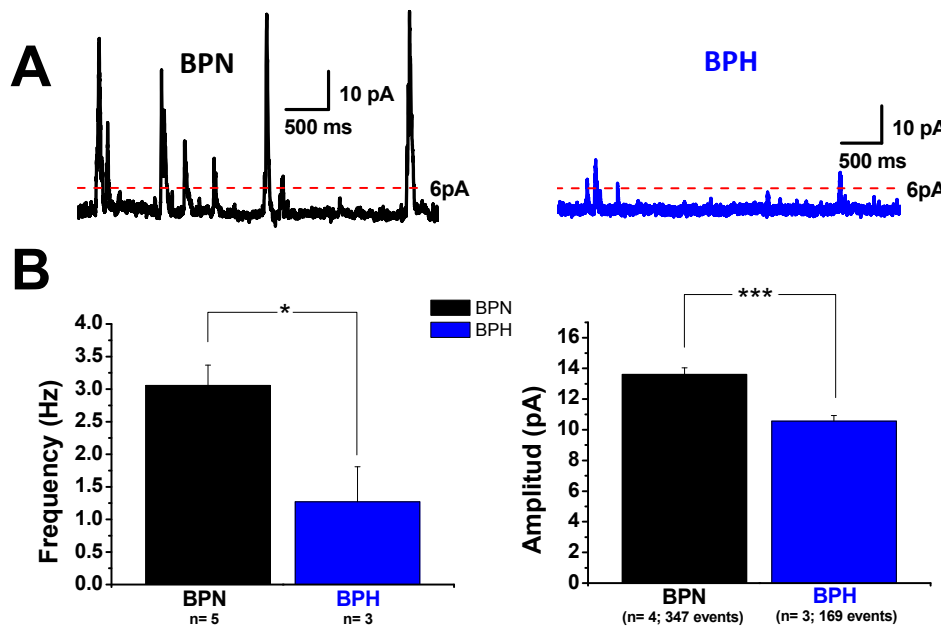
Figure 4.40 A: Spontaneous whole-cell BK currents in BPN and BPH myocytes at a holding potential of -40 mV. Currents were obtained in the amphotericin-perforated patch configuration. Only BK currens with an amplitude ≥ 6pA were analyzed. B: Bar plots summarizing mean ±SEM BK current event frequencies (left) and amplitudes (right) in BPN and BPH. *P<0.05 and ***P<0.001.

4.5.2 STOCs frequency and amplitude

Ca^{2+} sparks are the physiological activators of large-conductance, Ca^{2+}-activated K^+ (BK_{Ca}) channels in vascular smooth muscle (Nelson *et al.*, 1995). On the other hand, BK_{Ca} channels are important regulators of vascular smooth muscle membrane potential (Brayden & Nelson, 1992). Thus, it is possible that the bigger amplitude of Ca^{2+} spark events in BPH myocytes result in bigger hyperpolarizing BK_{Ca} currents. To test this hypothesis, BK_{Ca} channel function was assessed in VSMCs from normotensive and hypertensive animals measuring STOC activity at membrane potentials close to the resting membrane potential (-40 mV, Figure 4.40). The frequency of STOCs events in BPH was 1.27±0.53 Hz, approximately 59% smaller than the frequency observed in BPN cells (3.05±0.31 Hz, Figure 4.40B left pane). In addition, BK current amplitudes were about 33% smaller in BPH than in BPN myocytes (Figure 4.40B right panel).

Surprisingly, these data show that VSMCs from BPH animals, in spite of having larger Ca^{2+} sparklets and larger Ca^{2+} sparks, have smaller and less frequent spontaneous BK_{Ca} currents than VSMCs from BPN animals. This uncoupling between sparks and STOCs in BPH myocytes may be associated with the reported downregulation of the β_1 subunit of the BK_{Ca} in BPH mesenteric arteries (Moreno-Dominguez *et al.*, 2009), since the BK_{Ca} β_1 subunit enhances the sensitivity of BK_{Ca} channels to activation by physiological changes in $[Ca^{2+}]$ (Cox & Aldrich,

2000). A downregulation of the BK_{Ca} β_1 subunit has been also found in genetic hypertension (Amberg & Santana, 2003) and is consistent with results obtained in β_1-knockout mice (Patterson *et al.*, 2002).

4.5.3 BK channel Ca^{2+} sensitivity

Then, we decided to test the hypothesis that sparks and STOCs are uncoupled due to the downregulation of the β_1 subunit of the BK_{Ca} measuring the Ca^{2+} sensitivity of BK_{Ca} channels from BPN and BPH myocytes. We measured the single channel activity of BK_{Ca} channels present in excised membrane patches at four different Ca^{2+} concentrations (1, 5.5, 10 and 100 µM). Upper panels of figure 4.41 shows sample traces obtained at -40 mV and with four different $[Ca^{2+}]_i$. It is evident that the open probability of BK_{Ca} channels from BPH cells (right panel) was smaller than that of channels from BPN cells (left panel). The number of channels in the patch was also smaller in BPH cells, in agreement with the also reported decrease of the α subunit of BK_{Ca} in BPH cells (Moreno-Dominguez *et al.*, 2009). Both, a decrease of Ca^{2+} sensitivity and a reduction in the number of functional BK_{Ca} channels in the membrane could contribute to the smaller and less frequents STOCs in BPH myocytes. Then, we decided to explore channel activity both at different membrane potentials and with different $[Ca^{2+}]_I$ (Figure 4.41, lower pannels). In these graphs we represent the voltage and Ca^{2+} dependence of channel activity, measured as **nP_o**, obtained in inside-out patches from BPH (right panel) and BPH (left panel) cells.

Since **nP_o** is smaller in BPH patches at highly depolarized voltages and at saturating Ca^{2+}, we can conclude that the number BK_{Ca} channels in the plasma membrane of BPH cells is smaller than in BPN cells. Moreover, while **nPo** activation curves obtained at very high (10 and 100 µM) and very low (0 and 1 µM) Ca^{2+} concentrations are very similar in BPN and BPH cells, curves obtained at intermediate (5.5 µM) Ca^{2+} concentrations are clearly shifted to the right in BPH myocytes, indicating a decreased Ca^{2+} sensitivity. This is consistent with the reported decrease in mRNA expression of BK_{Ca} α and β_1 subunits in BPH cells. Therefore, since BK_{Ca} Ca^{2+} sensitivity is decreased in BPH cells, the consequent negative feedback mechanism that hyperpolarizes smooth muscle and thereby opposes vasoconstriction is reduced in these cells.
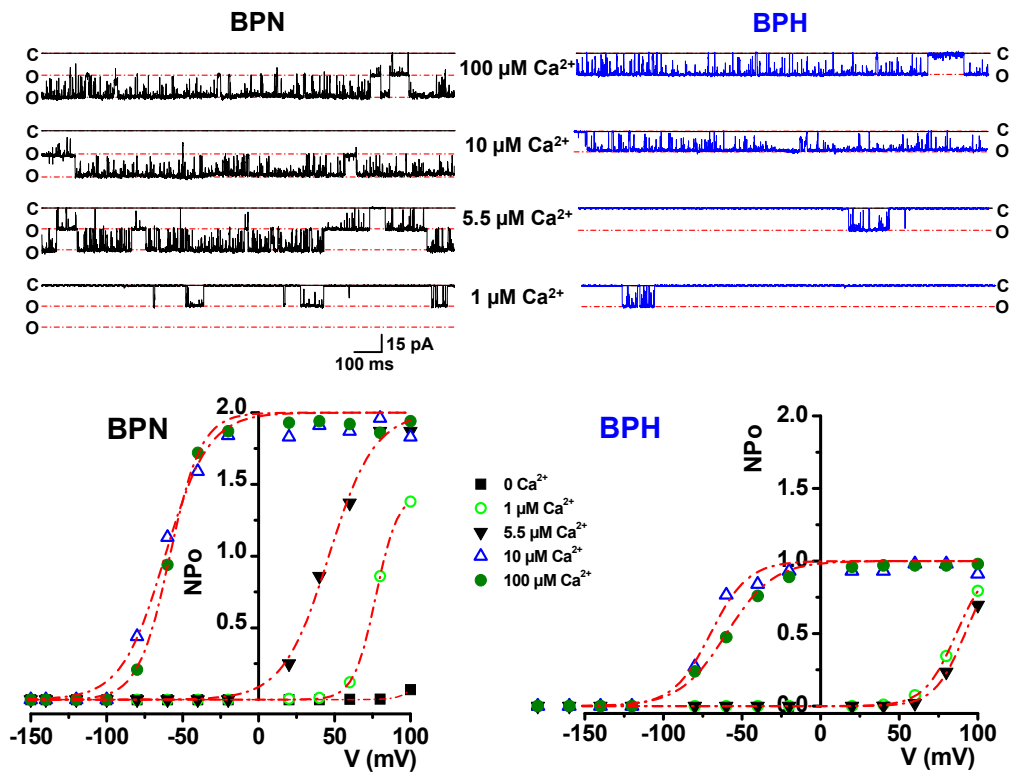
Figure 4.41 *Ca²⁺ sensitivity of BK_Ca channels in inside-out patches (HP -40 mV) from BPN and BPH myocytes. Shown at left BPN and righ BPH are representative BK_Ca channel records in the presence of 100, 10, 5.5 and 1 μM Ca²⁺ concetration. Voltage-activation curves of the BK_Ca channels measured in BPN (left) and BPH (right) myocytes under diferent Ca²⁺ concentrations are shown in the bottom panels. NPo is plotted as a function of membrane potential. The red lines represent a fit of a Boltzmann function.*

5 DISCUSSION

In the present study, using a mouse model of essential hypertension, we aimed to determine changes in K$^+$ conductances that could have an impact on the resting V_M of VSMCs and hence participate in the changes in excitability observed in the arteries from hypertensive animals. In addition, we have also explored the changes of LTCCs and the molecular composition of their ancillary subunits that would modify the Ca^{2+} influx and contribute to the differences observed between BPN and BPH. Here we show changes in Kir channel subunit expression and current, as well as changes in LTCCs and their molecular composition. However, the LTCC changes in BPH VSMCs are complex and diverse and likely affecting global and local changes in Ca^{2+} in different ways. How these changes contribute to the hypertensive phenotype is unclear, but taken as a whole, data presented in this thesis clearly demonstrate that changes have to be interpreted in a global context, and all differences must be integrated in order to properly understand the phenotypic change.

Pressure myography data obtained in BPN and BPH mesenteric arteries show that while passive changes in diameter in response to increased pressure are similar in the two groups, the active pressure-induced vasoconstriction and hence the myogenic tone are larger at all pressure values in BPH arteries (Fig. 4.2 and 4.3), indicating an increased vascular reactivity.

This increased vascular reactivity may be due to several reasons: (1) more depolarized cells due to an impaired potassium channel, leading to an increase in intracellular Ca^{2+} concentration and vasoconstriction, (2) changes in the molecular composition of LTCCs that would alter biophysical properties of the channel leading to increased Ca^{2+} influx and arterial contraction and (3) a more reactivity or sensitivity of the contractile machinery.

We hypothesize that this increased excitability could be related to the more depolarizing resting potential observed in BPH VSMCs (Fig. 4.4) and explained by changes in the functional expression of K$^+$ channels. We have chosen inward rectifier K$^+$ channels as good candidates *a priori* for that role, as they are active at values near resting V_M. Moreover, given the high resting input resistance of VSMCs (Fig. 4.6;(Nelson *et al.*, 1990)) it is plausible that small changes in the functional contribution of these K$^+$ channels, such as a slight decrease in the number of available channels, could lead to a significant depolarization and then vasoconstriction.

Our data show that there is in fact a decrease in the expression of some molecular constituents of the classical K_{IR} channels in mesenteric VSMCs (Kir2.1 and also Kir4.1) as well as in all the components of the K_{ATP} channels (albeit the decrease of SUR2 was moderate and failed to be statistically significant under all the conditions tested). These changes show a good

correlation with the electrophysiological properties of VSMCs from BPN and BPH mice, as we found a decrease of both K_{IR} and K_{ATP} currents and a diminished contribution of these channels to resting V_M in BPH VSMCs.
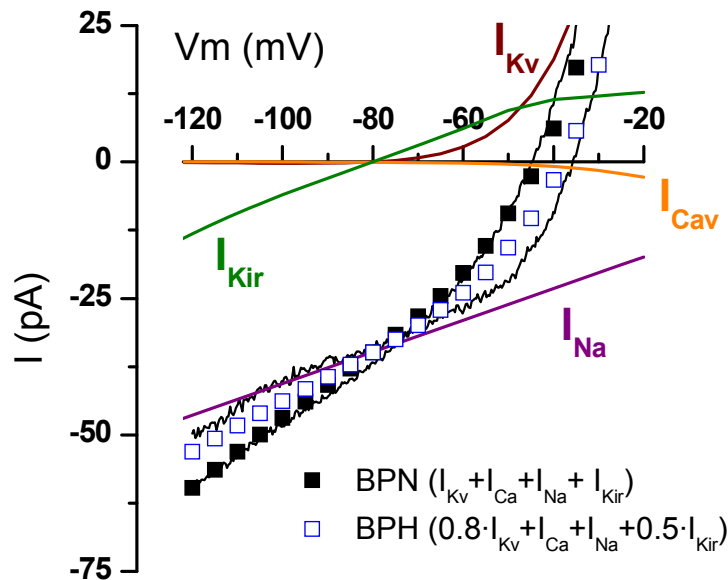
Figure 5.1 *Minimal conductance model required to simulate the whole-cell I–V relationship in BPN and BPH mesenteric VSMCs Whole-cell currents in the range between −120 and −20 mV are simply simulated by the addition of four parallel conductances mediated by inward rectifying channels (KIR plus KATP, IKir), voltage-dependent K+ (IKv) and Ca2+ (ICaV) channels and a voltage-independent inward cationic current (INa). The conductance mediating INa in the simulation has the required value to account for total current at the K+ reversal potential. Grey squares represent the simulated current for BPN currents, and open squares the simulated current for BPH currents. This simulation was obtained by decreasing Kir conductance to 50% and Kv conductance by 20%. The actual experimental data depicted in Fig. 4.5 are also represented in the figure.*

The present work does not preclude the existence of changes in the functional expression of other ionic conductances that could also be participating in the changes in excitability observed in BPH cells, but it is clear that a decreased K^+ conductance at values around and below resting V_M is needed to explain the observed changes in excitability (Fig. 4.5). In fact, the average currents obtained in perforated patch experiments in BPN and BPH cells can be reasonably reproduced through simple calculations based on a parallel conductance model (Fig. 5.1). Assuming that at any voltage between −120 and −20 mV total membrane current is the arithmetic sum of currents through inward rectifying (K_{IR} plus K_{ATP}), voltage-dependent K^+ (K_V) and Ca^{2+} (Ca_V) channels and a putative Na^+-dependent inward current (mediated for example by TRP channels), actual data obtained in VSMCs from BPN mice can be reasonably

reproduced. The calculation depicted for BPH currents includes the reduction of the K_V current amplitude previously reported in BPH cells (Moreno-Dominguez et al. 2009) and a decrease of the current through inward rectifying K^+ channels by 50%. As shown in Fig. 5.1, these changes generate a total current that closely mimics the changes observed in BPH cells, namely a reduction in the total current amplitude at −150 mV, a decrease of the slope conductance at potentials closed to E_K and a shift of the resting V_M towards more depolarized potentials. Actually, the fact that no other changes are needed is experimentally supported, as whole currents at E_K are very similar in BPN and BPH mice (Fig. 4.5).

5.1 Vascular bed distribution of inward rectifier K^+ channels

We also provide a characterization of the expression pattern of the different molecular constituents of inward rectifier K^+ channels in five different vascular beds both in normotensive and in hypertensive animals. Our results confirm the predominant expression of Kir2.1 transcripts in small vessels and the more homogeneous expression of the molecular components of K_{ATP} channels. Also, while hypertension induces significant changes in the expression of K_{ATP} channel transcripts in most vascular beds explored (Fig. 4.9 and 4.10), the changes in expression of Kir2.1 are very clearly restricted to renal and mesenteric arteries. We also detected a moderate expression of members of the G-protein gated inward rectifier K^+ channels (GIRK, Kir3.x), especially in cerebral and renal vessels. Surprisingly, some members of the K^+ transport channels (i.e. Kir1.x and Kir4.x channels) were detected in the mRNA expression studies. Kir4.1 mRNA was found in all vascular beds explored at levels similar to those of Kir2.1 transcripts, and its expression was significantly smaller in aorta and mesenteric arteries from BPH mice. These channels have been previously found in glial cells and in renal and gastric epithelium (Hibino *et al.* 2010), but this is the first report of their presence in VSMCs. Also, we have confirmed the expression of Kir4.1 protein in mesenteric VSMCs (Fig. 4.11). Lack of specific inhibitors has precluded further characterization of these channels, although their sensitivity to Ba^{2+} blockade suggests that these changes in expression could contribute to the overall changes in K_{IR} currents reported in this work. Kir1.1 (first described as ROMK1) is expressed only in cerebral arteries and at very high levels in renal arteries and it is one of the few channels whose expression is upregulated in hypertension. Kir1.1 knockout causes a renal salt wasting phenotype associated with hyperaldosteronism and hypotension (Bartter syndrome; reviewed by Hibino *et al.* 2010). As in the case of Kir4.1, Kir1.1 channel

expression has been described only in renal epithelium, and also in some cortical neurons, but it would be interesting to explore its possible function in VSMCs from those vascular beds.

5.2 Functional expression of K_{IR} and K_{ATP} channels in mesenteric arteries

In mesenteric VSMCs, we found that current density due to K_{IR} channels was smaller than current density through K_{ATP} channels in all the conditions studied (in perforated patch it represented 49% of K_{ATP} current density at −150 mV, see Fig. 4.13-16). In fact, while the contribution of K_{ATP} channels to V_M and basal tone in mesenteric arteries has been reported in several studies (reviewed by Quayle *et al.* 1997), the functional role of K_{IR} channels in this preparation is still debated. Several studies report expression of K_{IR} transcripts (mainly Kir2.1) in mesenteric VSMCs (Bradley *et al.* 1999; Kim *et al.* 2005; Smith *et al.* 2008), and a role of these channels in VSMC excitability (either in isolated cells or in whole mesenteric arteries) was reported in some studies (Kim *et al.* 2005) but not in others (Crane *et al.* 2003; Brochet & Langton, 2006; Smith *et al.* 2008). These discrepancies could be attributed to differences in the experimental setting, the size of the arteries used or the species under study. Additionally, they could reflect a minor contribution of these channels to set resting V_M in mesenteric arteries, as such discrepancies are absent in other preparations in which they are clearly relevant, such as cerebral or coronary arteries (Quayle *et al.* 1997).

Here, we detected expression of mRNA and protein for K_{IR} channels in mesenteric VSMCs, and also found a consistent functional contribution of these channels both in isolated cells and in whole arteries in which endothelium has been removed. The role of the channels was explored pharmacologically by studying Ba^{2+}-sensitive changes in current density, resting V_M and contractile responses. $BaCl_2$ is a rather non-specific blocker for many other potassium channels, although with higher Kd values, so that at concentrations up to 50–100 µM it can be considered as a selective inhibitor of the classical K_{IR} channels in vascular smooth muscle (Quayle *et al.* 1997; Zaritsky *et al.* 2000; Brayden, 2002; Park *et al.* 2008). We found a significant effect at concentrations of 30 µM and lower (see representative traces in Fig. 18*A*), supporting the presence of functional K_{IR} channels in our preparation.

In contrast to K_{IR} channels, the expression and functional role of K_{ATP} channels in mesenteric arteries is better established (Nelson *et al.* 1990; Nelson & Quayle, 1995; Hibino *et al.* 2010). The ability of glibenclamide to elicit a significant depolarization of mesenteric VSMCs is consistent with a major contribution of K_{ATP} channels to total K^+ conductance (Jiang *et al.* 2007), and is also supported by the presence of glibenclamide and pinacidil-sensitive currents in these cells.

5.3 Changes in K_{IR} and K_{ATP} channels in essential hypertension

We found a reduction in Kir2.1 and Kir4.1 mRNA transcripts upon hypertension, leading to a decrease of K_{IR} channel current density in isolated mesenteric VSMCs. Interestingly, although the $BaCl_2$ depolarizing response is clearly smaller in BPH cells, the contractile response of BPH mesenteric arteries to $BaCl_2$ is not significantly different. As VSMCs from BPH arteries are depolarized, the lack of differences in their response to $BaCl_2$ may simply reflect the fact that BPH arteries require smaller depolarizations to produce a Ca^{2+} entry equivalent to that obtained in BPN animals.

The available data regarding changes in K_{IR} channels in other models of hypertension are limited to their expression in cerebral arteries, where several authors have reported a decrease of the Ba^{2+}-sensitive vasodilator responses to moderate increases in extracellular K^+ (McCarron & Halpern, 1990; Chrissobolis & Sobey, 2003), suggesting an impairment of cerebral K_{IR} channels during chronic hypertension. However, there are no systematic studies of the changes of K_{IR} channels in other vascular beds and their contribution to the increased vascular tone or the development of high blood pressure. It is interesting to note that the majority of the data on the function of K_{IR} channels in the vasculature are derived from coronary and cerebral arteries. While these preparations are amenable for studying the role of ion channels in vascular tone control due to their relevant intrinsic control and their prominent myogenic tone, they may be less sensitive to the changes induced by essential hypertension, as their marked auto-regulation protects these vascular beds from systemic changes in blood pressure.

The data from BPH mesenteric arteries show a noticeable decrease in both the expression and the functional contribution of K_{ATP} channels to VSMC excitability. Our findings fit well with some previous reports indicating an impairment of the function of vascular K_{ATP} channels during hypertension (Sobey, 2001). However, decreased expression of Kir6.1/SUR2B protein in hypertensive aortas with preserved functional responses to K_{ATP} openers has also been reported (Blanco-Rivero *et al.* 2008). A reason for the discrepancy with our work may rely on the different vascular bed used, as the impact of changes in conductance vessels in the development of hypertension is expected to be minor. It is noteworthy that there is a change not only in the functional expression of K_{ATP} channels in BPH vessels, but also in the fraction of these channels that are active at rest (Fig. 4.17C). Our data in perforated patch using glibenclamide and pinacidil suggest that around half of the K_{ATP} channels expressed at the plasma membrane are active under basal conditions in normotensive VSMCs, but this fraction increases to more than 70% in BPH VSMCs (Fig. 4.16B and 4.17B). This observation could

explain previous reports indicating that K_{ATP} channel activators are less potent dilators in vivo in cerebral vessels of chronically hypertensive rats (Takaba et al. 1996), and is relevant for hypertension therapy, because it would imply that K_{ATP} channel dysfunction in hypertension may also interfere with vascular responsiveness to treatment with K^+ channel openers.

5.4 Contribution of the BPN/BPH model for understanding the molecular basis of hypertension

The model used in this study (BPH mice) has a moderate hypertensive phenotype, obtained by phenotypic selection. This particular model closely resembles the most common forms of human hypertension, as a genome-wide differential analysis in BPH and BPN mice has shown the involvement of several systems in the pathology of hypertension, reinforcing its multifactorial and complex nature (Friese *et al.* 2005). For that reason, the characterization of K_{IR} and K_{ATP} channels in this model allows us to draw some conclusions regarding the contribution of these channels to the development of essential hypertension, and also to frame the available data from knockout models. It could also provide a complementary approach for the study of the molecular determinants of essential hypertension, as so far there are no reports of genetic associations of Kir2.1, Kir4.1 or Kir6.1 genetic variants and hypertension in humans. While studies on Kir2.x$^{-/-}$ animals have not addressed directly the issue of their contribution to blood pressure, they indicate that Kir2.1 (but not Kir2.2) expression in VSMCs is required for K_{IR} currents and K^+-induced dilations in cerebral arteries (Zaritsky *et al.* 2000). With respect to knockout models of vascular K_{ATP} channels, there are two available Kir6.1$^{-/-}$ (Miki *et al.* 2002; Seino & Miki, 2004) and SUR2$^{-/-}$ (Chutkow *et al.* 2002). In both cases there is a complete loss of vascular K_{ATP} currents and a phenotype that highlights the critical role of this channel in regulating episodic vasomotor activity and vascular tone, especially in coronary arteries. However, only SUR2$^{-/-}$ mice show elevated blood pressure. In the light of our findings showing a decrease of both Kir6.1 and SUR2 mRNA in mesenteric VSMCs from BPH animals, we infer that SUR2 proteins may have other cellular partners that could compensate for the increased vascular tone observed in the absence of functional K_{ATP} channels in Kir6.1$^{-/-}$ animals.

In summary, we present here a characterization of inward rectifying K^+ channels in normotensive and hypertensive mesenteric arteries that spans from the mRNA to the protein, their function in isolated cells and their contribution to the function of the pressurized arteries. Our data support the hypothesis that changes in the functional expression of K_{IR} and K_{ATP} channels are relevant for the development of a hypertensive phenotype in a naturally

139

occurring form of hypertension, as they could be key determinants of membrane depolarization in hypertensive VSMCs.

5.5 Calcium channels remodelling in hypertension

The vascular ion channel remodeling during hypertension appear to involve a down regulation of K^+ (K_V and K_{IR}) channels in VSMCs form arteries exposed to high blood pressure (Cox *et al.*, 2001;Weston *et al.*, 2010;Martens & Gelband, 1996) that causes a depolarized resting membrane potential in VSMCs. Besides, the higher intraluminal pressure and enhanced sympathetic neural output that is characteristic of hypertensive animals may also promote arterial depolarization and activation of LTCCs. The final consequence may be a Ca^{2+}-dependent increase in peripheral vascular resistance that contributes to the progression of blood pressure elevation.

Given the tight relationship between resting membrane potential, calcium influx through LTCCs and vascular tone, it is not surprising that many studies during the past decade have shown that hypertension is associated with an elevated Ca^{2+} influx through arterial α_{1c} channels. However, while in some of these studies this finding is only indicating that the more depolarized resting membrane potential of VSMCs in hypertensive arteries determines that a larger fraction of LTCCs are open at rest, in other cases changes in the expression, the modulation or the kinetics of LTCCs are demonstrated in hypertensive animals. The best characterized animal models of essential hypertension are rat models, and included genetically hypertensive models (SHR, for spontaneously hypertensive rats), salt-induced hypertensive rats (the Dahl salt-sensitive rats) and renal hypertension models obtained with surgical approaches, such as the partial ligation of the aorta between the left and right renal arteries, to selectively elevate blood pressure in the right renal artery, or the partial renal artery ligation (Goldblatt 2-kidney 1-clip model, (Goldblatt *et al.*, 1934). In all these models, it has been described that even short term exposure to high intravascular pressures appears to upregulate the α_{1c} subunit and the number of functional LTCCs in VSMCs (Lozinskaya & Cox, 1997;Martens & Gelband, 1996;Simard *et al.*, 1998;Pesic *et al.*, 2004). In some of these studies, it is shown that depolarization per se promotes α_{1c} subunit expression in the VSMCs of small arteries, suggesting that this "myogenic stimulus" that represents the elevated blood pressure may both activate existing LTCCs and increase the number of LTCCs channels in VSMCs during the evolution of hypertension (Pesic *et al.*, 2004;Sonkusare *et al.*, 2006b). However, this increase in LTCCs expression is not consistently found in all cases and some important discrepancies have been pointed out. As an example, LTCC current density has been reported to increase in young

Conclusions

SHR, when blood pressure values are normal, but the difference disappear in old, hypertensive animals (Ohya *et al.*, 1993). Also, in SHR rats, and in spite of the finding of an increased calcium channel function, a decrease in the number of DHP receptors determined with binding studies in living cells has been reported (Hermsmeyer *et al.*, 1995). In that study, a defect in calcium-dependent inactivation has been proposed to contribute to the molecular etiology of genetic hypertension. Finally, in contrast to studies in renal hypertension and SHR rats in which an increase in the maximal conductance through LTCCs was described, in the Dahl-salt-sensitive rats, no changes in the maximal conductance were found, but the voltage-dependent availability was altered (Ohya *et al.*, 2000). Moreover, the alterations of LTCCs were induced by dietary salt loading in Dahl rats, but appeared after the development of hypertension in renal hypertensive rats, and before hypertension in SHR rats, indicating that the mechanisms involved differ among models.

The obvious differences between our study and previous published work regarding LTCCs remodelling in hypertension can be attributed in a large part to substantial differences in the animal models used. The most important of these differences, apart from species and vascular bed related ones, relies on the natural history of hypertension in those models. While our BPH animals show a moderate hypertension that develops in adult life, the spontaneous hypertensive rat model does not exactly mimic the essential hypertension in humans, mainly for two reasons: (1) this model shows a severe hypertension and (2) SHRs reproducibly develop hypertension in young adulthood rather than in middle age as in human (Doggrell & Brown, 1998). The renal hypertension model also leads to very severe hypertension that develops over a short time course. While, as mentioned before, there is no need to invoke changes in the expression and/or the function of LTCCs to understand the development of essential hypertension, it is possible that the differences between our model and these extreme hypertension models can be explained by an upregulation of LTCCs in these later ones that creates a positive feedback for calcium influx and increased arterial tone.

Our findings demonstrate that VSMCs from BPH mice present lower LTCC mRNA expression and a decreased density of nifedipine sensitive calcium currents. Despite this, BPH LTCCs operate at higher open probabilities at rest, present a longer mean open time and are grouped in bigger clusters than BPN. Our data suggest that these differences are probably due to different ancillary subunit composition of the LTCCS. These changes are rather complex, and global and local effects on Ca^{2+} changes in BPH myocytes could be quite different if we consider other changes in these cells, such a more depolarized membrane potential and a minor contribution of BK_{Ca} channels to control cell excitability.

141

5.6 LTCCs functional expression

In this study, we found differences in whole-cell Ca^{2+} currents density in myocytes from small mesenteric arteries of BPH compared with myocytes from BPN. Peak Ca^{2+} current density was smaller in myocytes from BPH than those from BPN at all voltages between −20 and +60 mV, with no significant difference in voltage dependence (Figure 4.20). The smaller currents recorded in the BPH were not the result of differences in cell size, as the currents were normalized to cell capacitance. Possible explanations for these differences in BPH Ca^{2+} current density could include (a) a different type of Ca^{2+} channel in the membrane, (b) an intracellular mediator that could act as an inhibitor of LTCCs currents, and (c) a decrease in the number of channels or in their open probability.

a. A different type of Ca^{2+} channel?

Previous studies of Ca^{2+} currents in vascular myocytes in hypertension have suggested the presence of two Ca^{2+} channel types, L and T (Hermsmeyer & Rusch, 1989). However, L–type channels are predominant in VSMCs from mesenteric arteries (Sonkusare *et al.*, 2006b). In the present study in myocytes from BPN and BPH, we found evidence for only one current component, the L-type. The evidence is twofold: Pharmacological, as the channel is blocked by nifedipine, indicating its dihydropyridine-sensitivity (Figure 4.22) and biophysical, as its kinetic behaviour (voltage dependence, activation and deactivation kinetics) is similar in both strains and corresponds to the properties of LTCCs. So, under the conditions of the present study, the macroscopic currents recorded can be reliably attributed to LTCCs exclusively, with no evidence of differences in the type of calcium channels expressed between BPN and BPH cells.

b. An intracellular inhibitory mediator in BPH VSMCs?

The perforated-path technique was used to test the hypothesis of an intracellular mediator, which could act as an inhibitor of LTCCs currents in the hypertensive strain, as in this technique the formation of small pores in cell membrane, does not disturb cell metabolism or intracellular milieu (Horn & Marty, 1988). In this regard, it is well known that LTCCs activity may be modulated by intracellular Ca^{2+} and Mg^{2+}, pH, G proteins, ATP, IP3, the cyclic nucleotides cAMP and cGMP, protein kinase C, phosphatases, tyrosine kinases and calmodulin (Hughes, 1995). Indeed, when BPH and BPN inward Ba^{2+} currents were compared using perforated-patch vs. conventional whole cell recording in mesenteric artery myocytes, the perforated-patch currents were smaller than conventional whole cell currents (Figure 4.21). However, the differences in the current density when comparing BPH relative to BPN were the same as in the whole cell recordings. Thus, Ba^{2+} currents differences during conventional

whole cell recording are not due to a washout of some cytoplasmic constituent of the VSMCs, so we can also eliminate the hypothesis of an inhibitor of LTCCs currents differentially expressed in the hypertensive strain.

c. *Changes in the number or the kinetics of LTCCs?*

Regarding the possibility of a different number of Ca^{2+} channels in hypertensive VSMCs, the electrophysiological and pharmacological properties of the LTCCs was tested further by examining the effects of BayK 8644, an LTCC opener which binds to the α_1 subunit modifying channel kinetics and evoking a large cation influx. BayK 8644 enhanced the whole cell LTCCs Ba^{2+} current by an increase in single-channel conductance together with the recruitment of a longer-duration open state (Tavalin *et al.*, 2004;Peterson & Catterall, 2006).

In the present study, we found that BayK 8644 increases Ba^{2+} inward current in both preparations and that Ba^{2+} currents also exhibit similar kinetics in BPN and BPH cells. The Ba^{2+} currents in the presence of BayK were still larger in BPN cells, but differences in current density between BPN and BPH cells were greatly diminished, as potentiation by BayK was significantly larger in BPH cells (Figure 4.23). In other studies, VSMCs from genetically hypertensive or experimentally induced hypertensive animals also exhibit greater sensitivity to the Ca^{2+} channel agonist BayK-8644 (Bruner & Webb, 1990). However, it should be noted that the contractile effect of BayK-8644 in hypertensive arteries may just reflect the fact that a larger fraction of LTCCs are open as a consequence of the more depolarized resting membrane potential in hypertensive arteries (Aoki & Asano, 1986). Our analysis of the steepness and midpoint potential of activation (Figure 4.24C) show no differences between BPN and BPH Ba^{2+} currents, excluding changes in the voltage-dependent properties of the channel in control conditions or in response to Bay K 8644.

Whole-cell calcium current amplitude is described by the following relationship:

$$I_{Ca} = n \cdot P_o \cdot g_u (V_M - E_{Ca})$$

where **n** is the number of channels in the membrane, **P_o** is the open probability, **g_u** is the unitary single channel conductance, **V_M** is the membrane potential and **E_{Ca}** is the reversal potential for Ca^{2+} ions.

Under voltage clamp, only **n**, **P_o** or **g_u** can be different between BPN and BPH cells. Single channel conductance seems to be the same in both cells (as inferred from sparklet amplitudes data, Figure 4.37). If we assume that BayK-8644 moves the channels both in BPN and BPH cells towards the same, longer-duration open state, we could consider that **P_o** is close to 1 in both

cases. Then, differences between LTCC currents must be due to a reduced number of LTCC in the BPH VSMCs plasma membrane. Several aspects of the data presented in this thesis are compatible with these assumptions (see below). However, the observed differences in the activity of LTCCs at rest (Ca^{2+} sparklets) are clearly not related to a decrease in the number of channels in the membrane. Other differences reported in this work, mainly related with a possible change in the composition of auxiliary subunits could be the responsible of the observed differences in Ca^{2+} sparklet activity.

5.7 Changes in the composition of LTCCs in hypertension

Our data from quantitative PCR could detect mRNA expression of several calcium channel pore forming α_1 subunits, being the Cav1.2 (α_{1c}) the most abundantly represented. We also detect mRNA expression for the $\alpha_2\delta$ isoforms 1-3, for all β subunits and for γ isoforms 1, 4 and 6. When comparing with BPH, our data indicate a significant reduction in the mRNA expression levels of the pore forming α_1 subunit (Figure 4.25), which correlates with the decreased Ba^{2+} current density described above (see Figure 4.20). In addition, all the γ and the β_2 accessory subunits exhibited a decreased expression in BPH, while only one accessory subunit ($\alpha_2\delta_3$) showed an increased expression in BPH. Previous studies indicate that α_1 and $\alpha_2\delta$ mRNA and protein are higher in cerebral arteries of hypertensive SHRs than WKY rat controls (Bannister *et al.*, 2012). In contrast, angiotensin II-induced hypertension did not alter neither α_1 nor β_3 mRNA but elevated α_1 and β_3 protein in cultured mesenteric arteries (Kharade *et al.*, 2013). These findings led to the proposal that hypertension may not be associated with changes in α_1 message but modification of LTCCs auxiliary subununits composition. Nevertheless, in order to get a first approximation to the possible changes in the composition of the LTCC channelosome, we have expressed the relative abundance of the mRNA for accessory subunits as a function of the levels of the α_1 (Figure 4.26). This simplistic approach suggests that BPH LTCCs are more likely to associate with $\alpha_2\delta$ subunits than BPN LTCCs. While association and modulation of α_{1c} with γ subunits in VSMCs is not clear, it is well known that $\alpha_2\delta$ and β auxiliary subunits modify channel properties: they can increase the activation and inactivation kinetics (Singer *et al.*, 1991), control the open probability (Shistik *et al.*, 1995) and contribute to the stability of the channel on the cell membrane.

With this assumption, we tested the hypothesis that the observed functional differences could be the consequence of changes in the L-type calcium channel chanelosome with a combined approach: (a) we use the antiepileptic drug gabapentin (GBP) as a tool to explore the presence and functional contribution of $\alpha_2\delta$ subunits to LTCCs in VSMCs (Davies *et al.*, 2007) and (b) we

compare the properties of native currents with currents obtained by heterologous expression of different subunits compositions.

a. *Lessons from GBP effects on LTCCs in native cells*

Gabapentin (GBP) was originally developed as an analogue of γ-amino-butyric acid (GABA), but is now believed to have no effect on GABA receptors or transporters (Taylor, 2009a). A structural domain in the α_2 protein of the $\alpha_2\delta$ subunit was identified by sequence homology as a von Willebrand factor type A domain (VWA), a site known to mediate interaction with extracellular matrix proteins (Whittaker & Hynes, 2002;Marais *et al.*, 2001b).

Acute effects of GBP on Ca^{2+} currents produced variable results. GBP has been shown to inhibit a variety of Ca^{2+} currents, including L-, N-, and P/Q-type (Cheng & Chiou, 2006). However, other studies show no acute effect of GBP on Ca^{2+} currents (Hendrich *et al.*, 2008a). On the contrary, in our study, also based on an acute application of the drug, we found that GBP increased LTCCs currents, being this effect significantly different in BPH and BPN VSMCs (Figures 4.27 and 4.30A). These differences can be related to differences in Ca^{2+} channel isoforms (both for the pore forming and accesory subunits) or in the auxiliary subunits present. In any case, if GBP is a specific ligand of $\alpha_2\delta_x$ subunits, the differential effect observed in BPN and BPH cells correlates well with the increased proportion of $\alpha_2\delta$ mRNA expression in BPH (Figure 4.26). Two indirect evidences demonstrate that the effects of GBP on LTCCs are due to its specific binding to $\alpha_2\delta$ subunits: in the heterologous system, we could not see any effect of the drug in any L-type channel subunit combination in which $\alpha_2\delta$ subunit was not present (Figure 4.30B), and in the native system, we demonstrate the lost of the effect of GBP upon removal of the α_2 subunit by treatment with DTT (Figure 4.28). DTT is a reducing agent that cleaves the $\alpha_2\delta$ accessory subunit by breaking the disulfide bridge that holds them together, eliminating the binding site of gabapentin from the LTCC channelosome (Marais *et al.*, 2001a).

Ca^{2+} channel $\alpha_2\delta$-1 and $\alpha_2\delta$-2 subunits were proposed to be the main site of action of GBPs (Dooley *et al.*, 2007). Since individual $\alpha_2\delta$ subtype may associate with different α_1 Ca^{2+} channels (Hobom *et al.*, 2000), it is expected that GBPs should affect various types of Ca^{2+} channels depending on the tissue and/or cell studied. Therefore it is not surprising that GBP effect is not similar in all cell preparations. This finding may reflect a biovariability in the target binding interactions of GBPs. Several reports indicate that GBPs reduced the cellular influx of Ca^{2+} via LTCCs in synaptosome fractions prepared from brain tissue (Fink *et al.*, 2002), in isolated rat neurons (Stefani *et al.*, 2001) and in dorsal root ganglion cells (Freiman *et al.*, 2001). On the other hand, there are many reports that have failed to detect any acute GBP-

mediated change in Ca^{2+} channel currents recorded from hippocampal neurons (Schumacher *et al.*, 1998), Purkinje cells (Dolphin, 2003) or PC12 cells (Vega-Hernandez & Felix, 2002). Also, in the light of our findings showing a clear biphasic dose-response curve for the effect of GBP in BPN cells, the lack of effect of some of these studies can be attributed to an inadequate GBP concentration. It is remarkable that we only observed this potentiating effect with 100µM GBP on LTCC from BPH cells. At this dose, GBP did not affect the amplitude of LTCCs from BPN mesenteric VSMCs, calcium currents from superior cervical ganglion (SCG) neurons or calcium currents from pituitary cells from BPN or BPH animals (Figure4.29). These other preparations were selected to exclude a change in the response to GBP as a consequence of the preparation (BPN or BPH animals) or the type of channels involved (L-type in mesenteric, L-type of neural origin in pituitary cells and a mixture of L- and N-type channels in SCG).

Finally, it is significant that a recent study from the group of Jaggar identify $\alpha_2\delta$ subunits as essential elements for plasma membrane expression of LTCCs in arterial myocytes (Bannister *et al.*, 2009). In a more recent work they found that in cerebral arteries of SHR rats, age-dependent development of hypertension was associated with an unequal elevation in $\alpha_2\delta$-1 and $Ca_V1.2\alpha_1$ mRNA and protein in cerebral artery myocytes, with $\alpha_2\delta$-1 increasing more than $Ca_V1.2\alpha_1$. The elevation in $\alpha_2\delta$-1 expression that promotes surface trafficking of $Ca_V1.2$ channels in cerebral artery myocytes leads to an increase in $Ca_V1.2$ current-density and a reduction in current inactivation that induces vasoconstriction (Bannister *et al.*, 2012). Apart from the already mentioned differences between the SHR model and ours, it is interesting that the changes in LTCCs in this model are also attributed to differences in the molecular composition of the channel in hypertensive animals.

b. *Lessons from heterologously expressed LTCCs*

In addition to $\alpha_2\delta$ subunits, LTCCs in VSMCs also associate with different β subunits whose coexpression is able to modulate the properties of the currents. Coexpression of β subunits with various α_1 subunits increased peak current (Singer *et al.*, 1991), due to an elevation in the number of functional surface membrane channels and by facilitating channel pore opening (Kamp *et al.*, 1996). Also, changes in the kinetics of the current associated with the presence of β subunits have been described both in native and heterologous systems (Lacinova, 2005;Castellano *et al.*, 1993). Our expression data are in agreement with previous data in the literature which indicate that the β_3 subunit is the main subtype expressed in VSMCs although β_2 subunits has also a significant expression (Murakami *et al.*, 2003c). We found that for this later subunit, mRNA expression levels were decreased in BPH. As native LTCCs in VSMCs are

probably composed of a heterogeneous mixture of at least $Ca_V1.2\alpha_1$, $\alpha_2\delta$, β_2 and β_3 subunits, it can be difficult to find the molecular correlate of the differential modulation of the currents by GBP, and for that reason we decided to explore the effects of the drug by coexpressing the subunits in different combinations in a heterologous system.

Our data confirm the specificity of GBP for $\alpha_2\delta$ subunits, as we could not find modulatory effects in combinations not including this subunit. With regards to the concentration-response relationship for the acute effect of GBP, a biphasic curve for GBP (similar to that of BPN) was obtained when co-expressing $\alpha_1 + \alpha_2\delta$ subunits (in the absence of β subunits), while a response similar to that observed in BPH was obtained by co-transfection of HEK with $\alpha_1 + \alpha_2\delta + \beta_2$ subunits (Figure 4.30B). These results suggest that the different response to GBP between BPN and BPH cells can be due to a different proportion of the β_2 subunits in the functional LTCCs. These results do not correlate with the β_2 subunit mRNA changes observed in BPN VSMCs, but are in good agreement with the differences in protein expression described by western-blot (Figure 4.31B). This is a peculiar case where a decrease in mRNA expression is associated with an increase in protein levels in the cells.

Regarding the role of β subunits in hypertension, it is interesting to point out that in a very recent publication, changes in the expression of β_3 subunits was linked to calcium channel upregulation in mice made hypertensive by angiotensin II infusion (Kharade *et al.*, 2013). Similarly, studies on $\beta_3^{-/-}$ mice have shown that VSMCs express fewer $Cav_{1.2}$ channels compared with wild-type (WT) mice, implying that $Cav\beta$ contributes to the basal expression of $Cav_{1.2}$ channels in VSMCs in vivo (Murakami *et al.*, 2003a). In agreement with this data, we found a decreased expression of β_2 subunits in BPH mice that could be contributing to a decreased LTCC density.

Data presented in this thesis and published in the literature are far from providing a clear pictutre of the role of LTCCs in the genesis and manteinance of the hypertensive phenotype. More data and a deeper knowledge of the functional consequences of having a different composition of auxiliary subunits are needed. Nevertheless, our data, and the recent papers on the subject already cited above clearly point towards the composition of the channelosome as an important player in the genesis and developing of hypertension.

5.8 Functional activity of LTCCs in basal conditions

Data presented in this work clearly demonstrate that essential hypertension can occur in the absence of an upregulation of LTCCs. However, in the absence of other changes, a reduction in

the number of LTCCs will lead to a lower blood pressure. For that reason, if BPH cells show a lower calcium current density, the regulatory mechanisms of $[Ca^{2+}]_i$ in VSMC must be modified in a compensatory manner. These compensatory mechanisms could affect the kinetic behavior of the channels under physiological conditions or, alternatively, can be due to changes in related molecules, such as BK channels, RyR receptors, Ca^{2+} pumps or Na^+/Ca^{2+} exchanger or to changes on the functional coupling between LTCCs and these other molecules. To explore these possibilities, we performed an optical analysis of Ca^{2+}-permeable ion channel activity, using TIRF microscopy to analyze Ca^{2+} sparklets (Navedo *et al.*, 2005).

Considering the strong voltage-dependence of LTCC activation and broad expression of functional LTCCs throughout the plasmalemma of arterial smooth muscle cells, it was long assumed that channel activation is random and that all LTCCs have a similar open probability at a given membrane potential. However, the laboratory of Santana reported that subpopulations of LTCCs in isolated arterial myocytes operate in a continuously high open probability mode, producing distinct sites of Ca^{2+} influx (Navedo *et al.*, 2005). The spatial distribution of LTCC sparklet sites in arterial myocytes, although varied between cells, is not a random process, indicating that LTCC activation occurs at defined sites within the myocyte surface membrane (Santana & Navedo, 2009).

Identification of sarcolemmal L-type Cav1.2 channels as the molecular entity underlying Ca^{2+} sparklets in arterial myocytes is based on multiple pharmacological, biophysical, and molecular biological studies. First, Ca^{2+} sparklets are eliminated by DHP antagonists and enhanced by DHP agonists and are insensitive to intracellular store depletion with thapsigargin. Furthermore, unlike Ca^{2+} release events from intracellular stores, Ca^{2+} sparklets are rapidly eliminated by the removal of extracellular Ca^{2+}. Second, unlike Ca^{2+} release events from intracellular Ca^{2+} stores, Ca^{2+} sparklets are associated with an inward L-type Ca^{2+} current. Consistent with this, Ca^{2+} sparklets have similar voltage dependencies of amplitude and activity as $Cav_{1.2}$ channels (Navedo *et al.*, 2005). Third, heterologous expression of the pore-forming Cav1.2 (i.e. α_{1C}) subunit with accessory β_3 and $\alpha_2\delta$-1 subunits in tsA-201 cells recapitulates LTCC sparklets with identical pharmacological and biophysical properties as Ca^{2+} sparklets in native smooth muscle cells (Navedo *et al.*, 2006). Finally, arterial myocytes expressing DPH-insensitive $Cav_{1.2}$ channels produce DPH-insensitive Ca^{2+} sparklets (Navedo *et al.*, 2007).

LTCCs sparklets have been described displaying several activity modes; namely silent, low and high (i.e. persistent). A silent LTCC sparklet refers to a typically dormant site, which can be triggered by LTCC agonists, for instance. Low activity sparklets show intermittent, transient

openings, whereas high activity ("persistent") sparklet sites are characterized by prolonged openings and nearly continuous Ca^{2+} influx (Navedo *et al.*, 2005). In our study we only considered sparklets at low and high open probability. An amplitude histogram for these events was fitted with a multi-component Gaussian function, revealing the quantal nature of Ca^{2+} influx through LTCCs (Figure 4.37). Both BPN and BPH showed a single quantal unit of Ca^{2+} influx that typically elevated [Ca^{2+}]$_i$ in the vicinity of the channel by ~37 nM in the presence of 20 mM external Ca^{2+}. These data confirm the absence of differences in the single channel conductance of LTCCs between BPN and BPH mice.

The "sparklets" data presented in this study are observed at hyperpolarized membrane potentials (−70 mV), so that we are analyzing the behavior of LTCCs at resting, basal conditions. Under these conditions, small clusters of seemingly coupled channels operate continuously at high open probabilities creating sites of sustained Ca^{2+} influx. We found no significant differences in the number of sparklets sites per cell between BPN and BPH, but we did observe a greater activity of LTCCs in high-activity Ca^{2+} sparklet sites in BPH. Examination of the amplitude distribution produced by LTCC sparklets led to a remarkable finding, the simultaneous openings of independently gating channels, suggesting that a group of several LTCCs may activate and inactivate in a independently or synchronous manner in the same sparklet site (Figure 4.37 insets). Several reports indicate that LTCCs form clusters, and can gate coordinately along the sarcolemma of VSMCs (Navedo & Santana, 2012). In this regard, our data suggest that BPH and BPN LTCCs are differentially distributed throughout the sarcolemma of VSMCs: while most BPN LTCCs channels diffuse in clusters of 2 to 5 channels, BPH form clusters of 2 to 7 channels. Altogether our findings show that BPH LTCCs under physiological conditions present a higher open probability, with longer mean open time and are organized in bigger clusters. With this organization, the activation of LTCCs in BPH will lead to an increased Ca^{2+} influx at rest. The physiological implications of sustained Ca^{2+} influx via clusters of LTCCs are profound. LTCCs in high activity Ca^{2+} influx mode increase local [Ca^{2+}]$_i$ and can activate nearby Ca^{2+}-sensitive proteins such as calmodulin, surface membrane Ca^{2+}-activated ion channels, and ryanodine receptors. LTCCs in persistent Ca^{2+} influx mode may indirectly influence SR function, elevating SR Ca^{2+} load. Therefore, by this way sparklets could increase the frequency of RyR-mediated Ca^{2+} sparks and activation of nearby large conductance Ca^{2+}-activated K$^+$ (BK$_{Ca}$) channels, ultimately promoting hyperpolarization and decreased LTCC activation. It is interesting to point out, that although produced by <1% of the functional L-type Ca^{2+} channels located in an area representing <1% of the total surface membrane, persistent Ca^{2+} sparklets are a major contributor to Ca^{2+} influx and [Ca^{2+}]$_i$ in arterial

myocytes (Navedo *et al.*, 2005). In the light of this observation, our findings in BPH cells are significant because they raise the possibility that the targeting (and not the number) of L-type calcium channels to the sarcolemma of arterial myocytes is critical for local persistent Ca^{2+} sparklet activity and hence for the regulation of arterial wall $[Ca^{2+}]_i$, myogenic tone, blood pressure, and the development of hypertension. In BPH mice, the spatial organization and the kinetic behavior of LTCCs will promote a larger Ca^{2+} influx at rest, leading to increased arterial tone and hypertension.

At this point, it is worthy to note the apparent paradox of how less LTCC present in the BPH plasma membrane could have a pro-hypertensive effect. Global and local changes could not only be very different, but could also have different physiological functions. In this case, fewer channels in the membrane seem to be more active (Ca^{2+} sparklets). Furthermore, if we take into account that BPH cells are depolarized and that BK_{Ca} channels in these cells are less functional (see below) the paradox becomes easily understandable.

It will be interesting to explore what are the determinants of this different spatial organization of LTCCs between BPN and BPH with such relevant functional consequences. In this regard, a recent study of the group of Santana suggest that the scaffolding protein, AKAP150 (A-kinase anchoring protein 150) is required for local targeting of PKCα to the sarcolemma of arterial myocytes and for PKCα-dependent persistent Ca^{2+} sparklet activity, but not for rare, stochastic L-type Ca^{2+} channel activity. This suggests that AKAP150/PKCα signaling does not increase L-type Ca^{2+} channel activity globally. Rather, this signaling complex increases Ca^{2+} influx locally by selectively coercing small clusters of L-type Ca^{2+} channels to operate in a persistent gating mode that create sites of sustained Ca^{2+} influx (Navedo *et al.*, 2008). These results have important functional consequences, as AKAP150$^{-/-}$ mice were hypotensive under control conditions and, unlike WT, did not develop hypertension during chronic angiotensin II infusion. In this same line, it will be interesting to explore in our model of hypertension the molecular determinants of the clustering of LTCC in sparklets sites, and, following our previous findings to explore whether this different localization can be related to the different subunit composition of the LTCCs in BPH animals.

5.9 Uncoupling in Ca^{2+} SPARKs and BK STOCs

Local intracellular Ca^{2+} transients, termed Ca^{2+} sparks, are caused by the coordinated opening of a cluster of ryanodine-sensitive Ca^{2+} release channels in the sarcoplasmic reticulum of VSMCs. Ca^{2+} sparks also have a profound negative-feedback effect on contractility by

decreasing Ca^{2+} entry through membrane potential hyperpolarization, caused by activation of large-conductance, Ca^{2+}-sensitive K^+ channels (Jaggar *et al.*, 2000). Alterations in spark-STOCs coupling may be an important event in the development of hypertension, since Ca^{2+} sparks are the physiological activators of BK_{Ca} channels and decreased BK_{Ca} activity has been related to membrane depolarization and vasoconstriction (Plüger *et al.*, 2000;Brenner *et al.*, 2000). Three major lines of evidence indicate that BK_{Ca} channel coupling to Ca^{2+} sparks is important in controlling vascular tone and blood pressure. First, inhibition of Ca^{2+} sparks constricts cerebral arteries (Nelson *et al.*, 1995). Second, vasodilators enhance coupling (Jaggar *et al.*, 2002), whereas vasoconstrictors decrease the activation of BK_{Ca} channels by Ca^{2+} sparks (Bonev *et al.*, 1997). Third, targeted deletion of the β_1 subunit uncouples BK_{Ca} channels from Ca^{2+} sparks and is, by itself, sufficient to induce hypertension (Plüger *et al.*, 2000).

Our data indicate that there is a clear uncoupling between Ca^{2+} spark and STOCs activities in BPH vascular myocytes. In comparation to BPN, the frequency and amplitude of spontaneous BK_{Ca} currents in BPH cells was small in despite higher Ca^{2+} spark amplitude (Figure 4.39-41). In addition, single channel data indicate that Ca^{2+} sensitivity of BK_{Ca} channels in BPH is lower than in BPN cells (Figure 4.43-44). The downregulation of the α and β_1 subunits of the BK_{Ca} channel described in a previous work in our lab (Moreno-Dominguez *et al.*, 2009) may underly the lower Ca^{2+} sensitivity of BK_{Ca} channels in BPH cells, contributing to the more depolarized V_M and to the enhanced vasoconstriction in these cells.

5.10 General conclusion

In most clinical cases of essential hypertension, there is an increased resistance due to an abnormal constriction of the small arteries and arterioles. The diameter of these vessels is determined by a dynamic interplay between K^+ and Ca^{2+} channels expressed in the plasma membrane of VSMCs, so that the opening of K^+ channels leads to hyperpolarization, closure of calcium channels and vasodilatation while closure of K^+ channels depolarizes VSMCs leading to the opening of Ca^{2+} channels that results in an increased intracellular Ca^{2+} and vasoconstriction. In this thesis we have explored the remodelling of inward-rectifier K^+ channels and LTCCs in VSMCs from a mouse model of essential hypertension. Results are summarized in the cartoon depicted in figure 5.2.

As expected, we have found an increased myogenic response in BPH arteries that could be a consequence of the more depolarized V_M observed in hypertensive VSMCs. When characterizing the changes in the expression of inward rectifier K^+ channels we found a decrease in the expression of Kir2.1, Kir4.1, Kir6.x and SUR2 mRNA in BPH VSMCs, and a
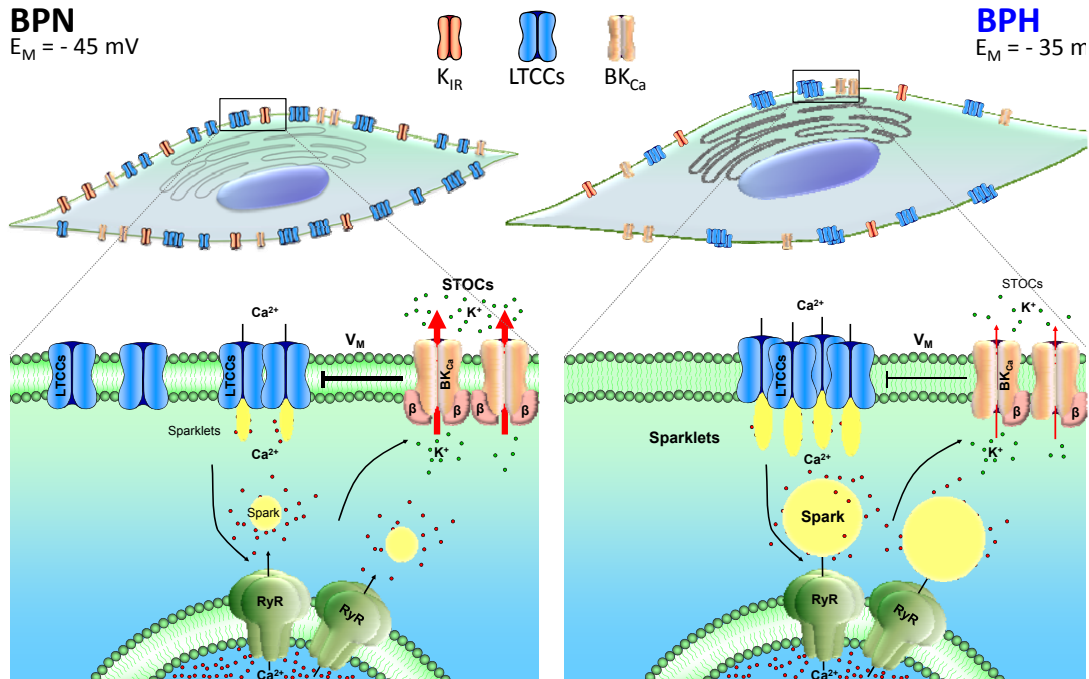
Figure 5.2 *Possible distribution and action of LTCCs on Ca^{2+} sparks, BK$_{Ca}$ channels and membrane potential in BPN and BPH arterial smooth muscle cells. BPH LTCCs spatial organization in bigger clusters increases local Ca^{+2} sparklets amplitude. Increased BPH Ca^{2+} influx through LTCCs increases the activity of RyR channels in the ER of the BPH myocytes. Ca^{2+} sparks activation normally also increases the activity of BK$_{Ca}$ channels, which is manifested by an elevation in STOC amplitude and membrane hyperpolarization. However, frequency and amplitud of BPH STOCs result in a significant decrease due to reduced BK$_{Ca}$ Ca^{2+} sensitivity. This difference can be explained by the lower expression of the BK$_{Ca}$ channel β subunit. BPH lower Ca^{2+} spark activation of the BK$_{Ca}$ channels reduce the negative feed-feedback (black arrow), leading to lower membrane hyperpolarization.*

decreased functional contribution of both K$_{IR}$ and K$_{ATP}$ channels in isolated BPH VSMCs. However, only the effect of K$_{ATP}$ channel modulators was impaired when exploring vascular tone, suggesting that decreased functional expression of K$_{ATP}$ channels may be an important element in the remodeling of VSMCs in essential hypertension. These changes are sufficient to explain the 10 mV depolarization at rest observed in BPH cells.

Regarding changes in the functional contribution of calcium channels, mRNA and protein expression studies and the functional characterization of LTCCs with electrophysiological and optical techniques have disclosed complex changes in the composition of LTCCs channelosome in BPH cells. Interestingly, while LTCCs are decreased in BPH at a global level, their local and basal activities seem to be higher in the hypertensive cells.

This apparent paradox, a higher activity with a downregulated expression, gives us an interesting lesson about the inherent danger in extracting general conclusions without a

complete understanding of all the elements playing a role in a complex and very nonlinear response such as the relationship between V_M, intracellular calcium and contraction.

Moreover, changes in LTCCs in BPH cells can only be properly interpreted in the context of other changes that clearly determine their role controlling intracellular Ca^{2+}. Those changes are obviously those affecting inward-rectifier channels, that compel BPH cells to work under a depolarized membrane potential, and those affecting BK_{Ca} Ca^{2+} sensitivity, that let fewer but more active LTCCs in the membrane to operate in a pro-contractile state in BPH cells.

Hypertension may be regarded as a narrative involving increased VSMC contractility, elevated blood pressure and increased mortality. However, the story can be told in different ways through the involvement of different characters that change in subtle and varied ways with time to achieve the same result of increased contractility. It is therefore not surprising that we are still so far from understanding how to change the end of the story and ensure longer patient survival.

6 CONCLUSIONS

1. BPH mice show a moderate, essential hypertension. Systolic, diastolic and mean arterial pressure are slightly but significantly elevated in BPH. Consistent with this hypertensive phenotype, mesenteric arteries from BPH mice are hyper-reactive, developing myogenic tone at lower pressures, and resting E_M values in mesenteric VSMCs from BPH mice are more depolarized

2. Depolarization of BPH VSMCs can be explained by a decreased in K^+ conductance, due to changes in functional expression of K_{IR} and K_{ATP} channels. We found that BPH VSMCs from mesenteric arteries show a noticeable decrease in the expression (both at the mRNA and protein level) and the functional contribution of K_{IR} and K_{ATP} channels to VSMC excitability.

3. However, when exploring the contribution of K_{IR} and K_{ATP} channels to arterial tone in myography experiments, only the response to K_{ATP} channel blockers and activators was impaired. These data indicate that the changes in K_{ATP} channels could be an important determinant of the hypertensive phenotype in resistance arteries, representing the main change responsible for VSMCs depolarization in BPH mice.

4. Macroscopic whole-cell LTCCs currents are decreased in BPH VSMCs. This decreased is also observed in perforated-patch recordings, excluding the contribution of intracellular mediators to the changes. However, differences in LTCCs currents in BPN and BPH cells are diminished in the presence of BayK, indicating that BPH cells have both fewer LTCCs and a different subunit composition with distinct kinetic behavior.

5. Expression data demonstrates that BPH have also a lower expression of Cav1.2α_1 mRNA and protein, as well as changes in the expression of the accessory subunits that could determine changes in the molecular composition of the LTCCs in the membrane of BPH VSMCs.

6. The functional contribution the accessory subunits to the LTCCs was disclosed with the use of gabapentin (GBP), a selective ligand of $\alpha_2\delta$ subunits. At 100µM, GBP did not modify LTCCs currents in BPN VSMCs while potentiated BPH currents. The study of the GBP concentration–response relationship indicated that the response obtained in $\alpha_1+\alpha_2\delta$ and $\alpha_1+\alpha_2\delta+\beta_2$ cotransfected HEK cells is similar to that obtained in BPN and BPH VSMCs, respectively. These data strongly suggest that differences in LTCCs BPH are related with the increased expression of β_2 subunit in these cells.

7. Ca^{2+} sparklet analysis by TIRF shows differences between BPN and BPH VSMCS. Sparklets from BPH cells have a higher site density, a greater activity of the high open

probability state, a longer duration of the open state and a larger amplitude, suggesting that BPH LTCCs are organized in bigger clusters than BPN. These data show that in spite of the decreased global expression of LTCCs, local Ca^{2+} signaling through LTCCs is increased in BPH cells

8. The increased Ca^{2+} sparklet activity in the hypertension model leads to a increased amplitude of Ca^{2+} sparks, but there is not a corresponding increase in the activity of BK_{Ca} channels, as we observed a decrease in the frequency and amplitude of STOCs from BPH cells. The uncoupling between Ca^{2+} sparks and BK_{Ca} channels can be attributed to a decreased expression of the BK_{Ca} channel β_1 subunit in the hypertensive phenotype, which reduces the Ca^{2+} sensitivity of BK_{Ca} channels. These changes determine a decreased contribution of the hyperpolarizing effect of BK_{Ca} channels that exacerbate membrane depolarization in BPH VSMCs.

9. Altogether, our data support the hypothesis that the changes in the functional expression of K_{IR}, K_{ATP}, BK_{Ca} and L-Type calcium channels are relevant to development of an essential hypertension, as they could be key determinants of membrane depolarization and increased Ca^{2+} influx in hypertensive VSMCs.

7 REFERENCES

Aaronson, P. I. & Ward, J. P. T. (2004). *The Cardiovascular System*, 2nd ed. Oxford.

Aguilar, H. N. & Mitchell, B. F. (2010). Physiological pathways and molecular mechanisms regulating uterine contractility. *Hum.Reprod.Update.* **16**, 725-744.

Aiello, E. A., Clement-Chomienne, O., Sontag, D. P., Walsh, M. P., & Cole, W. C. (1996). Protein kinase C inhibits delayed rectifier K+ current in rabbit vascular smooth muscle cells. *Am J Physiol* **271**, H109-H119.

Aiello, E. A., Malcolm, A. T., Walsh, M. P., & Cole, W. C. (1998). Beta-adrenoceptor activation and PKA regulate delayed rectifier K+ channels of vascular smooth muscle cells. *Am J Physiol* **275**, H448-H459.

Aird, W. C. (2007). Phenotypic heterogeneity of the endothelium: I. Structure, function, and mechanisms. *Circ Res* **100**, 158-173.

Amberg, G. C., Bonev, A. D., Rossow, C. F., Nelson, M. T., & Santana, L. F. (2003). Modulation of the molecular composition of large conductance, Ca^{2+} activated K$^+$ channels in vascular smooth muscle during hypertension. *J Clin.Invest* **112**, 717-724.

Amberg, G. C. & Santana, L. F. (2003). Downregulation of the BK Channel β1 Subunit in Genetic Hypertension. *Circulation Research* **93**, 965-971.

Anwar, M. A., Shalhoub, J., Lim, C. S., Gohel, M. S., & Davies, A. H. (2012). The effect of pressure-induced mechanical stretch on vascular wall differential gene expression. *J Vasc Res* **49**, 463-478.

Aoki, K. & Asano, M. (1986). Effects of Bay K 8644 and nifedipine on femoral arteries of spontaneously hypertensive rats. *Br J Pharmacol* **88**, 221-230.

Arikkath, J. & Campbell, K. P. (2003). Auxiliary subunits: essential components of the voltage-gated calcium channel complex. *Current Opinion in Neurobiology* **13**, 298-307.

Arribas, S. M., Gonzalez, J. M., Briones, A. M., Somoza, B., Daly, C. J., Vila, E., Gonzalez, M. C., & McGrath, J. C. (2007). Confocal myography for the study of hypertensive vascular remodelling. *Clin Hemorheol.Microcirc.* **37**, 205-210.

Axelrod, D. (2001). Total internal reflection fluorescence microscopy in cell biology. *Traffic.* **2**, 764-774.

Bahring, R., Milligan, C. J., Vardanyan, V., Engeland, B., Young, B. A., Dannenberg, J., Waldschutz, R., Edwards, J. P., Wray, D., & Pongs, O. (2001). Coupling of voltage-dependent potassium channel inactivation and oxidoreductase active site of Kvbeta subunits. *J Biol Chem* **276**, 22923-22929.

Bannister, J. P., Thomas-Gatewood, C. M., Neeb, Z. P., Adebiyi, A., Cheng, X., & Jaggar, J. H. (2011). Ca(V)1.2 channel N-terminal splice variants modulate functional surface expression in resistance size artery smooth muscle cells. *J Biol Chem* **286**, 15058-15066.

Bannister, J. P., Adebiyi, A., Zhao, G., Narayanan, D., Thomas, C. M., Feng, J. Y., & Jaggar, J. H. (2009). Smooth Muscle Cell alpha2-delta1 Subunits Are Essential for Vasoregulation by CaV1.2 Channels. *Circulation Research* **105**, 948-955.

Bannister, J. P., Bulley, S., Narayanan, D., Thomas-Gatewood, C., Luzny, P., Pachuau, J., & Jaggar, J. H. (2012). Transcriptional Upregulation of ¦2¦-1 Elevates Arterial Smooth Muscle Cell Voltage-Dependent Ca2+ Channel Surface Expression and Cerebrovascular Constriction in Genetic Hypertension / Novelty and Significance. *Hypertension* **60**, 1006-1015.

Beech, D. J. & Bolton, T. B. (1989). A voltage-dependent outward current with fast kinetics in single smooth muscle cells isolated from rabbit portal vein. *The Journal of Physiology* **412**, 397-414.

Berger, M. G., Vandier, C., Bonnet, P., Jackson, W. F., & Rusch, N. J. (1998). Intracellular acidosis differentially regulates KV channels in

References

coronary and pulmonary vascular muscle. *Am J Physiol* **275**, H1351-H1359.

Berridge, M. J. (1993). Inositol trisphosphate and calcium signalling. *Nature* **361**, 315-325.

Berridge, M. J. (1995). Capacitative calcium entry. *Biochemical Journal* **312 (Pt 1)**, 1-11.

Berridge, M. J. (2008). Smooth muscle cell calcium activation mechanisms. *The Journal of Physiology* **586**, 5047-5061.

Bichet, D., Haass, F. A., & Jan, L. Y. (2003). Merging functional studies with structures of inward-rectifier K+ channels. *Nat Rev Neurosci* **4**, 957-967.

Blaustein, M. P. (1996). Endogenous ouabain: role in the pathogenesis of hypertension. *Kidney Int.* **49**, 1748-1753.

Bolton, T. B. (1979). Mechanisms of action of transmitters and other substances on smooth muscle. *Physiol Rev* **59**, 606-718.

Bonev, A. D., Jaggar, J. H., Rubart, M., & Nelson, M. T. (1997). Activators of protein kinase C decrease Ca2+ spark frequency in smooth muscle cells from cerebral arteries. *Am J Physiol* **273**, C2090-C2095.

Brayden, J. E. & Nelson, M. T. (1992). Regulation of arterial tone by activation of calcium-dependent potassium channels. *Science* **256**, 532-535.

Brayden, J. E. (2002). Functional Roles Of KATP Channels In Vascular Smooth Muscle. *Clinical and Experimental Pharmacology and Physiology* **29**, 312-316.

Brenner, R., Perez, G. J., Bonev, A. D., Eckman, D. M., Kosek, J. C., Wiler, S. W., Patterson, A. J., Nelson, M. T., & Aldrich, R. W. (2000). Vasoregulation by the β1 subunit of the calcium-activated potassium channel. *Nature* **407**, 870-876.

Brown, A. M., Yatani, A., Codina, J., & Birnbaumer, L. (1989). G protein-gated channels. A third major category of ionic channels. *Am.J.Hypertens.* **2**, 124-127.

Brown, J. P., Dissanayake, V. U., Briggs, A. R., Milic, M. R., & Gee, N. S. (1998). Isolation of the [3H]gabapentin-binding protein/alpha 2 delta Ca2+ channel subunit from porcine brain: development of a radioligand binding assay for alpha 2 delta subunits using [3H]leucine. *Anal.Biochem* **255**, 236-243.

Bruner, C. A. & Webb, R. C. (1990). Increased vascular reactivity to Bay K 8644 in genetic hypertension. *Pharmacology* **41**, 24-35.

Carretero, O. A. & Oparil, S. (2000). Essential hypertension. Part I: definition and etiology. *Circulation* **101**, 329-335.

Castellano, A., Wei, X., Birnbaumer, L., & Perez-Reyes, E. (1993). Cloning and expression of a third calcium channel beta subunit. *J Biol Chem* **268**, 3450-3455.

Catalucci, D., Zhang, D. H., DeSantiago, J., Aimond, F., Barbara, G., Chemin, J., Bonci, D. +., Picht, E., Rusconi, F., Dalton, N. D., Peterson, K. L., Richard, S., Bers, D. M., Brown, J. H., & Condorelli, G. (2009). Akt regulates L-type Ca2+ channel activity by modulating Cav+¦1 protein stability. *The Journal of Cell Biology* **184**, 923-933.

Catterall, W. A. (2000b). Structure and regulation of voltage-gated Ca2+ channels. *Annu.Rev Cell Dev.Biol* **16**, 521-555.

Catterall, W. A. (2000a). Structure and regulation of voltage-gated Ca2+ channels. *Annu.Rev Cell Dev.Biol* **16**, 521-555.

Catterall, W. A. & Curtis, B. M. (1987). Molecular properties of voltage-sensitive calcium channels. *Soc Gen.Physiol Ser.* **41**, 201-213.

Catterall, W. A., Perez-Reyes, E., Snutch, T. P., & Striessnig, J. (2005). International Union of Pharmacology. XLVIII. Nomenclature and structure-function relationships of voltage-gated calcium channels. *Pharmacological Reviews* **57**, 411-425.

Cheng, H., Song, L. S., Shirokova, N., Gonzalez, A., Lakatta, E. G., Rios, E., & Stern, M. D. (1999). Amplitude distribution of calcium sparks in confocal images: theory and studies with an automatic detection method. *Biophys.J.* **76**, 606-617.

Cheng, J. K. & Chiou, L. C. (2006). Mechanisms of the antinociceptive action of gabapentin. *J Pharmacol Sci* **100**, 471-486.

Cheng, L., Fu, J., Tsukamoto, A., & Hawley, R. G. (1996). Use of green fluorescent protein variants to monitor gene transfer and expression in mammalian cells. *Nat Biotechnol.* **14**, 606-609.

Cheong, A., Dedman, A. M., Xu, S. Z., & Beech, D. J. (2001). K-v alpha 1 channels in murine arterioles: differential cellular expression and regulation of diameter. *American Journal of Physiology-Heart and Circulatory Physiology* **281**, H1057-H1065.

Cheung, D. W. (1984). Membrane potential of vascular smooth muscle and hypertension in spontaneously hypertensive rats. *Can.J Physiol Pharmacol* **62**, 957-960.

Chobanian, A. V., Bakris, G. L., Black, H. R., Cushman, W. C., Green, L. A., Izzo, J. L., Jr., Jones, D. W., Materson, B. J., Oparil, S., Wright, J. T., Jr., Roccella, E. J., & the National High Blood Pressure Education Program Coordinating Committee (2003). Seventh Report of the Joint National Committee on Prevention, Detection, Evaluation, and Treatment of High Blood Pressure. *Hypertension* **42**, 1206-1252.

Christ, G. J., Spray, D. C., El Sabban, M., Moore, L. K., & Brink, P. R. (1996). Gap Junctions in Vascular Tissues: Evaluating the Role of Intercellular Communication in the Modulation of Vasomotor Tone. *Circulation Research* **79**, 631-646.

Chutkow, W. A., Pu, J., Wheeler, M. T., Wada, T., Makielski, J. C., Burant, C. F., & McNally, E. M. (2002). Episodic coronary artery vasospasm and hypertension develop in the absence of Sur2 K(ATP) channels. *J Clin Invest* **110**, 203-208.

Cohen, C. J. & McCarthy, R. T. (1987). Nimodipine block of calcium channels in rat anterior pituitary cells. *Journal of Physiology* **387**, 195-225.

Cox, D. H. & Aldrich, R. W. (2000). Role of the beta1 subunit in large-conductance Ca(2+)-activated K(+) channel gating energetics. Mechanisms of enhanced Ca(2+) sensitivity. *J.Gen.Physiol* **116**, 411-432.

Cox, R. H. & Rusch, N. J. (2002). New expression profiles of voltage-gated ion channels in arteries exposed to high blood pressure. *Microcirculation.* **9**, 243-257.

Cox, R. H., Folander, K., & Swanson, R. (2001). Differential Expression of Voltage-Gated K+ Channel Genes in Arteries From Spontaneously Hypertensive and Wistar-Kyoto Rats. *Hypertension* **37**, 1315-1322.

Cox, R. H. & Petrou, S. (1999). Ca2+ influx inhibits voltage-dependent and augments Ca2+-dependent K+ currents in arterial myocytes. *AJP - Cell Physiology* **277**, C51-C63.

Craig, R., Smith, R., & Kendrick-Jones, J. (1983). Light-chain phosphorylation controls the conformation of vertebrate non-muscle and smooth muscle myosin molecules. *Nature* **302**, 436-439.

Craig, R. & Woodhead, J. L. (2006). Structure and function of myosin filaments. *Current Opinion in Structural Biology* **16**, 204-212.

Cui, Y., Tran, S., Tinker, A., & Clapp, L. H. (2002). The Molecular Composition of KATP Channels in Human Pulmonary Artery Smooth Muscle Cells and Their Modulation by Growth. *American Journal of Respiratory Cell and Molecular Biology* **26**, 135-143.

Davies, A., Douglas, L., Hendrich, J., Wratten, J., Tran, V. M., Foucault, I., Koch, D., Pratt, W. S., Saibil, H. R., & Dolphin, A. C. (2006). The calcium channel alpha2delta-2 subunit partitions with CaV2.1 into lipid rafts in cerebellum: implications for localization and function. *J Neurosci* **26**, 8748-8757.

References

Davies, A., Hendrich, J., Van Minh, A. T., Wratten, J., Douglas, L., & Dolphin, A. C. (2007). Functional biology of the [alpha]2[delta] subunits of voltage-gated calcium channels. *Trends in Pharmacological Sciences* **28**, 220-228.

Davis, M. J., Donovitz, J. A., & Hood, J. D. (1992). Stretch-activated single-channel and whole cell currents in vascular smooth muscle cells. *Am J Physiol* **262**, C1083-C1088.

Davis, M. J. & Hill, M. A. (1999). Signaling mechanisms underlying the vascular myogenic response. *Physiol Rev.* **79**, 387-423.

de Wit, C., Boettcher, M., & Schmidt, V. J. (2008). Signaling across myoendothelial gap junctions--fact or fiction? *Cell Commun.Adhes.* **15**, 231-245.

DEL CASTILLO, J. & Katz, B. (1954). Quantal components of the end-plate potential. *Journal of Physiology* **124**, 560-573.

Demuro, A. & Parker, I. (2004). Imaging the activity and localization of single voltage-gated Ca(2+) channels by total internal reflection fluorescence microscopy. *Biophys.J* **86**, 3250-3259.

Dick, G. M. & Tune, J. D. (2010). Role of potassium channels in coronary vasodilation. *Exp Biol Med (Maywood.)* **235**, 10-22.

Dietrich, A., Schnitzler, M., Gollasch, M., Gross, V., Storch, U., Dubrovska, G., Obst, M., Yildirim, E., Salanova, B., Kalwa, H., Essin, K., Pinkenburg, O., Luft, F. C., Gudermann, T., & Birnbaumer, L. (2005). Increased Vascular Smooth Muscle Contractility in TRPC6-/- Mice. *Molecular and Cellular Biology* **25**, 6980-6989.

Doggrell, S. A. & Brown, L. (1998). Rat models of hypertension, cardiac hypertrophy and failure. *Cardiovascular Research* **39**, 89-105.

Dolphin, A. C. (2003). Beta subunits of voltage-gated calcium channels. *J Bioenerg.Biomembr.* **35**, 599-620.

Dolphin, A. C. (2009). Calcium channel diversity: multiple roles of calcium channel subunits. *Current Opinion in Neurobiology* **19**, 237-244.

Dooley, D. J., Taylor, C. P., Donevan, S., & Feltner, D. (2007). Ca2+ channel [alpha]2[delta] ligands: novel modulators of neurotransmission. *Trends in Pharmacological Sciences* **28**, 75-82.

Drab, M., Verkade, P., Elger, M., Kasper, M., Lohn, M., Lauterbach, B., Menne, J., Lindschau, C., Mende, F., Luft, F. C., Schedl, A., Haller, H., & Kurzchalia, T. V. (2001). Loss of Caveolae, Vascular Dysfunction, and Pulmonary Defects in Caveolin-1 Gene-Disrupted Mice. *Science* **293**, 2449-2452.

Draeger, A., Amos, W. B., Ikebe, M., & Small, J. V. (1990). The cytoskeletal and contractile apparatus of smooth muscle: contraction bands and segmentation of the contractile elements. *J Cell Biol* **111**, 2463-2473.

Eddinger, T. J. & Meer, D. P. (2007). Myosin II isoforms in smooth muscle: heterogeneity and function. *AJP - Cell Physiology* **293**, C493-C508.

Fernandez-Tenorio, M., Gonzalez-Rodriguez, P., Porras, C., Castellano, A., Moosmang, S., Hofmann, F., Urena, J., & Lopez-Barneo, J. (2010). Short Communication: Genetic Ablation of L-Type Ca2+ Channels Abolishes Depolarization-Induced Ca2+ Release in Arterial Smooth Muscle. *Circulation Research* **106**, 1285-1289.

Field, M. J., Cox, P. J., Stott, E., Melrose, H., Offord, J., Su, T. Z., Bramwell, S., Corradini, L., England, S., Winks, J., Kinloch, R. A., Hendrich, J., Dolphin, A. C., Webb, T., & Williams, D. (2006). Identification of the alpha2-delta-1 subunit of voltage-dependent calcium channels as a molecular target for pain mediating the analgesic actions of pregabalin. *Proc Natl.Acad.Sci U S.A* **103**, 17537-17542.

Fink, K., Dooley, D. J., Meder, W. P., Suman-Chauhan, N., Duffy, S., Clusmann, H., & Gothert, M. (2002). Inhibition of neuronal Ca(2+) influx by gabapentin and pregabalin in the human neocortex. *Neuropharmacology* **42**, 229-236.

Firth, A. L., Remillard, C. V., & Yuan, J. X. (2007). TRP channels in hypertension. *Biochim.Biophys.Acta* **1772**, 895-906.

Franco-Obregon, A., Ureña, J., & López-Barneo, J. (1995). Oxigen-sensitive calcium channels in vascular smooth muscle and their possible role in arterial relaxation. *Proc.Natl.Acad.Sci.U.S.A.* **92**, 4715-4719.

Freiman, T. M., Kukolja, J., Heinemeyer, J., Eckhardt, K., Aranda, H., Rominger, A., Dooley, D. J., Zentner, J., & Feuerstein, T. J. (2001). Modulation of K+-evoked [3H]-noradrenaline release from rat and human brain slices by gabapentin: involvement of KATP channels. *Naunyn Schmiedebergs Arch.Pharmacol* **363**, 537-542.

Gabella, G. (1984). Structural apparatus for force transmission in smooth muscles. *Physiological Reviews* **64**, 455-477.

Gee, N. S., Brown, J. P., Dissanayake, V. U., Offord, J., Thurlow, R., & Woodruff, G. N. (1996b). The novel anticonvulsant drug, gabapentin (Neurontin), binds to the alpha2delta subunit of a calcium channel. *J Biol Chem* **271**, 5768-5776.

Gee, N. S., Brown, J. P., Dissanayake, V. U., Offord, J., Thurlow, R., & Woodruff, G. N. (1996a). The novel anticonvulsant drug, gabapentin (Neurontin), binds to the alpha2delta subunit of a calcium channel. *J Biol Chem* **271**, 5768-5776.

Gibson, A., McFadzean, I., Wallace, P., & Wayman, C. P. (1998). Capacitative Ca2+ entry and the regulation of smooth muscle tone. *Trends Pharmacol.Sci* **19**, 266-269.

Goldblatt, H., Lynch, J., Hanzal, R. F., & Summerville, W. W. (1934). STUDIES ON EXPERIMENTAL HYPERTENSION: I. THE PRODUCTION OF PERSISTENT ELEVATION OF SYSTOLIC BLOOD PRESSURE BY MEANS OF RENAL ISCHEMIA. *The Journal of Experimental Medicine* **59**, 347-379.

Gorlach, A., Klappa, P., & Kietzmann, T. (2006). The endoplasmic reticulum: folding, calcium homeostasis, signaling, and redox control. *Antioxid.Redox Signal* **8**, 1391-1418.

Guharay, F. & Sachs, F. (1984). Stretch-activated single ion channel currents in tissue-cultured embryonic chick skeletal muscle. *Journal of Physiology* **352**, 685-701.

Gunst, S. J. & Zhang, W. (2008). Actin cytoskeletal dynamics in smooth muscle: a new paradigm for the regulation of smooth muscle contraction. *AJP - Cell Physiology* **295**, C576-C587.

Gurnett, C. A., De Waard, M., & Campbell, K. P. (1996). Dual function of the voltage-dependent Ca2+ channel alpha 2 delta subunit in current stimulation and subunit interaction. *Neuron* **16**, 431-440.

Haeusler, G. (1983). Contraction, membrane potential, and calcium fluxes in rabbit pulmonary arterial muscle. *Fed.Proc* **42**, 263-268.

Harder, D. R., Brann, L., & Halpern, W. (1983). Altered membrane electrical properties of smooth muscle cells from small cerebral arteries of hypertensive rats. *Blood Vessels* **20**, 154-160.

Harder, D. R., Smeda, J., & Lombard, J. (1985). Enhanced myogenic depolarization in hypertensive cerebral arterial muscle. *Circulation Research* **57**, 319-322.

Hartshorne, D. J., Ito, M., & Erdodi, F. (2004). Role of protein phosphatase type 1 in contractile functions: myosin phosphatase. *J Biol Chem* **279**, 37211-37214.

Hayashi, K., Epstein, M., & Saruta, T. (1996). Altered myogenic responsiveness of the renal microvasculature in experimental hypertension. *J Hypertens.* **14**, 1387-1401.

Heistad, D. D., Mayhan, W. G., Coyle, P., & Baumbach, G. L. (1990). Impaired dilatation of cerebral arterioles in chronic hypertension. *Blood Vessels* **27**, 258-262.

References

Hendrich, J., Van Minh, A. T., Heblich, F., Nieto-Rostro, M., Watschinger, K., Striessnig, J., Wratten, J., Davies, A., & Dolphin, A. C. (2008b). Pharmacological disruption of calcium channel trafficking by the alpha2delta ligand gabapentin. *Proc Natl.Acad.Sci U S.A* **105**, 3628-3633.

Hendrich, J., Van Minh, A. T., Heblich, F., Nieto-Rostro, M., Watschinger, K., Striessnig, J., Wratten, J., Davies, A., & Dolphin, A. C. (2008a). Pharmacological disruption of calcium channel trafficking by the alpha2delta ligand gabapentin. *Proc Natl.Acad.Sci U S.A* **105**, 3628-3633.

Hermsmeyer, K. & Rusch, N. J. (1989). Calcium channel alterations in genetic hypertension. *Hypertension* **14**, 453-456.

Hermsmeyer, K., White, A. C., & Triggle, D. J. (1995). Decreased Dihydropyridine Receptor Number in Hypertensive Rat Vascular Muscle Cells. *Hypertension* **25**, 731-734.

Hess, P. & Tsien, R. W. (1984). Mechanism of ion permeation through calcium channels. *Nature* **309**, 453-456.

Hibino, H., Inanobe, A., Furutani, K., Murakami, S., Findlay, I., & Kurachi, Y. (2010). Inwardly Rectifying Potassium Channels: Their Structure, Function, and Physiological Roles. *Physiological Reviews* **90**, 291-366.

Hill, M. A., Zou, H., Potocnik, S. J., Meininger, G. A., & Davis, M. J. (2001). Invited review: arteriolar smooth muscle mechanotransduction: Ca(2+) signaling pathways underlying myogenic reactivity. *J Appl.Physiol* **91**, 973-983.

Hirenallur-S DK, Haworth, S. T., Leming, J. T., Chang, J., Hernandez, G., Gordon, J. B., & Rusch, N. J. (2008). Upregulation of vascular calcium channels in neonatal piglets with hypoxia-induced pulmonary hypertension. *Am J Physiol Lung Cell Mol Physiol* **295**, L915-L924.

Hobom, M., Dai, S., Marais, E., Lacinova, L., Hofmann, F., & Klugbauer, N. (2000). Neuronal distribution and functional characterization of the calcium channel alpha2delta-2 subunit. *Eur.J Neurosci* **12**, 1217-1226.

Horn, R. & Marty, A. (1988). Muscarinic activation of ionic currents measured by a new whole-cell recording method. *J Gen.Physiol* **92**, 145-159.

Horowitz, A., Menice, C. B., Laporte, R., & Morgan, K. G. (1996). Mechanisms of smooth muscle contraction. *Physiol Rev.* **76**, 967-1003.

Hughes, A. D. (1995). Calcium channels in vascular smooth muscle cells. *J Vasc Res* **32**, 353-370.

Hullin, R., Singer-Lahat, D., Freichel, M., Biel, M., Dascal, N., Hofmann, F., & Flockerzi, V. (1992). Calcium channel beta subunit heterogeneity: functional expression of cloned cDNA from heart, aorta and brain. *EMBO J* **11**, 885-890.

Jackson, W. F. (2000). Ion Channels and Vascular Tone. *Hypertension* **35**, 173.

Jaggar, J. H., Porter, V. A., Lederer, W. J., & Nelson, M. T. (2000). Calcium sparks in smooth muscle. *AJP - Cell Physiology* **278**, C235-C256.

Jaggar, J. H., Leffler, C. W., Cheranov, S. Y., Tcheranova, D., E, S., & Cheng, X. (2002). Carbon Monoxide Dilates Cerebral Arterioles by Enhancing the Coupling of Ca2+ Sparks to Ca2+-Activated K+ Channels. *Circulation Research* **91**, 610-617.

Jentsch, T. J. (1996). Chloride channels: a molecular perspective. *Curr.Opin.Neurobiol.* **6**, 303-310.

Jepps, T. A., Chadha, P. S., Davis, A. J., Harhun, M. I., Cockerill, G. W., Olesen, S. P., Hansen, R. S., & Greenwood, I. A. (2011). Downregulation of Kv7.4 channel activity in primary and secondary hypertension. *Circulation* **124**, 602-611.

Johnson, J. D., Snyder, C., Walsh, M., & Flynn, M. (1996). Effects of myosin light chain kinase and peptides on Ca2+ exchange with the N- and

C-terminal Ca2+ binding sites of calmodulin. *J Biol Chem* **271**, 761-767.

Kamp, T. J., Perez-Garcia, M. T., & Marban, E. (1996). Enhancement of ionic current and charge movement by coexpression of calcium channel beta 1A subunit with alpha 1C subunit in a human embryonic kidney cell line. *J.Physiol (Lond)* **492 (Pt 1)**, 89-96.

Keef, K. D., Hume, J. R., & Zhong, J. (2001). Regulation of cardiac and smooth muscle Ca(2+) channels (Ca(V)1.2a,b) by protein kinases. *AJP - Cell Physiology* **281**, C1743-C1756.

Kharade, S. V., Sonkusare, S. K., Srivastava, A. K., Thakali, K. M., Fletcher, T. W., Rhee, S. W., & Rusch, N. J. (2013). The β3 Subunit Contributes to Vascular Calcium Channel Upregulation and Hypertension in Angiotensin II–Infused C57BL/6 Mice. *Hypertension* **61**, 137-142.

Kitazono, T., Heistad, D. D., & Faraci, F. M. (1993). ATP-sensitive potassium channels in the basilar artery during chronic hypertension. *Hypertension* **22**, 677-681.

Klabunde, R. E. (2005)., 2ª ed. Baltimore, Maryland.

Klugbauer, N., Lacinova, L., Marais, E., Hobom, M., & Hofmann, F. (1999). Molecular diversity of the calcium channel alpha2delta subunit. *J Neurosci* **19**, 684-691.

Knot, H. J. & Nelson, M. T. (1998). Regulation of arterial diameter and wall [Ca2+] in cerebral arteries of rat by membrane potential and intravascular pressure. *Journal of Physiology* **508 (Pt 1)**, 199-209.

Knot, H. J., Zimmermann, P. A., & Nelson, M. T. (1996). Extracellular K^+-induced hyperpolarizations and dilatations of rat coronary and cerebral arteries involve inward rectifier K^+ channels. *J.Physiol* **492 (Pt 2)**, 419-430.

Ko, E. A., Han, J., Jung, I. D., & Park, W. S. (2008). Physiological roles of K+ channels in

vascular smooth muscle cells. *Jornal of Smooth Muscle Research* **44**, 65-81.

Koch, W. J., Ellinor, P. T., & Schwartz, A. (1990). cDNA cloning of a dihydropyridine-sensitive calcium channel from rat aorta. Evidence for the existence of alternatively spliced forms. *J Biol Chem* **265**, 17786-17791.

Korovkina, V. P. & England, S. K. (2002). Molecular diversity of vascular potassium channel isoforms. *Clin Exp Pharmacol Physiol* **29**, 317-323.

Lacinova, L. (2005). Voltage-dependent calcium channels. *Gen.Physiol Biophys.* **24 Suppl 1**, 1-78.

Landsberg, J. W. & Yuan, J. X. J. (2004). Calcium and TRP Channels in Pulmonary Vascular Smooth Muscle Cell Proliferation. *News in Physiological Sciences* **19**, 44-50.

Large, W. A. & Wang, Q. (1996). Characteristics and physiological role of the Ca(2+)-activated Cl- conductance in smooth muscle. *AJP - Cell Physiology* **271**, C435-C454.

Ledoux, J., Werner, M. E., Brayden, J. E., & Nelson, M. T. (2006). Calcium-Activated Potassium Channels and the Regulation of Vascular Tone. *Physiology* **21**, 69-78.

Lee, K. S. & Tsien, R. W. (1984). High selectivity of calcium channels in single dialysed heart cells of the guinea-pig. *Journal of Physiology* **354**, 253-272.

Letts, V. A., Felix, R., Biddlecome, G. H., Arikkath, J., Mahaffey, C. L., Valenzuela, A., Bartlett, F. S., Mori, Y., Campbell, K. P., & Frankel, W. N. (1998). The mouse stargazer gene encodes a neuronal Ca2+-channel gamma subunit. *Nat Genet.* **19**, 340-347.

Levick J.R. (2003). *An Introduction to Cardiovascular Physiology.*, Fourth ed.

Levy, M. N. & Pappano, A. J. (2007). *Cardiovascular Physiology*, 9th ed. Philadelphia.

References

Liao, P. & Soong, T. W. (2010). CaV1.2 channelopathies: from arrhythmias to autism, bipolar disorder, and immunodeficiency. *Pflugers Arch.* **460**, 353-359.

Livak, K. J. & Schmittgen, T. D. (2001). Analysis of relative gene expression data using real-time quantitative PCR and the 2(-Delta Delta C(T)) Method. *Methods* **25**, 402-408.

Lozinskaya, I. M. & Cox, R. H. (1997). Effects of age on Ca2+ currents in small mesenteric artery myocytes from Wistar-Kyoto and spontaneously hypertensive rats. *Hypertension* **29**, 1329-1336.

Makarewich, C. A., Correll, R. N., Gao, H., Zhang, H., Yang, B., Berretta, R. M., Rizzo, V., Molkentin, J. D., & Houser, S. R. (2012). A caveolae-targeted L-type Ca(2)+ channel antagonist inhibits hypertrophic signaling without reducing cardiac contractility. *Circulation Research* **110**, 669-674.

Marais, E., Klugbauer, N., & Hofmann, F. (2001b). Calcium channel alpha(2)delta subunits-structure and Gabapentin binding. *Molecular Pharmacology* **59**, 1243-1248.

Marais, E., Klugbauer, N., & Hofmann, F. (2001a). Calcium channel alpha(2)delta subunits-structure and Gabapentin binding. *Mol Pharmacol* **59**, 1243-1248.

Maravall, M., Mainen, Z. F., Sabatini, B. L., & Svoboda, K. (2000). Estimating intracellular calcium concentrations and buffering without wavelength ratioing. *Biophys.J.* **78**, 2655-2667.

Martens, J. R. & Gelband, C. H. (1996). Alterations in rat interlobar artery membrane potential and K+ channels in genetic and nongenetic hypertension. *Circulation Research* **79**, 295-301.

Martinez-Lemus, L. A., Hill, M. A., & Meininger, G. A. (2009). The plastic nature of the vascular wall: a continuum of remodeling events contributing to control of arteriolar diameter and structure. *Physiology (Bethesda.)* **24**, 45-57.

Mathar, I., Vennekens, R., Meissner, M., Kees, F., Van der, M. G., Camacho Londono, J. E., Uhl, S., Voets, T., Hummel, B., van den, B. A., Herijgers, P., Nilius, B., Flockerzi, V., Schweda, F., & Freichel, M. (2010). Increased catecholamine secretion contributes to hypertension in TRPM4-deficient mice. *J Clin Invest* **120**, 3267-3279.

McCarron, J. G. & Halpern, W. (1990). Impaired potassium-induced dilation in hypertensive rat cerebral arteries does not reflect altered Na+,K(+)-ATPase dilation. *Circulation Research* **67**, 1035-1039.

McGrath, J. C., Deighan, C., Briones, A. M., Shafaroudi, M. M., McBride, M., Adler, J., Arribas, S. M., Vila, E., & Daly, C. J. (2005). New aspects of vascular remodelling: the involvement of all vascular cell types. *Experimental Physiology* **90**, 469-475.

Mehta, P. K. & Griendling, K. K. (2007). Angiotensin II cell signaling: physiological and pathological effects in the cardiovascular system. *AJP - Cell Physiology* **292**, C82-C97.

Meredith, A. L., Thorneloe, K. S., Werner, M. E., Nelson, M. T., & Aldrich, R. W. (2004). Overactive bladder and incontinence in the absence of the BK large conductance Ca2+-activated K+ channel. *J Biol Chem.* **279**, 36746-36752.

Michelakis, E. D., Reeve, H. L., Huang, J. M., Tolarova, S., Nelson, D. P., Weir, E. K., & Archer, S. L. (1997). Potassium channel diversity in vascular smooth muscle cells. *Can.J.Physiol Pharmacol.* **75**, 889-897.

Mikami, A., Imoto, K., Tanabe, T., Niidome, T., Mori, Y., Takeshima, H., Narumiya, S., & Numa, S. (1989). Primary Structure and Functional Expression of the Cardiac Dihydropyridine-Sensitive Calcium-Channel. *Nature* **340**, 230-233.

Miki, T., Suzuki, M., Shibasaki, T., Uemura, H., Sato, T., Yamaguchi, K., Koseki, H., Iwanaga, T., Nakaya, H., & Seino, S. (2002). Mouse model of Prinzmetal angina by disruption of the inward rectifier Kir6.1. *Nat Med* **8**, 466-472.

Milner, R. E., Famulski, K. S., & Michalak, M. (1992). Calcium binding proteins in the

sarcoplasmic/endoplasmic reticulum of muscle and nonmuscle cells. *Mol Cell Biochem* **112**, 1-13.

Mindell, J. A. (2008). The chloride channel's appendix. *Nat Struct.Mol Biol* **15**, 781-783.

Mintz, I. M., Adams, M. E., & Bean, B. P. (1992). P-type calcium channels in rat central and peripheral neurons. *Neuron* **9**, 85-95.

Mohrman DE & Heller LJ (2003). *Cardiovascular Physiology*, 5th ed. Lange Medical Books/McGraw-Hill, New York.

Moosmang, S., Schulla, V., Welling, A., Feil, R., Feil, S., Wegener, J. W., Hofmann, F., & Klugbauer, N. (2003). Dominant role of smooth muscle L-type calcium channel Cav1.2 for blood pressure regulation. *EMBO J* **22**, 6027-6034.

Moreno-Dominguez, A., Cidad, P., Miguel-Velado, E., Lopez-Lopez, J. R., & Perez-Garcia, M. T. (2009). De novo expression of Kv6.3 contributes to changes in vascular smooth muscle cell excitability in a hypertensive mice strain. *Journal of Physiology* **587**, 625-640.

Murakami, M., Yamamura, H., Suzuki, T., Kang, M. G., Ohya, S., Murakami, A., Miyoshi, I., Sasano, H., Muraki, K., Hano, T., Kasai, N., Nakayama, S., Campbell, K. P., Flockerzi, V., Imaizumi, Y., Yanagisawa, T., & Iijima, T. (2003). Modified Cardiovascular L-type Channels in Mice Lacking the Voltage-dependent Ca2+ Channel +¦3 Subunit. *Journal of Biological Chemistry* **278**, 43261-43267.

Murphy, R. A. & Rembold, C. M. (2005). The latch-bridge hypothesis of smooth muscle contraction. *Can.J Physiol Pharmacol* **83**, 857-864.

Navedo, M. F. & Santana, L. F. (2012). Ca(V)1.2 sparklets in heart and vascular smooth muscle. *J Mol Cell Cardiol.*

Navedo, M. F., Amberg, G. C., Nieves, M., Molkentin, J. D., & Santana, L. F. (2006). Mechanisms Underlying Heterogeneous Ca2+ Sparklet Activity in Arterial Smooth Muscle. *The Journal of General Physiology* **127**, 611-622.

Navedo, M. F., Amberg, G. C., Votaw, V. S., & Santana, L. F. (2005). Constitutively active L-type Ca2+ channels. *Proceedings of the National Academy of Sciences of the United States of America* **102**, 11112-11117.

Navedo, M. F., Amberg, G. C., Westenbroek, R. E., Sinnegger-Brauns, M. J., Catterall, W. A., Striessnig, J., & Santana, L. F. (2007). Cav1.3 channels produce persistent calcium sparklets, but Cav1.2 channels are responsible for sparklets in mouse arterial smooth muscle. *AJP - Heart and Circulatory Physiology* **293**, H1359-H1370.

Navedo, M. F., Cheng, E. P., Yuan, C., Votaw, S., Molkentin, J. D., Scott, J. D., & Santana, L. F. (2010). Increased Coupled Gating of L-Type Ca2+ Channels During Hypertension and Timothy Syndrome. *Circulation Research* **106**, 748-756.

Navedo, M. F., Nieves-Cintron, M., Amberg, G. C., Yuan, C., Votaw, V. S., Lederer, W. J., McKnight, G. S., & Santana, L. F. (2008). AKAP150 Is Required for Stuttering Persistent Ca2+ Sparklets and Angiotensin II-Induced Hypertension. *Circulation Research* **102**, e1-11.

Nelson, M. T., Cheng, H., Rubart, M., Santana, L. F., Bonev, A. D., Knot, H. J., & Lederer, W. J. (1995). Relaxation of arterial smooth muscle by calcium sparks. *Science* **270**, 633-637.

Nelson, M. T., Patlak, J. B., Worley, J. F., & Standen, N. B. (1990). Calcium channels, potassium channels, and voltage dependence of arterial smooth muscle tone. *Am J Physiol* **259**, C3-18.

Nelson, M. T. & Quayle, J. M. (1995). Physiological roles and properties of potassium channels in arterial smooth muscle. *AJP - Cell Physiology* **268**, C799-C822.

Obermair, G. J., Tuluc, P., & Flucher, B. E. (2008). Auxiliary Ca(2+) channel subunits: lessons learned from muscle. *Curr.Opin.Pharmacol* **8**, 311-318.

Ohya, Y., Abe, I., Fujii, K., Takata, Y., & Fujishima, M. (1993). Voltage-dependent Ca2+ channels in resistance arteries from

References

spontaneously hypertensive rats. *Circulation Research* **73**, 1090-1099.

Ohya, Y., Fujii, K., Eto, K., Abe, I., & Fujishima, M. (2000). Voltage-dependent Ca2+ channels in resistance arteries from Dahl salt-sensitive rats. *Hypertens.Res* **23**, 701-707.

Ohya, Y., Setoguchi, M., Fujii, K., Nagao, T., Abe, I., & Fujishima, M. (1996). Impaired Action of Levcromakalim on ATP-Sensitive K+ Channels in Mesenteric Artery Cells From Spontaneously Hypertensive Rats. *Hypertension* **27**, 1234-1239.

Onishi, H., Wakabayashi, T., Kamata, T., & Watanabe, S. (1983). Electron microscopic studies of myosin molecules from chicken gizzard muscle II: The effect of thiophosphorylation of the 20K-dalton light chain on the ATP-induced change in the conformation of myosin monomers. *J Biochem* **94**, 1147-1154.

Owsianik, G., Talavera, K., Voets, T., & Nilius, B. (2006). Permeation and selectivity of TRP channels. *Annu.Rev Physiol* **68**, 685-717.

Pang, L., Koren, G., Wang, Z., & Nattel, S. (2003). Tissue-specific expression of two human Ca(v)1.2 isoforms under the control of distinct 5' flanking regulatory elements. *FEBS Lett.* **546**, 349-354.

Parekh, A. B. & Penner, R. (1997). Store depletion and calcium influx. *Physiol Rev* **77**, 901-930.

Park, K. S., Kim, Y., Lee, Y. H., Earm, Y. E., & Ho, W. K. (2003). Mechanosensitive cation channels in arterial smooth muscle cells are activated by diacylglycerol and inhibited by phospholipase C inhibitor. *Circulation Research* **93**, 557-564.

Patterson, A. J., Henrie-Olson, J., & Brenner, R. (2002). Vasoregulation at the molecular level: a role for the beta1 subunit of the calcium-activated potassium (BK) channel. *Trends Cardiovasc Med* **12**, 78-82.

Pedersen, S. F., Owsianik, G., & Nilius, B. (2005). TRP channels: an overview. *Cell Calcium* **38**, 233-252.

Pesic, A., Madden, J. A., Pesic, M., & Rusch, N. J. (2004). High Blood Pressure Upregulates Arterial L-Type Ca^{2+} Channels: Is Membrane Depolarization the Signal? *Circulation Research* **94**, e97-104.

Peterson, B. Z. & Catterall, W. A. (2006). Allosteric Interactions Required for High-Affinity Binding of Dihydropyridine Antagonists to CaV1.1 Channels Are Modulated by Calcium in the Pore. *Molecular Pharmacology* **70**, 667-675.

Pinterova, M., Kunes, J., & Zicha, J. (2011). Altered neural and vascular mechanisms in hypertension. *Physiol Res* **60**, 381-402.

Plüger, S., Faulhaber, J., Furstenau, M., Lohn, M., Waldschutz, R., Gollasch, M., Haller, H., Luft, F. C., Ehmke, H., & Pongs, O. (2000). Mice With Disrupted BK Channel β1 Subunit Gene Feature Abnormal Ca^{2+} Spark/STOC Coupling and Elevated Blood Pressure. *Circulation Research* **87**, e53-e60.

Pongs, O. & Schwarz, J. R. (2010). Ancillary Subunits Associated With Voltage-Dependent K+ Channels. *Physiological Reviews* **90**, 755-796.

Pratt, P. F., Bonnet, S., Ludwig, L. M., Bonnet, P., & Rusch, N. J. (2002). Upregulation of L-type Ca2+ channels in mesenteric and skeletal arteries of SHR. *Hypertension* **40**, 214-219.

Putney, J. W., Jr. (1986). A model for receptor-regulated calcium entry. *Cell Calcium* **7**, 1-12.

Qin, N., Yagel, S., Momplaisir, M. L., Codd, E. E., & D'Andrea, M. R. (2002). Molecular cloning and characterization of the human voltage-gated calcium channel alpha(2)delta-4 subunit. *Molecular Pharmacology* **62**, 485-496.

Quayle, J. M., McCarron, J. G., Brayden, J. E., & Nelson, M. T. (1993). Inward rectifier K+ currents in smooth muscle cells from rat resistance-sized cerebral arteries. *Am J Physiol* **265**, C1363-C1370.

Quayle, J. M., Nelson, M. T., & Standen, N. B. (1997). ATP-sensitive and inwardly rectifying

potassium channels in smooth muscle. *Physiol Rev.* **77**, 1165-1232.

Raikar, L. S., Vallejo, J., Lloyd, P. G., & Hardin, C. D. (2006). Overexpression of caveolin-1 results in increased plasma membrane targeting of glycolytic enzymes: the structural basis for a membrane associated metabolic compartment. *J Cell Biochem* **98**, 861-871.

Rubart, M., Patlak, J. B., & Nelson, M. T. (1996). Ca2+ currents in cerebral artery smooth muscle cells of rat at physiological Ca2+ concentrations. *J Gen.Physiol* **107**, 459-472.

Sah, P. (1996). Ca^{2+}-activated K^{+} currents in neurones: types, physiological roles and modulation. *Trends Neurosci.* **19**, 150-154.

Sanders, K. M. (2001). Invited review: mechanisms of calcium handling in smooth muscles. *Journal of Applied Physiology* **91**, 1438-1449.

Santana, L. F. & Navedo, M. F. (2009). Molecular and biophysical mechanisms of Ca2+ sparklets in smooth muscle. *Journal of Molecular and Cellular Cardiology* **In Press, Corrected Proof**.

Schlager, G. (1981). Longevity in Spontaneously Hypertensive Mice. *Experimental Gerontology* **16**, 325-330.

Schlager, G. & Sides, J. (1997). Characterization of hypertensive and hypotensive inbred strains of mice. *Lab Anim Sci.* **47**, 288-292.

Schreiber, M. & Salkoff, L. (1997). A novel calcium-sensing domain in the BK channel. *Biophysical Journal* **73**, 1355-1363.

Schumacher, T. B., Beck, H., Steinhauser, C., Schramm, J., & Elger, C. E. (1998). Effects of phenytoin, carbamazepine, and gabapentin on calcium channels in hippocampal granule cells from patients with temporal lobe epilepsy. *Epilepsia* **39**, 355-363.

Schwencke, C., Schmeisser, A., Walter, C., Wachter, R., Pannach, S., Weck, B., Braun-Dullaeus, R. C., Kasper, M., & Strasser, R. H.

(2005). Decreased caveolin-1 in atheroma: loss of antiproliferative control of vascular smooth muscle cells in atherosclerosis. *Cardiovasc Res* **68**, 128-135.

Seino, S. & Miki, T. (2004). Gene targeting approach to clarification of ion channel function: studies of Kir6.x null mice. *The Journal of Physiology* **554**, 295-300.

Sharif-Naeini, R., Dedman, A., Folgering, J. H., Duprat, F., Patel, A., Nilius, B., & Honore, E. (2008). TRP channels and mechanosensory transduction: insights into the arterial myogenic response. *Pflugers Arch.* **456**, 529-540.

Shistik, E., Ivanina, T., Puri, T., Hosey, M., & Dascal, N. (1995). Ca2+ current enhancement by alpha 2/delta and beta subunits in Xenopus oocytes: contribution of changes in channel gating and alpha 1 protein level. *Journal of Physiology* **489 (Pt 1)**, 55-62.

Siegel, G., Walter, A., Schnalke, F., Schmidt, A., Buddecke, E., Loirand, G., & Stock, G. (1991). Potassium channel activation, hyperpolarization, and vascular relaxation. *Z.Kardiol.* **80 Suppl 7**, 9-24.

Sigworth, F. J. & Sine, S. M. (1987). Data transformations for improved display and fitting of single-channel dwell time histograms. *Biophys.J* **52**, 1047-1054.

Simard, J. M., Li, X., & Tewari, K. (1998). Increase in functional Ca2+ channels in cerebral smooth muscle with renal hypertension. *Circulation Research* **82**, 1330-1337.

Singer, D., Biel, M., Lotan, I., Flockerzi, V., Hofmann, F., & Dascal, N. (1991). The roles of the subunits in the function of the calcium channel. *Science* **253**, 1553-1557.

Smith, P. D., Brett, S. E., Luykenaar, K. D., Sandow, S. L., Marrelli, S. P., Vigmond, E. J., & Welsh, D. G. (2008). KIR channels function as electrical amplifiers in rat vascular smooth muscle. *Journal of Physiology* **586**, 1147-1160.

References

Sobey, C. G. (2001). Potassium channel function in vascular disease. *Arteriosclerosis, Thrombosis, and Vascular Biology* **21**, 28-38.

Somlyo, A. P. & Somlyo, A. V. (2003). Ca^{2+} sensitivity of smooth muscle and nonmuscle myosin II: modulated by G proteins, kinases, and myosin phosphatase. *Physiol Rev.* **83**, 1325-1358.

Sonkusare, S., Palade, P. T., Marsh, J. D., Telemaque, S., Pesic, A., & Rusch, N. J. (2006). Vascular calcium channels and high blood pressure: Pathophysiology and therapeutic implications. *Vascular Pharmacology* **44**, 131-142.

Standen, N. B. & Quayle, J. M. (1998). K+ channel modulation in arterial smooth muscle. *Acta Physiol Scand.* **164**, 549-557.

Stefani, A., Spadoni, F., Giacomini, P., Lavaroni, F., & Bernardi, G. (2001). The effects of gabapentin on different ligand- and voltage-gated currents in isolated cortical neurons. *Epilepsy Res* **43**, 239-248.

Sutton, K. G., Martin, D. J., Pinnock, R. D., Lee, K., & Scott, R. H. (2002). Gabapentin inhibits high-threshold calcium channel currents in cultured rat dorsal root ganglion neurones. *Br J Pharmacol* **135**, 257-265.

Taggart, M. J. & Morgan, K. G. (2007). Regulation of the uterine contractile apparatus and cytoskeleton. *Semin.Cell Dev.Biol* **18**, 296-304.

Tanaka, Y., Koike, K., & Toro, L. (2004). MaxiK channel roles in blood vessel relaxations induced by endothelium-derived relaxing factors and their molecular mechanisms. *J Smooth Muscle Res* **40**, 125-153.

Tang, D. D. (2008). Intermediate filaments in smooth muscle. *American Journal of Physiology - Cell Physiology* **294**, C869-C878.

Tavalin, S. J., Shepherd, D., Cloues, R. K., Bowden, S. E., & Marrion, N. V. (2004). Modulation of single channels underlying hippocampal L-type current enhancement by agonists depends on the permeant ion. *Journal of Neurophysiology* **92**, 824-837.

Taylor, C. P. (2009b). Mechanisms of analgesia by gabapentin and pregabalin--calcium channel alpha2-delta [Cavalpha2-delta] ligands. *Pain* **142**, 13-16.

Taylor, C. P. (2009a). Mechanisms of analgesia by gabapentin and pregabalin--calcium channel alpha2-delta [Cavalpha2-delta] ligands. *Pain* **142**, 13-16.

Teramoto, N. (2006). Physiological roles of ATP-sensitive K+ channels in smooth muscle. *The Journal of Physiology Online* **572**, 617-624.

Terzic, A., Jahangir, A., & Kurachi, Y. (1995). Cardiac ATP-sensitive K+ channels: regulation by intracellular nucleotides and K+ channel-opening drugs. *Am J Physiol* **269**, C525-C545.

Thompson, S. M. (1986). Relations between chord and slope conductances and equivalent electromotive forces. *American Journal of Physiology - Cell Physiology* **250**, C333-C339.

Tzellos, T. G., Papazisis, G., Amaniti, E., & Kouvelas, D. (2008). Efficacy of pregabalin and gabapentin for neuropathic pain in spinal-cord injury: an evidence-based evaluation of the literature. *Eur.J Clin Pharmacol* **64**, 851-858.

Vega-Hernandez, A. & Felix, R. (2002). Down-regulation of N-type voltage-activated Ca2+ channels by gabapentin. *Cell Mol Neurobiol.* **22**, 185-190.

Vennekens, R. (2011). Emerging concepts for the role of TRP channels in the cardiovascular system. *Journal of Physiology* **589**, 1527-1534.

Wagenseil, J. E. & Mecham, R. P. (2009). Vascular extracellular matrix and arterial mechanics. *Physiol Rev* **89**, 957-989.

Wamhoff, B. R., Bowles, D. K., & Owens, G. K. (2006). Excitation-transcription coupling in arterial smooth muscle. *Circulation Research* **98**, 868-878.

Wang, W. Z., Saada, N., Dai, B., Pang, L., & Palade, P. (2006). Vascular-specific increase in exon 1B-encoded CAV1.2 channels in spontaneously hypertensive rats. *Am J Hypertens.* **19**, 823-831.

Weston, A. H., Porter, E. L., Harno, E., & Edwards, G. (2010). Impairment of endothelial SK(Ca) channels and of downstream hyperpolarizing pathways in mesenteric arteries from spontaneously hypertensive rats. *Br J Pharmacol* **160**, 836-843.

Whittaker, C. A. & Hynes, R. O. (2002). Distribution and evolution of von Willebrand/integrin A domains: widely dispersed domains with roles in cell adhesion and elsewhere. *Mol Biol Cell* **13**, 3369-3387.

Wickenden, A. D. (2002). K+ channels as therapeutic drug targets. *Pharmacology & Therapeutics* **94**, 157-182.

Woodruff, M. L., Sampath, A. P., Matthews, H. R., Krasnoperova, N. V., Lem, J., & Fain, G. L. (2002). Measurement of cytoplasmic calcium concentration in the rods of wild-type and transducin knock-out mice. *Journal of Physiology* **542**, 843-854.

Yang, J., Jan, Y. N., & Jan, L. Y. (1995). Determination of the subunit stoichiometry of an inwardly rectifying potassium channel. *Neuron* **15**, 1441-1447.

Yuan, J. S., Reed, A., Chen, F., & Stewart, C. N., Jr. (2006). Statistical analysis of real-time PCR data. *BMC.Bioinformatics* **7**, 85.

Zaritsky, J. J., Eckman, D. M., Wellman, G. C., Nelson, M. T., & Schwarz, T. L. (2000). Targeted disruption of Kir2.1 and Kir2.2 genes reveals the essential role of the inwardly rectifying K(+) current in K(+)-mediated vasodilation. *Circulation Research* **87**, 160-166.

Zhou, J. G., Qiu, Q. Y., Zhang, Z., Liu, Y. J., & Guan, Y. Y. (2006). Evidence for capacitative and non-capacitative Ca2+ entry pathways coexist in A10 vascular smooth muscle cells. *Life Sci* **78**, 1558-1563.

Zong, Z. Q., Zhou, J. Y., & Tanabe, T. (1994). Molecular Determinants of Calcium-Dependent Inactivation in Cardiac L-Type Calcium Channels. *Biochemical and Biophysical Research Communications* **201**, 1117-1123.

8 APPENDIX

8.1 Poiseuille's Law

The resistance of the systemic circulation to flow is located chiefly in the tiny terminal arteries and arterioles. Total peripheral resistance is the pressure drop required to drive unit flow through the systemic circulation. Resistance to flow arises exclusively from the internal friction within the fluid. It is not caused by friction at the tube wall, because there is no flow at the wall surface, owing to the laminar flow. Furthermore, resistance to flow is greatly affected by tube radius, because the rate at which one lamina slides past the adjacent one is greater in narrow tubes than wide tubes, for a given flow.

The factors governing tube resistance were first elucidated by physician Jean Leonard Marie Poiseuille, around 1840, in a meticulous study of water flowing through glass capillary tubes. Studying the steady, laminar flow of a Newtonian fluid (water, plasma) along a straight cylindrical tube, Poiseuille established that resistance R is inversely proportional to tube radius raised to the fourth power, r^4. Also, resistance is directly proportional to fluid viscosity η and tube length L:

$$R = \frac{8\,\eta\,L}{\pi\,r^4}$$
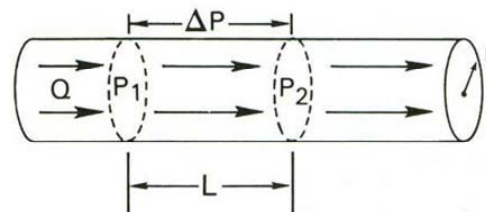
POISEUILLE'S LAW
$$Q = \frac{\Delta P}{\eta\,L} \cdot \frac{r^4}{8} \cdot \pi$$

8.2 Lambert-Beer Law

The equation of Lambert-Beer is used to correlate absorbance to concentration using the next equation:

$$A = E \cdot b \cdot c$$

Where **A** is the measured absorbance (or optical density, OD) represented as absorbance units (A), **E** is the wavelength-dependent molar absorptivity coefficient (or molar extinction coefficient) with units of ($M^{-1} \cdot cm^{-1}$), **b** is the sample thickness in (cm) and c is the analyte concentration in (mol/litre) or molarity (M).

The Lambert-Beer equation is modified to measure nucleic acids concentration. In this case, using a molar extinction coefficient whose units are ng · cm/ml. Now the equation is expressed:

$$c = \frac{A \cdot e}{b}$$

Where **c** is the concentration of nucleic acids in ng / µl, **A** is the absorbance in absorbance units, **e** is the molar extinction coefficient in ng · cm / µl and **b** is the sample length in cm.

The molar extinction coefficients accepted for nucleic acids are:

- Double-stranded DNA: 50 ng·cm/µl
- Simple-stranded DNA: 33 ng·cm/µl
- RNA: 40ng·cm/µl

The A260/A280 ratio was used to calculate the purity of both DNA and RNA. An A260/A280 ratio> 2 is generally accepted as a "pure RNA". If the ratio is less than 2, it is indicative of contamination by proteins, phenolic compounds or other compounds whose absorbance is close to 280nm.

Quantified RNA was treated with the DNAse, RNAase-Free DNase I (Ambion) to remove possible contaminations with genomic DNA from the samples.

8.3 Darcy's Law

Darcy was a French civil war engineer who studied the flow of water through the gravel beds of the fountains in Dijon. In 1856 Darcy reported that flow in the steady state, Q, is linearly proportional to the pressure difference between two points, $P_1 - P_2$. That is to say:

$$Q = K\,(P_1 - P_2) = \frac{(P_1 - P_2)}{R}$$

The proportionality coefficient K is called the hydraulic conductance, which is is effect the ease of flow. Its reciprocal is called the hydraulic resistance, R- the difficulty of flow. Darcy´s law can be applied to channels of any geometry, including blood vessels.

The flow through the systemic circulation is the cardiac output, CO, and the pressure difference driving it equal mean aortic pressure P_a minus the central venus pressure CVP. The systemic resistance is called the total peripheral resistance or TPR. Putting these symbols into Darcy´s law, we have:

$$CO = \frac{(P_a - CVP)}{TPR}$$

All blood pressures are concentionally expressed as pressure above atmospheric pressure , and since CVP is close to atmospheric pressure, CVP ≈ 0. Thus this equation simplifies to:

$$P_a = CO \cdot TPR$$

Therefore mean arterial pressure is determined by cardiac output and total peripheral resistance.

8.4 Patch-Clamp technique

AL.Hodgkin and AF.Huxley revolutionized research of ion channels in 1952 because they described the model that explains the ionic mechanisms underlying the initiation and propagation of action potentials in the squid giant axon (Hodgkin *et al.*, 1952;Hodgkin & Huxley, 1952c;Hodgkin & Huxley, 1952d;Hodgkin & Huxley, 1952b;Hodgkin & Huxley, 1952a). They received the 1963 Nobel Prize in Physiology or Medicine for this work. This advance in scientific research was preceded by the introduction of a new technique: the "Voltage Clamp".

The Voltage Clamp technique allows the membrane potential of a cell to be held or clamped and measure the current that flows through the membrane to maintain this voltage. This is important because many of the ion channels in the membrane of a neuron are voltage-gated ion channels, which open only when the membrane voltage is within a certain range. Initially, the technique combined the use of two intracellular electrodes. One of these is to measure the voltage of the membrane potential, and the other is to conduct electrical current into or out of the cell. An amplifier compares the real voltage of the cell with the voltage set, and introduce into the circuit the current required to achieve this voltage. The injected current is exactly equal in amplitude but opposite in sign to that flows across the cell membrane. Thus, the voltage clamp technique indicates how membrane potential influences the ion currents through the membrane and indirectly how the currents flowing through the cell plasmalemma determined the membrane potential.

Although the "Voltage Clamp" not reproduce a physiological process is interesting for three reasons:

1. Clamp or hold the voltage eliminates the capacitive current, except for a short period time, just before a voltage pulse.
2. Currents flowing through the membrane are proportional to the conductance of the cell i.e., the number of open channels.
3. The voltage clamp can control the main factor that determines the opening of voltage operated ion channel.

In 1976 B.Sackmann and E.Neher refined the "Voltage Clamp" method developing the "Patch-Clamp" technique or voltage clamp in membrane patches. This discovery allowed the study of single channel for the first time (Neher & Sakmann, 1976;Neher *et al.*, 1978;Hamill *et al.*, 1981). The ability to record single channel currents revolutionized the study of ion channels because it allowed the single channel conductance and kinetics to be observed directly. Neher and Sakmann received the Nobel Prize in Physiology or Medicine in 1991 for this update version of the voltage clamp technique.

This new technique is based on the use of large microelectrodes that does no penetrate the cell but forms a very tight seal with its membrane. These very high-resistance seals (>1GΩ) can be formed between the cell membrane and the small tip of a micropipette when gentle suction is applied to the pipet interior. The micropipette has an electrode inside, which inject the current required to maintain the fixed membrane potential. Using different stimulation protocols, resulting ionic currents are recorded with an electronic amplifier connected to the micropipette.

8.4.1 Patch-Clamp configurations

There are four main patch clamp configurations: cell attached, inside out and outside out and whole cell (Hamill *et al.*, 1981). The first three of these may be used to record single-channel currents from small patch of the membrane while the last is used to record the whole-cell currents flowing through all of the cell membrane.

Cell-attached: this configuration is the starting point for all of the others. The micropipette tip forms a high resistance seal against membrane of an intact cell. Thus this configuration is very useful for studying the properties of ion channels under physiological conditions. It also been used to determine whether the effects of a substance are mediated by a direct interaction with an ion channel or indirectly, via the generation of a cytosolic second messenger. However,

has two disadvantages: the composition of the internal solution and the membrane potential are unknown.

Inside-out: this configuration is obtained from a cell-attached patch configuration, where the pipette is pulled away. The result is an isolated membrane patch with the cytosolic side facing the bath. Inside-out configuration allow the properties of the single-channels currents to be studied under controlled ionic conditions and is ideal for studying the effects of cytoslic factors on channels activity. The inside-out patches are difficult to obtain and involves a extra step, destruction of the vesicle that can be formed on the pipette tip.

Whole cell: this configuration is obtained by forming a cell-attached patch and then destroying the patch membrane with lightly negative pressure. This provides electrical access to the cell interior and so enables measurement of the whole-cell current. It has the advantages that the extracellular side can be superfused and intracellular solutions can be manipulated, but the disadvantage that the soluble cytosolic constituents are lost from the cell because they dialyse with the pipette solution.

Outside-out: outside-out patch is obtained by simply pulling away the patch pipette from a whole-cell configuration. The extracellular membrane surface of the out-side patch faces the bath solution. This configuration may be used to study channels gated by extracellular ligands. As in the whole-cell configuration there is washout of cytosolic factors.

8.4.2 Special configurations

Perforated-patch: In this variation of whole-cell recording, after GΩ seal formation the patch membrane is not ruptured by suction. Instead, the patch membrane is permeabilised with a pore forming antibiotic or antifungal such as amphotericin B, nystatin or gramicidin. The pores formed are permeable to monovalent cations, such as K^+, but divalent cations, anions and molecules of high molecular weight are impermeant. This configuration therefore allows electrical access to the cell interior while retaining cell metabolism and intracellular messenger systems intact.

Hamill, O. P., Marty, A., Neher, E., Sakmann, B., & Sigworth, F. J. (1981). Improved patch clamp techniques for high-resolution current recordings from cells and cell-free membrane patches. *Pflugers Archiv - European Journal of Physiology* **391**, 85-100.

Hodgkin, A. L. & Huxley, A. F. (1952a). A quantitative description of membrane current and its application to conduction and excitation in nerve. *J.Physiol.(Lond.)* **117**, 500-544.

Hodgkin, A. L. & Huxley, A. F. (1952b). Currents Carried by Sodium and Potassium Ions through the Membrane of the Giant axon of *Loligo*. *J.Physiol.(Lond.)* **116**, 449-472.

Hodgkin, A. L. & Huxley, A. F. (1952c). The Components of Membrane Conductance in the Giant axon of *Loligo*. *J.Physiol.(Lond.)* **116**, 473-496.

Hodgkin, A. L. & Huxley, A. F. (1952d). The dual effect of membrane potential on sodium conductance in the Giant axon of *Loligo*. *J.Physiol.(Lond.)* **116**, 497-506.

Hodgkin, A. L., Huxley, A. F., & Katz, B. (1952). Measurement of Current-Voltage Relations in The Membrane of The Giant axon of *Loligo*. *J.Physiol.(Lond.)* **116**, 424-448.

Neher, E. & Sakmann, B. (1976). Single-channel currents recorded from membrane of denervated frog muscle fibres. *Nature* **260**, 799-802.

Neher, E., Sakmann, B., & Steinbach, J. H. (1978). The extracellular patch clamp: a method for resolving currents through individual open channels in biological membranes. *Pflugers Arch.* **375**, 219-228.

9 RESUMEN

1.1INTRODUCCIÓN

La **hipertensión arterial** (HTA) es una enfermedad que afecta a cerca del 30% de la población adulta en los países desarrollados (Chobanian *et al.*, 2003). Además, es un factor de riesgo que aumenta las probabilidades de padecer diferentes patologías cardiovasculares como infarto cardiaco, derrame cerebral e insuficiencia renal. El 95% de los casos de HTA se diagnostican como **hipertensión esencial** (HTE), siendo imposible identificar la causa de la elevada presión arterial. Sin embargo, diferentes estudios apoyan la hipótesis de que la HTE se desarrolla como consecuencia de múltiples factores genéticos y ambientales.

La HTE se define como el aumento sostenido de las resistencias periféricas totales (RPT) del sistema cardiovascular (SC). El SC esta formado por el corazón y los vasos sanguíneos, que podemos clasificar según el tamaño en: arterias, arteriolas, capilares, vénulas y venas. La actividad contráctil de las células del musculo liso que forman la pared de arterias y arteriolas es el principal determinante de las RPT en la circulación vascular. Los vasos sanguíneos se encuentran normalmente en un estado de contracción parcial denominado **tono basal** (Nelson & Quayle, 1995), desde el cual pueden contraerse o dilatarse dependiendo de las necesidades de perfusión. El **potencial de membrana** (E_M) de las VSMCs a través de los canales de Ca^{2+} dependientes de voltage (VDCCs) es el principal factor que regula la $[Ca^{2+}]_i$ y por tanto el tono vascular (Knot & Nelson, 1998). Por este motivo, la contracción en musculo liso vascular se encuentra estrechamente acoplada al E_M, de forma que una despolarización aumenta la contracción y una hiperpolarización la inhibe (Haeusler, 1983b). Como los canales de K^+ juegan un papel principal en establecer el E_M de las VSMCs, son determinantes en el control del tono vascular y en el diámetro de los vasos. Al menos cuatro tipos de diferentes de canales de potasio han sido identificados en VSMCs: los rectificadores hacia dentro (inward rectifiers K^+ channels, K_{IR}), los voltaje dependientes (voltage-dependent K^+ channels, Kv), los sensibles a ATP (ATP-gated K^+ channels, K_{ATP}) y los sensibles a Ca^{2+} (Ca^{2+} gated K^+ channels, BK_{Ca}) (Nelson & Quayle, 1995). Estos cuatro tipos de canales de K^+ junto con los VDCCs están implicados directa o indirectamente en la regulación del tono vascular.

1.2 OBJETIVOS

El objetivo de esta tesis es determinar los mecanismos iónicos que se encuentran alterados en un modelo murino de hipertensión esencial. Para ello se ha estudiado: el remodelado eléctrico de los canales de K^+ (los cuales controlan el E_M) y la composición molecular y función de los canales de calcio tipo-L (LTCCs), la principal vía de entrada de Ca^{2+} al interior celular.

1.3 MATERIALES

El modelo de HTE utilizado presenta una hipertension moderada que se desarrolla en el individuo adulto. Estos ratones se han obtenido cruzando ocho cepas distintas de ratones, por lo que comparten un fondo genético similar. Tras múltiples generaciones seleccionando fenotípicamente los ratones en función de su presión arterial se han obtenido dos cepas distintas, una cepa de ratones hipertensos (BPH, blood pressure high) y sus respectivos controles normotensos (BPN, blood pressure normal).

Para llevar a cabo los objetivos propuestos se ha recurrido a técnicas electrofisiológicas como el patch-clamp para estudiar las corrientes iónicas a través de los canales de K^+ y Ca^{2+} y el current-clamp para examinar la contribución de los diferentes canales al E_M. Se han utilizado las configuraciones de whole-cell (para estudiar corrientes en célula entera), perforated-patch (para examinar las corrientes sin alterar el medio intracelular) y el single channel (para estudiar las propiedades eléctricas de los BK_{Ca}). Además, se ha utilizado un miógrafo de presión para caracterizar las funciones fisiológicas y propiedades de los vasos de resistencia de los ratones BPN y BPH. Así mismo, también se ha utilizado la miografía para investigar la contribución de los canales de K^+ (K_{IR} y K_{ATP}) al tono vascular.

Las técnicas moleculares como PCR cuantitativa y el western blot se han utilizado para caracterizar los niveles de expresión de los distintos canales iónicos desde el RNAm hasta las proteínas.

La imagen de calcio tanto con el TIRF (fluorescencia de reflexión interna total) como con el swept-field confocal (confocal de barrido) han sido utilizados para examinar la entrada de Ca^{2+} al interior celular a través de los LTCCs ("sparklets"), así como la salida de calcio desde el retículo sarcoplasmatico (SR) a través de los canales acoplados a receptores de rianodina (RyR), "sparks".

1.4 RESULTADOS

1.4.1 Estudio de los canales de K^+

Mediante electrofisiología se comprobó que las células de musculo liso vascular (VSMCs) disociadas de arterias mesentericas de BPH presentaban una menor conductancia a K^+ que las de BPN. Esta menor conductancia podría explicar el E_M mas despolarizado observado en las VSMCs de BPH. Mediante qPCR se comprobó que había una disminución de los niveles de

expresión de los canales K_{IR} (Kir2.1 y Kir4.1) y de los K_{ATP} (Kir6.1 y SUR2). Sin embargo esta menor expresión de RNAm, sólo se tradujo en una reducción de las proteínas Kir4.1, SUR2 y mas notablemente en Kir6.1. La expresión funcional de estos canales se evaluó utilizando la técnica de whole-cell y de parche perforado. De esta forma, se confirmó midiendo densidad de corriente, que tanto los canales K_{IR} como los K_{ATP} estaban disminuidos en BPH, siendo estos últimos los que lo hacían de forma más significativa. Mediante estudios de current-clamp se evidenció la menor contribución de los canales K_{ATP} al establecimiento del E_M en los miocitos de ratones BPH. Por ultimo, se analizó la contribución de ambos canales al tono vascular y por tanto al fenotipo hypertensivo mediante miografía. En estos experimentos los canales K_{IR} no mostraron diferencias significativas entre BPN y BPH, sin embargo la contribución de los canales K_{ATP} al tono vascular se encontraba significativamente reducida en las arterias de BPH.

1.4.2 Estudio de los canales de Ca^{2+}

La caracterización funcional de las corrientes de Ca^{2+} se evaluó mediante técnicas electrofisiológicas en VSMCs de ratones BPN y BPH. Primero se comprobó que la corriente de Ca^{2+} en estas células se debía principalmente a canales de calcio tipo-L, ya que la mayor parte de la corriente se bloquea con nifedipina (bloqueante de los canales tipo-L) y porque las propiedades fisiológicas y cinéticas de las corrientes son características de los LTCCs.

La densidad de corriente a través de los LTCCs tanto en whole-cell como en parche-perforado se encontraba significativamente disminuida en las células BPH, con lo que se descarto la presencia de un inhibidor intracelular de la corriente en los miocitos de ratones BPH. El uso del BayK-8644 (agonista de los LTCCs) produjo un aumento significativo de ambas corrientes, sin embargo el efecto potenciador del BayK fue mayor en BPH. Esto sugiere que las células BPH tienen tanto una menor población de LTCCs como una composición de subunidades diferentes.

Los análisis de RT-PCR revelaron un descenso en los niveles de expresión de RNAm en las subunidades α_{1C} y β_2 y un aumento significativo en los de la subunidad $\alpha_2\delta$. Esta diferencia en la composición de las subunidades podría explicar las diferencias funcionales observadas en las corrientes.

Utilizamos la gabapentina (GBP), un ligando de la subunidad $\alpha_2\delta$, para explorar la contribución de esta subunidad a las corrientes mediadas por los LTCCs. El efecto de esta droga producía un mayor incremento de la corriente en BPH que en BPN, sugiriendo que en BPH esta subunidad se encuentra más disponible para formar un LTCCs funcional. Para una mejor caracterización del efecto de la GBP se recurrió a curvas dosis respuesta en células nativas y en HEKs

trasnfectadas con las diferentes subunidades. Los efectos de la GBP sobre las corrientes de los LTCCs mostraron ciertas similitudes entre los BPN y las HEKs co-trasnfectadas con $\alpha_1+\alpha_2\delta$ y entre los BPH y las HEKs co-transfectadas con $\alpha_1+\alpha_2\delta+\beta_2$. Estos resultados confirmaron que la presencia de $\alpha_2\delta$ es necesaria para la unión de la GBP y que las diferencias entre BPN y BPH podrían deberse a la diferente proporción de las subunidades β.

La organización y función de los LTCCs se estudió mediante la observación de la entrada de Ca^{2+} utilizando la técnica del TIRF. Los resultados obtenidos permitieron comprobar que en condiciones fisiológicas los LTCCs de las células BPH funcionan con mayor probabilidad de apertura, están en estado abierto durante más tiempo y se organizan en grupos mayores que los de BPN.

1.4.3 Acoplamiento spark-STOCs

El acoplamiento entre la salida de Ca^{2+} del SR a través de los RyR "spark" y las corrientes espontaneas y transitorias a través de los BK_{Ca} "STOCs" es un mecanismo de freno a la contracción ya que supone la hiperpolarización de la VSMCs. En las células BPH la amplitud de los sparks de Ca^{2+} está significativamente aumentada comparada con la de BPN, sin embargo esto no supone un aumento de las STOCs en estas células. Al medir mediante parche perforado STOCs en BPH, vimos una pronunciada disminución tanto de la frecuencia como de la amplitud de estas señales. Estos datos podían explicarse por la reducción de la subunidad β_1 de los canales BK_{Ca}, que regula su sensibilidad a Ca^{2+}. Mediante registros de single-channel se comprobó que el número se canales y su sensibilidad a calcio estaban disminuidos en las células de los ratones BPH.

1.5 DISCUSION

En la mayoría de los casos de HTE las causas de la elevada presión arterial se atribuyen a un origen multifactorial, tanto a factores genéticos como ambientales. Nuestro modelo de hipertensión obtenido por selección fenotípica mediante diversos cruces es un claro ejemplo de cómo múltiples y sutiles cambios pueden contribuir a la génensis de un fenotipo hipertensivo. Así, la elevada respuesta miogénica presente en las arterias de los ratones BPH podría ser una consecuencia de múltiples factores:

1. El potencial de membrana de reposo despolarizado en las células BPH ($\sim$10 mV).

2. La disminución de la contribución funcional de los canales K_{IR} y K_{ATP} en las VSMCs de BPH, aunque hemos comprobado que solo los K_{ATP} afectan al tono vascular en BPH.

3. La menor población o la diferente composición de los LTCCs en la membrana de las miocitos en BPH.

4. La mayor actividad de los LTCCs debido a la mayor probabilidad de apertura, un estado abierto mas prolongado y a su organización en grupos mas grandes.

5. El desacoplamiento que se produce entre sparks y STOCs reduciendo el freno a la contracción.

En resumen, nuestros datos apoyan la hipótesis de que cambios en la expresión funcional de los canales KIR, K_{ATP}, BK_{Ca} y LTCCs son importantes en el desarrollo de la HTE, ya que podrían ser determinantes principales en la despolarización del E_M y en el incremento de la entrada de Ca^{2+} en las VSMCs de ratones hipertensos.